Towards Improving Volcanic Mass Flow Hazard Assessment at New Zealand Stratovolcanoes

A thesis presented in partial fulfilment of the requirements for the degree of

Doctor of Philosophy

In

Earth Science

Massey University, Palmerston North, New Zealand.

Jonathan N. Procter

2009

Abstract

The most common hazards for communities surrounding mountain-forming stratovolcanoes are mass flows of a range of types. Determining their frequency, characteristics and distribution is a major focus of hazard mapping efforts. Recent improvements in computer power and numerical models have meant that simulation of mass flow scenarios is a new tool available for hazard analysis. Its application to hazard mapping, land use planning and emergency management awaits robust evaluation of the conditions under which simulation tools are effective. This study focuses on this question in attempting to improve mass-flow hazard assessments at the typical stratovolcanoes of Mts. Taranaki and Ruapehu in New Zealand. On Mt. Ruapehu, Titan2D modelling was applied to forecast behaviour of non-cohesive lahars in the Whangaehu River, primarily produced by Crater Lake break-outs, such as on 18 March 2007. The simulations were accurate in predicting inundation area, bifurcation, super-elevation, hydraulic ponding, velocity and travel times of the lahar to 9-10 km. A 6×10^6 m^3 simulated granular flow had a minimum discharge of 1800-2100 m^3/s at the apex of the Whangaehu Fan, 9-10 km from source, comparable to all historic information. The modelling implied that it was highly unlikely for a flow of this nature to overtop a lahar training dyke (bund) at the fan-apex location and avulse northward into a more vulnerable catchment. Beyond this point, the model could not cope with the rapid and complex changes in rheology of these non-cohesive lahars. At Mt. Taranaki chronostratigraphic grouping of mapped past lahar deposits often clouds the actual series of landscape forming processes and hence variations in hazard that occurred over time. Here, patterns of mass flows following emplacement of a 7 km^3 debris avalanche deposit were examined from field geology and Titan2D modelling to define a three-stage recovery process, where lahars of different types and sources were focused initially beside and later on top of the debris avalanche deposit for up to 10 000 years. Results from Titan2D were used to identify source areas of mass flows at different stages and their probable rheologies. Debris avalanche emplacement at Mt. Taranaki was investigated on the c. 7 ka B.P. Opua Formation with the help of Titan2D

simulations to identify initial collapse parameters and major flow paths. Once again, the simulations were reliable in proximal reaches, but could not reproduce the rheological transformations from an initial collapsing/sliding pile through to a cohesive clay-rich flow with long runout. In a further example, past block-and-ash flows (BAFs) and dense pyroclastic flow deposits northwest of the current crater were analysed to define the range of realistic model parameters for Titan2D simulations. These could be incorporated inside a Geographic Information System to produce a gradational map of relative probabilities of inundation by future BAF events that took both modelling and geological variability into account. This study highlights that computational models are now reaching the stage where a holistic approach can be taken to hazard analysis that combines both geological mapping and simulation of mass flow scenarios in a probabilistic framework to provide better tools for decision makers and land-use planners.

Acknowledgements

I would like to thank my supervisors for guiding me through this research: Prof. Vince Neall for his wisdom and depth of knowledge of geology; Mr Mike Tuohy for his unique methods and approaches to GIS as well as his related anecdotes; and Prof. Mike Sheridan for providing a new dimension to understanding and studying geology from a computational and modelling basis.

This research would not have been possible without the encouragement, close collaboration and meticulous direction of my supervisor, A/Prof. Shane Cronin who also provided the March 2007 Ruapehu lahar on cue, as well as an unpredictable and mind-boggling journey over the past years.

The Geophysical Mass Flow Group at the State University of New York at Buffalo (Profs. Mike Sheridan and Abani Patra) provided valuable knowledge and the Titan2D toolkit, as well as access to their geology laboratories and Scanning Electron Microscope. I would particularly like to thank Dr. Keith Dalbey for providing assistance and introducing me to linux, programming, uncertainty and super-computing in trailers.

At Massey University I would like to thank Dr. Kat Holt for speedy laboratory work, Dr. Thomas Platz for assistance in the field (and always having his cellphone ready in case of an emergency) and Matt Irwin for a surly and direct approach to answering my many GIS questions. Dr. Gert Lube also provided invaluable theoretical background and advice as well as many ponderous questions. Comments and proof-reading from Dr. Kate Arentsen were very helpful and much appreciated. I also thank all the post graduate students in the Earth Science department for providing an interesting experience and many distractions.

I would not have been able to undertake this research without the financial support of the Foundation for Research Science and Technology (FRST) Tuapapa Putaiao Maori Fellowship. I also greatly appreciate the financial support from the Freemasons Scholarship, the Puke Ariki/George Mason Trust Scholarship, Massey University and the FRST Living with Volcanic Risk programme. I would particularly like to acknowledge the financial and cultural support of Tanenuiarangi Manawatu Inc. who also provided an invaluable retreat.

I am very grateful to my parents who have kept me focussed and supported me throughout this process and been ready and willing to help whenever required.

Finally, I would like to thank my fiancée Dr. Anke Zernack whose immeasurable support kept me encouraged to persevere. While providing priceless field work assistance, proof-reading and organisation, Anke also provided thoughtful and understanding discussions about everything. Thanks for also introducing me to German culture and for saying yes.

TABLE OF CONTENTS

List of Tables

List of Figures

CHAPTER 1

Introduction

1.1. Research Problem

Mts. Taranaki and Ruapehu are the two highest volcanoes in New Zealand and are iconic features for the surrounding community as well as being held in great respect by Maori. Mt. Ruapehu has erupted on many occasions throughout its known history, producing destructive lahars upon nearly every major eruption. The tragedy of Christmas Eve, 1953, where 151 lives were lost, is a demonstration of how deadly these events can be (O'Shea, 1954; Manville, 2004). Mt. Taranaki, even though not having erupted in the last 200 years (Neall et al., 1986; Turner et al., 2008), remains a silent menace of enormous hazard potential, compounded by the fact that over 100 000 people live around its flanks. Geologic investigations of Taranaki volcano (Neall, 1979; Alloway, 1989) have revealed that debris avalanches, lahars, mass flows and pyroclastic flows were frequent throughout its entire geologic past. Hence mass flows are the main hazards defined on the current hazard map (Neall and Alloway, 1996). This map, although being the best hazard-management resource available, is potentially limited by the fact that it is constructed on the basis of the known distributions of past lahars. Long-term ongoing changes in landscape may render it inaccurate, and upon the onset of eruptive activity, rapid modification of the upper edifice may render the map completely irrelevant.

A hazard management tool is required that can be updated for changes in crater geometry and upper edifice geomorphology and is applicable to scenario or probabilistic forecasting, before and during crises. To meet this need, several computational hazard modelling tools are currently under development, using

differing types of physical flow theory, mathematical solutions and computer engineering. The main simulation tools in use include empirically based, block-sliding models (e.g. Sheridan and Kover, 1996); empirical, statistically based inundation models (Schilling, 1998); and more advanced numerical simulations based on physical Coulomb models utilising shallow-water theory (Iverson and Denlinger, 2001 USGS; Pitman et al., 2003, Geophysical Mass Flow Group, SUNY Buffalo). The most visual and useful outputs of these models for risk management purposes are when flows are simulated across digital representations of natural terrain (Digital Elevation Models, DEMs) within geographical information systems (GIS). This not only allows modelling and forecasting of hazards, but also overlaying of remotely sensed and socio-economic data. From such GIS analysis, scenario impact and direct risk assessments can be made. The application and development of these numerical models remains, however, at a very early stage. Many problems exists in understanding the basic physical theory of two-phase flows, further problems lie in conversion of that physical theory to a mathematical solution, and this is additionally complicated by difficulties in efficiently computing the resulting sets of equations. The models overcoming these issues use only a small set of criteria to control their behaviour. These may or may not relate to real physical parameters. Due to these limitations, the new generation computational models must be tested in detail before their forecasts can be trusted for application to hazard and risk management.

The research undertaken in this study focuses on:

1. Evaluating the utility of numerical mass flow models for hazard forecasting and management at NZ volcanoes; and

2. Assisting in the development of numerical mass-flow models for hazard forecasting through detailed testing and analysis on real-world example flows.

This study concentrates on a variety of mass-flow types at Mt. Ruapehu (non-cohesive lahars) and Mt. Taranaki (dry rockfalls, pyroclastic flows, lahars and debris avalanches). Field-based sedimentology, inundation, and where possible, dynamic data were collected for input and evaluation of the Titan2D computational modelling toolkit. Based on these evaluations, interpretations are made of the most appropriate predictive "boundary conditions" in the modelling approaches used. In addition, assessments are made of the applicability for the different types of processes considered at the two volcanoes. The final phase is to apply the best modelling approach in both a deterministic and probabilistic fashion to forecast inundation-hazard areas around the two volcanoes. These results are evaluated against current hazard assessments and appropriate updates and modifications to these are suggested. In addition, a first-order risk analysis is carried out in order to demonstrate the applicability of these models to volcanic risk management.

The overall outcomes expected from this research are improved assessments and forecasts of volcanic hazard at Ruapehu and Egmont (Mt. Taranaki) volcanoes. In addition, methods by which modelling can be used to increase volcanic hazard awareness are demonstrated, including the use of a range of visualisation techniques for effective communication of hazard forecasting results.

1.2. Regional Geological Setting

The subduction of the Pacific Plate under the Indo-Australian Plate is a major influence controlling the geological and tectonic setting of New Zealand for the last 45 Ma

(Sdrolias and Muller, 2006) (fig. 1.1). The highly active subduction zone extending 2800 km from Tonga to New Zealand consists of three segments, with the New Zealand section forming in continental crust (Cole, 1982). The dip of the Benioff zone is around 50-70° beneath New Zealand (Adams and Ware, 1977; Ewart et al., 1977) to a depth of around 100 km. A study by Wallace et al. (2004) showed that deformation processes in the North Island of New Zealand are complex and dominated by several North Island tectonic blocks that rotate at c. 0.5-3.8°/Ma relative to the Australian Plate; the poles of rotation (with the exception of that of the Wanganui block) relative to the Pacific Plate are centred where the thick and buoyant Chatham Rise encroaches on the margin. This complex system of rotating blocks results in convergence between the plates decreasing southward with the subduction becoming progressively more oblique beneath the North Island. Subduction no longer occurs and strike-slip motion develops along the South Island Fault systems where the Alpine Fault system dominates (Cole et al., 1995; Norris and Cooper, 2000) (fig. 1.1).

1.2.1. Taupo Volcanic Zone

The Taupo Volcanic Zone (TVZ) is the southern expression of the Tonga-Kermadec subduction system and the main locus of continental arc volcanism in the North Island, New Zealand (Cole, 1979, 1986; Gamble et al., 1993a & b; Wilson et al., 1995) (fig. 1.1). The TVZ lies within a depression that extends 250 km from White Island in the north-east to Mount Ruapehu in the south-west. Extensional faulting, vent positions and calderas define its structural boundaries (Wilson et al., 1995) and it is characterised by thin (12-15 km) continental crust and exceptionally high heat flow (Stern, 1987; Bibby et al., 1995; Hochstein, 1995). The rates of extension are about 7 mm/yr in the north and 18 mm/yr in the south, with subsidence rates of approximately 1-2 mm/yr (Cole et al., 1995).

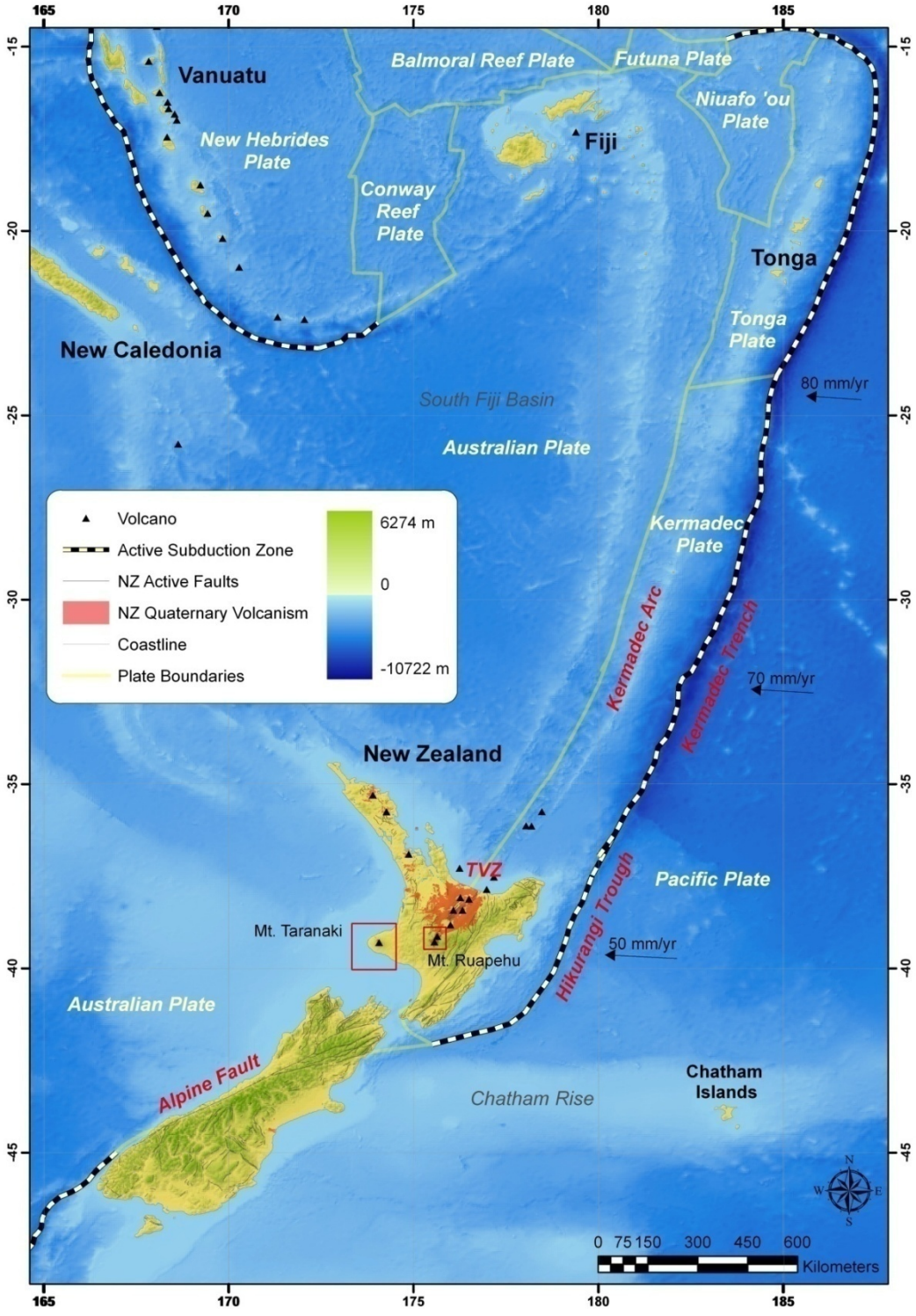

Figure 1-1. New Zealand regional setting. Map showing the Tonga-Kermadec-Hikurangi subduction system with numbers indicating convergence rates. On the South Island the plate boundary is marked by strike slip plate motion of the Alpine Fault. Plate boundaries are based on those of Bird (2003), bathymetric and elevation data is courtesy of GEODAS NOAA. Red boxes indicate the study areas of Mt. Ruapehu and Mt. Taranaki. Taupo Volcanic Zone (TVZ) is shown by the red filled area representing NZ Quaternary volcanism. Data projected in WGS 84.

Three periods of volcanic activity are used to define the TVZ (Wilson et al., 1995). Old TVZ represents activity from 2 Ma to 340 000 yrs ago; young TVZ encompasses volcanism between 340 000 to 65 000 yrs ago; and the modern TVZ; volcanic activity since 65 000 yrs. Andesitic volcanism in the TVZ is believed to have started at 2 Ma with rhyolitic activity beginning later at 1.6 Ma (Wilson et al., 1995). The TVZ from < 2 Ma is considered to be part of a migrating arc which has been active for more than 20 Ma (Stern, 1985, 1987; Cole et al., 1995). Over the past 4 Ma, the active volcanic front of this arc is thought to have migrated south-eastward at a rate of c. 20 mm/yr (Smith et al., 1989; Cole et al., 1995). Differences in age and type of volcanism throughout the TVZ may be a result of its variable and segmented nature (Wilson et al., 1995), rather than a direct relationship to the propagating southward arc. Active andesite volcanism dominates the northern and southern extremities of the TVZ (Cole et al., 1986; Houghton and Nairn, 1991; Price et al., 2005). The Tongariro Volcanic Centre (TgVC) at the southern end comprises 12 eruptive centres and four major andesitic massifs, Kakaramea, Pihanga, Tongariro, and Ruapehu, as well as a few satellite cones (Cole, 1978). Gamble et al. (2003) give a maximum age of c. 340 ka for the inception of volcanism at Ruapehu and Tongariro volcanoes.

1.2.2. Taranaki Volcanism

The Taranaki volcanic succession represents the most westerly expression of subduction-related volcanism in the North Island (Hatherton, 1969), and lies ~180 km above the westward-dipping Wadati-Benioff zone (Adams and Ware 1977; Stewart et al., 1996) and around 400 km away from the trench (fig 1.1). Recent work by Stern et al. (2006) suggests that Taranaki magmatism might not be directly related to the present day subduction system, but could instead be associated with lithospheric delamination. Sherburn and White (2005) showed that there is an area where there is no brittle deformation under Mt. Taranaki, implying low degrees of partial melting;

they also highlighted that there may be no link to the subduction system. The Taranaki Volcanic Lineament is located 130 km west of Mt. Ruapehu and is geochemically and tectonically distinct from the TVZ. The Taranaki NW-SE-trending volcanic lineament (oblique to the arc front) and related volcanism has migrated south-eastward through time with Sugar Loaf Islands (1.75 Ma), Kaitake (0.75 Ma), Pouakai (0.5 Ma) and Mt. Taranaki/Egmont (c. 0.15 Ma) (Neall, 1979). The Sugar Loaf Islands are remnant plugs and dykes while Pouakai and Kaitake are highly eroded remnants of former cones. Pouakai Volcanic activity is thought to have started at c. 670 ka and terminated with a catastrophic edifice failure producing the Maitahi debris avalanche c. 270 000 years ago (Gaylord et al., 1993; Neall, 2003). Mt. Taranaki/Egmont Volcano is the youngest and most southerly expression of volcanism along the lineament. Volcanic activity at this centre began >200 ka (Zernack, 2009) with the last known eruption occurring at either AD 1755 (Neall et al., 1986) or ~AD 1800 according to Platz (2007). The Taranaki peninsula is a near semi-circular ringplain made up of overlapping fans of volcaniclastic sediments, including debris-avalanche, debris-flow, pyroclastic flow, and fluvial deposits.

1.2.2.1. Mt. Taranaki Geology

The Taranaki peninsula represents the largest onshore region within the Taranaki Basin (King and Thrasher, 1996) (fig 1.2). The sedimentary basin sequence is built up of sand, silt- and mudstones with intercalated shell beds, and records a period of regional transgression with higher order eustatic sea-level cycles (Kamp et al., 2004) from the late Cretaceous to early Miocene, followed by a regressive phase that is still ongoing (King and Thrasher, 1996). The Taranaki Basin is cut by numerous active and inactive Quaternary faults (King, 1991; King and Thrasher, 1996). The orientation of Quaternary and active faults, which include the Inglewood and Norfolk Fault to the northeast of Mt. Taranaki, the Oaonui Fault to the south-west, and the Ararata Fault in the south-

east near Hawera (Hull and Dellow, 1993), is NE-SW. The alignment of volcanic vents provides an indicator of the more recent stress field as these tend to occur normal to the extension direction (Nakamura, 1977). The SSE migration of the Taranaki volcanoes and the N-S alignment of Mt. Taranaki summit, Fanthams Peak and several lava domes (Neall, 1971) differ significantly from the NW-SE orientation of the observed faults. The volcanic alignment and assumed stress field might therefore represent that the current situation and normal faulting in western Taranaki may be a relic of the past stress regime activated by major eruptive activity at the Taranaki volcanoes (Sherburn and White, 2006). The present geomorphology of the Taranaki peninsula is not related to its subsurface structure but was predominantly formed by Quaternary volcanism and its sedimentary products, which unconformably overlie the Tertiary basement.

Mount Taranaki/Mount Egmont (2518 m) (referred to throughout the remainder of this thesis as Mt. Taranaki) is a near symmetrical shaped andesitic stratovolcano considered to be the largest in the North Island of New Zealand (Platz, 2007; Zernack 2009) (fig 1.2). Its conical symmetry is broken by Fanthams Peak, a 1967 m high parasitic cone to the south of the crater and active over the last 7 ka (Neall et al., 1986). The earliest identified activity of Mt. Taranaki is indicated by the Motunui debris-avalanche deposit preserved in the coastal cliffs of North Taranaki, cut by the c. 127 ka Rapanui marine bench (Pillans, 1983). The characteristics and volume of the deposit imply that Mt. Taranaki was already a volcanic edifice of considerable height at that time (Zernack, 2009). The current Mt. Taranaki massif is made up of alternating layers of lavas and pyroclastic deposits that are younger than 14 ka (Neall, 1979). Mt. Taranaki lithologies range from vesicular red and black scoria through to non-vesicular to holocrystalline, porphyric lavas (Neall et al., 1986; Stewart et al., 1996). Common inclusions are fragments of older eruptives and basement or cognate rocks such as diorite, gabbro, hornblendite, and Tertiary sediments, as well as rare metamorphic and

mantle xenoliths (Price et al., 1999). Mt. Taranaki lavas are holocrystalline to hypocrystalline in thin-section with crystal contents of 25-55%. Phenocryst assemblages are dominated by plagioclase, clinopyroxene, titanomagnetite, and hornblende. The geochemical composition of Mt. Taranaki eruptives ranges from high-alumina basalt through to andesite and is dominated by high-K basaltic andesite (Price et al., 1992). K_2O abundance varies with time as magmas become progressively more K-rich with decreasing age (Zernack, 2009). The massif provides a record of predominantly cone-building events such as explosive and effusive activity. The eruptive activity over the last c. 18 ka is characterised by moderate to large sized sub-Plinian eruptions on c. 330 yr intervals, interspersed with more frequent effusive and dome-forming events (Alloway et al., 1995; Turner et al., 2008). The most recent activity is confined to the North Western sector of the massif from 600 yrs B.P., commonly termed the Maero Eruptive period which is characterised by dome-forming and dome collapse episodes and one sub-Plinian eruption in AD1655 (Burrell Lapilli eruption) (Platz et al., 2007). The last major landscape altering event at Mt. Taranaki, the Tahurangi eruption, was considered to be in AD1755 (Druce, 1966), while Platz (2007) postulates from mass flow deposits near the current crater that the last dome forming event may have occurred at ~1800 AD.

The relatively young massif has a volume of c. 12 km^3, while the apron of epiclastic and pyroclastic material surrounding the volcano makes up 150 km^3 and preserves the record of older volcanic activity especially within tephras, debris avalanche, lahar and fluvial deposits (Neall et al., 1986). This “ring plain” covers an area of c. 1000 km^2 and is nearly circular in outline. At least four debris-avalanche deposits in west and south Taranaki have been mapped (Neall 1979; Neall et al., 1986), named the Opua, Warea (the southern lobe Wr3), Pungarehu and Stratford Formations. Another three avalanche deposits (Ngaere, Okawa and Motunui Formations) were identified to the

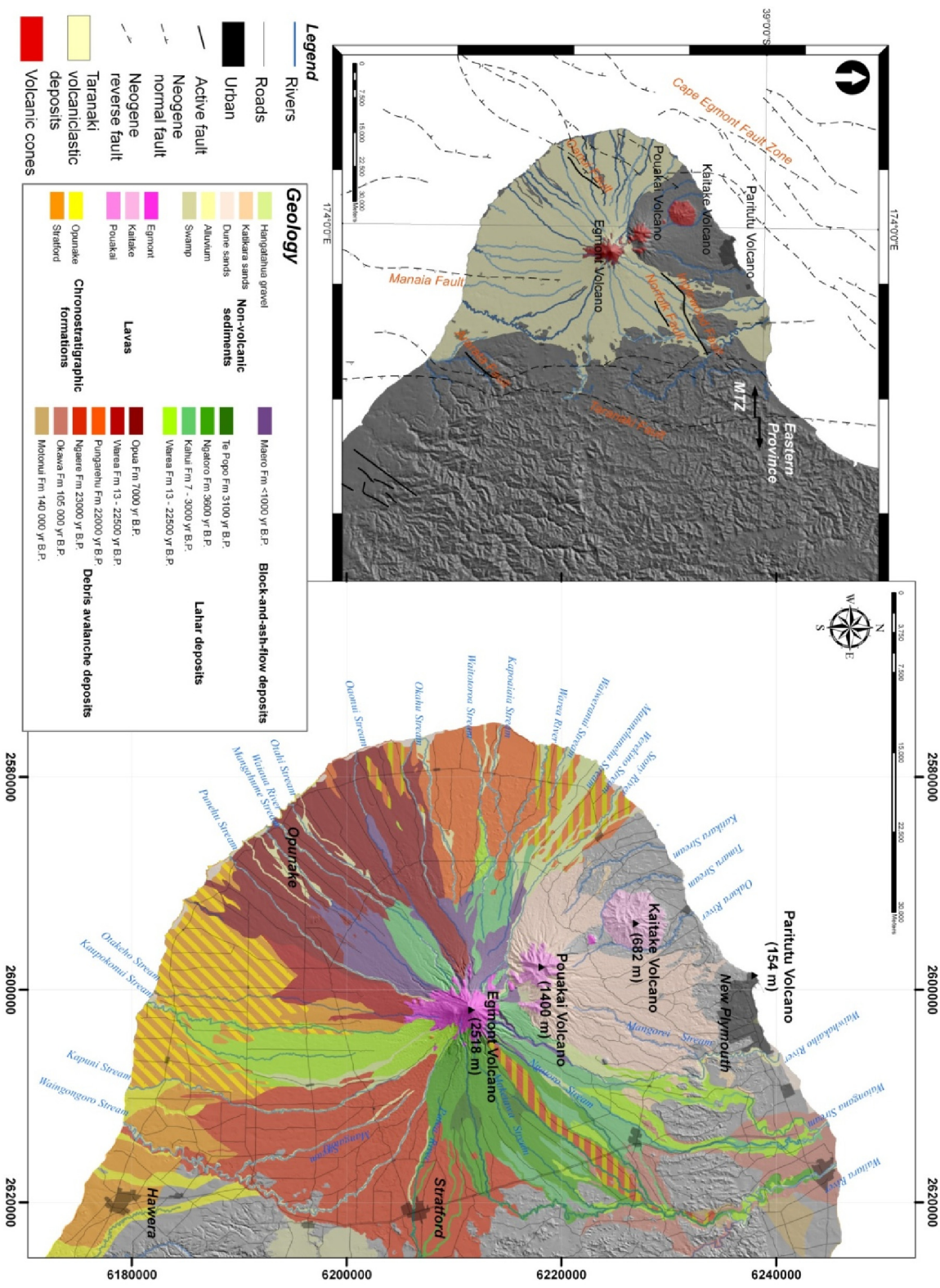

Figure 1-2. Map of the geology of Mt. Taranaki and Taranaki peninsula. Inset map showing the Taranaki region and indicative faults from Sherburn and White (2005) projected in WGS 84. Main map showing the Quaternary volcanic geology of Mt. Taranaki and its ring plain. Geology based on that of Neall and Alloway (2004) projected in NZ map grid.

north-east and south-east of the volcano by Alloway et al. (2005). The largest known edifice failure at Mt. Taranaki produced the c.20 ka Pungarehu Formation for which the calculated deposited onshore volume is c. 7.5 km^3 (Ui et al., 1986).

The debris avalanches were able to spread out on a relatively unconfined, gently dissected, ringplain to form broad fans around the volcano. The deposits form a characteristic hummocky/mound dominated landscape with a higher density of large hills along the main dispersal axes that reduce in spatial density and size laterally and with increasing distance from source (Palmer and Neall, 1991). Zernack (2009) recognised that 14 debris-avalanche deposits, together with their associated debris-flow deposits, recorded large-scale edifice-destruction events. In contrast, phases of cone growth comprised series of eruptive periods separated by intervals of quiescence. Accumulation on the ringplain during these constructional phases was dominated by lahars, i.e. debris flows and hyperconcentrated flows, and tephras.

Neall (1979) and Neall and Alloway (2004) recognise five lahar (debris flow to flood) deposits with the oldest being the Opunake Fm., followed by the Warea Fm. (22 500 – 13 000 yrs. B.P), Kahui Fm. (7 000 – 13 000 yrs. B.P.), the Ngatoro and Te Popo Fm. (3500 yrs. B.P.) and the Hangatahua Gravels (<500 yrs. flood deposits). These chrono-stratigraphic formations represent thick sequences of volcaniclastic diamictons and breccias originating from distinct catchments on the massif.

1.2.3. Mt Ruapehu Geology

The Tongariro Volcanic Centre (TgVC) consists of four main andesite stratovolcanoes, Kakaramea-Tihia, Pihanga, Tongariro and Ruapehu. The latter two stratovolcanoes are surrounded by a ring plain of similar lahar, debris avalanche, fluvial and tephra deposits. The absolute age of the start of volcanism is not known, but andesite pebbles found in the lower Pleistocene conglomerates along the Wanganui coastline have been dated at 1.7 Ma (Donoghue, 1991). The oldest lavas in the TgVC were dated by Hobden et al. (1996) at 0.27±0.2 Ma. The oldest dated lavas on Tongariro are 0.26 Ma, on Ruapehu 0.23 Ma and Kakaramea 0.22 Ma (Cole et al., 1986). TgVC lavas range between basalts and dacites (52-67% SiO_2) with most being medium-K silicic and basaltic andesites (Cole et al., 1986). The petrology of the pre- and post-50 ka eruptions is distinct, with the younger material being higher in silica and the older rocks being olivine bearing. There have been four lithofacies identified by Cole et al. (1986) and Hackett and Houghton (1989) in the TgVC of central and flank vent, proximal cone-building, distal ring-plain and satellite vents.

Mount Ruapehu is the largest composite stratovolcano in the TgVC with an estimated volume of 110 km^3 (Hackett and Houghton, 1987) (fig. 1.3). Grindley (1960) produced the first geology maps of the area; Topping (1973) compiled the first stratigraphic columns of tephra deposits; and Hackett and Houghton (1987) have provided the most recent geochemical based lithofacies stratigraphy of the massif. Hackett (1985) identified four different phases of cone building or Formations: the Whakapapa (<10 ka), Mangawhero (eastern segment, 20-29 ka), Mangawhero (southwestern segment, 37-53 ka), Wahianoa (130-147 ka) and the Te Herenga (183-205 ka) (fig. 1.3). The ring plain deposits and associated tephra deposits have been described in detail by Cronin

et al. (1996a), Cronin and Neall (1997), Donoghue et al. (1997), Lecointre et al. (1998) and Donoghue and Neall (2001). More detailed stratigraphic and geochemical investigations of smaller areas on the volcano have been made by Nakagawa et al. (1998), Nairn et al. (1998), Smith et al. (1999), and Waight et al. (1999).

Mt. Ruapehu has a large ring plain with an approximate volume of 100 km^3 (Hackett and Houghton, 1989) and is made up largely of laharic, debris avalanche, fluvial and tephra deposits. The ring plain contains a more detailed record of the eruptive history of Ruapehu than the cone itself. The southeastern ring plain was mapped in detail by Donoghue (1991). Using dated rhyolitic and andesitic tephras as marker beds above and below the lahar deposits, a chronology and stratigraphy was determined for the last 22 600 yrs. B.P. Five formations were defined: Onetapu Formation (1850 years B.P. to present), Manutahi Formation (5370-3200 years B.P.), Mangaio Formation (4600 years B.P.), Tangatu Formation (14 700-5400 years B.P.) and Te Heuheu Formation (>22 600-14 700 years B.P.) (Donoghue and Neall, 2001). The construction of the southeastern ring plain between the ages of 22 600 and 14 700 years B.P. was characterised by aggradation, with the associated eruptions of the large-scale Bullot Formation tephras (Donoghue and Neall, 2001). These deposits relate to the Mangawhero Formation phase of cone building (Donoghue and Neall, 2001). At 25 000 yrs. B.P. the ring plain and lahars drained along the Moawhango River headwaters, with the Whangaehu River draining through Waiouru and Taihape. At <14 000 years B.P., uplift occurred on the eastern block of the Desert Road Fault, forcing the Whangaehu River to drain to the southwest (Villamor et al., 2007). This also caused the ring plain to aggrade along the Whangaehu River, building a large fan during the Holocene. Present-day lahars are confined to channels along the Whangaehu Fan,

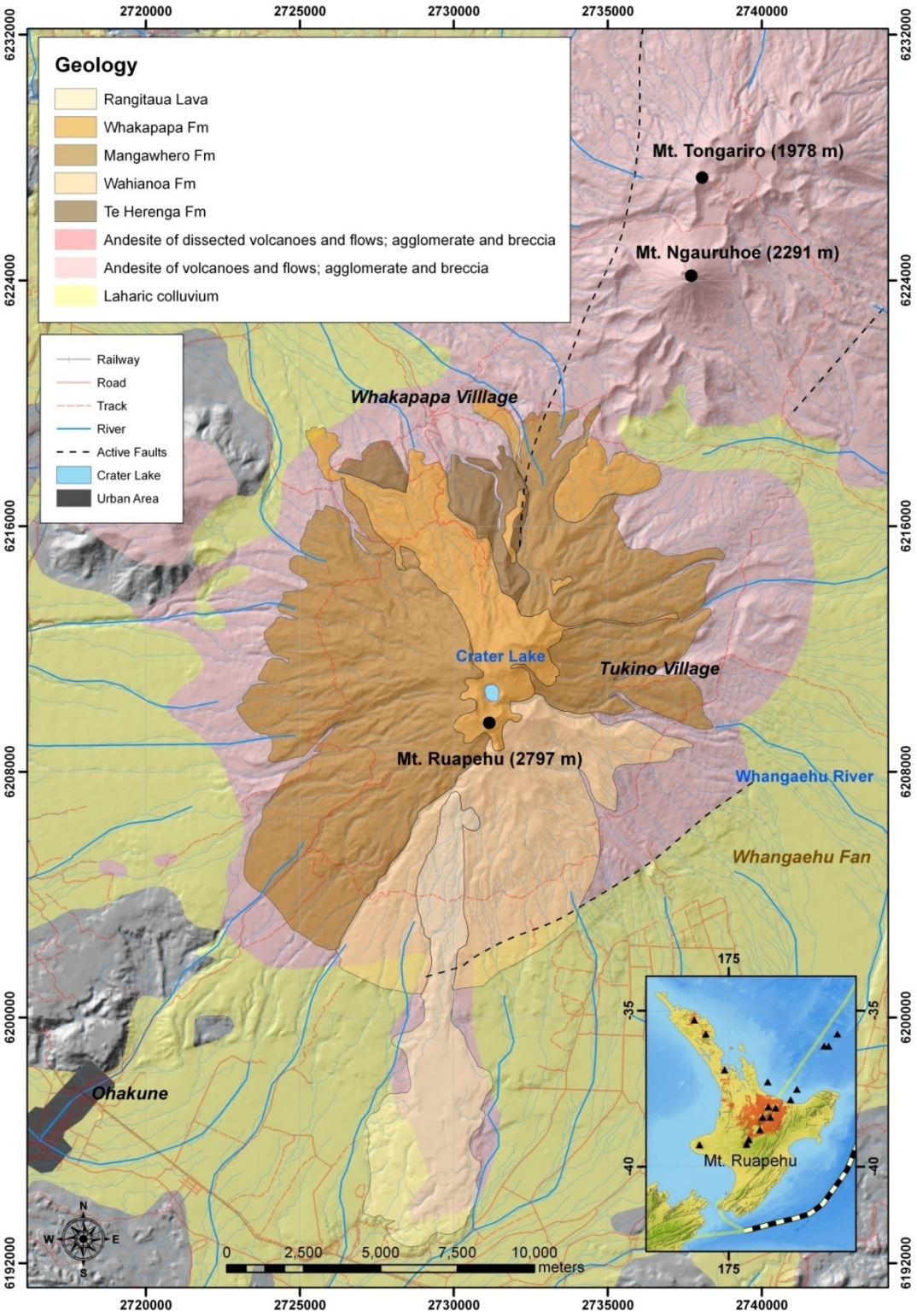

Figure 1-3. Map of the geology of Mt. Ruapehu and associated ring plain based on the geology of Hackett (1985) showing the associated geological formations of the massif and the surrounding ring plain geology. Supplied courtesy of the Institute of Geological and Science national, 1:1 000 000, geological dataset .

while other areas of the ringplain have been starved of sediment, causing incision of channels (Donoghue and Neall, 2001).

Epiclastic deposits of the northeastern ring plain of the TgVC were mapped in detail by Cronin (1996). A lahar-deposit stratigraphy for both volcanoes was created using known rhyolitic and andesitic tephras. Fifteen lahar deposition episodes were identified from >65 years B.P. to <2 ka. The most voluminous lahar deposits were produced during the cool and stormy climatic conditions of $\delta^{18}O$ stages 2 and 4 (Cronin et al., 1996a).

Hodgson (1993) describe the Onetapu Formation, which represents a sequence of at least 17 volcanic diamictons emplaced since c. 2000 yrs. B.P. by lahars along the Whangaehu River. Larger lahars were considered to be the result of collapses from walls holding summit crater lakes. Frequent smaller lahars resulted from phreatic/phreatomagmatic eruptions within the same basin as the present day Crater Lake, expelling lake waters onto the flanks of the volcano. Hodgson et al. (2007) and Cronin et al. (1997b) showed depositional evidence for many pre-historic lahars being much higher in discharges and volume than those observed over the last 100 years. The earliest historic record of a lahar in the Whangaehu catchment was in 1861 (Taylor 1861). Nineteen lahars were recorded in the Whangaehu catchment before 1995 (Hodgson 1993) and the 1995 eruptions of Ruapehu produced 26 lahars in less than 4 months (Cronin et al., 1997b).

1.3. Mass-Flow Classification and Rheology

Volcanic mass flow deposits are typically mapped and distinguished as: pyroclastic flow deposits, block-and-ash flow deposits, lahar deposits (including debris flow and hyperconcentrated flow units) or debris avalanche deposits. Volcanic mass-flows are dominantly gravity-driven (although sometimes initially accelerated by volcanic explosions), and involve rock materials as their primary solid component along with either water or gas as the fluidising component. Sediment-water mixture flows are the most common and they span a wide range of volumes, discharges, velocities, compositions, bulk rheologies, and flow hydraulics (Pierson, 1998). However, the nomenclature used to distinguish different types of volcanic mass-flows is often misleading (Pierson and Costa, 1987). The variation in nomenclature is mainly a result of the interdisciplinary study of volcanic mass-flow processes.

The classification of flows has been undertaken based on a variety of sedimentological, rheological and physical models along with theory of material behaviour (e.g. Takahashi, 1981; Costa, 1984; Costa and Williams, 1984; Johnson and Rodine, 1984; Pierson, 1986; Smith, 1986; Iverson and Denlinger, 1987; Pierson and Costa, 1987; O'Brien and Julien, 1988; Smith and Lowe, 1991; Whipple and Dunne, 1992; Coussot and Meunier, 1996; Cronin et al., 1999, 2000; Pierson, 2005b) or a mixture of all of these factors. In general flow categorisation is based on depositional models (Pierson and Scott, 1985; Smith, 1986; Rodolfo, 1989; Palmer and Neall, 1991; Smith and Lowe, 1991) or physical/rheological models (Beverage and Culbertson, 1964; Pierson, 1986; Coussot and Meunier, 1996). Additional classification factors include triggering mechanisms, sediment lithology, solids' concentration, velocity, duration, bed slope and physical processes during flow. Classifications based on flow dynamic properties

are difficult to apply to sedimentological studies (Smith, 1986) and vice versa (Coussot and Meunier, 1996). Beverage and Culbertson (1964) first categorised volcanic sediment-water flows based on solely the weight percentage of the two of sediment water components. Catergorisation of flow types based on sediments or deposits was made by Smith and Lowe (1991) (fig. 1.4) and by Scott et al. (1995) who defined the boundaries between clay-rich (cohesive lahars) and clay-poor (non-cohesive lahars) also providing more of a gradational spectrum of flow types (fig. 1.4). Pierson and Costa (1987) provided a classification (fig. 1.4) based more on the rheology of the flow and its constitutive components. This was further extended by Cronin et al. (2000) (fig. 1.4) attempting to conceptualise the flow as a wave with variety of processes producing spatially and temporally related deposits. Coussot and Meunir (1996) also provide a model based more on viscoplastic concepts of flow also being gradational from granular flows to Newtonian flows (fig. 1.4).

Observations of lahar flows in motion provide the basis of many depositional models by Pierson and Scott (1985) from the 1982 Mt. St. Helens lahars. They showed sediment concentration and rheology gradients through their length. They recorded 78 wt.% (57 vol.%) sediment at the head of the flow and 61 wt.% (37 vol.%) at the tail. The deposits included a debris flow portion which showed an extremely wide range in grain size (clay to gravel), very poor sorting, lack of cross-stratification, matrix-support, common inverse grading (coarsening upward) near bottom and normal grading (fining upward) near the top. The following hyperconcentrated flow phase was characterised by depositing a coarse sandy, clast-supported unit with poor sorting, faint horizontal stratification, and isolated lenses of gravel and pumice clasts. Cronin et al. (2000) observed a similar pattern of deposition at Mt. Ruapehu but dip samples showed a vertical flow stratification also existed, with a basal, mostly channel-confined, coarse,

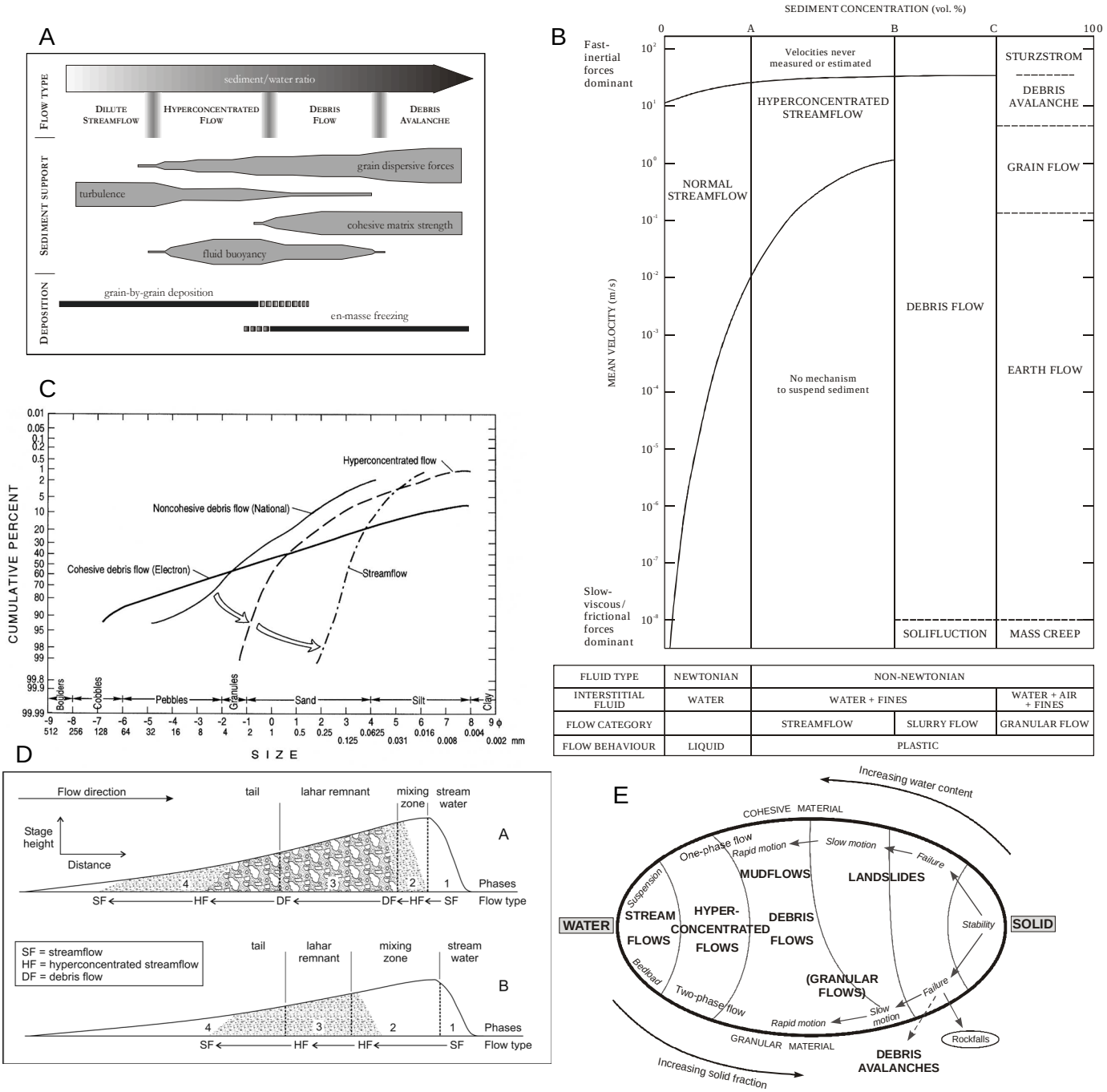

FLUID TYPE	NEWTONIAN	NON-NEWTONIAN		
INTERSTITIAL FLUID	WATER	WATER + FINES		WATER + AIR + FINES
FLOW CATEGORY		STREAMFLOW	SLURRY FLOW	GRANULAR FLOW
FLOW BEHAVIOUR	LIQUID	PLASTIC		

Figure 1-4. Concepts and categorisation of flow based on sedimentological or rheological criteria. A) Schematic illustration of sediment/water ratio, corresponding flow type, transport and depositional mechanisms (from Smith and Lowe 1991); B) rheologic classification of sediment-water flows from Pierson and Costa (1987); C) Cronin et al. (2000) concept of a lahar flow showing the transition of a debris flow to hyperconcentrated flow and related deposits through the passage of the event; D) cumulative curves of particle sizes in a typical cohesive lahar (Electron Mudflow) and non-cohesive lahar (National Lahar) of Mt.Rainier, USA. Downstream transitions occur from debris flows to hyperconcentrated flows; E) Classification of solid-water mixtures from Coussot and Meunier (1996).

sediment-concentrated portion of flow and an overlying dilute and finer grained portion with hyperconcentrated flow properties.

One of the most recognised sedimentological categorisations of volcanic mass flows follows that of Smith (1986), who interprets depositional features to classify flows ranging from fully turbulent, dilute stream flow through to viscous, laminar debris flow. In general normal stream flow deposits are characterised by laminar to cross bedded sands and gravels that are well sorted and exhibit imbrication. Debris flow deposits are characterised by poor sorting, a large range in clast sizes, a lack of stratification and clast imbrication and occasionally coarse-tail reverse grading. Hyperconcentrated flows are recognised as exhibiting characteristics of both end member types, with poor sorting and weak or incipient horizontal fabric or bedding. Methods of emplacement range from rapid grain by grain aggradation from the base of flows, or in some cases *en masse* stalling of flows (Smith and Lowe, 1991).

Physical models extend these flow observations to classify volcanic mass flows based on flow dynamics as well as the mechanical properties of the solid components and the fluid. Typical theoretical flow models include Bingham or viscoplastic fluids with uniform intrinsic shear strengths (Pierson, 1980; Major and Voight, 1986; Coussot and Proust, 1996; White, 2006). Major (1993) highlighted that viscosity increases with increasing sediment concentration and especially increasing clay fraction. These results drew attention to the collisional grain flow theory of the Bagnold model, according to which flow only occurs if gravitational driving forces overcome grain-collision stresses (Bagnold, 1954; Lowe, 1979; Major and Iverson, 1999; Vallance, 2000). Pierson and Costa (1987) developed a classification of sediment-water mixtures based on thresholds in rheologic behaviour according to deformation rate (mean flow velocity)

and sediment concentration, with a constant composition of components. Major and Pierson (1990, 1992) highlighted through experiments that sand content affected the yield strength and viscosity of the flow more than gravel fraction. It is also important to note that granular flow begins when the sediment concentration increases to the point where the mass loses the ability to liquefy and the bulk behaviour is dominated by friction and grain collisions. The importance of pore water pressure in the rheology of flows, grain transport and deposition was recognised through experiments by Major and Iverson (1999) and support Iverson's (1997a, 1997b) theories of mass flow movement occurring only when the fluid pressure within the flow is high enough to liquefy the debris and that deposition occurs when frictional stresses at the margins and flow front become too great.

1.3.1. Transitions between Depositional and Rheological Categories

The transition between differing flow rheologies and fluid mechanical properties has been highlighted by Scott (1988a), noting a major difference in properties occurs between non-cohesive (1-4% clay) and cohesive (>4% clay) debris flows. Scott et al. (2001) demonstrated transformation from debris avalanche to debris flows with the resulting debris flows typically being cohesive. Pierson and Scott (1985) and Cronin et al. (1999, 2000) examined the common transitions in non-cohesive lahars, with flow varying between debris flow to hyperconcentrated flow and streamflow. In general all of these transformations rely on either the incorporation of water or rock fragments from erosion/entrainment of sediment or water along the flow path, or the loss of material and water through deposition. These processes have been examined in part through experimental studies of small-scale, non-cohesive debris flows that show behaviour similar to natural flows (Major 1997). Depositional processes and deposit

morphology were strongly dependent on the water content of the source material and deposits developed by incremental vertical rather than horizontal accretion from shallow, successively overlapping surges. Some horizontal accretion also occurred in flow termination areas with later surges within unsteady flows locally pushing into and shouldering aside sediment, to override or lap against earlier deposited debris. Iverson (1997a, 1997b) explain that this process is due to the centre of the flow becoming more liquefied by concentrating pore water, leading to it becoming more mobile.

The process of incorporating material or water into moving flows (often termed bulking) is poorly understood, along with its impacts on flow rheology. Transformation in rheology has been observed from flows bulking up in sediment mass (Cronin et al., 1999, 2000). However, the nature of this transformation is complex and non-uniform, noting the common observation that non-cohesive lahars typically comprise a bedload region with high sediment concentration, subdivided into a lower collisional grain-flow zone and an upper saltation zone, with an overlying more dilute and finer-grained turbulent flow (Pierson, 2005b). This means that one flow can produce a range of deposition types at different locations or different times during its passage.

Repeated transformation between flow rheologies may also occur in non-cohesive lahars (Procter et al., 2009). This is often driven by low-sediment concentration flows being excellent at scouring and incorporating sediment along their path, which can then be consequently lost on sudden gradient changes. For example, at Mt. Pinatubo turbulent hyperconcentrated flows were more effective than debris flows at eroding banks and channels (Scott et al., 1996).

1.4. Numerical Modelling

Numerical characterisation of sediment-water mass flows comprise physical models of Newtonian flow (both laminar and turbulent), Bingham flow or dilatent-grain shearing flow with the models differentiated by the dominant flow mechanism, such as viscous deformation, friction or collision. A wide range of flow models and classifications reflect the large variety of processes within the water-sediment flow spectrum that are obviously gradational (Pierson and Costa, 1987), or may co-exist in a single flow at a single point in time (Cronin et al., 2000). With numerical mass flow characterisation, most grain-water flows are treated as homogenous and variably liquefied Coulomb grain flows in which pore-fluid pressure controls inter-granular friction and the degree of liquefaction (Iverson, 1997a, 1997b; Major and Iverson, 1999; Iverson and Denlinger, 2001).

Newtonian models usually apply Mannings (O'Brien et al., 1993), St. Venant (Carrivick, 2007), Navier-Stokes and Reynolds-averaged Navier-Stokes equations (Hluchy et al., 2002) to simulate a fluid along a channel (Acheson, 1990). These relationships account for shear stress and viscosity but do not factor in the effects of particles within a flow. For volcanic mass flow modelling, these approaches have been used to form a range of empirical models that relate to peak discharge and debris flow volume (e.g. Takahashi, 1981; Rickenmann, 1994).

Hungr (1995) divided grain flow modelling into two main categories, either (1) lumped mass models that idealise the sliding body as a single point and are unable to account for internal deformation, or (2) continuum models based on rheological formulae (e.g.

Newtonian, Bingham, Coulomb etc). Continuum numerical mass flow models have developed from describing two major non-dimensional regimes using either the Bagnold number, or the Savage number (Bagnold, 1954). The Bagnold number approach describes the interstitial fluid and the interaction of particles, particle density, packing, strain rate and viscosity of fluid; this results in the classification of flow as being either macroviscous or inertial. The Savage number focuses on the transfer of momentum between particles and the interparticle friction that develops. Flows are either in a collisional or frictional regime. The modelling of granular flows has hence focused on determination of Mohr-Coulomb stresses acting on piles of grains.

Volcanic mass flows encompass a range of particle-water and particle-gas flows (the latter known as pyroclastic flows and pyroclastic density currents). The latter flows, with a compressible phase (gas) have highly distinctive properties meaning that models to describe thier behaviour have evolved and diverged from traditional granular flow models such as that of Bagnold (1954). Pyroclastic density currents are generated from either a collapsing pyroclastic eruption column containing vesicular primary clasts, lithics and hot gas, or small examples may also be generated from the collapse of lava dome. The resulting gound-hugging flows can range in temperature up to 900°C and travel with speeds of 10-100's m/s resulting in runout distances of just a few km (Merapi, Indonesia) to beyond 50 km (Taupo, N.Z.), producing deposits with volumes ranging from 1 km^3 (e.g. Mt. St. Helens, U.S.A.) to 1000 km3 (e.g. Long Valley, California, U.S.A.) (Fisher & Schmincke, 1984). The flow rheology and fluidisation is typically strongly controlled by (hot) interstitial gas. These complex thermodynamic flows hence are generally is comprised of a dense (particle rich) basal region where the majority of the mass is transported, overridden by a more dilute particle-poor zone, Wilson, 1986).

The difficulty of sampling or measureing pyroclastic density currentsduring flow or deposition (due to the extreme danger posed by them) has lead to a range of interpretations and models of flow and depositional mechanisms derived from deposit sedimentology. The most widely accepted models assume that these are relatively dilute and turbulent flows that deposit incrementally, frictionally controlling runout from the rate of sedimentation (Fisher, 1966; Druitt, 1998). Sparks (1976) interpreted that small-volume, high-concentration flows travel in a laminar fashion and deposit by en-masse freezing rather than layer-by-layer accretion, which is similar to granular flow concepts (Savage & Hutter, 1989). Developments of these concepts have led to the progressive aggradation models of Branney and Kokelaar (1992) and Palladino & Valentines' (1995) model of emplacement through the kinetic energy loss from grain shearing.

In the absence of quantitatively characterising transport and emplacement mechanisms, they are inferred by applying sedimentological models derived from other depositional systems (e.g. water-particulate flows). Many of these interpretations (Sparks et al., 1973; Walker & Wilson, 1983) have identified both a separate "*dilute*" and "*dense*" flow system yet it is difficult to determine the interaction and transfer of both energy (and gas/particles) between these two phases. Numerical attempts, such as those by Doyle et al. (2008) provide some insights into the physical conditions of this process controlling the overall rheology of pyroclastic flows.

Highly energetic and large volume pyroclastic flows are uncommon in the stratigraphic record of many andesitic stratovolcanoes such as Mt. Taranaki and Mt. Ruapehu. The

most common pyroclastic flow units are the lava dome-sourced, block- and ash-flow deposits, at the lowest end of the mobility spectrum for pyroclastid density currents. These are further discussed in Chapter 6.

Savage and Hutter (1989) produced a set of equations of motion for a translating and deforming granular mass based on a Coulomb frictional resistance term. They balanced equations for mass and momentum and, making scaled arguments, developed a 1D model system similar to shallow water equations (c.f., Pitman et al., 2003). Iverson (1997b) extended the Savage and Hutter (1989) model to include the effects of pore fluid. Patra et al. (2005) combined models from Iverson and Denlinger (2001) and Pitman et al. (2003) using a finite-volume with a Gudunov solver, a conservative numerical scheme, to develop a system of local mesh refinement to simulate a mass flow. In relation to volcanic mass flows these simulations are limited by narrow range of friction parameters, thermodynamics, stress inhomogenity and compressibility, and erosion or the inclusion of additional material (Bursik et al., 2005). More recent models to account for many features of volcanic flows, such as clast break-up and erosion need to model discrete particles rather than continuum approaches (Bursik et al., 2005).

1.5. Computer Flow Simulations and Applications

Recent advances in computing power and graphical computer interfaces have allowed a user to both apply numerical models and develop hazard analyses with ease. In combination with Geographic Information Systems (GIS) and remotely sensed data,

the outputs of numerical simulations can be also easily and convincingly communicated to decision makers in a manner that requires little knowledge of either the hazard or numerical simulation. This may also present significant risk if a simulation tool is applied and treated as “black-box” by users with little knowledge of how the model works and under what conditions its results can be trusted. Intensive validation and testing of models are hence required under a range of conditions and applications.

Numerical simulation and characterisation of mass flows is either based on determining empirical relationships identified from experiments and flow observations (Rickenmann, 1995), or by comparing physics-based flow models to experimental or natural examples of flows (Denlinger and Iverson, 2001). Computer models of flow hazards can be one to three dimensional, with the latter producing the most visually useful outputs for educational purposes. All models attempt to simulate a flow of water (or any mass) from a discrete point to the next, or to reproduce several flow parameters across a complex natural terrain. The complexity of a numerical model increases as more physical characteristics are parameterised and included. Complexity and computational demand also strongly increases with the detail and resolution of the terrain representation over which the model runs, ranging from a simple series of cross-sections to a detailed sub-metre digital elevation model (DEM).

A 1D modelling methodology assumes one dominant spatial dimension with flow aligned to the centre of a channel that is represented as a series of cross-sections. Flow/water level is forecast from one cross-section to the next downstream. Generally a discharge model or set of St. Venant equations is propagated downstream, conserving the volume. Factors such as frictional resistance to the bed are usually

accounted for in the equations. The flow can only propagate in one direction and excess volume is considered to spill out of the channel into surrounding areas. The resulting data of volume and water levels at user defined points is usually extrapolated onto two dimensional cartographic displays. Typically the data is most useful in specific localised hazard analysis studies of infrastructure (e.g. Hancox et al. 1998). Examples of these types of models range from the statistical based LAHARZ (Schilling, 1998), to tools based on hydrological theory ArcGIS HYDRO (ESRI, 2007), HEC RAS (USA Army Core of Engineers) or Mike 11 (DHI).

Volcanic flow models such as that of the energy line/cone concept of Malin and Sheridan (1982) and the sliding block model, flow3D of Sheridan and Kover (1996) provide simulations that model solid flows in a similar fashion to 1D hydrological tools, with data represented on a three dimensional terrain by aggregating data from multiple flow runs with varying properties and starting locations. These models have been commonly used for volcanic hazard analyses and can be modified to account for contrasting flow rheologies, from Newtonian to granular flow and sliding solid masses.

Two-dimensional modelling techniques are also frequently applied to achieve more realistic outputs that can be related to natural landscapes. In these, vertical variations in flow properties such as sediment concentration, rheology, friction, viscosity etc., are summarised as vertically averaged values (O'Brien et al., 1993). This is a mathematical convenience that allows more ready solving of complex mathematical relationships for any type of flow. The principle is justified by the fact that the vertical depth component of any mass flow is typically miniscule in comparison to the dimensions of overall width and length. Hence, 2D models generally involve the solving of shallow water equations to predict flow levels and depth-averaged velocities. The models are

solved under a variety of numerical methods (e.g. finite element or finite volume), over differing representations of terrain/grid (e.g. Cartesian, structured or unstructured) (Pender and Neelz, 2007). 2D simulations are usually propagated across a raster-based terrain model or DEM and do not require a specific direction or channel to be identified. Computing power is often the greatest limiting factor to the resolution at which calculations and simulations are made, with the simplest case involving calculations made in every cell of a grid at every time step, even if simulated mass is not present in the majority of cells. To make computing more efficient, analysis of the DEM is usually applied to extract specific computational grids with high detail for catchments or channels (e.g. Carrivick et al., 2009). Examples of typical 2D hydrological flow models that have some capacity for handling sediment-laden floods include LISFLOOD (Bates and De Roo, 2000), TUFLOW (TUFLOW modelling software), MIKE 21 (DHI) and Delft 3D (Delft Inc). These models do not account for sediment concentration, yet models such as Flo-2D (Flo-2D Software Ltd.) do usually account for sediment by the incorporation and adaption of a Bingham flow.

The numerical simulation of pyroclastic flows has required a different approach that has either attempted to characterise the dilute gaseous (upper) phase or flow type, or the dense lithic rich basal component of the flow. The dilute gaseous part of flow is typically modelled using a multiphase approach, where the ash particles are contained in suspension and propagated mathematically utilising a generalised version of the Navier-Stokes equations (Todesco et al ., 2002; Neri & Dobran, 1994).

At the other end of the spectrum the simplest of models assumed the granular flow to move as a single mass or sliding block, which implies flows have a constant viscosity and yield strength. To account for more complex frictional regimes, a Mohr-Coulomb

model adaption was applied by Savage and Hutter (1989). Other simulations tend towards applying bulk continuum models, thus treating the entire phenomena is a single (fluid) phase (Denglinger, 1987; Takahashi & Tsujimoto, 2000). These models simulate grain flows separated by intergranular dispersive pressure in a frictional regime (Denglinger, 1987). This was widely applied to represent a number of mass flows of low volume with travel distances unexplained by Mohr-Coulomb models. Recent continuum descriptions of flows in a depth-averaged, shallow-water framework have been applied by Denglinger and Iverson (2001) by adding in Coulomb frictional resistance.

Continuum models are however limited by the physical generalisations made of the entire flow and by not accounting for the compressibility of a gas phase in pyroclastic density currents as well as any additional fluidisation generated by heating and release of magmatic gas, thus changing friction. Moreover the inability to account for depositional mechanisms and changes in mass during flow does provide some limitations. More recent models such as that of Doyle et al. (2007) can account for two phases (granular and gaseous) and assumptions for the transfer of mass between them. Alternative developments are based on discrete element models of individual particular interaction which are also proving to be applicable to pyroclastic and mass flows (Bursik et al., 2005), providing large scale computing resources are available.

The common factor that all flow models rely upon is a digital representation of the natural terrain. These can be determined from traditional surveying methods utilising GPS or from remotely sensed data such as stereo-orthophotography, LiDAR, or satellite radar. All methods collect the coordinates and height values of single points that must be interpolated into a digital terrain model or DEM. Methods to create raster or grid-

based terrain representations are many, the most reliable including triangulation of points and calculation of heights between points (or groups of points) from splines. DEM interpolation methods can be optimised for specific purposes, with the main aim for their use in flow modelling being to produce "hydrologically correct" representations of landscape (i.e., ensuring drainage networks are realistic) (Stevens et al., 2003). 1D models typically utilise cross-sections and the outputs are then locally extrapolated across a DEM. 2D models typically resample a DEM to simplify the terrain to save on computational power and time or sub-divide a catchment into smaller, more manageable sections, transferring the final outputs from the previous sections as starting criteria for the next section. More complex models use the full resolution of a DEM, but require large computing resources as in the case of Titan2D. For the purpose of this PhD study the DEMs used were created originally from stereo-orthophotography (resulting in vector-based spot heights and contours) and either represented as triangular irregular networks (TIN) or as a raster based interpolated grid (fig. 1.5).

1.6. The Titan2D group of codes

The original Titan2D model and its ongoing derivatives were developed by the Geophysical Mass Flow Group at the State University of New York at Buffalo. The model is designed for simulating mass flows by combining Coulomb numerical representations of granular flows with digital models of natural terrain (Pitman et al., 2003). Later models in the series can combine a viscous fluid component in varying proportions (Pitman and Le, 2005). The approach is 2D, based on a "depth-averaged" or "thin-layer" continuum solution of the conservation equations of mass and momentum for an incompressible mass (Pitman et al., 2003).

To increase processing efficiency and optimise the use of high-resolution DEMs, an "adaptive gridding" method and parallel processing has been incorporated into Titan2D (Patra et al., 2005). The adaptive grid process allows for the DEM to be dynamically sampled and resampled enabling the computational grid to be refined to capture the simulated flow features at a higher resolution as the flow evolves (Patra et al., 2005). This method also allows for better utilisation of a parallel computer network by dividing the DEM up and simulating grids over different machines.

The modelling approach has been to minimise the number of user-definable parameters to include only factors such as: initial pile volume and dimensions (refer to Appendix 1. Titan2D User Guide); starting location; internal angle of bed friction of the mass; basal friction between the mass and terrain (which can be varied by using a surface roughness map); solid/fluid fraction for two-phase flows; and a basal topography in the form of a DEM. Outputs of the simulation include flow run-out, flow inundation area, velocity and flow depth at any time-step. Stopping criteria for the simulations must be defined by numbers of computational steps, simulated time, or limit of grid. The model outputs at each time-step can be animated or individually exported into GIS for analysis.

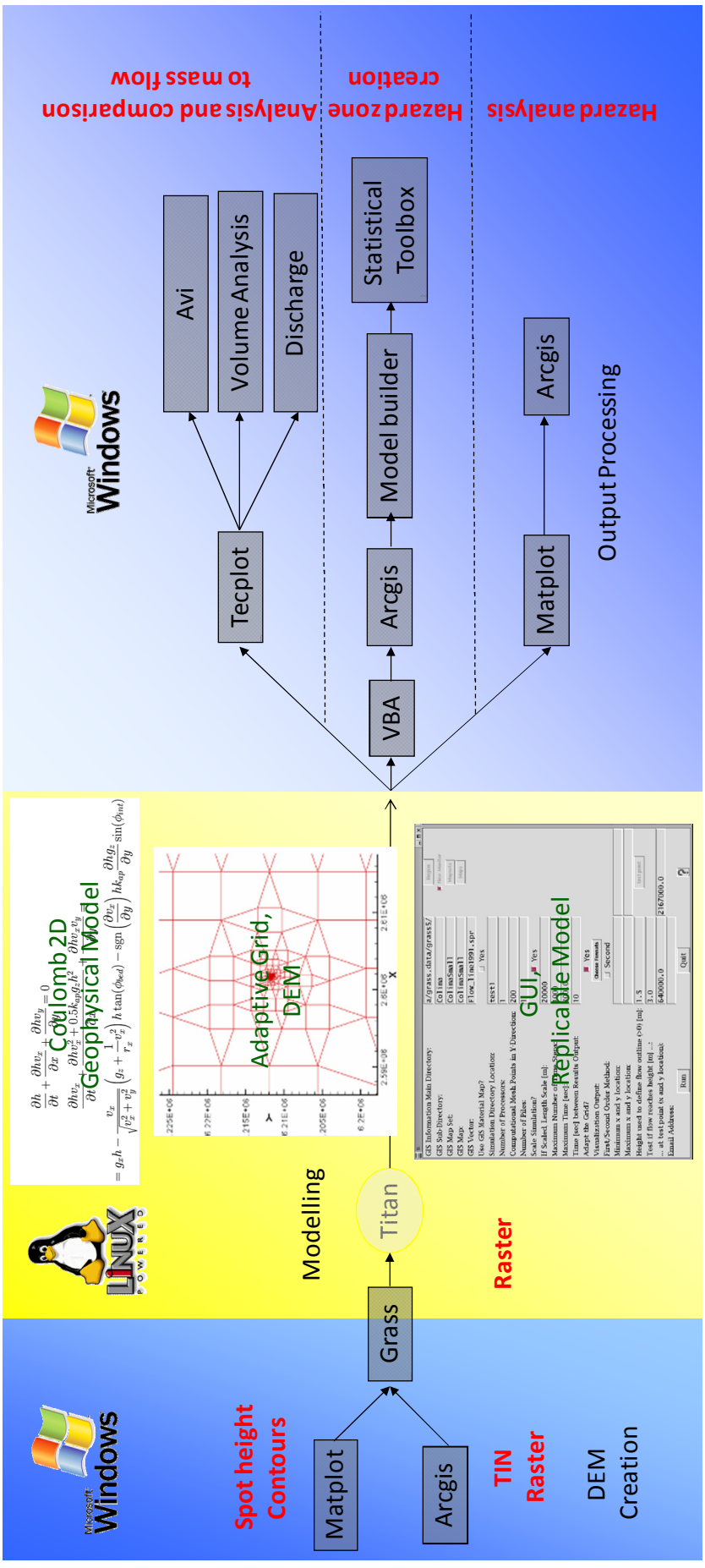
Hazard analysis
Hazard zone creation
Analysis and comparison to mass flow
Output Processing
Avi
Volume Analysis
Discharge
Statistical Toolbox
Model builder
Arcgis
Tecplot
Arcgis
Matplot
VBA
Windows
Coulomb 2D
Geophysical Model
Adaptive Grid, DEM
GUI, Replicable Model
Modelling
Titan
Grass
Raster
Matplot
Arcgis
Spot height Contours
TIN
Raster
DEM Creation
Windows
LINUX

Figure 1-5. (Previous page) Simplified flow chart of the software used and GIS processing of data for the Titan2D toolkit to undertake and produce hazard analyses for this study.

Titan2D allows a user to define a limited (low) number of input parameters in comparison to most other flow simulation models. While some of the modelling inputs such as starting pile position and its volume can be well based on natural real world data and measurements, the other main parameters of internal and basal friction cannot simply be derived from real world measurements. In theory and experimental situations they have been compared to and extrapolated from the angles inducing collapse of granular material from tilt-tables and the angles defined from analogue experimental flows (Iverson, 1997a). However, in general the selection of basal and internal friction angles/values has no fixed method and the parameters are typically tuned to the situation (primarily depending on the type of flow being examined, the slopes and length scales analysed and the potential for transformation of flow conditions and rheology along its path). The studies reported in this thesis has dealt with the issue of defining these modelling parameters by applying a range of different combinations loosely based on known ranges from published experimental studies. Final selections were based on modelling experimentation, comparison of outputs to past events, and systematic testing using basic statistical methods.

In conjunction with selection of inputs, the comparison of outputs to real world events lacks a standard methodology mostly because different workers are interested in simulating differing aspects of the mass flow hazard events (e.g. some are interested in travel times, while others may focus on inundation areas, inundation depths or flow velocities). Sheridan et al. (2005) provided a basic method of analysing the comparison of outputs to a real-world flow using the measure of whether the flow was in the (past event) inundation area or not. For the studies contained in this thesis,

outputs are compared to past event inundation areas, as well as a range of other measured parameters from known events, such as discharge, velocity, and travel times. The work of Dalbey et al. (2008) partly bridged the gap between real world parameters and optimisation of simulation input parameters, however the complex mathematics of multi-parameter optimisation in relation to models has not been included in the Titan2D tool kit yet, due to its additional numerical and programming complexities. The implementation and application of the model is described more fully in Appendix 1 containing the user guide of toolkit.

1.7. Hazard Mapping

Volcanic hazard assessment, and especially its mapping or zonation, remains a common goal at many volcanoes to the present day. One of the earliest cartographic representations of volcanic hazards was produced by the Volcanological Division of the Geological Survey of Indonesia in 1920 in response to eruptions at the volcanoes of Kelud, Merapi, Semeru, and Kawah Ijen on Java, as well as volcanoes on Sumatra, Flores, and other islands (noted in Crandell et al., 1984).

A modern standardised programme for the creation of hazard maps was established in the USA by the United States Geological Survey in 1967 (Crandell et al., 1984). The focus of this programme was the derivation from geological information of hazard-zonation maps, primarily describing relative levels of mass-flow hazards for each of Mt. Rainier (Crandell, 1973), Mt. Baker (Hyde and Crandell, 1978), Mount St. Helens (Crandell and Mullineaux, 1978), Mt. Hood (Crandell, 1980), and Mt. Shasta (Miller, 1980), as well as for the islands of Hawaii and Oahu in the State of Hawaii (Mullineaux and Peterson, 1974; Crandell, 1975). In addition, a hazard-zonation map specifically for

ashfall hazards was created for the western continental U.S. Following the eruption of Mt. St. Helens, where hazard maps formed an integral part of the volcano hazard management, this hazard mapping programme has grown to include other volcanoes as well as update the underlying stratigraphic information of existing hazard analysis such as at Mt. Adams (Scott et al. 1995), Mt. Baker (Gardner et al., 1995), Glacier Peak (Waitt et al., 1995), Mt. Rainier (Hoblitt et al., 1995) and Mount St. Helens (Wolfe and Pierson, 1995). These mapping approaches were converted by Schilling (1996) into a Geographic Information System (GIS) format, producing data sets that represent the hazard information from the assessments of the above volcanoes, incorporating both flow and ashfall hazard. The ongoing creation and promotion of these maps, along with the more recent production of digital GIS datasets and free access to this information is an important step in the greater uptake and use of hazards information for general public education as well as rural and urban planning.

The methods applied for all of the above-listed hazard maps were described by Crandell et al. (1984). These included: (1) field geological study to identify the types, scales, inundation areas and properties of volcanic and volcano-sedimentary events that have occurred at a volcano (2) recurrence intervals of these various types and scales of events based on stratigraphy and dating of deposits.

Volcanic hazard analysis in New Zealand, like in many countries, was re-prioritised and standardised after the 1980 Mount St. Helens eruptions. However, presently in New Zealand there seems to be a divergence of “general prediction” and “specific prediction” methods with very little interaction between the two. The main public hazard information on NZ volcanoes is encapsulated in a series of booklets, produced by the Volcanic Hazards Working Group of the Civil Defence Scientific Advisory

Committee (e.g. Neall et al., 1999), that cover seven volcanic areas and contain maps of individual volcanic hazards at a regional scale. The maps contained are very simplistic for ease of public understanding, but they provide little information and contain only a single or small number of zones. Frequency estimates are based on historic events in each of the landscapes. For some regions, further hazard mapping has been published, albeit less widely.

1.8. New Hazard vs. Risk

The concepts of hazard and risk, although used by lay-persons interchangeably, have quite distinct meanings. A natural hazard is defined by Burton et al. (1978) as "those elements of the physical environment, harmful to man and caused by forces extraneous to him." A volcanic event (eruption, lahar, etc.) is a natural phenomenon and is not a hazard until it affects humans, their activities or assets that they value. The impacts of a volcanic event are hence natural (geo) hazards. This definition led UNESCO (Varnes, 1984) to define a natural hazard as the probability of occurrence of a potentially damaging phenomenon within a specified period of time and within a given area. The susceptibility of a community to such hazard phenomena is often termed termed its “vulnerability”.

The concept of risk in association with natural hazardous phenomena is to encapsulate the magnitude of potential loss that could result from their impact on communities, such as expected number of fatalities, injuries, damage to property and disruption of

economic activity. UNESCO (1980) attempted to clarify the terminology used within natural hazard management in the following terms;

- Vulnerability; including identification of the magnitude of the event and specific features of the hazardous phenomena that impact upon the degree of loss potentially faced by a community,
- Value or Elements at risk; which includes possible infrastructure affected within a given area,
- Specific risk; expected degree of loss as a function of hazard, Value and vulnerability.

Volcanic risk assessments typical involve identifying the spatial extent of a range of hazardous events from geological mapping and then determining the frequency that each of these event-types and scales has occurred. Volcanic risk assessment usually entails identifying attributes of the population and its supporting infrastructure as well as specific features of the community that enhance its vulnerability or promote its resilience (including a range of factors from infrastructure quality, through to state of preparedness and past recent experience of similar events) (e.g., Magill & Blong, 2005). Magill and Blong (2005) also define volcanic risk quantitatively as;

Risk = likelihood x extent x effect,

and to include the total range of hazard types based on their probabilities as;

Risk = likelihood x extent x effect x probability (of event) x importance.

This allows for the hazards from multiple events and outcomes to be assessed and compared.

Overall the scope of this thesis concentrates on the realm of hazard and hazard forecasting, which then forms the foundations for later extended studies for risk assessment.

1.9. Research Objectives

Mass flows from high-elevation, steep and snow-covered volcanoes such as Mts. Taranaki, Ruapehu and Tongariro are the most common and potentially most deadly volcanic hazards faced by the surrounding communities. These include a variety of sediment-water or pyroclastic-gas mixtures, including: pyroclastic flows and block and ash flows (from collapse of volcanic plumes or domes); lahars (water-borne debris flows to hyperconcentrated flows), and debris avalanches (large-volume landslides caused by collapse of a sector of the volcanic edifice). New developments in computing, and growing understanding of the physical processes operating within this variety of mass flows, are leading the way toward numerical simulations of these events. Several models using different physical theories and numerical models have been developed, but few of these have ever been used as the cornerstone of real-world hazard mapping, nor within emergency management planning in association with volcanic crises. Evaluation and validation of the most promising of these models is required to confirm the conditions under which they can be relied upon for hazard analysis. For this, real-world data and examples are needed for calibration and testing. This project will aim to test the Titan2D mass flow model and examine the conditions under which it is useful for hazard analysis and geological event reconstruction.

Mass flow examples and data are readily available for a range of flow types from both Taranaki and Ruapehu. The tests of the Titan2D toolkit focus on a range of features including: its reliability for varying types and scales of flows; the parameter sensitivity; how it can be used to develop probabilistic hazard GIS layers; and its use for reconstructing processes occurring in past mass flow events. These simulation studies are to identify the most important predictive data that can be collected from the field to constrain models for assessment of pyroclastic flow, rock fall, lahar and debris

avalanche hazard from our major andesitic stratovolcanoes. Once the most reliable modelling approach is identified for each hazard type, this study will demonstrate how individual simulations can be used for developing probabilistic hazard layers and appropriate visualisation and volcanic risk communication strategies for improving the awareness and uptake of volcanic risk management by communities surrounding the two volcanoes.

1.10. Methods of Research

The research comprised the completion of the following tasks to determine methods for volcanic risk analysis;

1. Analysis of flow parameters from Ruapehu and Taranaki.
2. Mapping specific mass flow deposits for parameter collection.
3. DEM generation and evaluation.
4. Titan2D model testing with Taranaki/Ruapehu lahar data and comparisons.
5. Deterministic assessment – scenario development and modelling results.
6. Combining statistical methods with deterministic modelling to develop new hazard zones.
7. Preliminary risk analysis and discussion.

1.11. Thesis Contents

Chapter 2 is entitled, “Lahar hazard assessment and engineering mitigation for an alluvial fan with rapidly changing geomorphology: Whangaehu River, Mt. Ruapehu”. It focuses on determining the geomorphic factors contributing to lahar hazards on Mt. Ruapehu and applies the Titan2D toolkit as a hazard analysis tool, focussed at the critical points on the Whangaehu Fan where flows may spill northwards into a catchment containing many more people and economic activities at risk.

Collaborators/Authors

Shane J. Cronin – Provided assistance in surveying, access to historical data, manuscript editing and supervision. Ian C. Fuller - Provided assistance in surveying and manuscript editing. Michael Sheridan - Provided the Titan2D model and setup assistance. Vince E. Neall, and Harry Keys – Provided access to historical data.

Submitted to Journal – Geomorphology (March 2009)

Chapter 3 is entitled, “Evaluation of Titan2D forecasts for the anticipated lake breakout flood at Ruapehu Volcano” and takes the next step to develop the conditions under which Titan2D simulations can be used as a lahar hazard forecasting tool. It also examines the constraints of such forecasts and the parameters that can be relied upon under certain conditions, along with the constraints that need to be considered when simulating and forecasting such non-cohesive lahar flows on stratovolcanoes.

Collaborators/Authors

Shane J. Cronin – Provided assistance in model simulation, manuscript editing and supervision. Michael Sheridan and Abani Patra - Provided the Titan2D model and access to the State University of New York at Buffalo supercomputing facility.

Submitted to Journal – Journal of Volcanology and Geothermal Research (July 2009)

Chapter 4 is entitled, "Landscape and Sedimentary Response to Catastrophic Debris Avalanches, Western Taranaki, New Zealand" and it examines the utility of applying Titan2D to understanding geological processes of landscape readjustment and lahar generation in the aftermath of major catastrophic edifice failures. This study provides detail on the spectrum of flow rheologies generated in mass flows during the recovery of a ring-plain landscape and highlights input factors that need to be considered when applying this model to pre-historical example scenarios.

Collaborators/Authors

Shane J. Cronin – Provided assistance in fieldwork, manuscript editing and supervision. Anke V. Zernack – Provided assistance in field work and manuscript editing.

Published in Journal – Sedimentary Geology (submitted, 2007; accepted 2009)

Chapter 5 is entitled "Emplacement Mechanisms of the Opua Debris Avalanche from Mt Taranaki, New Zealand; Structural Analysis and Computer Simulation" and demonstrates geological and Titan2D modelling approaches to reconstruct the processes of emplacement of the youngest debris avalanche deposit from Mt.

Taranaki. The chapter also investigates rheological criteria defining this type of flow and the potential for Titan2D for forecasting debris avalanche hazard.

Collaborators/Authors

Shane J. Cronin – Provided assistance in fieldwork, manuscript editing and supervision. Anke V. Zernack – Provided assistance in field work and manuscript editing. Michael F. Sheridan – Provided access to SEM equipment.

Submitted to Journal – Earth Surface Processes and Landforms (submitted, 2009)

Chapter 6 is entitled "Mapping block-and-ash flow (BAFs) hazards based on Titan 2D simulations; a case study from Mt Taranaki, NZ" and it examines how Titan2D simulations can be used to simulate dome-collapse pyroclastic flows and cold rock avalanches from the summit area of Mt Taranaki. It also examines methods of taking modelling and simulation results from individual scenarios to create combined hazard zones and probabilistic hazard assessment.

Collaborators/Authors

Shane J. Cronin - Provided assistance in fieldwork, manuscript editing and supervision. Thomas Platz and Vince Neall – Provided information on the block-and-ash flow stratigraphy of Mt. Taranaki. Abani Patra, Keith Dalbey and Michael Sheridan - Provided the Titan2D model and access to the State University of New York at Buffalo supercomputing facility as well as assistance in programming.

Submitted to Journal – Natural Hazards (submitted, 2008; in review)

Chapter 7 & 8 comprises a wrap-up discussion based on the findings of the earlier chapters, integrating conclusions of the applicability and constraints of 2D modelling for mass flow hazards on stratovolcanoes, such as those in New Zealand.

CHAPTER 2

Lahar hazard assessment and engineering mitigation for an alluvial fan with rapidly changing geomorphology: Whangaehu River, Mt. Ruapehu.

J.N. Procter, S.J.Cronin[1], I.C. Fuller[1], M. Sheridan[2], V.E. Neall[1], and H. Keys[3]

1. Volcanic Risk Solutions, Institute of Natural Resources, Massey University, Private Bag 11 222, Palmerston North, NZ.

2. Geophysical Mass Flow Modelling Group, State University of New York at Buffalo, NY 14260, USA.

3. Department of Conservation, P.O. Box 10-420, Wellington, NZ.

Abstract

Rapid changes in small areas at the apex of alluvial fans may have devastating consequences by directing downstream flood or lahar impacts into catchments of widely varying population or infrastructure vulnerability. During a series of lahars in 1995 at Mt. Ruapehu, New Zealand, aggradation of the Whangaehu fan apex (draining the eastern edifice) caused the onset of avulsion of flows northward into the highly vulnerable Tongariro catchment. An earth training dike "or bund" was constructed to protect this catchment by retaining flows on the southern side and normal lahar outlet path to the south. Surveys in 2001, late 2005, and following a major lahar in March

2007 now show net degradation of a channel in the Whangaehu fan apex, bordered by the bund. This indicates a net increase in the channel capacity at this site and shows that the bund remains at its effective design capacity. Past hydrological modelling used for the bund design provided a large range of discharge estimates, but lacked precise constraints on the size and nature of lahars from eruption and lake break-out events. New modelling has been carried out using Titan2D to examine the impacts of a 6 x 10^6 m^3 volume granular flow down this catchment. This simulates either an eruption or lake-breakout induced lahar with a historically typical volumetric bulking factor of 4. These simulations predict minimum discharges between 1800-2100 m^3/s at the bund site. By comparison, the largest 1995 flow at this site was estimated at around 1200 m^3/s. Further, any single modelled flow from the normal outlet channel of Crater Lake could not be induced to overtop the bund because discharge appears to be limited by the narrow upper reaches of the Whangaehu Gorge. Theoretical discharge levels required to overtop the Bund are estimated to be >6800 m^3/s, assuming no aggradation of the channel by the decelerating flow. Maximum potential discharge at the bund site is additionally modified by potential bifurcation of lahars above a certain size threshold at a point 2.5 km upstream of the bund. A major side channel ('the chute') effectively diverts part of the flows away to the southern side of the Whangaehu Fan. This potential for splitting of the flow appears to have increased since 1995, due to aggradation of lahar deposits and reworked sediment in the area immediately upstream of the divide. Despite remaining at design capacity for lahar events in the Whangaehu, erosion of new channels following the 2007 lahar renders the bund vulnerable to undercutting.

2.1. Introduction

Alluvial fans are complex and sensitive landscape components, responding to an array of factors including tectonics (e.g. Dade, 2007), climate (e.g. Harvey, 1996), earthquake (Wang et al., 2001), fire (Meyer et al., 1992) and the magnitude and frequency of formative processes, notably debris flows and floods (Volker et al., 2007). The Whangaehu fan is no exception. Located on a catchment divide, the precise topography at the fan apex determines whether flow events draining the eastern flanks of Mt. Ruapehu (2797 m) are channelled south into the Whangaehu River or north into the Tongariro catchment with a narrow divide between the two (fig. 2.1). Frequent lahars in the Whangaehu River over the last c. 20 000 years result from the direct drainage of Crater Lake (at 2540 m) into this catchment (Donoghue, 1991; Hodgson, 1993; Cronin et al., 1997a & b). By contrast, the Tongariro catchment experienced comparatively fewer lahars during this period (Cronin et al., 1997c). There is a greater population and infrastructure at risk in the Tongariro catchment, including hydroelectric power and a major trout fishery, hence confinement of most Ruapehu lahars within the Whangaehu River is a preferable option to minimise risk.

During the 1995 Ruapehu eruptions it became apparent that the narrow drainage divide between the two catchments at the fan apex may have been more precarious than the geologic record suggested. Accumulation of tephra from the 1995 and 1996 Ruapehu eruptions (Hancox et al., 1997) led to Crater Lake rising by 6-7 m above its normal level. Collapse of this to generate a lahar, which occurred on 18 March 2007, was one of the hazard scenarios anticipated to potentially cross the drainage divide and possibly enter the Tongariro catchment. In planning for the anticipated 2007 lahar and in the historical context of the lahar-induced Tangiwai Rail disaster of 1953

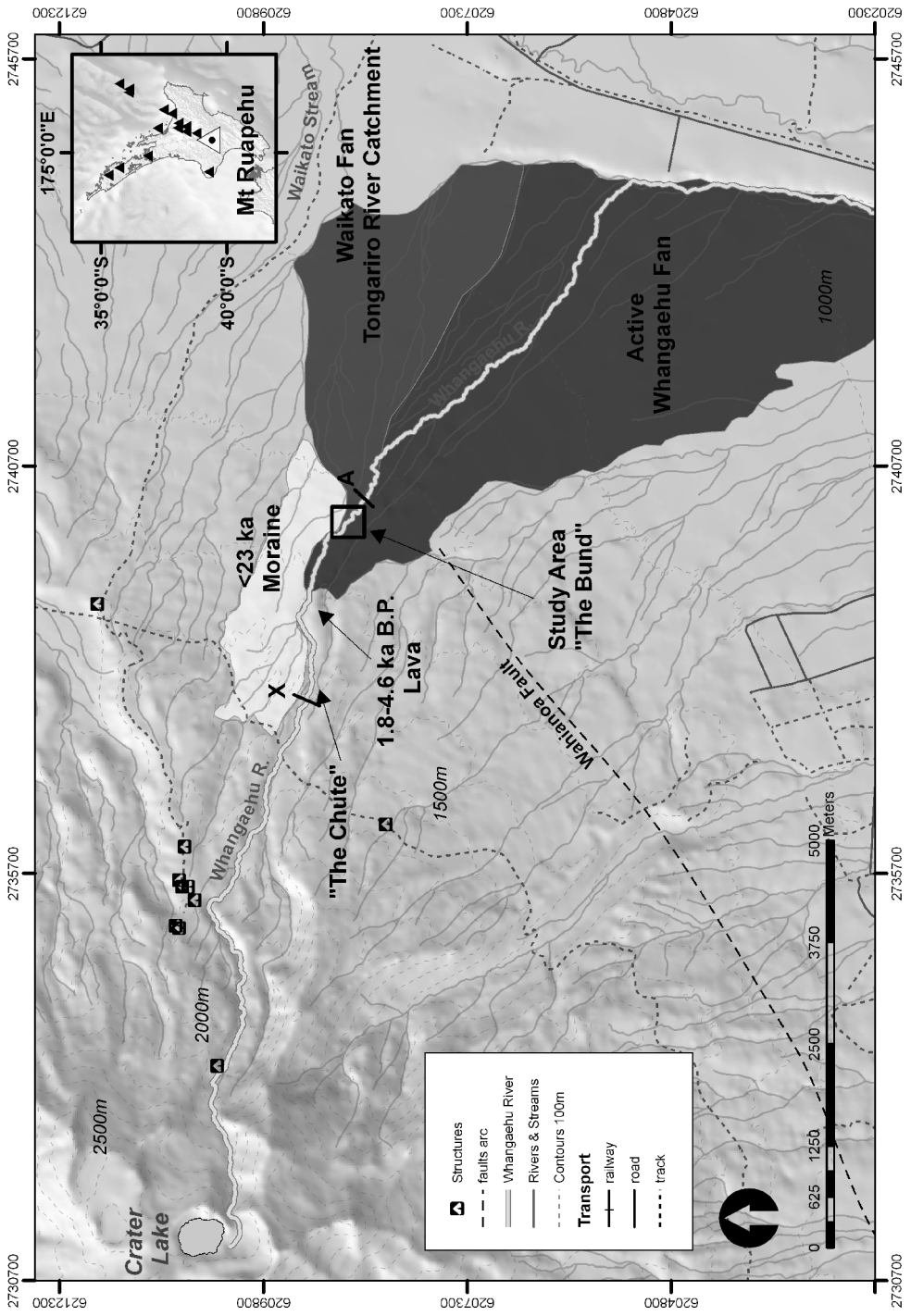

Figure 2-1. Location map of Mt. Ruapehu, North Island, New Zealand. Top Right, Ruapehu Volcano. Below, the (upper) Whangaehu River with the Whangaehu Fan highlighted. Box and line A indicate the study area across the current active Whangaehu River channel and the lahar deflection structure, the "bund". Line (X) indicates the point where lahars can bifurcate and enter the normally inactive channel referred to as the "Chute".

(O'Shea, 1954; Stillwell et al., 1954), a number of mitigation measures were developed with a focus on forecasts of the potential size of lahar that could be contained within the Whangaehu catchment.

One of the engineering-based hazard-mitigation measures was the construction of a lahar deflection dike (bund) at the apex of the Whangaehu fan. The design of this structure relied on a variety of computer simulations of lahar flow but these had to be carried out with only a few precise constraining details on flow discharge in this location. In addition, the suitability of lahar flow models applied and assumptions made in lahar-triggering calculations were widely questioned (Cronin, 2009, pers. Comm.).

The computer simulation of lahars is difficult due to their complex and changing rheology over time and space (Procter et al., in press). Lahars range in rheology from debris flow to hyperconcentrated flow (Pierson and Costa, 1987) and may contain between 20-70% by volume of sediment of variable grain size. Due to acceleration down-slope as well as local changes in channel slope, bed-lithology and width, can cause scour or rapid deposition, which in turn can alter lahar sediment concentrations repeatedly (Cronin et al., 1999). Few constraints on the interaction of particles, with each other within the fluid or with the bed, make it difficult to apply standard computer simulations of either granular mass flows or clear-water floods to lahars. Initial attempts in modelling Mt. Ruapehu lahars focused on the application of kinematic wave theory or other empirical mathematical functions to estimate travel time of a wave or flow front (Viganeux and Weir 1990; Fagents and Baloga, 2005). Other attempts have included applying the LAHARZ model, but only as a tool to validate differently generated DEMs (Stevens et al., 2003). Manville (2004) also applied

standard 1-D flood propagation models to hind-cast the 1953 lake-breakout lahar from Ruapehu and focused on more accurately describing the initial dam-break flood properties. The most recent attempt to simulate Mt. Ruapehu lahars has been the application of the commercial flood-routing package Delft3D (Carrivick et al., 2009). The application of this pure Newtonian fluid code has, however, highlighted problems in accurately simulating travel times and discharges of complex lahars with Newtonian fluid models. The majority of these methods also require simplified representations of the rough and complex terrain typically occurring in alpine volcanic catchments.

A further complication in numerical simulation of lahars is the change in flow volume and total mass with distance downstream. It has been demonstrated that lahars typically increase in volume or bulk-up by three to five times through incorporating sediment and water on upper volcano flanks (Cronin et al., 1997a & b; Pierson, 2002). Current hazard analyses for the Whangaehu catchment have used standard hydrological simulations, with development of a dam-breakout hydrograph and computation of its downstream propagation (Hancox et al., 1997). Webby and Forster (2002) attempted to simulate a volumetric increase or bulking by adjusting the Manning's n coefficient and adapting initial volume/discharge parameters. These approaches grossly simplify the complex nature of these lahars and are not able to be empirically or otherwise tested. This has led to a wide range of discharge values and travel time estimates being made available.

In this study we analyse the geology and geomorphology of the divide between two catchments, in particular at the apex of the active volcaniclastic fan (the Whangaehu fan) where a training dike or bund was constructed. The likelihood of the dike successfully diverting flow is analysed from channel changes during a series of lahars in

1995, along with three topographic surveys undertaken during 2001, 2005 and following the 18 March 2007 lahar. Processes leading to overflow of Crater Lake lahars into the Tongariro Catchment are described, along with a projection of the effectiveness of the current mitigation measures. In addition, computer simulations using the Titan2D granular flow code have been carried out to examine the extreme case of a fully sediment-laden debris flow to predict the flow inundation at the bund. These Titan2D simulations are also compared and contrasted to the properties measured from the March 2007 breakout lahar.

2.1.1 Eastern Mt Ruapehu catchments: Tongariro and Whangaehu Rivers

Widespread lahar deposits from >20 ka in the Upper Waikato Stream catchment attest to lahars generated on eastern Ruapehu entering the Tongariro River (Cronin et al., 1997b & c). The deposition record indicates that since 20 ka, only a few small lahars have entered this catchment via its southernmost tributary (Donoghue, 1991). The apparent cessation of lahars entering the Upper Waikato Stream is probably due to the formation of a lateral moraine during the last glacial maximum (fig. 2.1), which blocked direct drainage from the upper Whangaehu (Cronin et al. 1997b). This ridge, combined with the emplacement of a lava flow in the Whangaehu Canyon at some time between 1800-4600 yrs B.P. (Donoghue 1991), has narrowed the channel to a single thread stream that abuts the southwestern edge of the moraine (fig. 2.1). In the channel reach along the moraine, the Whangaehu River can cut down only 2 m below its normally base level before reaching solid (older than 1800-4600 yrs B.P) lava. This lava also forms the base of the moraine ridge, limiting the potential for northward lateral

erosion. This portion of channel is also crossed by the active Waihianoa Fault (Grindley, 1960), which may have generated an offset in the toe of the ridge that induces a southerly direction of the river. The main river flow path around this moraine also flips from being dominantly on the true-left to the true-right hand side of the larger channel.

The upper Whangaehu River is confined to a steep, deep, glacially modified valley that is bounded by lava flows for its first 8.5 km (fig. 2.2). The river forms a single thread channel controlled by the lava basement with minor, localised extremely coarse gravel, cobble and boulder bars. Below a slope break and the end of confinement at 9 km, the 7-8 km long and c. 10 km wide Whangaehu volcaniclastic fan begins, with the fan apex is not incised at this point. The path of the main channel thread is highly variable and modified by deposition and erosion during lahar events. During large lahars, flow may occur across many distributaries and overland by up to 700 m lateral extent (Cronin et al., 1997a). On the fan immediately downstream of the northward-confining moraine ridge, two ephemeral distributaries branch to the NE, travelling within 200 m of the southernmost tributary of the Upper Waikato Stream, before turning SE and rejoining the main Whangaehu channel up to 4 km downstream. At their closest approach only a few metres of relief separate the northernmost Whangaehu distributary and southernmost Upper Waikato tributary.

Two sites are critical potential overflow points to the Tongariro catchment. The first occurs upstream of the 1800-4600 yrs B.P. lava flow in the centre of Whangaehu valley (fig. 2.2). The second is the narrow and low divide between the closest tributaries of the Upper Waikato and Whangaehu catchments immediately downstream of the moraine (fig. 2.1). At the first location, flow of the Whangaehu normally travels

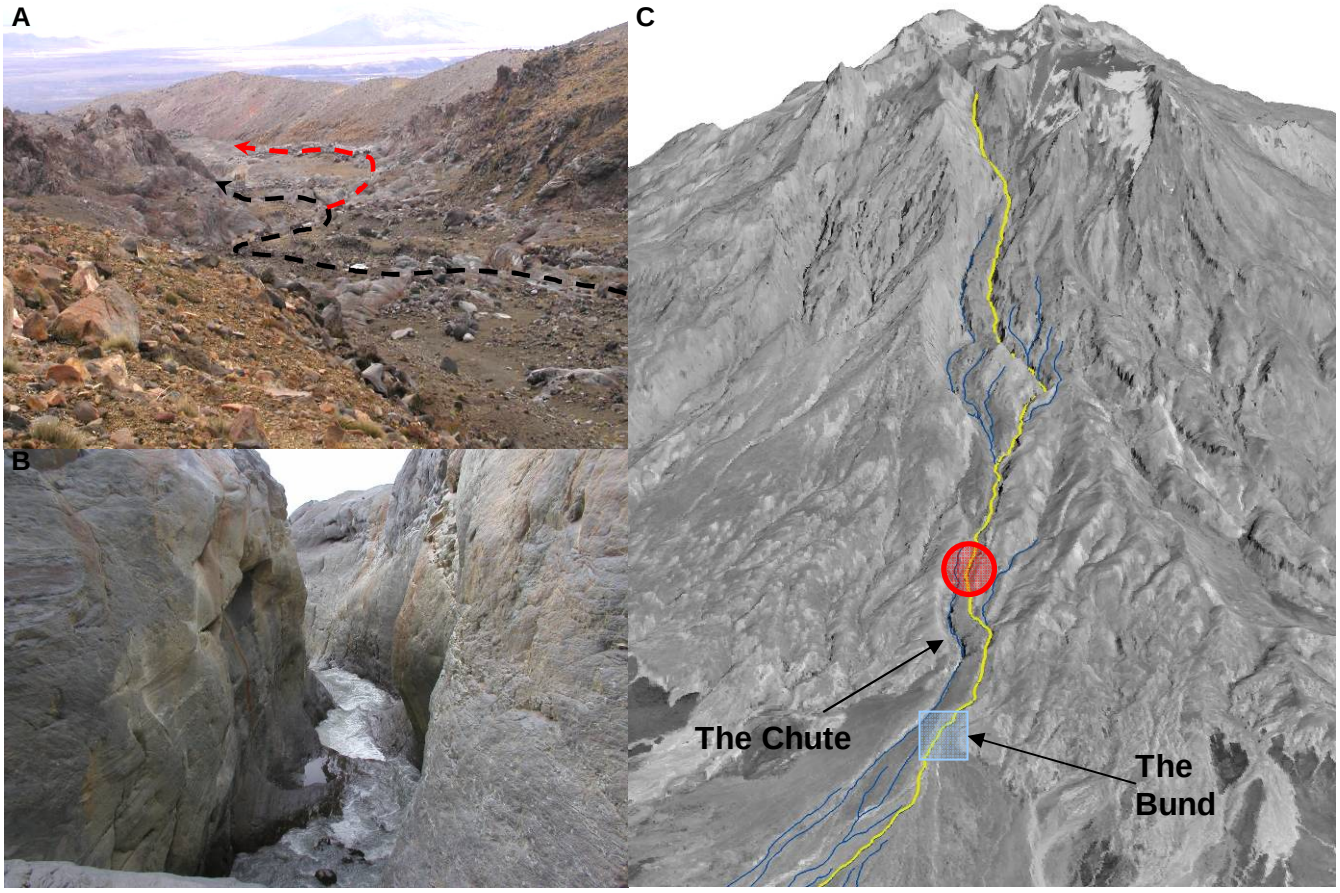

Figure 2-2. Geomorpphology of critical areas along the upper Whangaehu River; A) Entry (pre-2007 lahar) to the "Chute" ~7.5 km along the Whangaehu channel from the source Crater Lake. Note path of present normal Whangaehu streamflow (black line), and path of Chute spill over (in red). 1995-97 lahar deposits and reworked sediments cover the lava of the channel upstream of this divide; B) The main Whangaehu channel at the Chute location becomes constricted into a narrow hard-rock chasm which causes high discharge flows (e.g. lahars) to pond upstream and spill into the Chute; C) The Upper Whangaehu channel showing main flow channel (yellow) and the point at which divergence may occur during lahar flow. The upper split returns flow to the main channel, but the lower split (red circle) diverts flow into the "Chute" a channel to the south of the main flow, hence diverting it from the bund site and on a more direct and channelised path across the Whangaehu fan.

around the northern margin of the lava flow (fig. 2). However larger lahars, such as those in 1975During the 1995 eruptions of Mt Ruapehu, Crater Lake was emptied to produce at least 26 lahars (Cronin et al., 1997c) mostly confined to the Whangaehu River. During this period direct measurements of the lahars were consistently recorded at stations more than 42 km downstream and only very occasionally were observations made from the cone/fan area. Cronin et al. (1997a & b) equate the peak discharge of the largest 1995 flow, LH 4c, to the 1953 and 1975 lahars in the Whangaehu. The deposits of the major 1995 lahars in the uppermost fan area are

massive bouldery, muddy-sandy gravels with characteristics typically of debris flows (Cronin et al., 1997a). The flows at this point are considered to have had had a >60 vol. % sediment component, that resulted from water and debris expelled by eruption from the Crater Lake having eroded and entrained sediment from the upper channel and slopes. Velocities of the largest 1995 flows estimated by super-elevation at the fan head were around 9 m/s, with estimated peak discharges between 1400-1800 m^3/s (Cronin et al., 2000). The LH 4c flow occupied both the chute as well as tributaries of the Upper Waikato Stream and thus came very close to spilling into the Tongariro River. It cut channels up to 2 m deep leading northwestward from the main river channel and these were later used and deepened by lahars on three other occasions when they flooded into the northern distributaries.

During the 1995 lahar sequence, bed aggradation occurred rapidly in the apex area of the Whangaehu Fan (Cronin et al., 1997a). Between each lahar, major variations in the channel structure and location occurred at this critical location. The impact around halfway through the lahar sequence was a reduction in the cross-sectional area of the Whangaehu channel and a concentration of the channel thalweg on the true left bank (northern side). This increased the potential for lahars to avulse northward and enter the Upper Waikato Stream. On 25th September 1995, during the largest lahars of the eruption sequence, northward avulsion of LH 4c occurred from a channel that was initially 160 m^2 in cross-section. The channel capacity after LH 4c was only 52 m^2. Had similar sized lahars (with a discharge of c 1000 m^3/s) occurred after this event, the flows would have readily entered the Upper Waikato Stream. At least three and possibly five other lahars of magnitude LH 4c have occurred since 1860 (Hodgson 1993; Cronin et al. 1997a; Manville and Cronin, 2007).

The events required to cause a Crater Lake lahar to enter the Upper Waikato Stream are either a very large, 1 in c. 270 year lahar (c.f. Cronin et al., 1997a), or a moderately sized flow, equivalent to 1953, 1975, 1995 (LH4c) lahars, following a period of aggradation on the apex of the Whangaehu fan. The hazard is not just of the direct lahar effects in the Tongariro River, but also the potential for eventual capture of the Whangaehu River northward. While this may be an extreme case, acidic Crater Lake waters entering the high-value trout fishery of the Tongariro River and its delta into Lake Taupo would generate huge impacts on the river ecosystem and tourism economy as well as hydro-electric power stations on the river.

The Upper Waikato Stream is not the only route for a Crater Lake lahar to enter the Tongariro catchment. The (eastern) Mangatoetoenui Stream has also been a conduit for Crater-Lake-derived lahars in 1975 (Nairn et al. 1979) and 1895 (Allen 1902). Remobilised tephra lahars also occurred in this and other catchments of the Tongariro River following the major Ruapehu tephra eruptions of 1995 and 1996 (Cronin et al. 1996a&b).

2.1.2. Engineering mitigation measures – "The Bund"

An engineered structure was built to mitigate hazard for the stakeholders and communities in the Tongariro catchment, through protection of the north-trending distributaries and the Upper Waikato Stream (fig. 2.3). This involved construction of

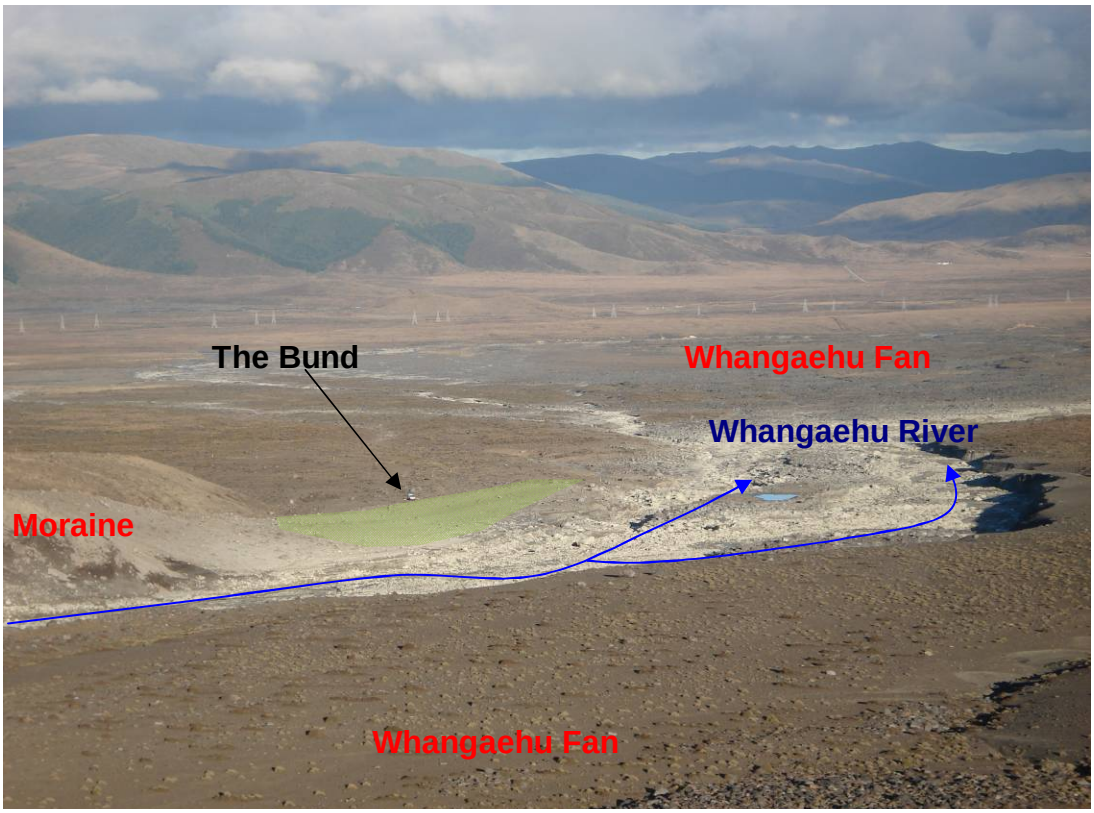

Figure 2-3. Study area of the Whangaehu River channel adjacent to the lahar deflection structure the bund (indicated by the arrow and highlighted green), further confining the river channel by extending the moraine. View is looking east, post the March 2007 lahar as shown by the light grey colour of the fine-grained deposits in the channel. Note the white vehicle at the end of the arrow for scale.

an earthen embankment or lahar-deflection structure, termed "the bund" that was planned from 2000 and completed in early 2002. The embankment is composed of gravel, sand and boulders bulldozed from the lahar channel and adjacent fan surface. The core materials were compacted, then armoured on the river side and topped with a layer of well-graded boulders up to 1.5 m in diameter.

At the same time, the Eastern Ruapehu Lahar Alarm & Warning System (ERLAWS) was put in place. This consists of Acoustic Flow Monitors (AFMs; Hadley and LaHusen,

1995) located adjacent to the Whangaehu River that trigger electronic paging devices and other automated warning responses. This was augmented with a trip-wire across the outlet of the Crater Lake and other monitoring instruments installed by scientific agencies (Manville and Cronin, 2007).

The other possible mitigation measures considered involved the enlargement of the southward-trending overflow channel upstream of the fan at the "Chute" (fig. 2.2). This would conduct a greater proportion of flow to a more southerly portion of the Whangaehu fan. However, due to its difficult access and hard lava base it would be a logistical and engineering challenge. Also given the rapid aggradation demonstrated by these lahars, constant maintenance work would be required.

The constructed bund is 285 m long and 20 m wide, with its crest 4 m above existing ground level (fig. 2.3). This height was based on a 2.2 m flow height at this point (2350 m^3/s discharge and 350-420 m^2 channel capacity), allowing for a 0.8 m error and 1 m of freeboard based on estimates of peak flow from Walder and O'Conner (1997) and Hancox et al. (1998) . Concerns over the structure's effectiveness focus on the effects of aggradation from the scale described during the 1995 lahars, and also on potential lateral erosion of the structure by lahar or meandering stream flow. If the channel aggraded to the level of the bund crest, it would probably be high enough for large flows to flood both southward and northward, thereby lessening the chances of a northward flow large enough to cross into the Upper Waikato Stream. Pierson (2002) also notes that this type of structure, in all known locations, usually withstands about 4 lahars before they need replacing.

2.2. 18 March 2007 Crater Lake Breakout Lahar

Ruapehu's Crater Lake filled behind a dam of unconsolidated pyroclastic debris at an erratic rate following the cessation of eruptions in 1996 (Keys, 2007). Signs of the imminent collapse of the dam began with seepage of Crater Lake water through intermediate porous layers in early 2007. At the same time, headward-sapping erosion scarps developed above the seeps on the outer downstream face of the dam. At 11:16 am (NZ summer time; GMT+12) on the 18 March, during a high-intensity rain storm, these scarps were deepened and cut back further, leading to a full collapse approximately 5 mins later (Manville and Cronin, 2007). Over the next 40 min ~1.3 x 10^6 m^3 of Crater Lake water was released through a 6.5 m x 40 m breach. The flood eroded and entrained sediment along the upper Whangaehu River to generate a lahar.

The lahar travelled followed the main channel of the Whangaehu River with a small portion flowing into the "chute" and then onto the southern Whangaehu Fan. All observations of the flow describe it as a "watery, fluid lahar" or hyperconcentrated streamflow rather than a fully sediment-laden debris flow. It was highly efficient at eroding and redepositing enormous amounts of bouldery sediment in the steep upper channel, with up to 6 m of down-cutting occurring in the upper channel and around 3-4 m of deposition at c. 6 km from source. The lahar monitoring station (seismic broadband, stage height and pore-pressure) at 6.5 km from source recorded a flow of 9 m depth, arriving in two major peaks at 11:26 am and 12:14 pm, with an average velocity of ~9-10 m/s, resulting in a peak discharge of 2250 m^3/s (Manville and Cronin, 2007) at that site. No instrumental recordings were made at the bund other than an arrival time of 24 mins being observed via responding agencies.

At the fan apex the lahar reorganised the channel, leaving deposits including a channel facies of clast-supported boulder bars and poorly sorted and horizontally bedded sandy gravels and a fine gravelly sand, overbank facies. Near the bund, the flow occupied a 140 m wide channel at peak flow depth of 5 m. The average front velocity estimated from the arrival time was 6.4 m/s, and peak flow velocity from super-elevation calculations was up to 7-8 m/s. The flow encroached onto a formed embankment in front of the bund but did not flow against the bund itself. A complex sequence of deposition and erosion occured in the channel at the apex, including formation of 1-2 m high and 20 m long gravel/boulder bars and parallel adjacent channels. The embankment in front of the bund appears to have directed flow eastward so that flow occupied distributary channels to the southeast that were not occupied during the 1995 events.

2.3. Fan Apex/Bund Area Geomorphic Change 1995-2007

Changes to the fan apex area were surveyed in 2001, 2005 and 2007. The uppermost surveyed profile is in a similar position to those observations made using tape and level methods during the 1995 lahar events. No detailed quantitative comparison can be made, yet there was clearly significant erosion of the channel between 1995 and 2001 with the reorganisation of lahar deposit as the river environment attempted to reach a stable situation after the 1995 lahars. Topographic surveys were undertaken during 2001, 2005 and following the 18 March 2007 lahar using RTK-GPS (and supplementary LiDAR data in 2007) (fig. 2.4). All

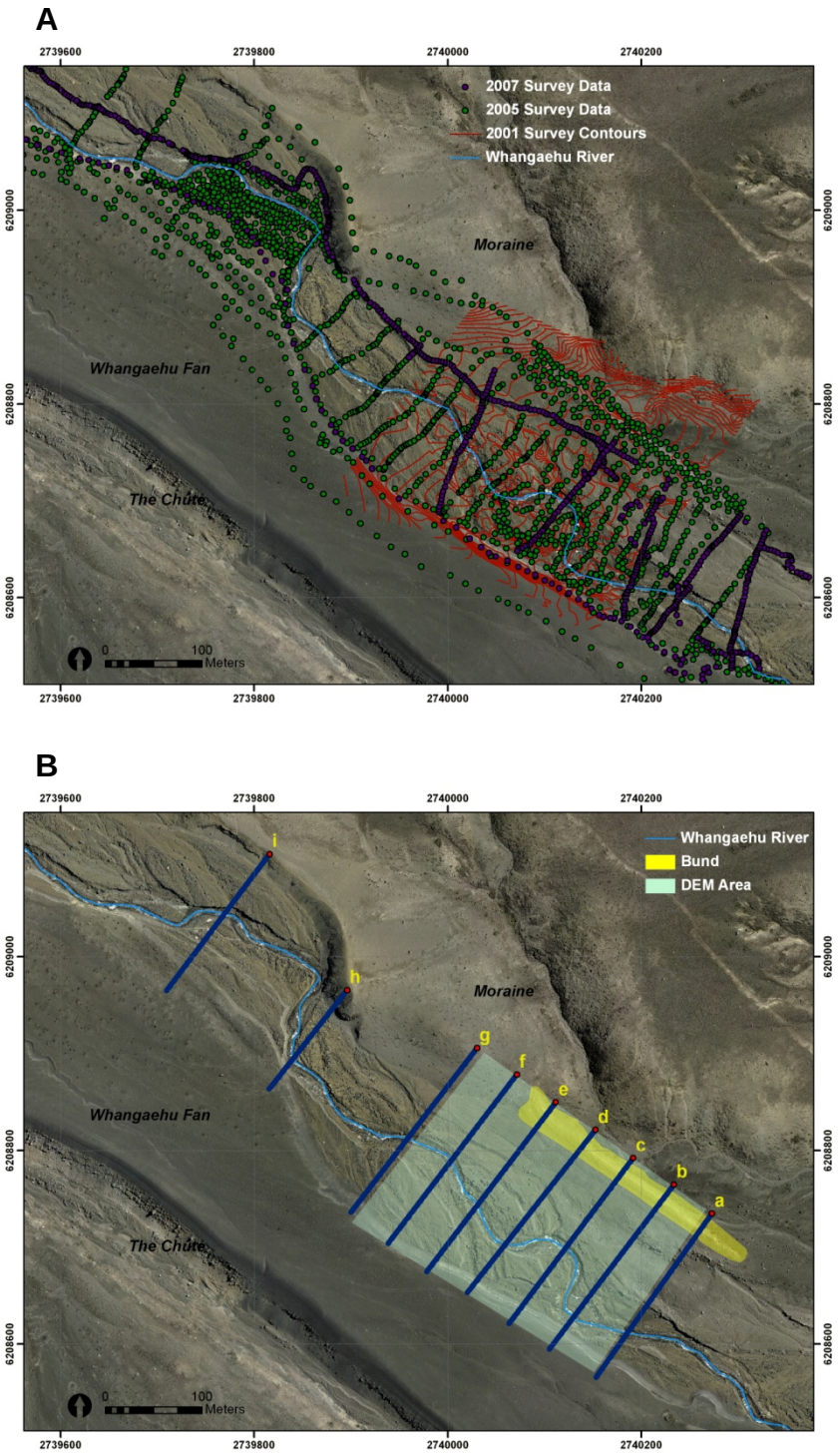

Figure 2-4. A) Study area (river flowing from left to right) showing the survey data contour and point data (with 2005 ortho-photography) collected 2001, 2005 and 2007; B) Location of cross-section lines indicating the respective comparative cross-sections from each survey 2001, 2005 and 2007. Rectangular area represents the boundary of the DEMs created from the survey data used in topographic change analysis.

surveys were compared as cross-sectional lines and data were converted in a DEM (Digital Elevation Model) (ArcGIS - GRID) to calculate differences in elevation and volumetric changes. For interpretation of the GPS-surveyed cross-section changes, only differences of >0.5 m are considered significant because the 2001 survey data has postings only every 10-20 m in many cases. DEMs were created at 1 m resolution.

2.4. Changes from 2001-2005

Between 2001 and 2005, profiles A-E (fig. 2.5) alongside the bund demonstrate net degradation occurred across the main channel, with changes mostly between 1-4 m. Net changes become smaller in an upstream direction, with profiles above profile-line F showing little net change. Profiles G and H (fig. 2.5) show some narrowing of the channel due to bank collapse. Additionally, profile H (fig. 2.5) shows erosion of the true-left bank where the river contacts the moraine on a channel curve upstream of the bund. Upstream of the moraine channel bend, comparison of the profiles becomes more difficult, because there is more divergence between the two data sources. Despite this variation, the base level of the channel was in bedrock during the 2005 survey, implying that little change in bed elevation has occurred over this reach between the two surveys.

The major change in the bund area since 2001 has been net degradation, particularly within the active channel region in front on the bund (fig. 2.6). Around 54 000 m^3 of material was removed from this area between the two surveys, and in places channels are scoured up to c. 8 m deep. Several abandoned channels are

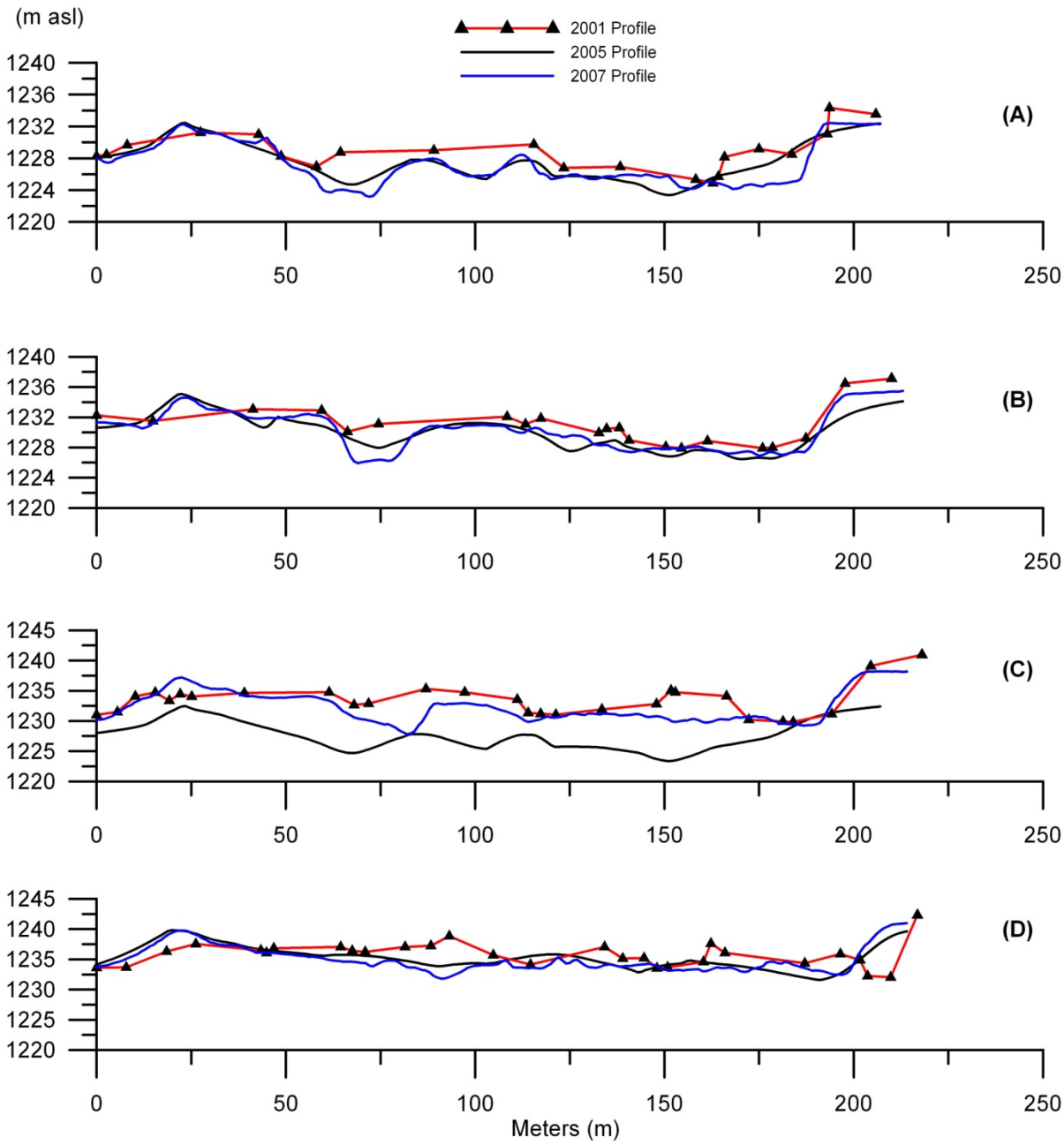

Figure 2-5. Graphs of the cross-sections A-I comparing the changing elevation (m. asl.) along those lines from 2001, 2005 and 2007. Constructed from surveyed spot heights; 2001 points shown on cross-section lines, 2005 are surveyed at 0.5 m intervals, and 2007 from 0.5 m resolution points.

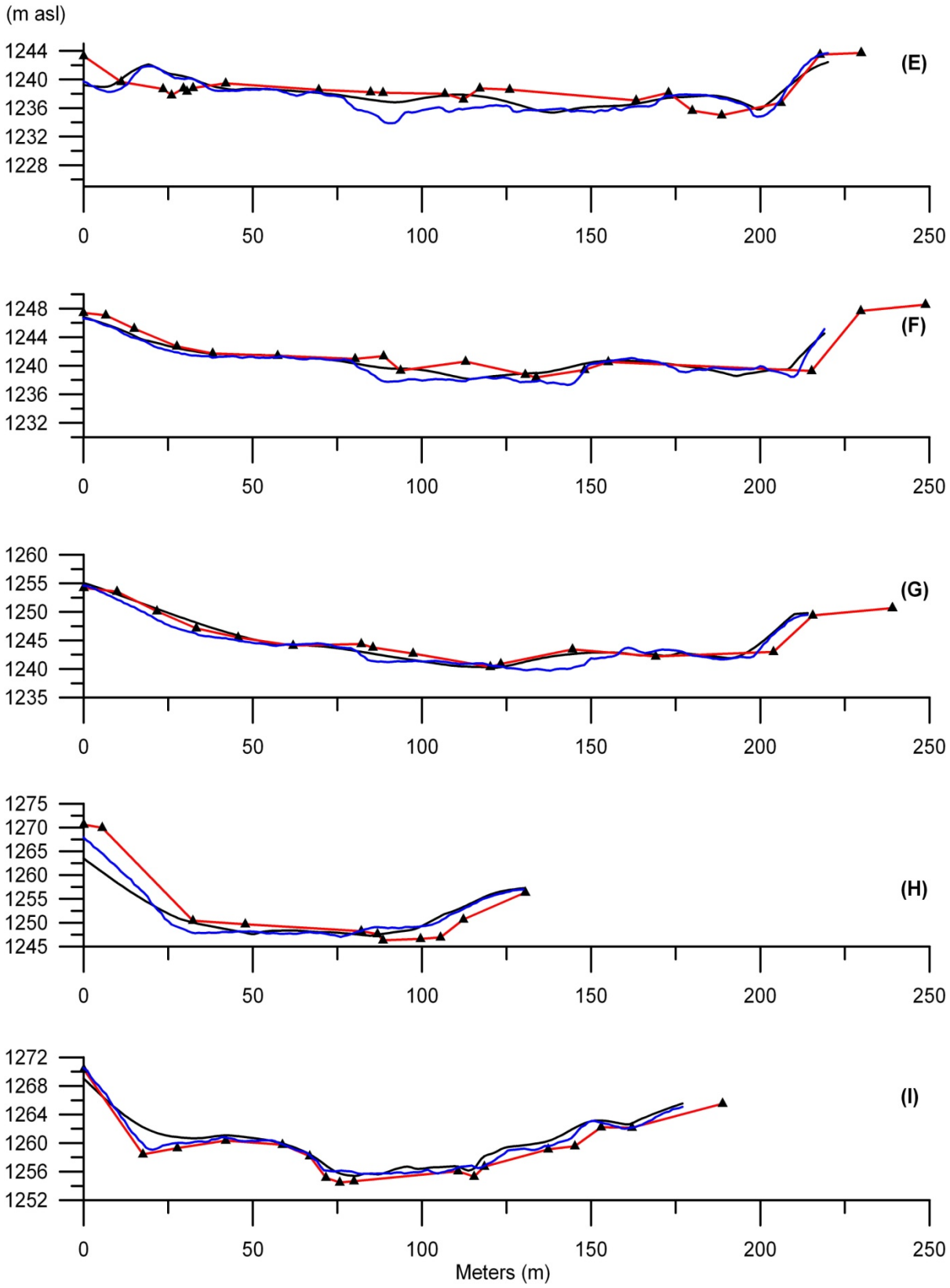
(m asl)
1244
1240
1236
1232
1228
(E)
0
50
100
150
200
250
1248
1244
1240
1236
1232
(F)
0
50
100
150
200
250
1260
1255
1250
1245
1240
1235
(G)
0
50
100
150
200
250
1275
1270
1265
1260
1255
1250
1245
(H)
0
50
100
150
200
250
1272
1268
1264
1260
1256
1252
(I)
0
50
100
150
200
250
Meters (m)

present, and these show signs of being abandoned due to ongoing preferential down-cutting in marginal areas of the active channel (fig. 2.6) and bar formation in the centre of the channel opposite the bund. Additionally, downstream of the bund area, channelised areas seen on 1999 orthophotos have been widened and in some cases deepened, with many new exposures of the underlying, distinctive yellow-brown, clay-rich Mangaio Fm. debris avalanche deposit (c. 4000 yrs B.P., Donoghue, 1991).

Net changes in the immediate bund area between the two survey periods also include a gain of 20 000 m^3. This change mostly includes construction of the bund (11 000 m^3) along the true-left bank, although aggradation in the order of 1-2 m occurred at the upstream end of the area near the true-right bank caused by its collapse. Minor depositional "highs" occur in mid-channel, representing local shifting and redeposition of sediment in the active channel.

2.5. Changes after the 18 March 2007 lahar

The lahar of 18 March 2007 dramatically altered the channel in the bund area. Major changes in stream position occurred, as well as the reactivation of abandoned stream channels (fig. 2.5. and fig. 2.6). Despite the aggradation of bars, primarily in the centre of the channel opposite the bund, the overall effect was of net erosion of 35 500 m^3. The channel thalweg moved from the true right hand side to a deeper (5-8 m deep) channel on the true left hand side, starting at approximately the midpoint of the bund (fig. 2.6). This newly formed channel accounts for the majority of the material eroded. The channel also cut into the end of the constructed platform at the front of the bund,

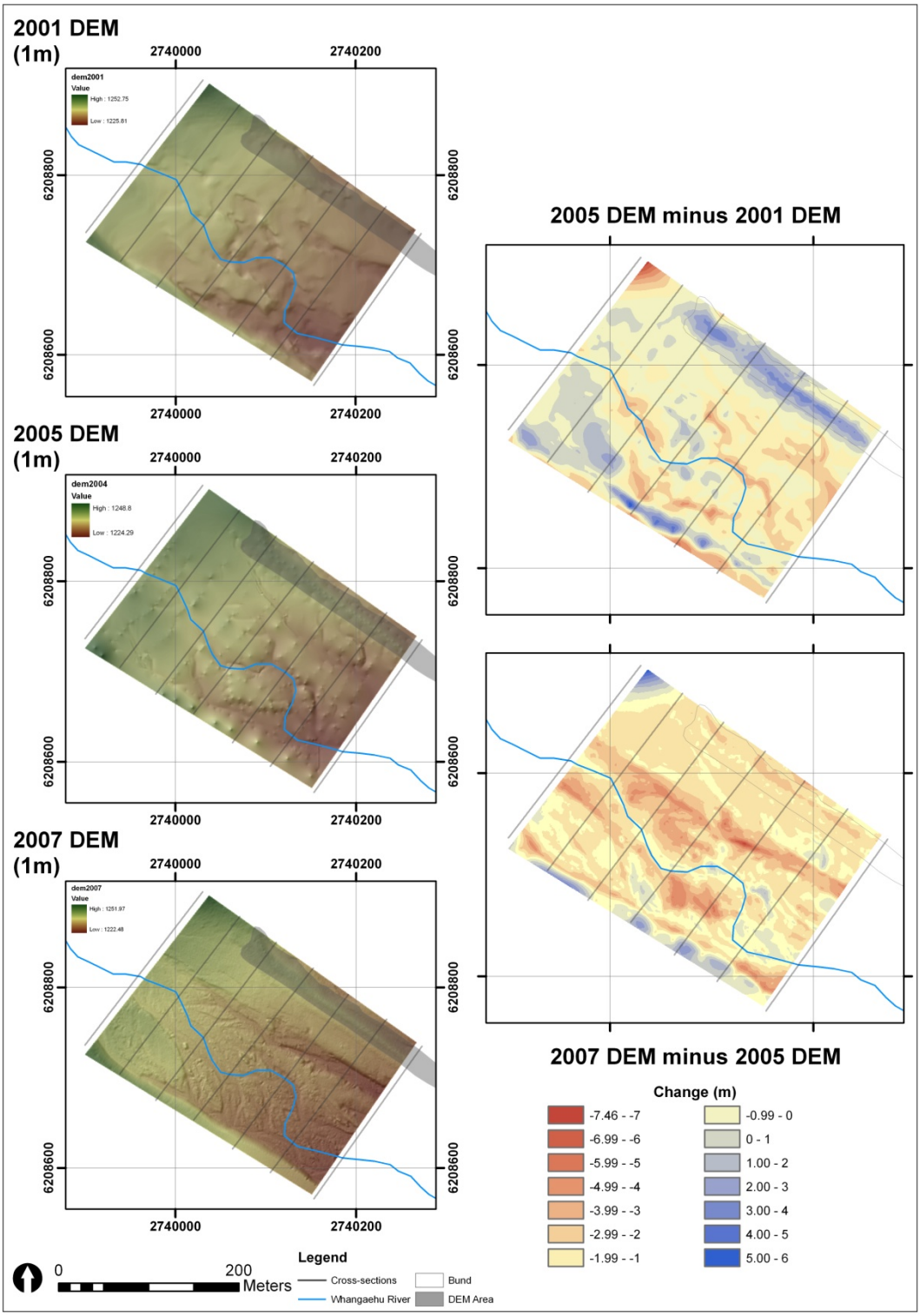

Figure 2-6. Digital elevation models of the analysis area constructed from the survey (2001, 2005 and 2007) data on the left hand side. On the right hand side, difference maps constructed from subtracting DEMs, 2005-2001 and 2007-2005 with difference shown in metres displaying erosion in red and aggradation in blue. 2005-2001 difference map shows a pattern channel braiding starting to occur whereas 2007-2005 map displays the erosive nature of a lahar.

with lahar flow occupying downstream channels north to northeast of the bund. Directly opposite the bund, a bar in the centre of the channel survived the lahar and became more prominent due to erosion either side of it. The main channel (to the south of the bund and true right of the channel) filled in with sandy gravels to create a more boxed shape. Despite undergoing net erosion from the lahar, there was a clear pattern of localised bed reorganisation to smooth and flatten the channel (fig. 2.6).

Other changes upstream of the bund include the deposition of material on the true right side of the channel, directly opposite the moraine, following a major bend in the river (fig. 2.5). This deposition followed a similar pattern to that of the previous 5 years; however, the 1-2 m thick bouldery gravel bar was completely removed.

2.6. Past Flow Modelling Applied to Risk Assessment and the Bund construction

Initial assessments of lahar hazards following the 1995/96 Ruapehu eruptions were undertaken by Hancox et al. (1998) using standard 1-D hydrograhic models constrained by eyewitness accounts and measurements taken from the 1975 and 1953 lahars. Later analysis (Webby and Forster, 2002; Manville, 2004) applied Manning's open channel flow formula for estimating discharge flow as a function of channel morphology, roughness and slope. Onset hydrographs from a dam-collapse breakout of Crater Lake were calculated for different initial conditions: outlet/breach dimensions, water volume, and mode of dam collapse (piping, overtopping and rapid down-cutting).

The first calculated values for an outbreak flood (Walder & O'Conner, 1997; Hancox et al., 1998) were:

Volume of tephra dam:	~3 x 10^5 m^3
Drop in water level:	6.5 m
Water Volume:	1.4 x 10^6 m^3
Erosion rate of dam:	10 to 100 m/h
Outlet Peak Discharge:	480-850 m^3/s
Breach width:	30 m

From these values Hancox et al. (1998) calculated discharges of 1500-1600 m^3/s at the bund area, with flow arriving 20-25 minutes after breakout. These models all applied relationships derived for Newtonian fluid flow and did not take into account the different rheological nature of lahars (debris flows to hyperconcentrated flows) that may be carrying sediment loads up to 70 vol.% (Pierson and Scott, 1985). Pierson (2002) and Cronin et al. (1999) also noted that lahars can rapidly change their properties by either incorporating massive amounts of sediment along some reaches of flow (e.g. upper few km from source), or depositing material in broader, lower gradient stretches. This process markedly changes the volume and discharge of lahars, which cannot be predicted by hydrological approaches. From 1995 lahars on Mt. Ruapehu and other global examples, it was estimated that these incorporation or

bulking processes may lead to a three- to five-fold increase in original breakout volume (Cronin et al, 1999; Pierson, 2002).

Webby and Forster (2002) re-modelled the breakout lahar using a 1-dimensional shallow water equation approach that incorporated an energy dissipation parameter to account for the bulking and de-bulking of a lahar. This value was adjusted to account for bulking factors of 3.3 to 5x the original breakout volume, resulting in 24 simulations, giving a broad range of discharge and travel times at various points along the channel and at the bund (Qp = 500-3500 m^3/s, flow depth = 3.5 - 6 m, peak flow travel time = 16-25 min). They recognised that the variable flow behaviour observed in lahars due to interactions between particles, clay and water made their rheology difficult to simulate.

More recently Manville (2004) undertook a paleohydraulic analysis of the 1953 Crater Lake breakout lahar. This revised simulation of the dam outbreak used various dam-collapse models and constraints on initial channel dimensions and constrictions of flow through an ice cave. Modelling of the lahar was carried out using 1-dimensional flood routing software, Boss DAMBRK (Fread, 1988). It used an initial assumed hydrograph, cross-sectional areas of calculation sites and application of varying Manning's n coefficient to account for bulking and de-bulking. The Manning's parameter was tuned to fit modelled observations to known values in some locations. Hence for the 1953 event the simulated flow velocity was 5-7 m/s at the bund, with peak discharge between 1700-2000 m^3/s and travel time to this point ~18-20 min.

Descriptions of pre-historic and historic lahars and their deposits at the bund (Donoghue, 1991; Cronin et al., 2000) imply that flows in this reach are typically either debris flows or rapidly transforming into hyperconcentrated flows. To effectively simulate debris flow conditions, the interaction of sediment particles and their effect on the rheology of the flow needs to be taken into account. Such flows are likely to have substantially different velocity than typical Newtonian flood flows.

2.7. Computer Simulation of Debris Flows– Titan2D

The mass flow model Titan2D (Pitman et al., 2003) is a code based on a model for an incompressible Coulomb continuum, a depth-averaged "shallow-water" granular flow (after Iverson and Denlinger, 2001; Pitman et al., 2003). The original code was designed for application to "dry" granular masses, not wet debris flows such as at Ruapehu; however, within the context of other hazard modelling approaches Titan2D offers a possibility of simulating highly concentrated debris flows at the lowest end of the mobility spectrum at Ruapehu, particularly those travelling along the Whangaehu Gorge reach of the channel. In addition, a two-phase version exists that allows various combinations of fluid flow with granular flow. The unique and most advantageous part of the Titan2D model is that the calculations are solved over a natural terrain represented by an irregular terrain model i.e. an original DEM that does not require any simplification or user modification. This is carried out using a parallel, adaptive mesh utilising a Godunov solver. In addition by using a Message Passing Interface (MPI), simulations can be distributed between multiple processors to increase computational efficiency (Patra et al., 2005), or run on a single processor such as on a personal computer.

The main parameters controlling the model include dimensions/volume of an initial mass and angles of "internal" and "basal" friction. Here, a series of runs was used to evaluate the parameter sensitivity in the upper Whangaehu River, by comparing (visually) model outputs to observations from past debris flows in the Whangaehu (particularly the 1995 LH 4c flow). Evaluation criteria included: surveyed cross-sectional areas at peak flow, inundation areas, travel times, instantaneous velocities, run-ups and other observations of avulsion behaviour. Internal friction angles allowed a subtle control on the lateral spread of the moving mass, and best results were found with angles between 30-35°, which is around the angle-of-repose of typical Ruapehu debris flow sediment. Basal friction angles allowed a level of control of the acceleration and velocity of the moving mass, and the best results were found with angles between 9-12°. The point where overall average slopes drop below 9° in the Whangaehu channel is approximately where historic debris flows begin to deposit sediment rather than solely entrain it. Initial starting pile volumes and dimensions made little difference to flow simulations in the upper part of the channel. Dimensions and volumes of 4×10^6 m^3 were used, based on bulking factors of 4-6 applied to a 1.5×10^6 m^3 water breakout from Crater Lake. Similar parameters are applied to the 2-phase model with the solid component being set to a constant of 60% of the mass.

Titan2D was run over a digital elevation model within the GRASS GIS package. In this case both 10 m and 5 m DEMs were used. DEMs were constructed by combining high-quality photogrammetry-derived point and breakline data of the channel with precise Real-Time-Kinetic-differential GPS (RTK-GPS)-surveyed data points in several parts of the channel, particularly the bund area. Triangular irregular networks (TINs) were constructed from the point data, to best capture drainage patterns, and these were in turn converted into raster DEMs at 5 and 10 m resolution for model runs. DEM

creation was carried out in ArcGIS (ESRI, 2007) and later converted into GRASS GIS raster formats.

The modelled pile was placed within the Crater Lake basin, which was “filled” on the DEM to the former lake outlet height. The tephra dam was subtracted from the basal DEM based on surveyed dimensions. Initial piles with an ovoid basal area were oriented with long-axis toward the lake outlet, to maximise the flow of the collapsing pile in this one area and to maximise discharge from the lake outlet.

A workstation with a single Intel Pentium 4 processor was used for this exercise, limiting the density of the mesh used for calculating model flow travel. An initial mesh size of 800 was used that may expand out to 800x4x4x4 = 51200 points being sampled at any one time with the distribution of these points altered in response to areas of greatest change via the adaptive mesh.

Model results include GIS point datasets that can be used to calculate flow thicknesses, mass and momentum, and inundation area. These datasets were converted and processed using ArcGIS with flow parameters being calculated from data within each calculation time-step.

2.7.1. Titan2D Modelling Results

Using mid-range (see above) conditions of a 4 x 10^6 m^3 starting volume (assuming a 4 times bulking factor from a 1.5 x 10^6 m^3 lake water outbreak), an internal friction angle of 35° (repose angle of dry lahar sediment), and a basal friction angle of 8° (transition from dominantly erosion to deposition along the Whangaehu channel), a simulated flow at the bund site would have a peak discharge/volume flux of 1800-2100 m^3/s, velocity of 4-6 m/s and a peak depth of 3.5-5 m (fig. 2.7). Discharge or volume flux calculations are made using the slope-area method (as applied in the hydrological models) using simulated tide-lines and surface slopes to allow direct comparison to those results.

2.8. Discussion

To evaluate the hazard posed by future lahars (2007 and onwards) on a lahar deflection structure and to examine if these may pose any greater risk to infrastructure in other catchments, two issues need to be considered. The first is identification of significant change in channel morphology since the 1995-1996 eruption that might alter travel times and inundation areas of lahars arriving to the apex of the Whangaehu fan at the bund. The second is the identification of significant channel change in relation to a single large scale event. This should be combined with an analysis of the suitability of a range of simulation tools to evaluate the capacity of the structure given different magnitudes of lahar events.

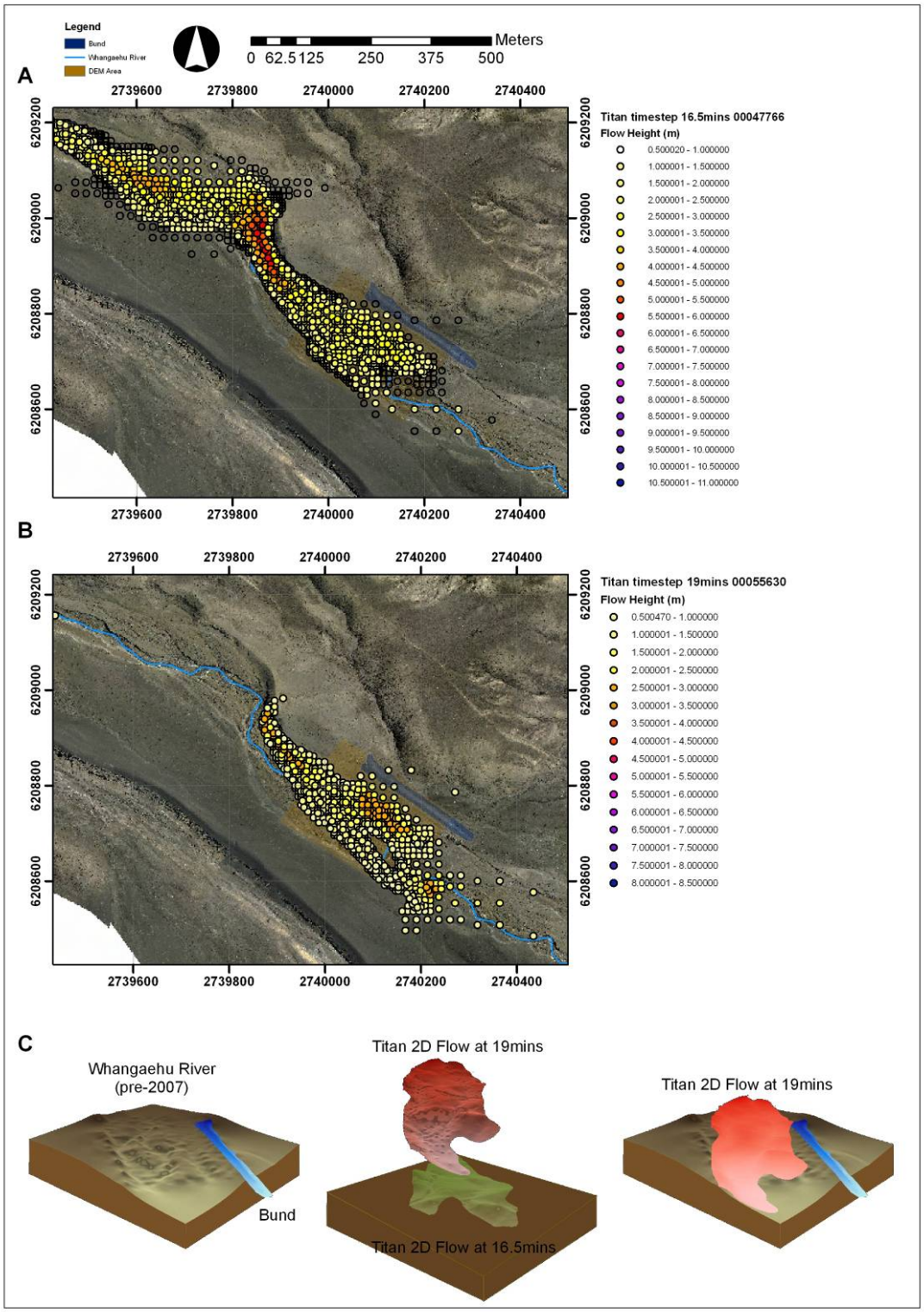

Figure 2-7. Example results of the Titan2D modelling, highlighted is one simulation (run number, 10/8) prior to the 2007 lahar, simulated on a terrain from 2005. The top image is the simulated peak of the flow arriving at 16.5 mins with the lower image indicating the preferred path to the true left of the simulated flow at 19 mins. Below those is a 3D representation of those peaks on the surveyed terrain.

2.8.1. Apex Geomorphology

The major change in the channel morphology has been the erosion through the 1995-1996 lahar deposits in the fan apex area. Following the 1995-1996 series of eruption-induced and rainfall-induced lahars, significant redistribution of sediment occurred throughout the Whangaehu channel system. In several locations deposition of lahar deposits or fluvially redeposited sediment has changed the course of stream flow and may contribute to unexpected changes in courses/channel distribution of future lahars in the catchment. From the period of 2001-2005, the river upstream of the bund eroded and occupied a single channel in the centre of the valley floor. Adjacent to the bund the river has undergone the greatest change. After 2001 the river was confined to a broad and braided channel between the bund and deposits of the clay-rich and resistant Mangaio Fm after flowing around the moraine. During the March 2007 lahar, major bed reworking occurred, which included development of a prominent central bouldery bar. The most dramatic change, over the 500m stretch, was erosion of 22 500 m^3 of sediment to form a channel (10-15 m wide x 5-8 m deep x 150 m long) on the true left, directly opposite the bund. The bund and the embankment in front of it is ~40 000 m^3. Pierson (2002) states that lahar deflection structures generally only last 4-5 events. Further reactivation and erosion of channels adjacent and downstream of the bund, suggests the bund may only exist for another 2 events of a similar size to the March 2007 event. During an eruption such as 1995-1996 with a series of events that empty the entire 10 x 10^6 m^3 of the Crater Lake, the structure may not last longer than the first few events or it could be rapidly inundated by aggradation.

One of the features controlling discharge into the apex of the Whangaehu fan area is the overflow site 2.5 km upstream at the Chute distributary. The Chute provides a

straight and hydraulically smooth channel for lahar flow over much of its length, spilling out onto the southern Whangaehu fan c. 15 km from source. Spill of significant proportions of lahar flow into the Chute has two main implications:

1. Decrease in the potential discharge and stage height of flows travelling down the main channel; i.e. an effective "cropping" of the hydrograph peak for the bund area.

2. Decrease in the travel time of some of the lahar flow onto the lower fan, by providing a straight and smooth travel path. This may potentially speed the arrival of a lahar in downstream areas, but only if a significant proportion (>30% of flow) were able to enter the Chute.

Entry of flow into the Chute would be encouraged by significant aggradation in the main channel at and upstream of the divide area. Up to 6 m thick 1995-1996 lahar deposits remain in this area, and much of the current channel base is formed in solid lava. The channel is also highly irregular and would generate highly heterogeneous and turbulent behaviour within a lahar flow travelling over it. In addition, significant hydraulic damming or ponding of lahars occur at this site, due to the transition from a broad (albeit irregular) channel, into a narrow, slot channel passing down the true left of the lava flow.

2.8.2. Analysis of Titan2D Model

One of the most attractive properties of the Titan2D code is the adaptive grid or refining mesh used in its calculation (Patra et al, 2005), which increases the resolution and sensitivity of models (especially of the flow front) to geomorphic features such as barriers and channel irregularities and broad-scale roughness. It also means that the flow path is not pre-selected by the user. Without the adaptive grid, computational requirements of using high-resolution DEMs necessitate splitting simulations into manageable sub-sections (Carrivick et al., 2009).

For the purpose of analysing small areas like the Whangaehu Fan apex, the Titan2D model allows a detailed focus on the dynamics of the flow front and later flow in relation to local topographic features. Super-elevation can be dynamically viewed around bends and conditions could be examined under which mass was split between two channels upstream of the bund.

Using a 5 m DEM with a complex terrain and channel morphology and a long flow path reached the limits of capability of single processor workstation, resulting in long computational times (up to several days). The detailed terrain and complex Crater Lake/outlet and channel conditions stretched the adaptive mesh to its limits along entire length of the flow. Unfortunately this may progressively degrade the possible mesh detail for the flow front with increasing distance from source. Under the constraints of a single processor workstation, the loss of detail at the flow front led to apparent dissipation of flow across the lower Whangaehu Fan.

2.8.3. Titan2D Simulated Flow Observations

These are the first 2-D computer simulations to model an entire flow from the Crater Lake outlet down the Whangaehu Gorge to the base of the mountain. Recent 2D hydrological modelling of Carrivick et al. (2009) using Delft 3D, was forced to apply an initial hydrograph at a point on the upper cone well below the Crater Lake outlet due to computational complexities of the upper channel. This also meant that initial effects of bulking and flow acceleration could not be accounted for.

The deep Whangaehu Gorge, a large glacially carved valley bounded by high (400m) lava cliffs, has confined all historic and known prehistoric flows, that utilise that flow path, for the first 7 km of flow. Within the Gorge a complex channel morphology occurs, with lahars having alternated between various paths. While these variations have few implications for local hazard, they provide insight into the dynamics of flows in response to various geomorphologic features, which may alter downstream peak discharge and lahar wave form. Using software such as Tecplot (Tecplot Inc., 2006), the time-step outputs from Titan2D simulations can be spliced to provide an animated visualisation of simulations in 3D allowing for immediate validation of model flow behaviour within expected ranges. Flows acting in a non-physical manner exhibit features such as ignoring the terrain and channel, extreme super-elevations and speeds, as well as a high variability in pile height and inundation area. Visual analysis of the simulations also allows for the identification of various signature features comparable to observed lahar events.

Several observations from the Titan2D animations compare well with observations of lahar events from 1995-1996 and the March 2007 event. All of the Titan2D simulations (using a DEM created from 1999-2000 data) consistently predicted avulsion of part of the flow into the Chute. Simulated inundation areas of the flow at 9 km correspond well with the mud lines of the largest 1995 lahars and the March 2007 event. Areas of super-elevation identified at 9 km in the simulation compare well with real event super-elevations of 2007. Velocities calculated from average momentum vectors produced within the simulations (4-6 m/s) at the bund compare well with the lower end of the observed velocities at between 9.1-4.6 m/s (Lahar LH 4c, 1995; Cronin et al., 2000) and the averaged arrival velocity for the 2007 lahar (6-7 m/s) as well as super-elevation calculated velocities of ~7 m/s.

2.8.4. Titan2D Hazard analysis

The Titan2D-calculated discharge or volume flux values are slightly lower than the Maximum Credible Design Flow (MCT3) rate of 2340 m^3/s used in the bund design. This is mostly due to the lower velocities predicted by the model (4-6 m/s) compared to the MCT3 flow's 6.7 m/s. The Titan2D discharges should hence be considered minimum values.

An example model flow entering the bund area is shown after 16 min 30s and 19 min (fig. 2.7). The arrival time to the bund area agrees well with those observed for 1995 lahars (e.g. Cronin et al., 1997a; 2000). The main control on the simulated flow routing appears to be a bend in the stream around the moraine, immediately upstream of the bund area; flow-ponding and run-up occurs at this point (fig. 2.7). Flow is contained within the main channel area along the bund reach of channel and the flow is primarily

oriented parallel to the bund (e.g. fig. 2.7). This is important in showing no direct or oblique impact of the modelled flow onto the bund, lowering the chances of direct bund erosion. However, the model shows re-activation and preference for the minor channel adjacent to the front of the bund.

Based on the Titan2D simulations, it appears that flow of reasonable dimensions (6-9 x 10^6 m^3, or 4-6 x bulking factor from a Crater Lake outbreak) should be well contained by the existing bund. For the example flow described above (6 x 10^6 m^3), there remains around 5.5-6 m freeboard at the lower end of the bund and c. 3.5-4 m at the upper end, based on the channel configuration surveyed in 2005. These freeboard values may be reduced by 1-2 m if there is significant wave development and unsteadiness in the flow, which is highly likely given the high degree of channel roughness in the area.

Any modelled flow starting at Crater Lake with an initial starting volume of 6 x 10^6 m^3 could not be induced to overtop the bund. This is because discharges of the modelled (and real) flows from the Crater Lake basin are limited in their early stages by the constricted initial path of the Whangaehu channel. Even with ever increasing volumes (up to 7 x 10^6 m^3) released from the Crater Lake basin, high enough discharges to overtop the bund could not be generated by the model. The only way bund overtopping could be achieved was by allowing flow to enter the Whangaehu channel by more than one path; i.e. an explosion scenario where water was rapidly ejected onto the Whangaehu Glacier as well as out the normal outlet channel.

Assuming multiple flow paths and using standard slope-area discharge calculations (e.g. McCuen, 1998) and the newly measured cross sections along the bund and channel, estimates of discharge required to overtop the bund can be calculated. Accurately evaluating the roughness of the channel (approximated by Manning's n), is the greatest source of uncertainty in these calculations. Values of 0.15 to 0.1 are used by Manville (2004) for the Whangaehu Gorge and Fan, respectively, but visual assessment and applying other empirical calculations result in n values of 0.07-0.075 for the specific channel reach along the bund. Based on the latter values, discharges in the order of >6800 m^3/s are required to overtop the bund. This is around 3.5 x the peak discharge calculated for a Titan2D-modelled flow of 6 x 10^6 m^3 in the bund reach. This assumes no modification of the channel by flow. However, it should be noted that a decelerating flow disgorging in this area has the potential for causing significant bed aggradation (such as observed in 1995), reducing channel capacity and possibly leading to overtopping of the bund at substantially lower discharges.

2.8.5. Titan2D as a Tool for Hazard Analysis

Application of Titan2D is an important supplementary hazard-analysis tool for traditional hydrological engineering problems such as this one. Being a granular flow model it provides another perspective on flowing materials with the rheology of debris flows (>60% sediment). Hazard analyses using standard hydrological models (e.g., Hancox et al., 1998, Webby and Forster, 2002) require estimation of a Manning's n factor, which in this case is used not only to represent frictional loss based on channel roughness, but is also being stretched to account for the potential rheological properties of a sediment-rich and non-Newtonian flow.

Data outputs of Titan2D do not automatically contain the information needed to calculate a mass flux or discharge-equivalent for comparison with hydrological methods. Instead, mass fluxes can be derived over a user-defined flow width. A more robust method of volumetric/mass flow rate would add an extra dimension to the hazard analysis. Also if resultant forces of the flow could be determined through mass/momentum vectors, assessments could be made on forces that a structure may have to withstand. Methods of determining the physics of debris flows (e.g., impact force, shear stress, viscosity; Costa, 1984) combined with methods to determine erosion and deposition would greatly aid hazard analysis and help determine the life expectancy of the bund.

2.9. Conclusions

Lahar hazard assessments can rarely be made at high precision along an entire flow path of several tens or hundreds of kilometres. Instead detailed studies must concentrate on critical points along channels. These may be obvious, or can be determined by initial simulations, by defining areas of potential avulsion or sudden possible changes in flow path. The apexes of coalescing fans, common around stratovolcanoes, are highly dynamic environments, where small changes in bed level or channel form may lead to major changes in flow path and downstream hazard. Focussing on the detailed hazard analysis at such a point on the apex of the Whangaehu fan, it is seen that lahars can be both locally intensely erosive and also depositional, but on a smaller scale. The deflection structure (the bund) was installed to protect northward flow avulsion of lahars. It is shown that the effectiveness of such deflection structures needs to be continually reassessed to account for ever changing channel morphology. This assessment of the Whangaehu bund from surveyed DEMs

has shown that, despite periods of apparent rapid channel aggradation following a series of small lahars over time, the net effect is erosion for larger lahars. Sudden erosion and deposition by lahars can reactivate older previously abandoned channels and result in unpredictable travel paths and impacts of subsquent events. At this site, measured net erosion provides some assurance that there is likely to be greater channel capacity for containing larger flows. However, the greatest risk remains that with repeated erosive events, the protection structure could simply be eroded away in as few as two further lahars.

Past computer simulations of lahar hazards and planning for mitigation structures have focused on the use of hydrologic flow codes that are designed for Newtonian flows. These require various degrees of abstraction to allow for both variations in basal friction/roughness and in the internal rheology of sediment-rich non-Newtonian lahars. Development of new computer codes that allow the user to model a range of the rheological spectrum should be applied alongside these Newtonian-fluid approaches. Titan2D was highly effective in the assessment of lahar properties in the upper 10 km of flow, in comparison to actual major lahars in 1995 and 2007. In particular, travel time and inundation were predicted very well. Further work is required to develop realistic outputs for volumetric flux measurements and parameters such as dynamic forces faced by channel walls or obstacles.

CHAPTER 3

Evaluation of Titan2D Modelling Forecasts for the 2007 Crater Lake Break-out Lahar, Mt. Ruapehu, New Zealand.

J.N. Procter, S.J. Cronin[1], M.F. Sheridan[2] and A.Patra[2]

1. Institute of Natural Resources, Massey University, Private Bag 11 222, Palmerston North, NZ.

2. Geophysical Mass Flow Modelling Group, State University of New York at Buffalo, NY 14260, USA.

Abstract

Following the 1995-1996 eruptions of Mt. Ruapehu, the hazard of a dam-breakout lahar was immediately recognised, because an unstable 7-9 m pile of volcaniclastic ejecta had accumulated over the former stable outlet of the normally 10 x 10^6 m^3 Crater Lake. Prior to the dam-breakout lahar of 18 March 2007, a range of flow scenarios down the eastern flanks of Mt. Ruapehu were simulated using the Titan2D mass flow numerical code to forecast flow travel times and inundation areas. Titan2D is a depth averaged code that solves the movement of a granular or two-phase mass over digital representations of natural terrains. We compared modelled scenarios, run before the 18 March 2007 break-out lahar of Ruapehu, to details from the actual event. The Titan2D models were accurate in predicting both the inundation areas and travel

times of the lahar at various key points down the volcano's flanks to 9 km. Beyond 9 km, and a major break in slope, the initial model parameters did not cope with the fundamental change that occurred in flow rheology. Velocity and discharge predicted at a lahar-deflection structure, "the bund", at 9 km from the Lake were up to 20% less than those of the actual 2007 flow, but matched closely those of the largest 1995 lahar at this location. Predicted paths of flow, including sites of avulsion, correlated well with those in the March 2007 event. In addition the simulations predicted dynamic behaviour such as super-elevation of flow in corners and hydraulic ponding that correspond to real-event measurements. This application shows that the Titan2D model can be used to reliably forecast certain parameters of lahar flow. However, care must be taken when choosing parameters and flow-length scales over which the comparison should be made.

3.1. Introduction

Lahars in historical times have killed over 50,000 people around the world (Skermer and VanDine, 2005). Overflow or break-out from volcanic lakes to produce lahars is a particularly common and deadly process at locations such as Kelut, Indonesia (1875 and 1990); Ruapehu, New Zealand (1953) and Parker, Philippines (1995) (Vallance, 2005). Mt. Ruapehu (2797m) is New Zealand's most active lahar-producing volcano (fig. 3.1). The composite, andesitic stratovolcano exhibits deep, glacially carved gorges and the 10 x 10^6 m^3 "Crater Lake" overlies its active vent (Christenson and Wood, 1993). Water and sediment are rapidly displaced from the Crater Lake during almost all phreatic and phreatomagmatic eruptions. At Mt. Ruapehu, there have been ~22 lahar events since 1861 in addition to 35 discrete lahars during the 1995 eruption sequence (Cronin et al., 1997a & b). Before the most recent break-out lahar on 18 March 2007,

the previous non-eruptive lahar from Crater Lake caused the most deadly disaster at Ruapehu on 24 December 1953, destroying the Tangiwai Rail Bridge and leading to the deaths of 151 people as a train was derailed into the still-flowing lahar (OShea, 1954). The 1953 dam-break mechanism was investigated by Gillon et al. (2006), and Manville (2004) conservatively estimated the rate of collapse to calculate a peak outlet discharge of ~530 m^3/s.

The term “lahar” is given to a gravity-driven, rapidly flowing mixture of (rock) debris and water from a volcano with a higher sediment concentration than normal stream flow and they may encompass a spectrum from debris flows to hyperconcentrated streamflows (Pierson and Costa, 1987). In addition to lake outbreak, lahars are generated by several other processes, including: debris avalanches, the melting of snow and ice by pyroclastic flows or tephra, and rainfall remobilisation of pyroclastic debris/tephra (Neall, 1976a & b). Lake-breakout lahars are at the more dilute end of the lahar spectrum, but are typically non-Newtonian, two phase mixtures of sediment and water, with sediment transported and suspended via grain-dispersive forces, and turbulence being dampened but not absent. They are also usually non-cohesive, having clay contents of <<5 wt.%. Beverage & Culbertson (1964) described hyperconcentrated flows as typically having sediment concentrations between 40 and 80 wt.% (20 to 60 vol.%). Volcanic-lake generated lahars usually display complex variations in sediment concentration due to erosion and entrainment of sediment along their flow paths (e.g., at Ruapehu, Cronin et al., 1999) and it is this variability causing “bulking” that plagues the accurate forecasting of downstream hazards from lake-breakout lahars.

Lahars are generally simulated with numerical models involving Navier-Stokes equations (assuming dominantly Newtonian flow), Bingham and Bagnold models

(assuming plastic or viscous characteristics), or Coulomb equations (for describing granular flow behaviour). The underlying physics for these was derived from field observations and laboratory experiments (e.g. Takahashi, 1980; Chen, 1988; Savage and Hutter, 1991; Major and Iverson, 1999; Denlinger and Iverson, 2001; and Pudasaini and Hutter, 2003). Few of these numerical models, however, have been transferred into computer simulations that replicate a lahar progressing over a natural terrain. In addition all of these numerical models need to be calibrated and tested against data from a series of real lahar events encompassing different natural behaviours and generation mechanisms. Computer flow simulations for hazard assessment have generally lagged behind development of theoretical models. A common model designed specifically for volcanic cones or volcanic environments is LAHARZ (Schilling, 1998), which uses statistical data of the planimetric area and cross-sectional data of past events to predict the potential lahar inundation, without providing any forecast of dynamic features of flows. The HEC-RAS series of models created by the US Army Corps of Engineers produces dynamic data for watery floods in a 1-D fashion, applying the hydrological Mannings "n" equations for prediction of flow velocity and discharge. More recently other commercially available 2D hydrological codes such as Flo-2D (based on the St Venant equations applied to hydraulics) and Delft 3D (based on solving of the Navier-Stokes equation in an incompressible shallow water framework) were applied to the simulation and forecasting of lahars at Guagua Pichincha Volcano, Ecuador (Canuti el al., 2002) and Ruapehu Volcano, New Zealand (Carrivick et al., 2009), respectively. Both models focus on the application and calibration to past events to determine factors such as inundation areas, velocity, discharge, and bed stress.

The anticipated 18 March 2007 breakout flood at Mt. Ruapehu provided an ideal opportunity to plan for an emergency response. However, for this to occur well-

constrained forecasting of the travel times and inundation areas was required. We applied the two-phase debris flow model of "Titan2D" developed by Pitman and Le (2005) to the problem. This model is based on a depth-averaged 'thin layer' granular debris flow containing a mixture of solid material and fluid. Constraints and parameters to run the model were derived from the debris flow/hyperconcentrated flow conditions witnessed and measured on the flanks of Mt. Ruapehu and in the Whangaehu Valley during lahars in 1995/96 (Cronin et al., 1997a). Measuring properties of the actual event of 18 March 2007 allowed us to undertake a rigorous test of the applicability and accuracy of the Titan2D model to forecasting lahar hazards in upper catchment areas.

3.1.1. Background

Mt. Ruapehu (2797 m) (fig. 3.1) is a 110 km^3 composite edifice is comprised of lava and pyroclastic products accumulated over c. 300 ka (Hackett and Houghton, 1987). Mt. Ruapehu is surrounded by a ring plain of epiclastic and pyroclastic deposits, dominantly the products of lahars (Donoghue, 1991; Cronin, 1996). The active crater vent of the volcano is covered by a lake that typically holds c. 10 x 10^6 m^3 of highly acidic water (Christenson and Wood, 1993). The only outlet for Crater Lake throughout historical record has directed outbreak and some eruption-triggered lahars down the Whangaehu catchment on the eastern flanks of the volcano. Water outbursts from Crater Lake typically rapidly erode and entrain sediment to transform into debris flows or sediment-rich hyperconcentrated flows within a few kilometres from the lake (Cronin et al., 1997a & b). The Crater Lake outlet was a focus for concern following the cessation of eruptive activity in 1996, from which 6-9 m thick unconsolidated pyroclastic debris was deposited on the lava rock rim (formed in 1945).

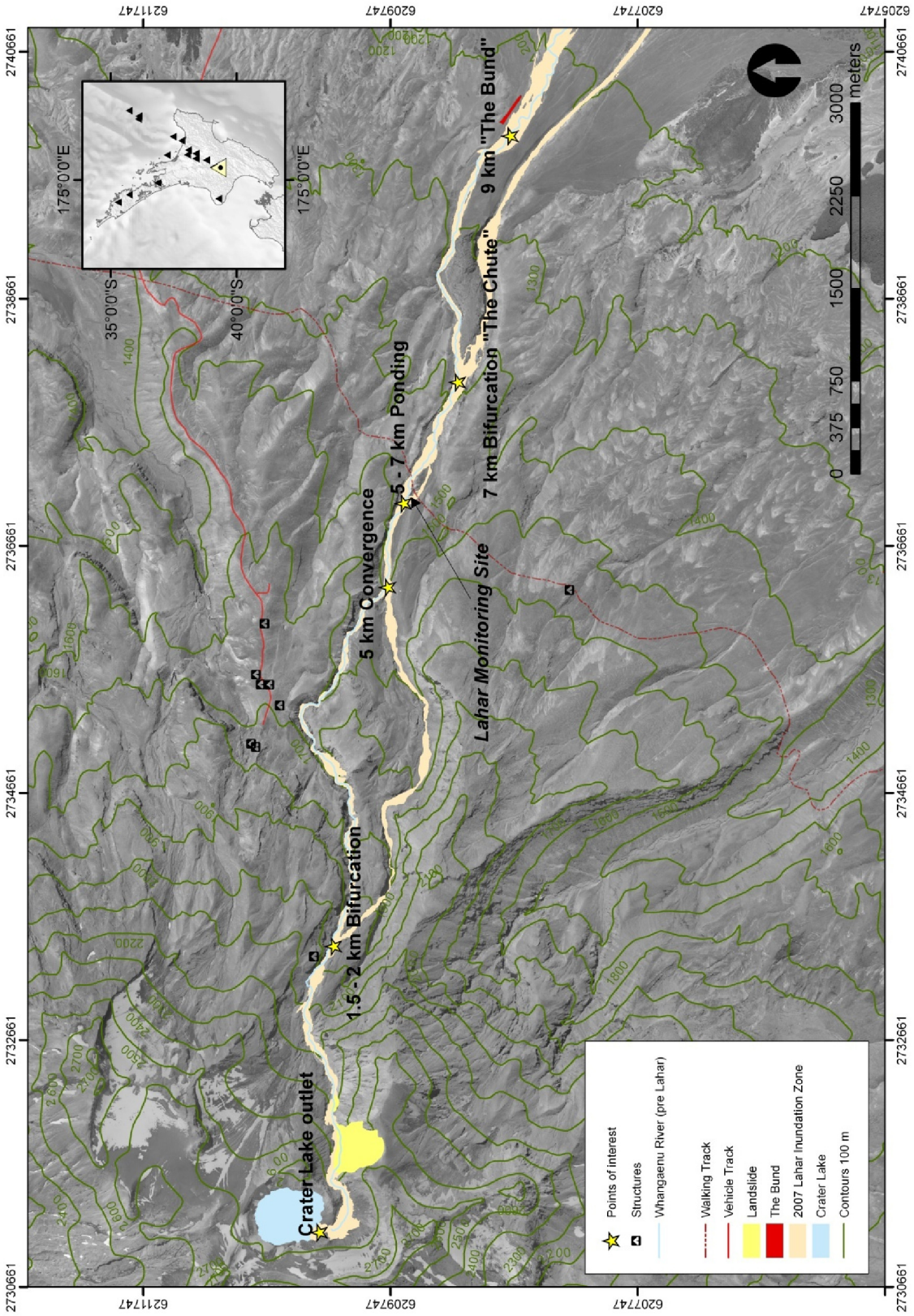

Figure 3-1. Location map and orthophoto of the eastern massif of Mt. Ruapehu showing the first ~10 km of inundation area of the 2007 lahar down the Whangaehu Valley. Identified are the sites of interest along the first 10 km. Inset map of the North Island of New Zealand and locations of volcanoes.

A previous dam-break lahar in 1953 occurred when warm waters of Crater Lake melted a tunnel through a glacier that was formerly located over the outlet region.

The upper Whangaehu River is confined in a narrow gorge between steep 100-400 m lava cliffs. The channel base is a mixture of hard lava with boulder and gravel fills in places. At 1900 m elevation and ~2 km from the lake outlet, the river bifurcates around a lava buttress, recombining into a single boulder-gravel based channel at around 1500 m elevation (<5km from source). At the crossing of a hiking trail, the Round the Mountain Track (RTMT), the channel gradient reduces to ~30° and meanders within a gravel-boulder bed up to 200 m wide. Below this point the river permanently occupies a hard-rock based channel around the northern margin of two lava flows (> 3000 yrs B.P.). Large historic lahars frequently occupy another channel on the southern margin of the lava flows to flow off the volcano (e.g., 1975, Purves, 1990; 1995, Cronin et al., 1997c), into a straight channel segment named “the chute” that leads flow to the southern part of the Whangaehu fan. The main northern channel leads into a 2 km stretch of gravel-bed channel that is weakly confined, before debouching onto the apex of the Whangaehu fan. Across the fan, the river occupies minor and changeable single and multiple ephemeral channels across a flat gradual (~10°) sloped surface.

3.1.2. Lahar observations at Mt. Ruapehu

Early studies of Mt. Ruapehu geology and hazards recognised the ubiquity of lahars in past eruptions (Nairn et al., 1979; Houghton et al., 1987). These were observed in greatest detail during a sequence of 35 lahars in the 1995-96 eruption episodes (Cronin et al., 1996b; Cronin et al., 1997a & b; Hodgson and Manville., 1999). The observed

and sampled flows spanned the range from non-cohesive debris flow to hyperconcentrated flow end members and Cronin et al. (1997a & b) distinguished four categories during the progression of the eruption: (1) initial snow slurry flows, (2) dilute lahars from large-scale sustained water expulsion from Crater Lake; (3) concentrated lahars from expulsion of Crater Lake water that entrained deposits of earlier flows; and (4) secondary lahars from rainfall-remobilisation of fall tephra. One of the flows (25 September 1995) was observed at 18 km, 42 km and 53-84 km from source, with the flow containing 61 wt.% sediment at 42 km and 46 wt.% by 84 km. Flow surfaces were smooth with a granular appearance of pebbles and floating sand in narrow reaches with common standing waves in broad shallow reaches (Cronin et al., 2000). Saltating, rolling and bouncing boulders were common and local flow velocities ranged between 9.1-4.6 m/s between 9 and 42 km from source. Cronin et al. (1999; 2000) identified a strong downstream variability in rheology in the 1995 flows, with most "bulking-up" from a flood to a debris flow in the first 5-9 km before diluting through sediment deposition beyond a major break in slope at 10 km. Pierson (2002) summarises that Ruapehu lahars bulk up to around five times the original volume of water released from Crater Lake. The debris flow deposits were massive, poorly-sorted, matrix-supported diamictons. Sand-dominated, weakly planar-bedded deposits were dominant in the catchment below 15-20 km from source.

Observations of the 1995 lahars are consistent with other hyperconcentrated flows (Pierson, 2005b), with movement of coarser particles in a dense underflow by saltation, while finer particles are suspended. Bingham models are thought to be appropriate to simulate aspects of these conditions (Pierson, 2005b); however, they do not account for the complex collisional interaction of particles observed to occur.

3.2. Observations of the 18 March 2007 Lahar

Ruapehu's Crater Lake filled behind a dam of pyroclastic breccia at an erratic rate following the cessation of eruptions in 1996 (Keys and Green, 2008). The dam collapsed at 11:16 am (NZ summer time; GMT+12) on 18 March 2007, during a high-intensity rain storm. Signs of the imminent collapse of the dam began with seepage of Crater Lake water months earlier through intermediate porous layers in the dam. During the rain storm, erosion scarps developed above the seeps on the outer downstream face of the dam, deepened and cut back further, leading to a full collapse. Over 40 min a 6.5 m x 40 m breach formed to release 1.3 x 10^6 m^3 of Crater Lake water that eroded and entrained sediment along the upper Whangaehu River to generate a lahar (fig. 3.1).

All eye witness observations, photos and video records show the flow behaved dominantly as a hyperconcentrated flow capable of moving large boulders by saltation and rolling. The flow was highly efficient at eroding and re-depositing bars and levees of coarse boulder gravels while it was on the flanks of Mt. Ruapehu. Up to 60 m of down-cutting occurred in isolated parts of the uppermost channel and 3-4 m of deposition was common at c. 6 km from source. A multi-component monitoring station (seismic broadband, stage height and pore-pressure) at 6.5 km recorded the flow being a steep wave up to 9 m in depth, arriving in two major peaks at 11:26 am and 12:14 am. From this an average arrival velocity of ~9-10 m/s can be calculated resulting in an estimated peak discharge at this location of 2250 m^3/s (Manville and Cronin, 2007). No instrumental recordings were made at the bund but an arrival time of 24 min was observed by responding agencies.

The lahar greatly reorganised channel morphology in gravel-boulder based reaches, leaving deposits ranging from boulder bars, clast-supported gravel and boulder sheets within the channel and sand gravels in overbank facies. Peak stage flow was dilute, leaving a wetted tide line washed clean of loose sediment in hard-rock stretches. At the base of the cone in the channel reach where the bund is located, a complex sequence of deposition and erosion is implied by numerous bars and channels being constructed and abandoned as flow was split between many changing braided distributaries. This corresponds with eyewitness reports and photographs of the flow at this point. Channels to the southeast of the bund that were not wetted in the largest 1995 lahars were occupied during this 2007 event. At peak discharge, the flow inundated up to 140 m across the channel with highly localised peak flow depths of up to 5 m. Average arrival velocity to this point was 6.4 m/s and super elevation measurements from a curve 300 m upstream of the bund yielded maximum instantaneous velocity measurements of 7-8 m/s. The flow wetted only the frontal embankment of the bund, remaining in the broad channel to the south of it.

3.3. Modelling of Mt. Ruapehu Lahars

Numerous models of mass flows exist (Takahashi, 1978; Hungr et al., 1984; Chen, 1988; Mizuyama and Kobashi, 1992; Iverson, 1997a; Rickenmann, 1999 and Iverson and Denlinger, 2001) but these are not normally constructed to provide 2-dimensional computer simulations of complex and variable sediment-water flows across simulated natural terrains. Application of hydrology-based simulation tools such as Flo-2D (Guagua Pichincha Volcano, Ecuador, Canuti et al., 2002; Mt. St. Helens, USA, Julien

and O'Brien, 1997), Delft3D (Kverkfjoll (jokulhlaups), Iceland, Carrivick, 2006) and HEC-RAS (Baitoushan Volcano, China, Yu et al., 2004) have been able to produce comparable inundation areas to test case lahars, yet many factors of the flow, including velocity, discharge, and travel time are not reliably forecast.

At Ruapehu, a number of attempts have been made to specifically forecast travel time and discharge at a number of critical points, mainly by adapting 1-D hydrological equations. The first paleohydraulic analysis of Ruapehu lahars was undertaken in the Government Inquiry into the 1953 lahar tragedy (O'Shea, 1954). These were focused on the Tangiwai Bridge site, 39 km from source. Here the 1953 flow had a peak stage of 6.1 m (Healy, 1954) from a bow wave, with other high water marks indicating a sustained 2.4 m rise. Stilwell et al. (1954) using slope-area methods calculated a discharge of 590-650 m^3/s. From field observations and experiments, Healy (1954) concluded that the lahar had a specific gravity of 1.6 and a concentration of 43 vol.% sediment.

Ruapehu lahar propagation was characterised using kinematic wave theory by Weir (1982) and Vignaux & Weir (1990). The method assumed that flow rate is a simple power function of depth and channel slope with a Mannings-type law to account for frictional losses. The determination of two constants describing these factors was made through analysis of a 1968 lahar, which was a small event possibly triggered by a single hydrothermal explosion from the Crater Lake. Applying the model with these constants to the 1953 lahar produced simulated volumes and peak discharge that differed by a factor of 3 (Vignaux & Weir, 1989). This in part was due to the assumption of a constant flow volume that, along with discharge and velocity, decays regularly over time, which is clearly not the case for most non-cohesive lahars (Cronin

et al., 1999; Pierson, 2002). A rule-of-thumb bulking factor for Ruapehu lahars implies a 3-5x increase in volume (Pierson, 2002).

Hancox et al. (2001) re-examined the 1953 lahar and calculated an outflow hydrograph with peak discharge at 250 m^3/s, based on development of an ice tunnel, 4.7 m in diameter and 500-600 m long over 30-35 mins. This required a bulking factor of 3.3 to produce a peak discharge of 590-650 m^3/s after 2.1-2.3 hours of travel when propagated downstream using MIKE11 (DHI software). Manville (2004) modelled 1953 dam failure and ice tunnel formation using the BOSS BREACH (Fread, 1987) code and propagated this starting hydrograph downstream using BOSS DAMBRK (Fread, 1988). This used bulking factors from the 1995-LH4c lahar (Cronin at el., 1997a & b; 2000), particle grain size and densities from the 1995/96 tephra dam at Crater Lake and constraining channel metrics from 1968 (Vignaux & Weir, 1990) to fit the observed 1953 peak discharge and travel time to Tangiwai.

Another approach was the application of LAHARZ (Schilling, 1998) to Ruapehu lahars by Stevens et al. (2003). The model was extremely sensitive to different digital elevation models (DEMs) produced by photogrammetry and the Shuttle Radar Topography Mission (SRTM). The well characterised historical lahar record at Ruapehu has been used to constrain other simplified numerical models (Fagents and Baloga, 2006) focussing on the propagation of a simple 1-D continuum model over changing slope. Fagents and Baloga (2006) recognised the need to adapt this approach to accurately simulate discharge downstream by incorporating influx and outflow of sediment to account for the changing rheology and density of the flow. Carrivick et al. (2007) provides a comprehensive reconstruction of a Ruapehu lahar event (18 March 2007) by applying DELFT 3D (Delft Software Inc.). The software utilises the St. Vernant

set of hydrodynamic equations that simulate Newtonian flows. With an input hydrograph based on Manville (2004) the resulting simulation matched 18 March 2007 peak instantaneous velocities up to 18 km from source, but the arrival time was significantly slower. Inundation areas were also similar except for the braided channel system across the Whangaehu fan. To enable effective computation, Carrivick et al. (2009) had to re-sample and simplify the 1m DEM as well as only utilise a modified and clipped channel area which removed some of the complex topographic structures that affect flow. Due to the low initial slopes of the Whangaehu River, the input hydrograph flow source had to be located c. 1 km downstream of the lake outlet for the simulation to run effectively.

3.4. Titan2D-Two Phase modelling at Ruapehu Volcano

Titan2D (Pitman et al., 2003) models use incompressible Coulomb continuum mathematics to model a depth-averaged "shallow-water" granular flow (after Savage and Hutter, 1989). The basic (one phase) form of the code was designed to simulate 2D motion of a "dry" granular mass across natural terrain. Its second generation (Pitman and Le, 2005) encompasses both granular and fluid flow, allowing for the simulation of (water laden) debris flows. Numerical characterisation of fluid within a debris flow was also carried out by Iverson and Denlinger (2001), who recognised the need to characterise the effect of interstitial fluid on a flow. Pitman and Le (2005) model each phase with mass and momentum balanced as individual constituents (after Anderson and Jackson, 1967) and simple interactions from Anderson et al. (1995), forming a system of hyperbolic equations. This numerical model is applied through a parallel, adaptive mesh utilising a Godunov solver, which allows for grid density to increase for high-resolution sampling of a DEM where rapid changes in mass occur (Patra et al.,

2005). The adaptive grid also enables de-focussing of the grid in areas of low change, thus enabling a large and complex DEM to be used for the entire simulation with high computational efficiency. Through a Message Passing Interface, the code can be run on multiple processors where highest resolution is required. A useful aspect of the Titan2D model is that DEMs of high resolution do not require any simplification or user modification to adjust for required computational power.

The main parameters controlling Titan2D simulations are the dimensions and volume of an initial mass, angles of "internal" and "basal" friction and the proportion of the granular/solid component. The input conditions applied to the Ruapehu lahar hazard assessment were based on a series of simulations using single-phase Titan2D (Procter et al., 2004), which evaluated parameter sensitivity in the upper Whangaehu River, by comparing model outputs to observations from past debris flows in the Whangaehu (particularly the 1995 LH 4c flow). Initial pile volumes and dimensions made little difference to flow simulations in the upper part of the channel.

A series of ~10 simulation runs were undertaken using two-phase Titan2D with internal and basal friction ranging between 15-30° and 10-15°, respectively. An initial computational mesh size of 800 was used that may expand out to 800x4x4x4 = 51200 points that can be sampled at any one time, with the distribution of these points changing in response to areas of greatest change via the adaptive mesh. The initial volume was placed within the Crater Lake basin that had been "filled" on the DEM to the level of the pre-1995 lake outlet height. This height was chosen, because it represents the level of hard rock beneath the 1995/1996 breccia dam. The breccia/tephra dam was subtracted from the basal DEM based on its surveyed dimensions. Simulation starting piles with an ovoid basal area were oriented with

long-axis toward the lake outlet, to maximise the flow of the collapsing pile in this one area and to maximise discharge from the lake outlet. A 5 x 10^6 m^3 pile was used, based on bulking factor of 3.3 on a 1.5 x 10^6 m^3 water breakout from Crater Lake. The solid component was set within the range 60-70%, the transitional conditions between hyperconcentrated flow and debris flow.

The topographic dataset used for the simulations was a 5 m grid DEM produced by combining high-quality point and breakline data of the channel from photogrammetry, with precise Real-Time-Kinetic-GPS (RTK-GPS) surveyed reaches in several locations along the channel. Triangular irregular networks (TINs) were constructed from the point data, to best capture drainage patterns, and these were converted into a raster DEM using ArcGIS (ESRI, 2008). Model results produced as CAD and ASCII point datasets were used to calculate maximum flow thickness, mass, momentum and inundation area. These datasets were processed using ArcGIS with flow parameters being calculated from data within each calculation time-step.

3.5. Results

10 simulations were undertaken displaying consistent results. Used in the hazard analysis display was 1 simulation (basal friction 10°, internal friction 17°), for ease of display, utilising 2 phase flow that encompassed the length of the study area (fig. 3.2). Evaluation of the model was through comparison with surveyed cross-sectional areas of peak flow, inundation areas, travel times, instantaneous velocities, run-ups and avulsion behaviour (table 3.1).

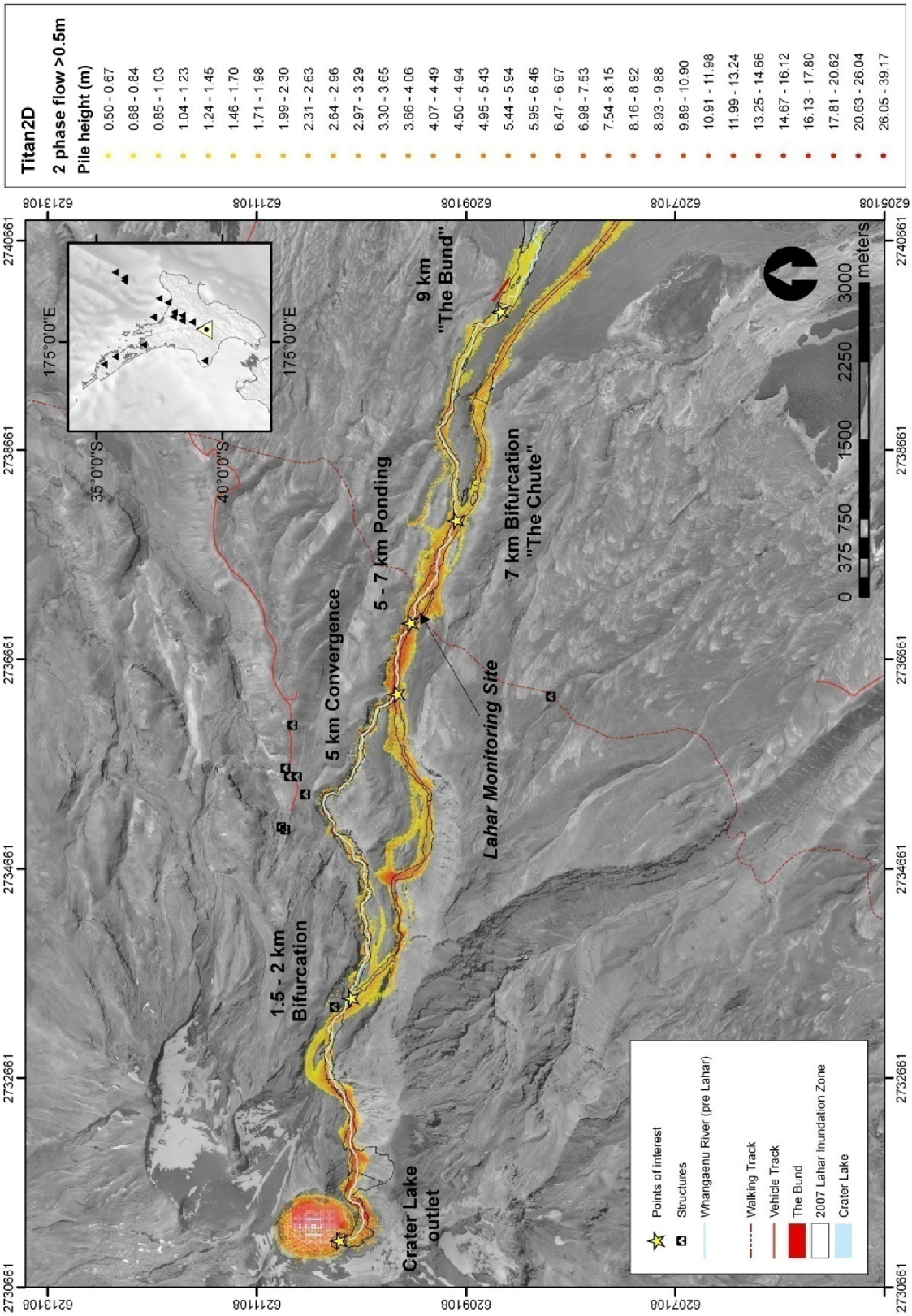

Figure 3-2. Map showing the representative Titan2D two phase combined outputs displayed against the inundation outline of the 2007 lahar.

3.5.1. Source – Crater Lake Outlet

The outlet of Crater Lake ($1x10^7$ m^3) was blocked with a 50 m wide x 90 m long x 6.5 m high barrier of pyroclastic breccia, comprising two distinct layers that corresponded with tephra sourced from the 1995-1996 eruptions. This dam could have impounded a maximum of 1.54×10^6 m^3 extra water in the lake basin. The 18 March 2007 collapse released 1.3×10^6 m^3 over up to 40 min with a peak discharge of 530 m^3/s (Manville and Cronin, 2007). This peak was based on the estimated drawdown in the lake from a fixed camera and duration of seismic signal on a geophone.

The simulation starting conditions of a collapsing static pile successfully produced a flow exiting the main current outlet with little loss from other low points in the crater rim (fig. 3.3). Two thirds of the starting volume exited the lake outlet within 8-10 min, with the remaining pile discharged over the next 10-15 min. While this reproduced the observed discharge time for most of the 18 March flow, peak simulated discharges for a range of pile dimensions were consistently higher, between ~776-7010 m^3/s. This was because, as described earlier, the starting volume was chosen to represent the already bulked lahar volume. The upper ~600 m reach of the Whangaehu channel is broad and of low-gradient (12-18°), Titan2D simulated the flow of a mass and inundation of this area comparatively well. This contrasts to previous models (Vigneaux and Weir, 1990; Manville, 2004; Fagents and Baloga, 2005) that were required to simplify or disregarded the first 1 km of modelled outputs (for 1D, numerical models), or initiate simulations from beyond this point.

Table 3-1. Comparison table of the 2007 lahar event and the Titan2D 2-phase simulation at key locations.

	Inundation width (m)		*Peak flow depth (m)*		*Travel time (mins:secs)*		*Average velocity (m/s)*	
	2007 Lahar[1]	**Titan2D**	**2007 Lahar[1]**	**Titan2D**	**2007 Lahar[2]**	**Titan2D[4]**	**2007 Lahar**	**Titan2D[3]**
ERLAWS 2 2 km	73	224	10	8	2.54	6	9.6	5.5
ERLAWS 3 5 km	102	136	13	16	6.54	8:36	8.6	9.6
RTMT 7 km	75	150	10	13	11.02	11.18	8.7	10.6
The Chute 7.5 km	141	167	9	5	-	-	-	-
The Bund 9 km	141	135	8	5	24	19	7.5	5.9

[1]Measured from LiDAR mapped inundation tide lines.
[2]Measured from arrival time on acoustic flow monitors.
[3]Identified from output file iterations

3.5.2. 2-5 km – Bifurcation

The simulations forecast a location of super-elevation of flow around a channel bend and localised hydraulic ponding at 1.5 km from source that matched the observed 2007 conditions (fig. 3.4). Between 2 and 5 km from source the models correctly indicated that bifurcation would occur between two channels after 6 minutes of flow onset, despite only a minor change in topography. The two channels are separated by a low (<10 m high) divide made up of sandy gravel fluvial and laharic deposits, with the southern branch containing the deposits of pre-historic lahars, but no evidence of historic events.

The modelled flow times to the Eastern Ruapehu Lahar Warning System (ERLAWS) Acoustic Flow Monitor (AFM) sites 2 and 3 were slightly faster than the 18 March 2007

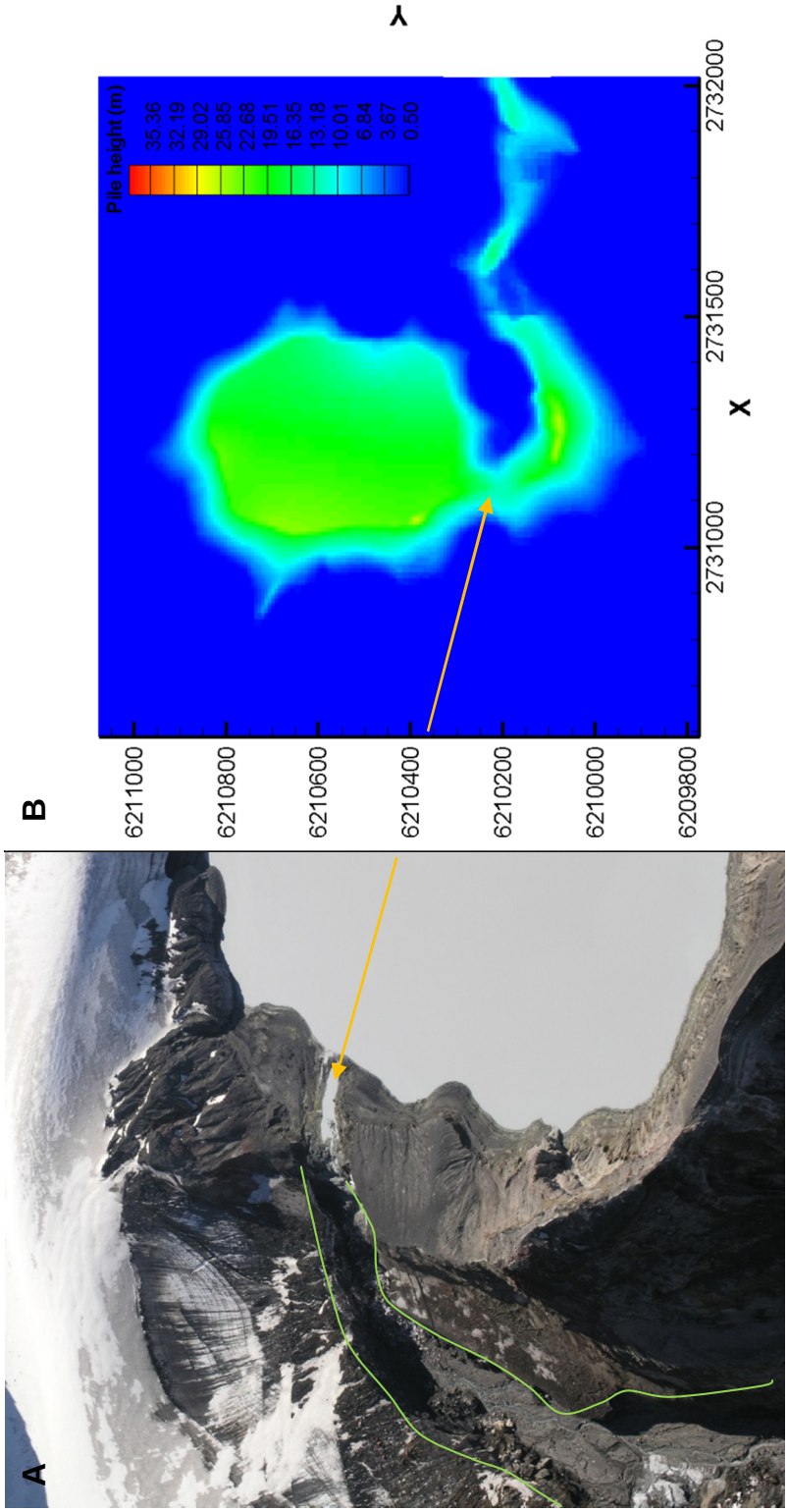

Figure 3-3. Crater Lake outlet. A) Photograph 5 days after the event showing the outlet and area of material eroded from the outlet. Green lines indicate the peak tide lines; B) Plot showing the mass flow inundation from the Titan2D simulation (after 3 minutes 10 seconds) of the same Crater Lake outlet area.

Figure 3-4. Bifurcation 2 km from source; white box indicates area of photo, arrow flow direction. A) Photograph of site and green lines indicating the peak inundation areas and flow direction; B) Titan2D plot of the simulated flow and; C) 3D view of th e Titan2D simulation.

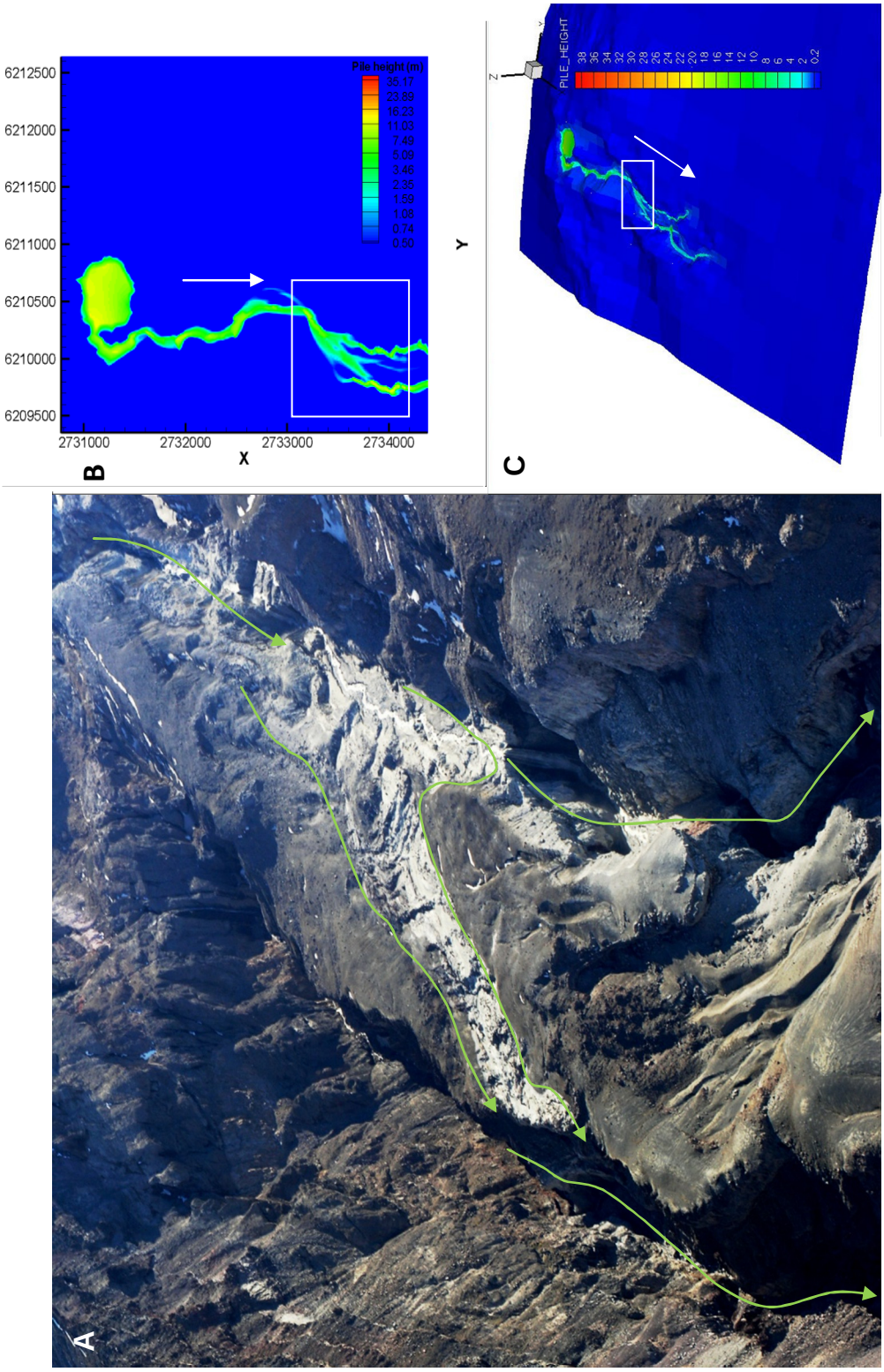

event, probably due to the modelled volumes in these reaches being higher than the volumes of the actual lahar that was still bulking up (Procter et al., in press). The modelled inundation areas were higher (by 70%) and showed occupation of a number of <20 m-long areas of channel avulsion that were not observed in the real event. These modelled features may be due to both the high initial volumes of the simulations and the relatively coarse resolution (5 m) of the DEM in relation to the narrow channel.

3.5.3. 5-7 km –Convergence and Ponding – Round the Mountain Track

From 5 km, at the point of bifurcated flow convergence, a strong decrease in slope occurs from 20° to 6° and the channel widens from 10 to 50 m. By this point, net erosion calculations indicated that the March 2007 flow had bulked to its maximum sediment content, achieving a total volume around 3 times that of the original lake breakout (Procter et al., in press). Despite the similarity of modelled and real flow volumes at this point, the simulations showed a greater area of inundation by up to 60% for this 2 km reach (fig. 3.5). At 5 km the lahar peak wetted area indicated a flow up to 10 m high while the Titan2D simulated a peak flowing height of 13 m (fig. 3.5 & 3.6).

At the 7 km mark a monitoring site had been installed that contained a radar stage gauge, broadband seismometer, AFM, and pore pressure meter (Manville and Cronin, 2007). Peak flow of the March event occurred at 11 min 52 s after the breakout, with a calculated average velocity of 9.4 m/s, and peak flow depth of 8.1 m. Observations and seismic records imply that the flow was turbulent throughout, with highest

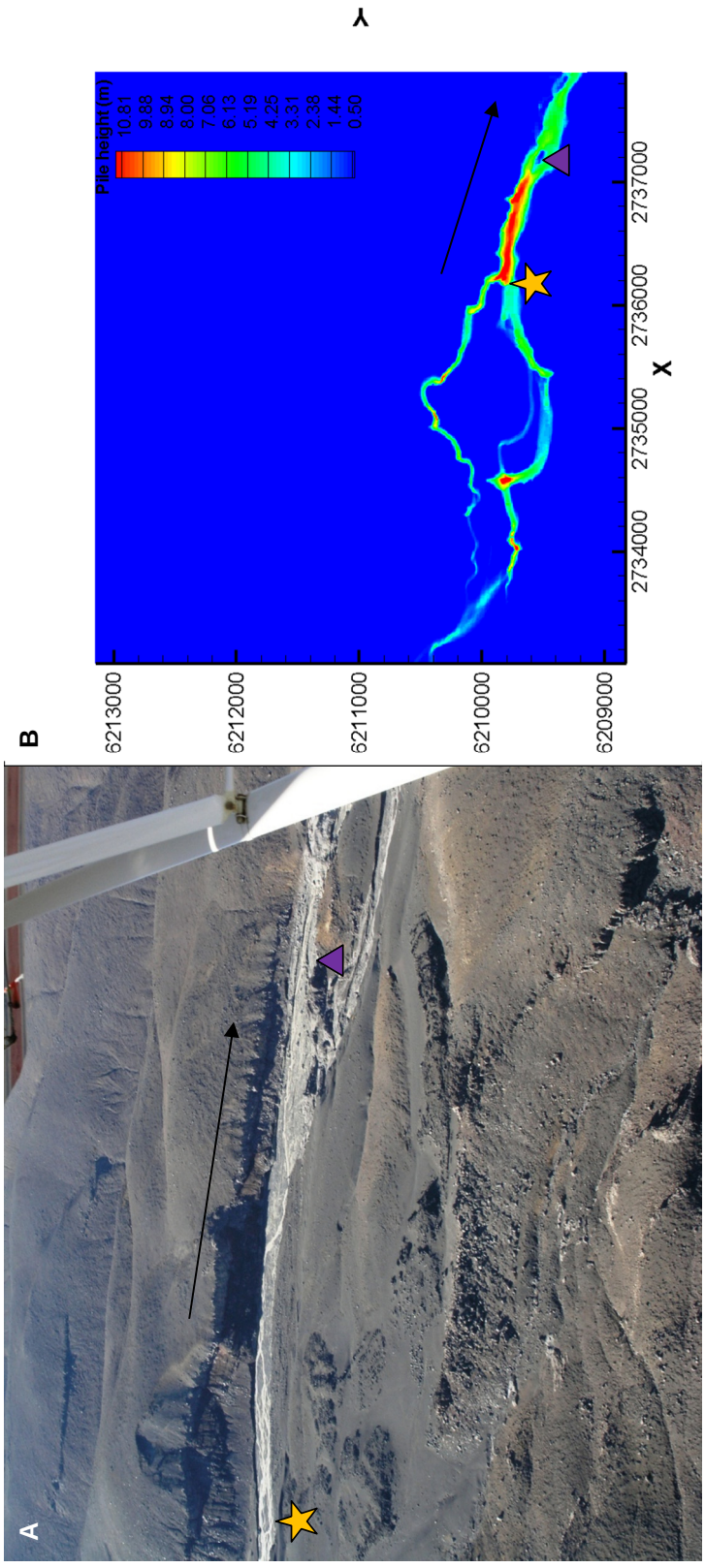

Figure 3-5. 5 – 6 km from source at the Round the Mountain Track (RTMT) with the star indicating the start of an area of ponding of the flow and deposition. The triangle marker identifies the location of a lahar monitoring station arrow marks flow direction; A) Photograph of site; B) Titan2D simulation for that stretch of river.

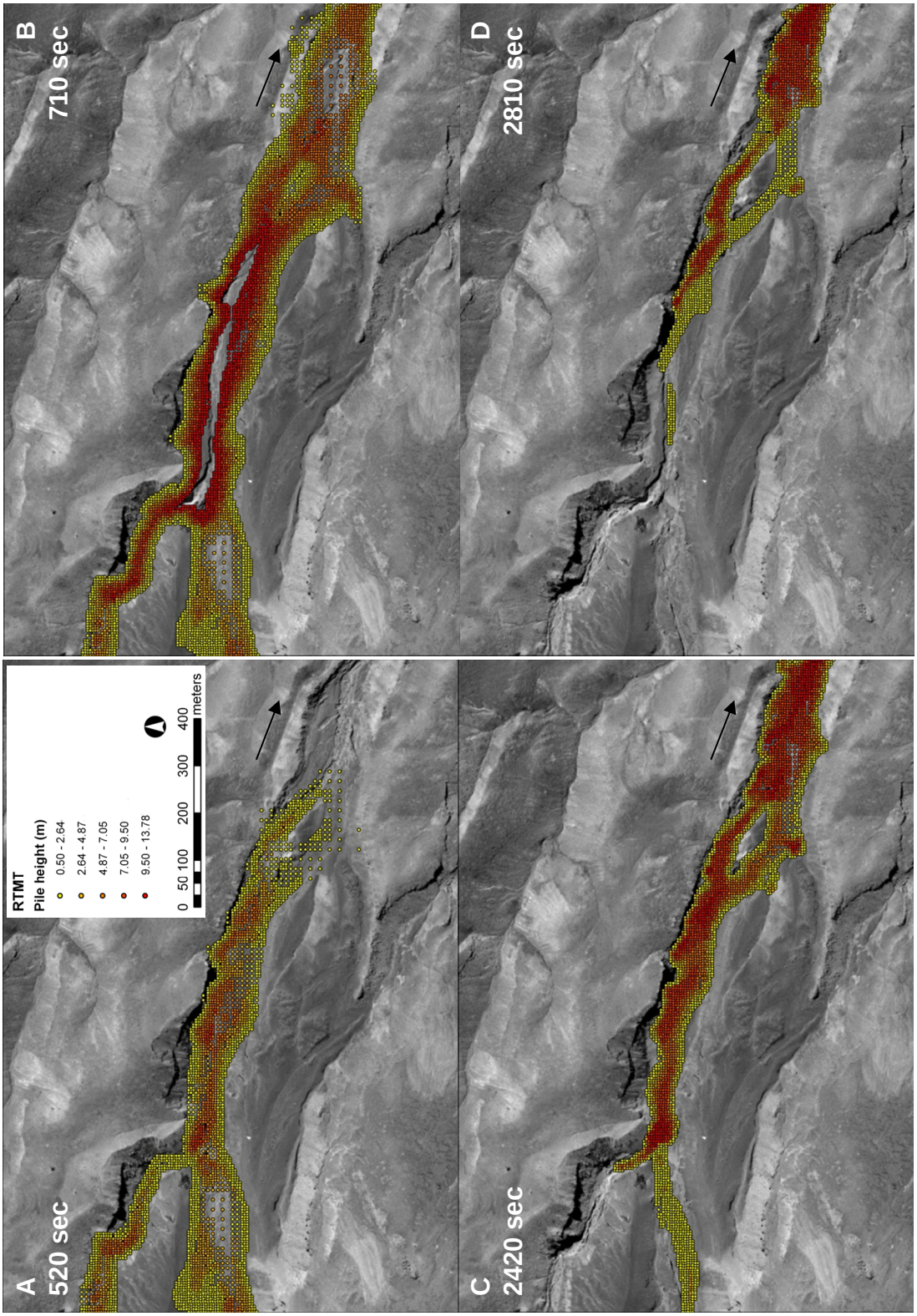

Figure 3-6. A – D represents the Titan2D passage of the simulation of the mass flow height through the 5 – 6 km stretch of river with the timestamp of outputted simulation iteration inset. Arrow indicates flow direction.

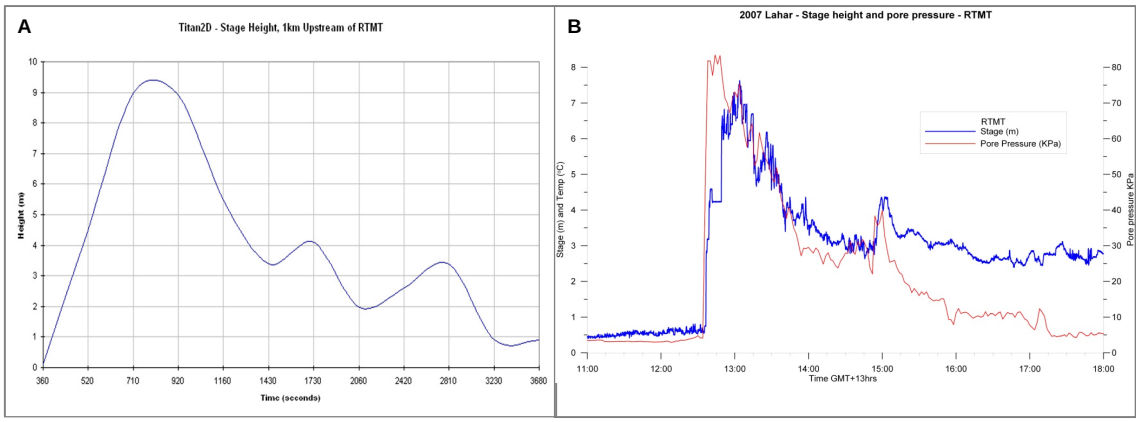

Figure 3-7. Comparison of A) the Titan2D calculated stage height from the (6km from source) lahar monitoring station and B). the recorded stage height and pore pressure stage height from the monitoring station.

sediment concentrations following the peak (Maniville and Cronin., 2007). Calculated peak discharge at this point was c. 2250 m^3/s. Both stage height and pore pressure data indicate that a period of hydraulic ponding occurred at this site of flow constriction for possibly the first 38 min of flow (fig. 3.7).

Titan2D simulations showed arrival at the site around 13 min after onset with an average travel velocity of 8.8 m/s. The simulated peak velocity at the station site was 5.7 m/s. The peak simulated flow depth was between 7-9 m (fig. 3.6). Animation of the simulations displayed 3 peaks in stage height, an initial peak with two smaller peaks (4 m and 3.5 m) that arrived at 28 min and 46 min from onset. This behaviour broadly mimicked the measured hydrograph of this site (fig. 3.7).

The Titan2D simulations compared well to the real event, and surprisingly matched the observed hydrograph at 7 km. Peaks and pulses within the flow have been recognised

in other lahars (e.g., Mt. Pinatubo, Philippines, Scott et al., 1996; Pierson, 2005b) yet the process behind this phenomenon is unclear. For the 2007 Ruapehu lahar it could be attributed to either a variation in the release of material from the Crater Lake breakout, or from variation and bifurcation in the flow path. The simulated variations could be related to feeding variations from the Crater Lake basin as the feeding pile sloshes backwards and forwards in the basin before flowing out, or also due to variations in flow path due to flow bifurcation. The Titan2D simulations also allowed plotting of changes of simulated flow over time, showing it migrating from the true-right to the true-left, which surprisingly mimicked the behaviour of the real flow, which migrated to the true left due to deposition of boulder deposits along the right side (fig. 3.6). The Titan2D model does not simulate deposition or channel bed changes, hence this appears to be only a coincidence.

Unfortunately it is extremely difficult to compare discharge (volumetric flux) between the simulations and the actual flow. Discharge is commonly used to estimate the hazard potential for floods and lahars (Scott et al., 2001; Lavigne and Suva, 2004) and is often an aim for calculation at hydrological instrumentation sites. There are problems in calculating this in nature, due to variations in bed level during lahar flow and difficulties in directly measuring the bulk material flow velocity. Titan2D records x and y momentum for each computational cell using the conservation of momentum and Coulomb equations and the average velocity for every output iteration, hence discharge at any single cross section cannot be reliably calculated.

3.5.4. 7-9km – Bifurcation – The Chute

At approximately the 8 km mark a portion of the lahar entered into an overflow channel referred to in the past as the "Chute". Lahars in 1975 (Purves, 1990), LH 4c in 1995 (Cronin et al., 1997a & b) and the March 2007 flow overflowed at this point, which feeds into a straight and hydraulically smooth channel before spilling out onto the southern Whangaehu Fan c. 5 km later. Titan2D simulates this bifurcation with highest flow depths in the area of 3-5 m compared to the actual ~3 m (fig. 3.8). The simulation suggests that there was some hydraulic ponding immediately upstream of the bifurcation, which if occurring in the actual flow may have triggered deposition and possible forcing of overflow into the Chute. Overflow of a proportion of lahar flow into the Chute may limit the maximum discharge at crucial structures and overflow points between 10-15 km in the main channel and may also influence the flow wave form farther from source once the two-subpaths recombined.

3.5.5. 9 km – Flow attenuation - Bund

At 9 km from source, the apex of the Whangaehu Fan has been a focus of hazard assessments since 1995 when the potential for avulsion of flows northward into the highly vulnerable Tongariro catchment was recognised (Keys and Green, 2008). An earth training dike or bund was constructed to protect this catchment by confining and directing flows into the normal lahar path to the south. This isolated area has no monitoring or measurement equipment. Inundation areas forecast by the Titan2D simulations are extremely similar to the actual inundation. The 18 March 2007 lahar took 18-20 min to reach this site, implying an average flow front velocity of 7.5-8.3 m/s. A peak flow velocity immediately upstream of the site, estimated by super-elevation (Apmann, 1973), was between 7-8 m/s. Alongside the bund, the peak flow depth was 5 m. The Titan2D simulations had average velocities of 5.9 m/s, peak flow

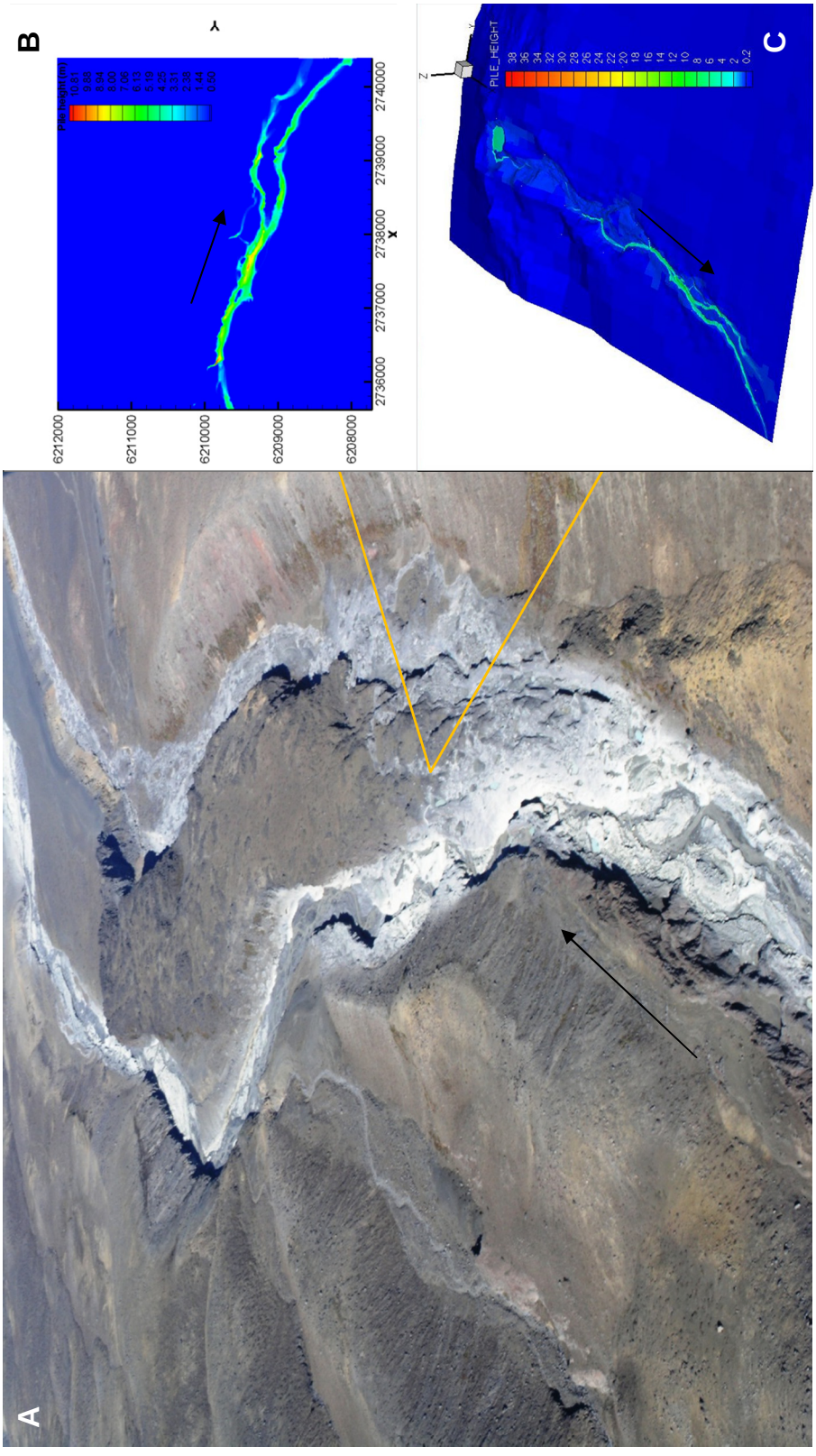

Figure 3-8. The Chute ~7 km from source, black arrows indicate flow direction. A) Photograph of site with the white mud coated surfaces indicating the peak inundation areas and flow direction; B) Titan2D plot of the simulated flow showing the same bifurcation of flow; C) 3D view of the Titan2D simulation at the same site.

depths of 5-6 m and a travel time for the peak flow to reach this site of 18 min (fig. 3.9).

Under normal flow conditions the wetted area is confined to a single, sinuous stream within a broad (130 m wide) channel containing large boulders and gravel/boulder bars. Following the March 2007 lahar the channel was entirely modified to form a braided channel bed. At this point, earlier studies imply that Ruapehu lahars are fully bulked (Pierson, 2002), probably displaying a debris flow rheology with a volume 3-5 times the original breakout, through incorporation of unconsolidated material along the channel (Procter et al., in press). Beyond this point the flow was expected to transform via deposition into a hyperconcentrated flow as occurred during 1995 examples (Cronin et al., 2000). Titan2D cannot simulate the flow past this point because with the computer power available, the adaptive mesh was not able to increase resolution enough for the flow to realistically propagate across the broad flat terrain. The fan also corresponds to a dramatic change in slope that generates major changes in flow rheology (Cronin et al., 2000), while the properties of the Titan2D simulated flow did not change. Similarly, the Delft3D model was unable to simulate the sudden changes in flow properties and/or rheology occurring over long runout distances (c.f., Carrivick et al., 2009).

3.6. Discussion

Titan2D simulations were able to reproduce the actual inundation area (>0.5 m) of the March 2007 lahar with c. 7-200% difference; however, this comparison is limited

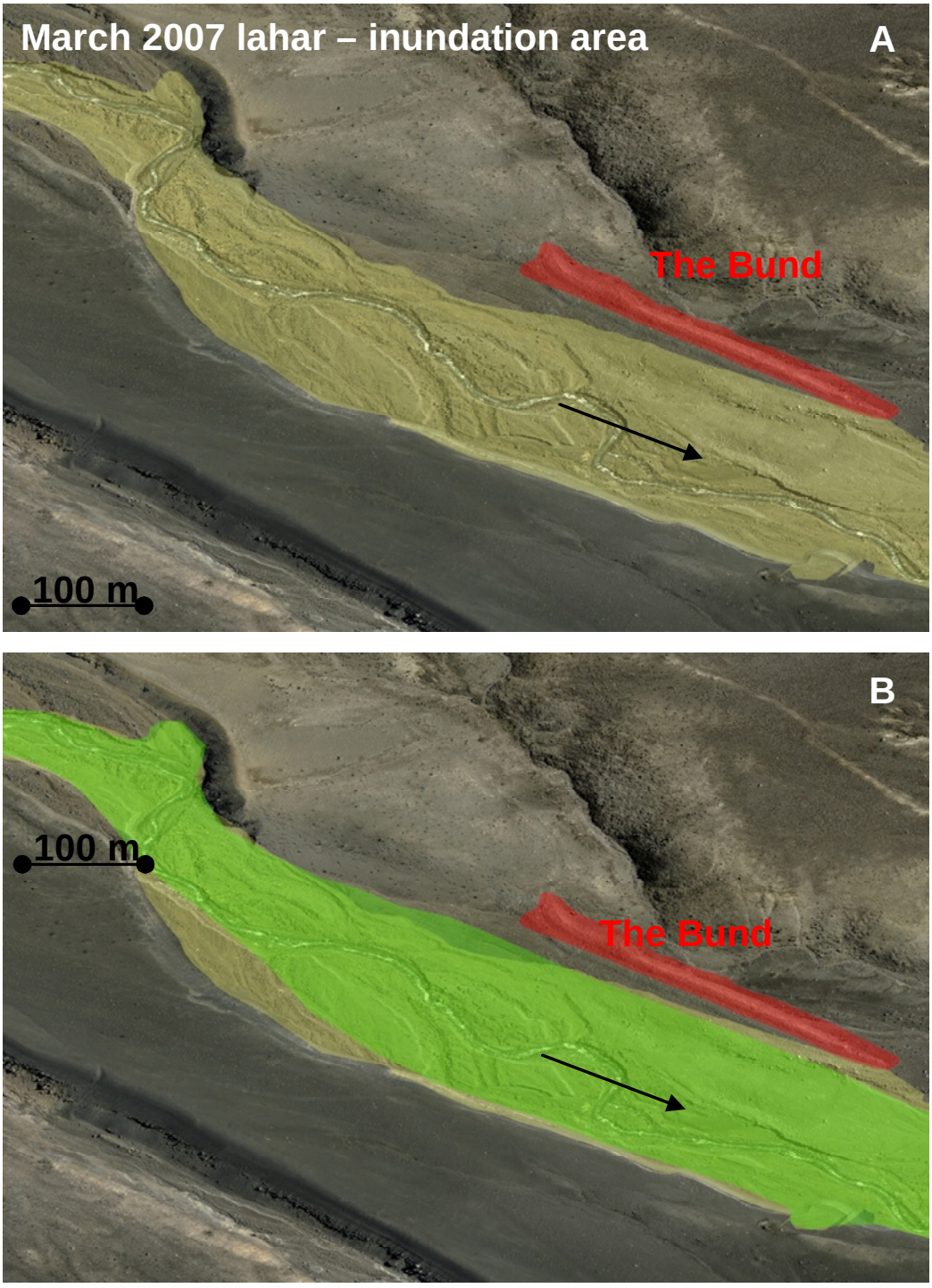

Figure 3-9. The bund ~9 km from source. Inundation area mapped of A) the 2007 lahar and B) Titan2D simulated inundation area overlayed. Note the bund highlighted in red and arrows indicate flow direction.

by comparing lahar inundation data measured (or digitised) at a 10-cm scale while the flow simulation is measured on a 20 m DEM (table 3.1). The arrival times of simulations varied 5-75% from actual flow front travel times (table 3.1). At specific sites simulated flow passage and real data match closely, particularly flow height/pile height. These parameters are easily determined from surveying the lahar channel and tide lines, and can be directly derived from Titan2D's output files. However, care must be taken in comparing these parameters, particularly since in real-world flows, the bed level of many channel reaches may rapidly deepen via erosion and/or shallow by deposition, impacting on the height of flow surface and hence inundation area. Repeated erosion and deposition cycles may occur throughout the passage of a lahar in any one location (Procter et al., in press).

Several other features of the Titan2D simulations reproduced many of the physical processes commonly observed in debris flows. As the simulated flow descended the steep and sinuous upper channel, it not only super-elevated around major channel bends, but it also generated a resulting surging and pulsing flow behaviour. These pulses and surges are observed particularly well on animations of the flow and in flow surface "snapshots" over the upper reaches and have wavelengths of between 150-300 m. These phenomena are similar to the observation of roll waves (Takahashi, 1981), although it is not certain that the models are actually capturing the physics of these empirically observed waves. Titan2D simulated flows exiting Crater Lake were constricted at a point c. 500 m from source following initial passage of the flow "head". Thus the head material of the flow could accelerate away from following material. This process repeated itself 2-3 times, generating successively smaller "pulses" of flow with wavelengths of between c. 3-5 km in the upper channel (periods of >300-500 s). Such pulses or packets of flow are often observed in areas where rain-triggered lahars are monitored (Doyle et al., in review) where they reflect either variable source areas of

flow generation or hydraulic ponding and segregation of flow. Either way, this apparent similarity between flow and model may not necessarily indicate a physical process in common.

3.6.1. Titan2D as a lahar simulation tool

Titan2D is a simulation tool that can be applied for many applications by the average computer user on a typical desktop computer (table 3.2). The only trade-off is that with lower computing power, there are fewer levels of complexity to which the adaptive grid may extend. This, in-turn, limits the effectiveness of models run over long distances with only desk-top computational power. The geomorphology of Mt. Ruapehu is particularly difficult in this respect, particularly when simulations are started from the Crater Lake basin area. In this case, it takes a long period before all starting materials have drained from the basin, leading to development of a leading portion of flow with dregs remaining in the basin. Despite these lagging materials not being significant for determining flow properties, their “sloshing” in the source area ties up computational time and grid resolution at the expense of resources at the flow front area.

Major slope breaks appear to be a significant problem in the running of Titan2D models, since these generate rapid deceleration and cessation of flow. This is probably due to the model being primarily based upon simulation of dry granular flow for its solid component.

Table 3-2. Summary table of the key features of Titan2D from this study highlighting issues of computer simulation of mass flows with comments for hazard planners and model developers.

Feature	Positive	Negative	Hazard analysis comments	Model developer challenges
Simulation of the first 10 km of lahar travel	Defines the flow path of a fully sediment laden debris flow.	Difficulties in simulating past the 10 km point due to sudden slope break and attenuation across a sedimentary fan.	Limited by the fact that a lahar over an entire catchment cannot be simulated in a single run. Requires supercomputing or dividing the flow into individual sections.	The adaptation of changing flow rheology to changing channel conditions needs to be developed.
Simulation across natural terrain	Simulations are sensitive to many of the small topographical changes that affect the flow and produce accurate travel times beyond 5 km.	Titan2D cannot simulate a situation where flow is deviated due to syn-lahar channel aggradation or bed modification.	For a sequence of lahars changing channel conditions must be anticipated and DEMs should be adjusted accordingly.	The incorporation of a changing terrain via erosion or deposition needs to be recognised.
Adaptive Grid	Defines a propagating flow across a natural terrain. Efficient use of computation power and time.	Long runout flows result in the computational grid retaining some complexity still at the tail of flow or in source areas, diminishing concentration of the propagating flow front.	Allows for a rapid simulation on a natural terrain without any modification or simplification.	The flow front characteristics need to be better characterised and adaptive grid complexity in tail regions of flow should be reduced.
Incorporation of proportions of sediment/water components	Simulates one set of respective components from source providing a combined inundation area and stage height.	Titan2D does not simulate erosion or deposition; therefore cannot simulate the bulking and de-bulking flow and resulting changing rheology.	While utilising a mass flow numerical basis (rather than fluid flow) there are still limitations on replicating a debris flow that goes through transition to hyperconcentrated flow.	Ability to model incorporation and deposition, as well as resulting variability in rheology need to be built into the numerical model.
Outputs files in a variety of formats containing numerous fields of data	Files contain pile height and momentum data.	Does not contain velocity data yet requires further analysis to determine this and mass flux at a point .	Traditional factors of lahar hazard parameters such as discharge and velocity require some further analysis interpretation.	Recognition that a hazard analysis tool requires specific outputs and data for specific users.
Source pile initiation	Simulates a mass flowing from source.	Can only simulate a mass collapsing and flowing from collapse under gravity.	There are limitations to scenarios modelled due to variable initiation.	More user-variable initiating criteria, such as hydrograph input, need to be developed.
Replicates some rheological conditions	Feature such as ponding and bifurcation occur in response of the flow to changing terrain conditions.	Changes in rheology from variable sediment loads cannot be simulated.	Unexpected variations between a real flow and simulated flow may occur.	Erosion and deposition of sediment needs to be incorporated.
Visualisation and animations	Output files based on computational iterations can be easily viewed and analysed.	Further conversion and data reorganisation for analysis in a GIS is required.	Further analysis requires time and methods that account for inherent uncertainties.	Recognition that for a rapid response, hazard outputs need to be easily converted for specific viewing or mapping software

In the case of hazard assessment, the applicability of any flow/flood simulation is dependent on the ease with which its outputs and the information contained can be viewed and analysed. Titan2D has a variety of outputs (grass GIS, HDF, Tecplot PLT, TitanViewer text) that may be used in most animation applications for viewing dynamic features and GIS packages for detailed analysis of inundation, depth and changes over time.

The primary limitation of Titan2D for modelling hazard of lahars is its inability to replicate erosion or deposition, including any variation in topography relating to this and any resulting changes in flow rheology. Titan2D can also not be used to determine parameters such as bed shear stress or basal friction that could be used as a proxy of erosion or deposition at any location. One of the most unique features of lahars is their ability to change rheology by erosion and deposition of material along their paths, even transforming repeatedly between hyperconcentrated flow and debris flow along their course (Pierson and Scott, 1985; Procter et al., in press). At Ruapehu, this transformation was mostly recognised beyond 10 km from source where debris flows leave the volcanic cone and attenuate by thinning and depositing across the volcaniclastic fan (Cronin et al., 2000; Manville, 2004). Titan2D cannot simulate this transformation because the abrupt change in slope causes the simulated flows to stall and terminate.

3.6.2. Parameter Comparison

The comparison of lahar events to computer simulations can be a challenge, particularly since there are few opportunities to capture data from unexpected lahar events. The primary descriptive measures from real-world flows are flow-surface

height (in relation to some fixed datum or a fixed bed), maximum surface velocity and occasionally discharge and flow density (sediment concentration). Post-event data readily captured include maximum inundation areas (tide-lines), super-elevation around bends and on obstacles in flow path, changes in channel form/depth and measures of erosion and deposition. In computer flow simulations factors including inundation area and run-out length are typically dependent on the definition of stopping criteria, such as simulated time, minimum thickness thresholds, or computational steps (c.f., Iverson, 1997a; Denlinger and Iverson, 2001; Pudasaini and Hutter 2003). Sheridan et al. (2005) used velocity, run-out and stage height to compare the effectives of Titan2D simulations to real-world data.

3.7. Conclusion

As a simulation tool Titan2D predicted the flow path and inundation area of 18 March 2007 break-out lahar with high overall accuracy. The simulation was able to reproduce number of characteristics of the flow:

- The flow of mass from a stationary pile out through the forecast dam break-out area,
- Simulation of pulses of material developed via flow constriction and channel path sinuosity,
- Simulation of short-period flow unsteadiness and features similar to roll-waves
- Bifurcation and flow avulsion,

- Super-elevation around bends,
- Hydraulic ponding leading to avulsion,
- Forecasting of travel times within 5-75% precision.
- Forecasting of flow depths and inundation with 7-200% precision.

As hazard analysis tools, computer simulations require the user to not only have an understanding of the results produced by the code but an appreciation of the suitability of the tool to the type of flow as well as all the uncertainties associated with the mathematical relationships used as well as those associated with (table 3.2). All computers models need to be used and analysed with rigorous evaluation before being applied for hazard analysis.

CHAPTER 4

Landscape and Sedimentary Response to Catastrophic Debris Avalanches, Western Taranaki, New Zealand.

J.N. Procter, S. J. Cronin[1], A.V. Zernack[1]

1. Institute of Natural Resources, Massey University, Private Bag 11 222, Palmerston North, NZ.

Abstract

Catastrophic volcanic debris avalanches reshape volcanic edifices with up to half of pre-collapse cone volumes being removed. Deposition from this debris avalanche deposit often fills and inundates the surrounding landscape and may permanently change the distribution of drainage networks. On the weakly-incised Mt. Taranaki ring plain, volcanic debris avalanche deposits typically form large, wedge-shaped (in plan view), flat-lying fans. Following volcanic debris avalanches, a period of intense re-sedimentation commonly begins on ring-plain areas, particularly in wet or temperate climates. This is exacerbated by large areas of denuded landscape, ongoing instability in the scarp/source region, damming of river/stream systems, and in some cases inherent instability of the volcanic debris avalanche deposits. In addition, on Mt. Taranaki, the collapse of a segment of the cone by volcanic debris avalanche often generates long periods of renewed volcanism, generating large volumes of juvenile

tephra onto unstable and un-vegetated slopes, or construction of new domes with associated rock falls and block-and-ash flows. The distal ring-plain impact from these post-debris avalanche conditions and processes is primarily accumulation of long-runout debris flow and hyperconcentrated flow deposits with a variety of lithologies and sedimentary character. Common to these post-debris avalanche units is evidence for high-water-content flows that are typically non-cohesive. Hence sedimentary variations in these units are high in lateral and longitudinal exposure in relation to local topography. The post-collapse deposits flank large-scale fans and hence similar lithological and chronological sequences can form on widely disparate sectors of the ring plain. These deposits on Mt. Taranaki provide a record of landscape response and ring plain evolution in three stages that divide the currently identified Warea Formation: 1. the deposition of broad fans of material adjacent to the debris avalanche unit; 2. channel formation and erosion of stage 1 deposits, primarily at the contact between debris avalanche deposits and the stage 1 deposits, and the refilling of these channels; 3. the development of broad tabular sheet flows on top of the debris avalanche, leaving sediments between debris avalanche mounds. After a volcanic debris avalanche, these processes represent an ever changing and evolving hazard-scape with hazard maps needing to be regularly updated to take account of which stage the sedimentary system is in.

4.1. Introduction

Water-mass flows from volcanoes (lahars) can either be syn- or post-eruptive, with numerous modes of generation (Vallance, 2000). Their widespread hazard in very large areas downstream of volcanic activity has also been well recognised worldwide such as in: Indonesia (Lavigne et al., 2000; Thouret et al., 2007); Alaska (Waythomas et

al., 2000); Pinatubo in the Philippines (Rodolfo, 1989; Janda et al., 1997); Nevado del Ruiz in Columbia (Pierson et al., 1990); and Ruapehu in New Zealand (Cronin et al., 1997a & b). The generation of large-volume lahars after catastrophic ignimbrite eruptions has also been recognised, such as in relation to the 26.5 ka Oruanui Ignimbrite (Manville and Wilson, 2004) and the 12 900 yr B.P. Laacher See eruption (Schmincke et al., 1999). Segschneider et al. (2002) also highlight that lahars are formed during the process of re-establishing hydrologic networks in distal drainages after landscape-filling ignimbrite eruptions, such as the 1.8 ka B.P. Taupo eruption. These examples focus on the re-establishment of previous drainage networks from events that were confined to, and filled, existing channels. Due to their origin (mostly from dam-breakouts) and pumice lithologies, lahars formed in these situations normally only span a narrow part of the rheological spectrum, i.e., the more water-rich end members. By contrast to ignimbrite examples, very few studies have examined the response of the landscape, the post-event lahars, and the alteration of drainage patterns after a large unconfined debris avalanche event.

Volcanic debris avalanches also generate a strong disequilibrium in the landscape and probably also alter the subsequent hazard-scape. Thouret (2004) refers to these phenomena as a geomorphic hazard; however, the processes behind the creation of this hazard are poorly recognised. Following the 1980 Mt. St. Helens eruption and debris avalanche, lahars were triggered by melting of snow and ice from pyroclastic flows and surges, high rainfall and glacial outburst floods (Major, 2003). In this case, the volcanic debris avalanche deposition within a large valley system meant that drainage patterns redeveloped more or less in the same location as previously, by eroding through the volcanic debris avalanche deposits. Initially this process caused very high sedimentation rates due to the increase in available erodible material and an increase in drainage area (Major, 2004). The majority of sediment was transported in

an increased frequency of short bursts or floods (transporting 10-100 times more sediment than pre-1980) over the 20+ years after the event (Major, 2004). These impacts were focused into one or two major catchments, hence the situation following large-scale fan-deposited debris avalanches is not well constrained.

In parallel with landscape-readjustment studies, research into prehistoric lahar events (Scott, 1985, 1988a & 1988b; Pierson, 1997; Vallance et al., 2003) provide examples of how the identification of deposits and stratigraphy can provide valuable insights into the hazards related to these events. The analysis of ring plain stratigraphy and lahar identification at Ruapehu Volcano, New Zealand (Cronin and Neall, 1997; Lecointre et al., 1998; Donoghue and Neall, 2001) provides a detailed description of past landscape construction and insights into future hazardous events. These studies highlight the importance of lahars and their deposits in altering the landscape. However, the holistic relationship between catastrophic debris avalanche events and lahar generation and frequency has not yet been addressed.

The volume of the ring plain of volcaniclastic deposits surrounding the andesitic Mt. Taranaki (2518 m) in western North Island, New Zealand (fig. 4.1) is up to 10-times that of the current upper edifice. This sedimentary record comprises a distinctive repeating sequence of lithofacies implying cyclic growth and destruction of the Mt. Taranaki edifice (Neall et al., 1986; Palmer et al., 1991; Zernack et al., 2009). This cycle includes long periods between major debris-avalanche collapses, when long run-out mass flows occur, forming volumetrically important and widespread deposits. The processes that formed these depositional packages, factors controlling their distribution, and their implications for the development and evolution of ring-plain landscapes are examined here. These units contrast with recent (<1000 yrs)

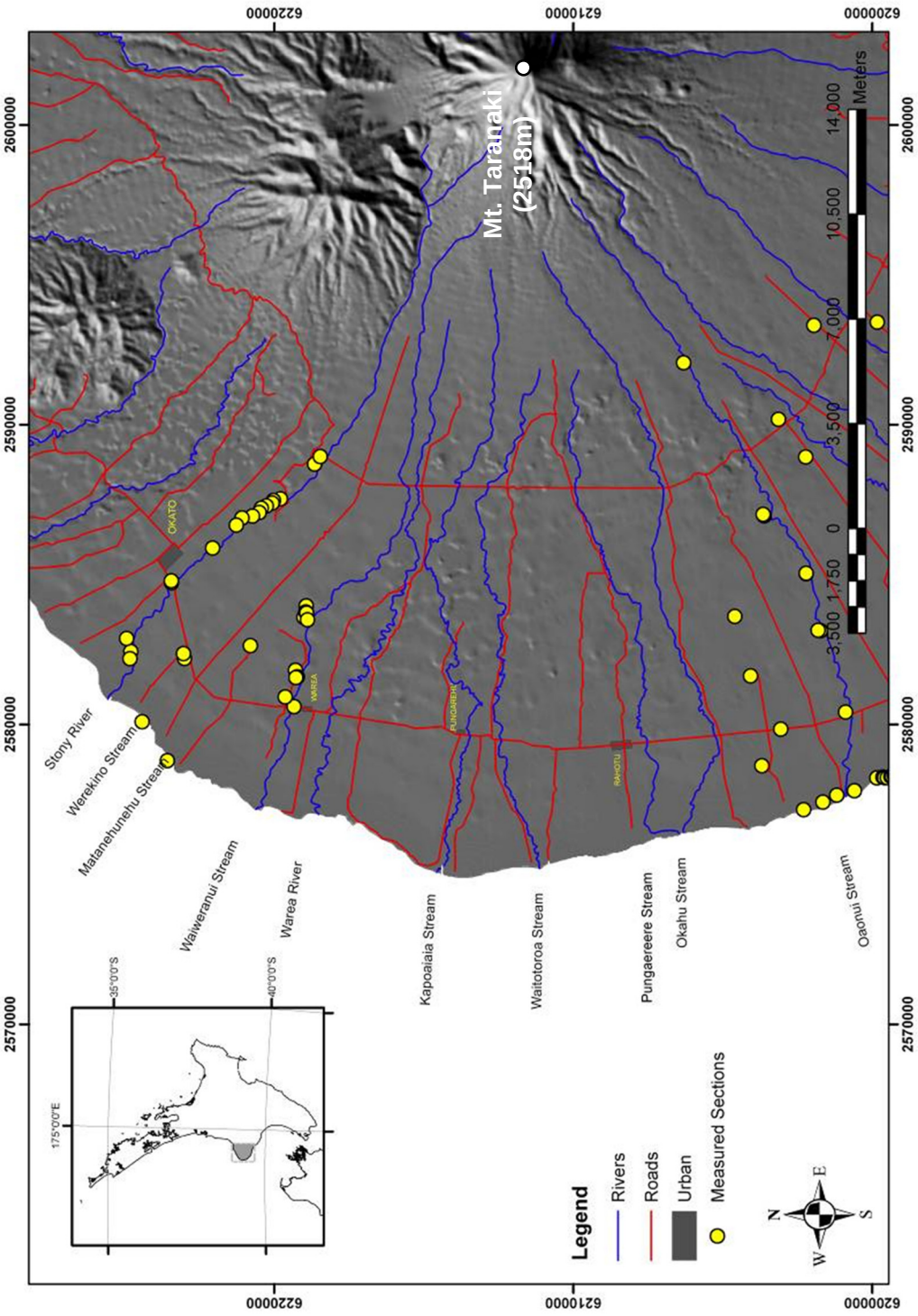

Figure 4-1. Location map, showing the western portion of the Taranaki region and volcano ringplain. Spots represent locations of described exposures.

volcaniclastic sedimentation surrounding Mt. Taranaki, which dominantly represents stream-flow reworking of dome-collapse related block-and-ash flow deposits (Neall, 1979). The source block-and-ash-flow deposits were confined to within 15 km of their parent summit dome, and result from small-scale eruptions (Platz et al., 2007). Lahars over this recent period appear to have been all low-volume events (<2 x 10^6 m^3) that were strongly confined to a few discrete channels around the volcano (Neall, 1979). Earlier episodes of lahars, the Warea Formation (Neall, 1979) which immediately followed volcanic debris avalanche emplacement, appear to have been one to two orders of magnitude larger in volume (Neall, 1979). The processes leading to this can be identified. The factors relating to edifice and landscape stability are not solely related to different magnitudes of eruptive activity in the past but are more significantly related to changing geomorphic processes. Recognition of such large-scale lahars and defining the conditions under which they form is an extremely important component of volcanic hazard assessment for any re-awakening volcano. The Warea Formation is investigated in terms of a modern volcano-sedimentological approach, and conclusions for sedimentary response are drawn from observed sedimentologic characteristics.

4.2. Geological setting: Mt. Taranaki/Egmont Volcano and ring plain

Mt Taranaki/Egmont (2518 m) is the youngest and most southerly of the Taranaki Quaternary volcanic succession (Neall et al., 1986). It has been active for at least 130 000 years, although the present cone (above c. 1200 m) is <10 000 years old. The cone comprises alternating layers of pyroxene-andesite and hornblende-andesite lavas and

fragmental volcanic deposits including tephra fall units, scoria-rich pyroclastic flow deposits and juvenile-lithic-rich block-and-ash flow deposits. Deep radiating valleys have formed on the middle-lower flanks of the cone feeding major separate catchments (fig. 4.3) that spill out onto a series of coalescing fans (the ring plain). Exposures in these streams and rivers on the ringplain were examined in this study to determine the types of unconsolidated volcaniclastic deposits present. Where possible, organic material and/or soils were collected for radiocarbon dating. Sediment samples (representative of lahar deposits) were also collected to further characterise properties indicative of parent flow rheology.

The Taranaki ring plain is dominated in western and southern parts by debris avalanche deposits, which provide a most dramatic volcanic landscape feature of large conical hills or mounds dominating the landscape (Neall, 1979, Ui et al., 1986, Palmer and Neall 1991, Alloway et al., 2005). Intercalated between these deposits are numerous smaller confined volcaniclastic diamicton sequences representing a series of more-confined lahar deposition systems. Neall (1979) identified five “laharic breccia” Formations as chronostratigraphic units within the last 140 000 years of the ring plain record. Of these units, the Warea (13-22 500 yrs.) and Kahui (7 000-13 000 yrs.) Formations radiate from several separate and apparently unrelated catchments on the massif and occupy numerous drainage systems (fig. 4.2). By contrast, other laharic formations occupy only single, confined sectors of the ringplain, representing coherent areas of active inundation during their respective time periods. The ring plain relief is dominated by the upper surfaces of volcanic debris avalanche deposits (e.g., Ui et al., 1986) and the major drainage channels exhibit only minor incision (<20 m).

4.2.1. Warea Formation

The Warea Formation (fig. 4.2) type area lies between the township of Warea and the Stony River in western Taranaki. The deposit forms large flat surfaces, intricately dispersed between and around the mounds of the older, underlying debris avalanche deposits. The unique characteristics of this intercalating deposit include its unusually strong lithification, its scoria-rich nature and the presence of radially fractured, breadcrusted volcanic bombs of +30 cm diameter. In addition to this location, Neall and Alloway (2004) identified a number of other similar deposit lobes originating from the cone in every major catchment and grouped them as a single chronostratigraphic unit emplaced in the interval 13 000-22 500 years B.P. Neall (1972) provides the only published account of possible generation and mode of emplacement for these deposits; that is, formation of lahars following major flank collapses with an accompanying supply of water, possibly from a crater-lake outbreak.

Field investigations of the Warea Formation breccias, laharic conglomerates and sandstones reported here were used to discriminate individual packets of deposits, constrain their periods of accumulation and determine their sources. The aims of this investigation were to examine the relationship between deposits emplaced in widely differing sectors of the volcano, infer the types of mass-flow processes that were active, and fit these units within the context of the overall development of the ring plain in response to known large-scale catastrophic events.

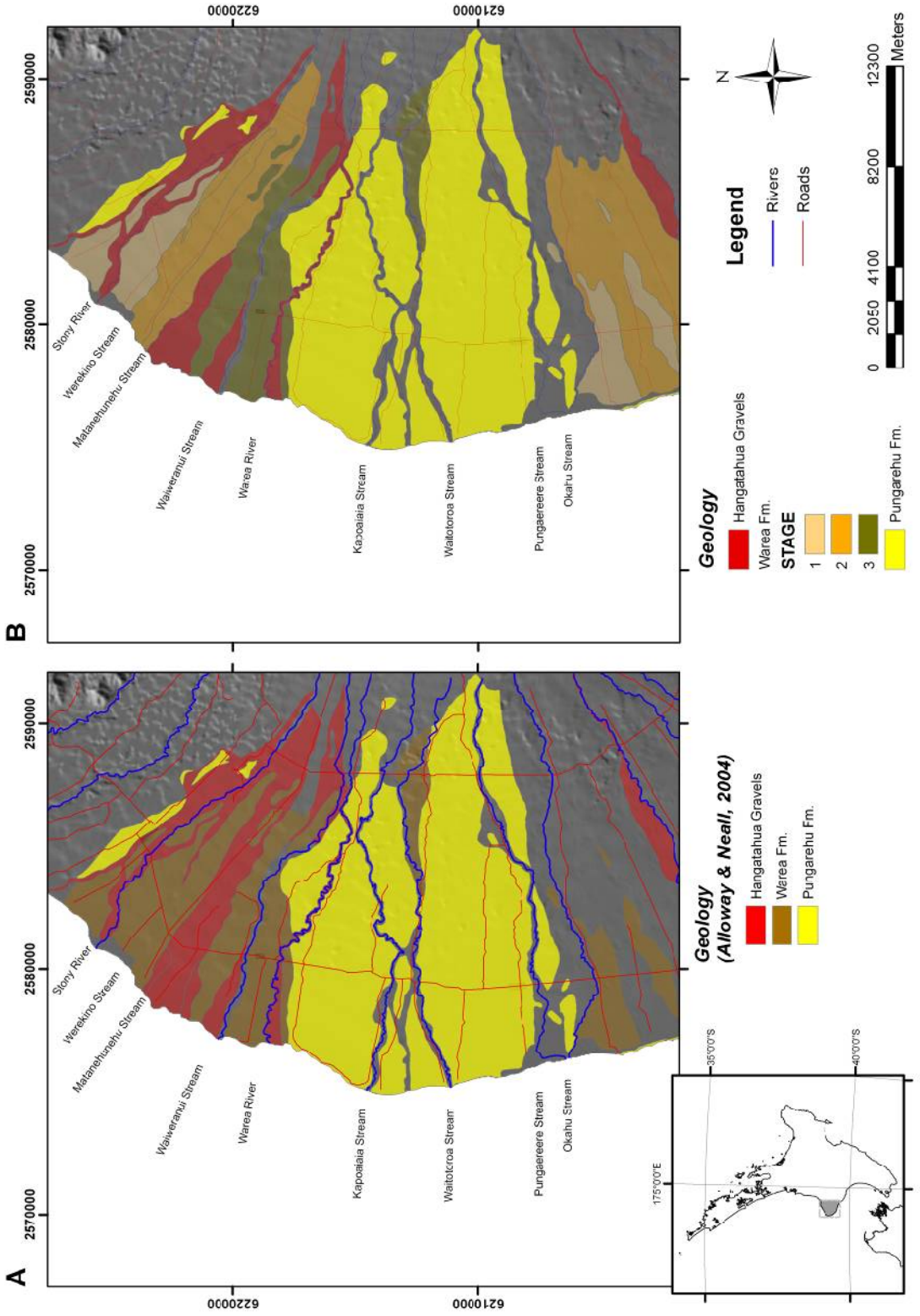

Figure 4-2. Geologic map of the western part of the Taranaki ringplain. Map A) Previous geology from Neall and Alloway (2004) with the three main chronostratigraphic units of the Pungarehu Fm. (central facies, debris flow facies), the Warea Fm. (adjacent to the lateral extents of the Pungarehu Fm.) and the Hangatahua Gravels (recent flood deposits), inundating present drainages). Map B) The revised geology from this study highlighting the progressive inundation of the lateral areas around the Pungarehu Fm. in three stages contained within the Warea Fm. from Neall and Alloway (2004).

4.3. Nomenclature

Mt. Taranaki diamicton units have been categorised as either lahar or debris avalanche deposits. They have similar textural characteristics (comparable fine-grained matrix containing fragmental clasts), but differing morphologies and distribution patterns. Debris avalanche deposits also contain mega-clasts (Neall, 1979, Palmer et al. 1991; Scott et al., 2001); i.e., single definable fragments of lithologically or stratigraphically coherent material as well as common *in situ* fractured clasts. Lahars are defined as "a rapidly flowing mixture of rock debris and water (other than normal stream flow) from a volcano" (Smith and Fritz, 1989). The term is then applied in general to flows with a range in sediment concentrations and rheologies. Lahars can be primary (syn-eruptive) or secondary (post-eruptive) (Vallance, 2000; Thouret, 2004) yet both types require an available source of unconsolidated material and water. Scott et al. (2001) distinguishes cohesive (clay rich, >3-5%) from non-cohesive (clay poor, <3-5%) flows that have very differing properties. The former are often derived from debris avalanche deposits and show little variation with distance (Vallance and Scott, 1997), while the latter go through a range of transformations relating to entrainment or loss of sediment along their paths (e.g. Cronin et al., 1999). Pierson and Costa (1987) and Pierson (2005b) classified the range of subaerial sediment-water flow types within lahars based upon their rheologic behaviour, particularly deformation rate, sediment transport mechanism, and sediment concentration/grainsize. This classification ranges through; debris avalanche/grain flow ("dry"), debris flow (very high yield strength, laminar flow and >75% sediment concentration), hyperconcentrated flow (onset of measurable yield strength, dampened turbulent flow, c. 20-60% sediment; after Beverage and Culbertson, 1964) and normal stream flow <20% by volume sediment. Resulting deposits do not exhibit a 1:1 relationship to flow rheologies because rapid and localised variations in depositional environments result in sudden transformations

from one rheology to another, producing at times complex deposits. Smith and Lowe (1991) and, Vessel and Davies (1981) also describe a continuum between hyperconcentrated flow and debris flow as well as transitional stages between the two in respect of deposit structures. Smith (1986) and Pierson (2005a) provide a framework of deposit structural features that can be applied to classifying likely parent-flow rheologies (Table 4.1).

4.4. Stratigraphy

The Warea Formation can be divided into 3 distinct packages (fig. 4.2) defined by stratigraphy and the distribution of deposits in specific sectors. The basal boundary of some of the packages is the Pungarehu Formation, a 16 km^3 debris avalanche deposit that inundates the majority of the western section of the ringplain (Alloway et al., 2005). The other time constraint of these Warea Formation deposits is the Oakura and Okato Tephra (identified by Neall, 1972) with the Oakura tephra providing a minimum age of 7000 years B.P. Each spatial package has a unique stratigraphy of stacked and on-lapping debris flow and hyperconcentrated flow deposits (fig. 4.3a-c). Previously, Oeo Stream sequences were also correlated to the Warea Formation (Neall, 1979; Neall and Alloway, 2004). New mapping of this study shows that despite being sedimentologically similar, these units are underlain by the c. 7000 yrs B.P. Opua Formation debris avalanche deposit and are hence unrelated.

Table 4-1. Sedimentary features of ring-plain deposits and their inferred mode of deposition.
Sediment type observed features (after Smith, 1986 & Cronin et al, 1997a & b)

Inferred Mode of Deposition	Key Features of Deposits
Normal Streamflow	o Horizontally/planar bedded sands o Bedded sands, silts, and gravels o Variable grain size, silt, sand, and gravels in layers and lenses o Individual layers and lenses well sorted o Strong development of dominantly wavy and cross-bedding o Clast supported o Maximum clast diameter 0.2 m
Fluvial Flood Event	o Horizontally/planar bedded sands o Bedded sands, silts, and gravels Variable grain size, silt, sand, and gravels in layers and lenses o Individual layers and lenses well sorted o Strong development of dominantly wavy and cross-bedding o Poly modal grainsize distribution o Imbrication o Clast supported, rounded clasts o Maximum clast diameter 1 m
Hyperconcentrated Flow	o Grain size dominantly med-coarse sand, supporting common pebbles and rare cobbles and boulders o Poorly sorted o Clast supported o Horizontal bedding discontinuous but overall planar or horizontal fabric o Larger clasts often in pebble or cobble "strings" or exhibit “layering” o Planar basal contact o Maximum clast diameter 1 m
Non-cohesive Debris Flow	o Sandy matrix massive diamictons o Very poorly sorted o Matrix supported o Massive, mostly ungraded or occasionally normally graded o Sub-rounded to angular clasts o Bimodal grainsize distribution o Planar basal contact o Maximum clast diameter 1—3 m
Cohesive Debris flow	o Silty matrix massive diamictons o Features as above except matrix dominated by silt and clay o Can contain hydrothermally altered pumice and lithic clasts o Ungraded or normally graded

Stage 1.

1. Stony (Hangatauhua) River 16-22.5 ka B.P.

The Stony River sequences of Warea Formation exhibit one of the greatest ranges in deposit types. A well-developed paleosol separates the lowermost units from Pungarehu Formation. At 13 km from source, four individual sandy horizontally bedded hyperconcentrated flow units are separated by individual paleosols containing no identifiable tephra beds. In the upper catchment (above 13 km), the Oakura Tephra (maximum age of 7000 yrs B.P.; Neall, 1972) overlies these units and the Okato Tephra is found with the Saunders Ash (16.1 ka B.P.; Neall, 1972) intermittently at its base. In the lower catchment the hyperconcentrated units are overlain by recent soils.

2. Oaonui Stream 17 702 ± 82 B.P.

The Oaonui Stream catchment exhibits a sequence of stratigraphy that varies so much over short distances that individual units cannot be easily correlated downstream. In general four hyperconcentrated flow units, separated by thin silt/mud layers, are contained between a paleosol (in some places peat) above the Pungarehu Formation beneath the overlying Hangatahua Formation (debris flows) in the upper catchment. The peat was dated at 17 702 ± 82 B.P. In some locations a debris flow/hyperconcentrated flow deposit occurs above the sequence that may relate to the 7 ka B.P. Opua Fm. (Neall, 1979). Underlying this possible Opua corellative is a tephric paleosol, possibly correlated to the Okato and Oakura Tephra.

Stage 2.

1. Matanehunehu Stream 14 826 ± 77 B.P.

The Matanehunehu Stream deposits and stratigraphy exhibit a much simpler stratigraphy. Paleosol and peat lenses occur in places above the Pungarehu Formation. These were 14C dated at 14 826 ± 77 B.P. Above this a single deposit of debris flow (upper catchment) or hyperconcentrated flow (lower catchment) origin occurs with a medial-ash rich soil covering it.

Stage 3.

1. Waiweranui Stream <22.5 ka B.P..

The Waiweranui Stream catchment contains very similar sequence to the Stony River. Above a paleosol the sequence consists of four, similarly sized debris flow deposits separated by sandy paleosols. The sequence is overlain only by recent soil development, while nearer the current river channel, three terraces occur, representing individual hyperconcentrated flow deposits correlated to the <1000 yrs. B.P. Hangatahua Gravels (Neall and Alloway, 2004).

2. Kapoaiaia Stream <22.5 ka.

In the Kapoaiaia Stream catchment, a single debris flow/hyperconcentrated flow deposit occurs above the underlying paleosol and Pungarehu Formation.

A

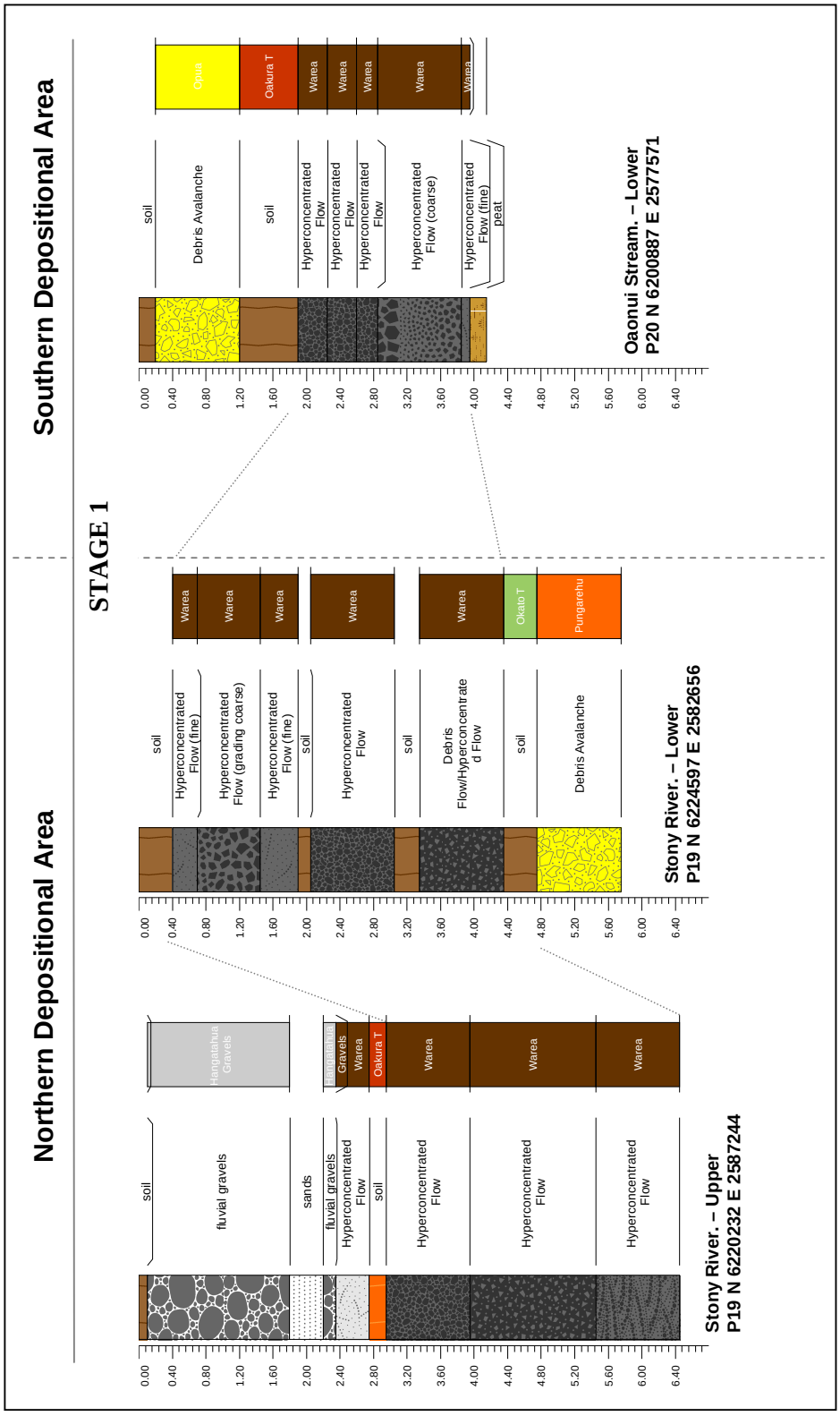
Northern Depositional Area
Southern Depositional Area
STAGE 1
Stony River. – Upper
P19 N 6220232 E 2587244
Stony River. – Lower
P19 N 6224597 E 2582656
Oaonui Stream. – Lower
P20 N 6200887 E 2577571
soil
fluvial gravels
sands
fluvial gravels
Hyperconcentrated Flow
soil
Hyperconcentrated Flow
Hyperconcentrated Flow
Hyperconcentrated Flow
Hangatahua Gravels
Gravels
Warea
Oakura T
Warea
Warea
Warea
soil
Hyperconcentrated Flow (fine)
Hyperconcentrated Flow (grading coarse)
Hyperconcentrated Flow (fine)
soil
Hyperconcentrated Flow
soil
Debris Flow/Hyperconcentrated Flow
soil
Debris Avalanche
Warea
Warea
Warea
Warea
Warea
Okato T
Pungarehu
soil
Debris Avalanche
soil
Hyperconcentrated Flow
Hyperconcentrated Flow
Hyperconcentrated Flow
Hyperconcentrated Flow (coarse)
Hyperconcentrated Flow (fine)
peat
Opua
Oakura T
Warea
Warea
Warea
Warea
Warea
0.00
0.40
0.80
1.20
1.60
2.00
2.40
2.80
3.20
3.60
4.00
4.40
4.80
5.20
5.60
6.00
6.40

B

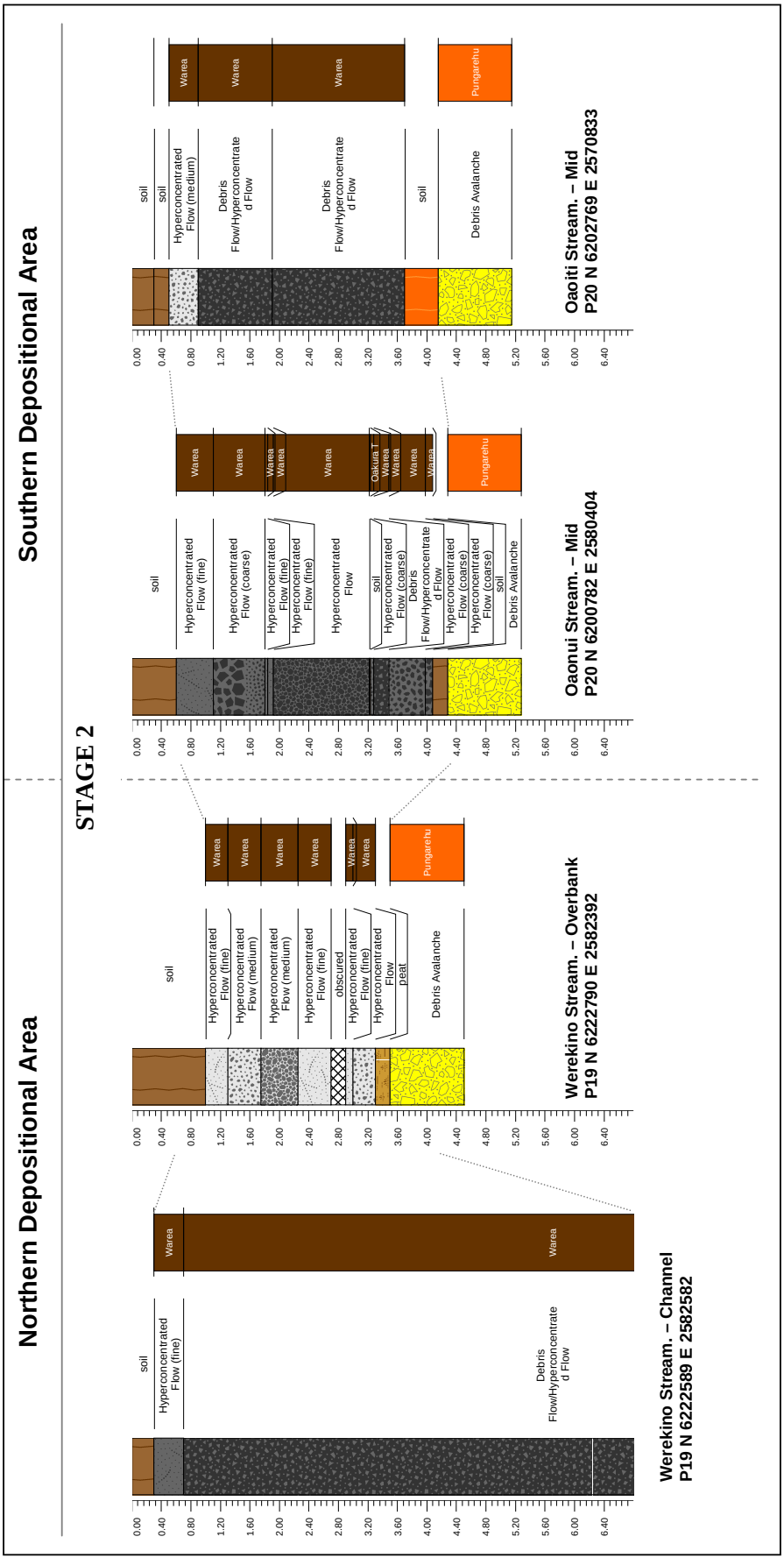
Northern Depositional Area
Southern Depositional Area
STAGE 2
Werekino Stream. – Channel
P19 N 6222589 E 2582582
Werekino Stream. – Overbank
P19 N 6222790 E 2582392
Oaonui Stream. – Mid
P20 N 6200782 E 2580404
Oaoiti Stream. – Mid
P20 N 6202769 E 2570833
soil
Hyperconcentrated Flow (fine)
Hyperconcentrated Flow (medium)
Hyperconcentrated Flow (coarse)
obscured
peat
Debris Avalanche
Debris Flow/Hyperconcentrated Flow
Warea
Oakura T
Pungarehu

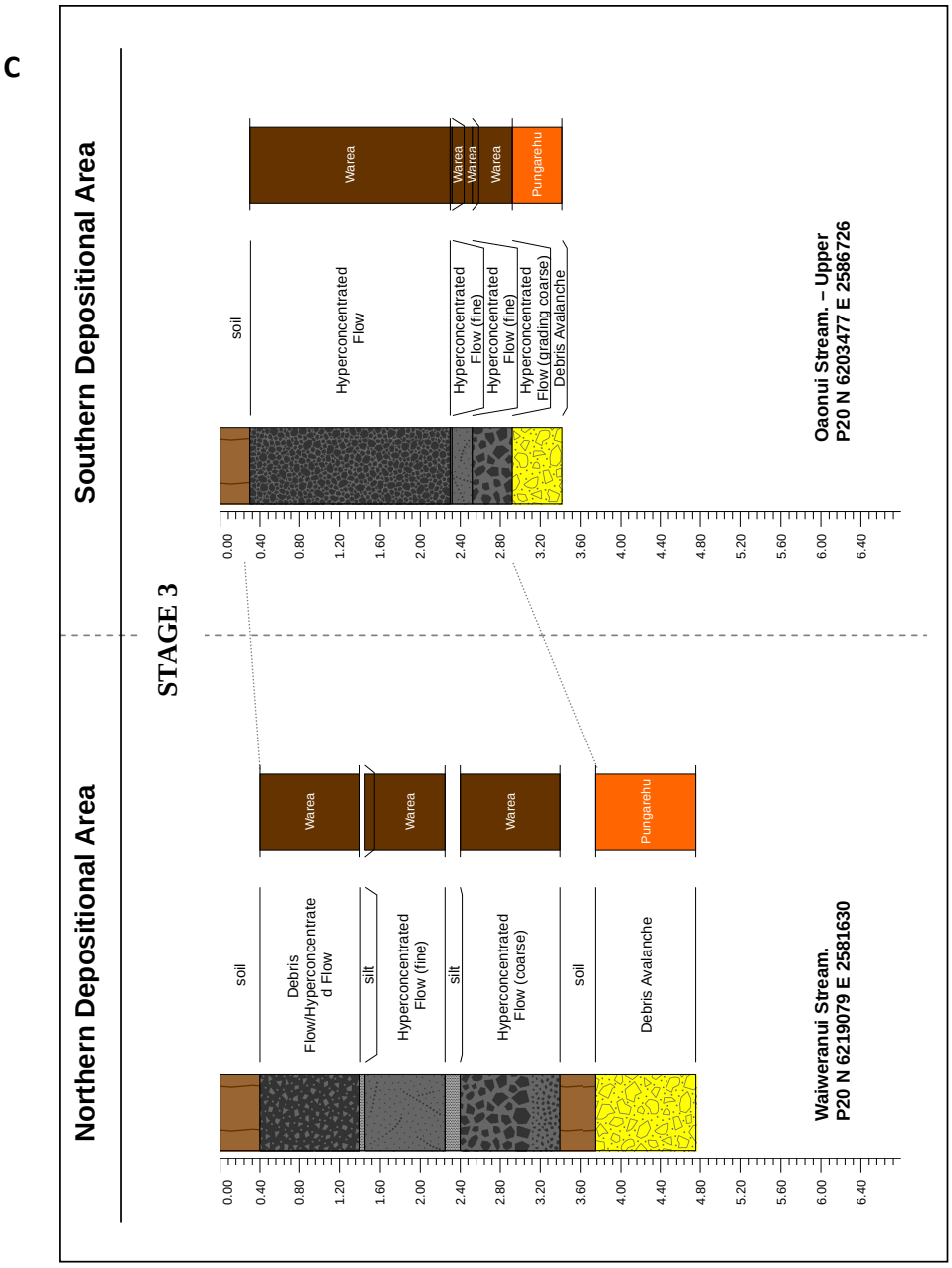

Figure 4-3. Phases and stratigraphy of each stage (1-3) of the emplacement of the Warea Formation; note, the northern and southern depositional areas refer to the respective margins of the Pungarehu Formation debris avalanche deposit. The column on the right of each measured section refers to the stratigraphy and formations from Neall and Alloway (2004). A) Stratigraphy of stage 1; B) Stratigraphy of stage 2; C) Stratigraphy of stage 3.

4.5. The Pungarehu debris avalanche and its possible landscape modification

The 22 100 ± 600 yrs B.P. Pungarehu Formation debris avalanche deposit (Neall, 1979; Ui et al., 1986; Alloway et al., 2005) covers an area of 200-250 km^2, west to north-west of the present day cone (fig. 4.2). The >7 km^3 on-land volume is spread in a broad fan with an average thickness of 30 m and run-out distance of 27 km. The avalanche was thought to have flowed in an unconfined fashion, yet in contrast to the other Taranaki debris avalanche deposits; it has a distinctive west-directed physiographic pattern of axial and marginal facies (Neall, 1979). The unit has pervasive yellow-brown, sandy clay, pumice-rich matrix that supports common basaltic-andesite to andesite clasts typically between 0.01 to 5 m in diameter, that are sub-angular, fractured or jigsaw cracked. Some highly fractured clasts form domains of dispersed clast fragments over an area of several square metres. One of the most characteristic features of this deposit is the presence of megaclasts up to several hundred metres in size, forming domains within the deposit that show complete (and variably deformed) sections of complete stratigraphy from the original source area. Hummocks and conical mounds are common and vary in size and shape across the deposit from: axial (dominated by fragmental clasts and large, closely spaced mounds) to marginal (dominated by inter-clast matrix) facies (Neall, 1979; Alloway, 1989; Palmer et al, 1991).

The volume of the Pungarehu Formation equates to around 50% of the current cone. Alloway et al. (2005) identified an earlier collapse of similar size immediately prior to this collapse event, producing the Ngaere Formation (5.85 km^3) a debris avalanche deposit over the east to south-east ringplain before 22.6 ka B.P. Following these two

enormous events, the ringplain was substantially altered, but more importantly the cone itself was completely destroyed. The Last Glacial Maximum then occurred (Alloway et al., 2007), with climatic conditions to 13 500 yrs B.P. contributing to the general lowering of vegetation levels and ongoing instability of high-elevation areas. At the same time, regrowth of the edifice appears to have started, with a steady rate of large-scale eruptions recorded (Alloway et al., 1995).

Following emplacement of the Pungarehu debris avalanche deposit, the following sedimentary response is postulated (fig. 4.4):

1. Aggradation of volcanic conglomerates at the outer margins of the debris avalanche fan from mass flows derived from an unstable scarp (eastern half of the massif still present) and the unvegetated Pungarehu Formation deposit.

2. Establishment of an incipient drainage network, followed by channel-controlled mass flows produced during rain-fall remobilisation of proximal tephra, block-and-ash-flow and scoria/pumice-flow deposits.

3. Broader spread of hyperconcentrated flows across the main debris avalanche surface generated from redistribution of proximal tephra and block-and-ash-flow deposits.

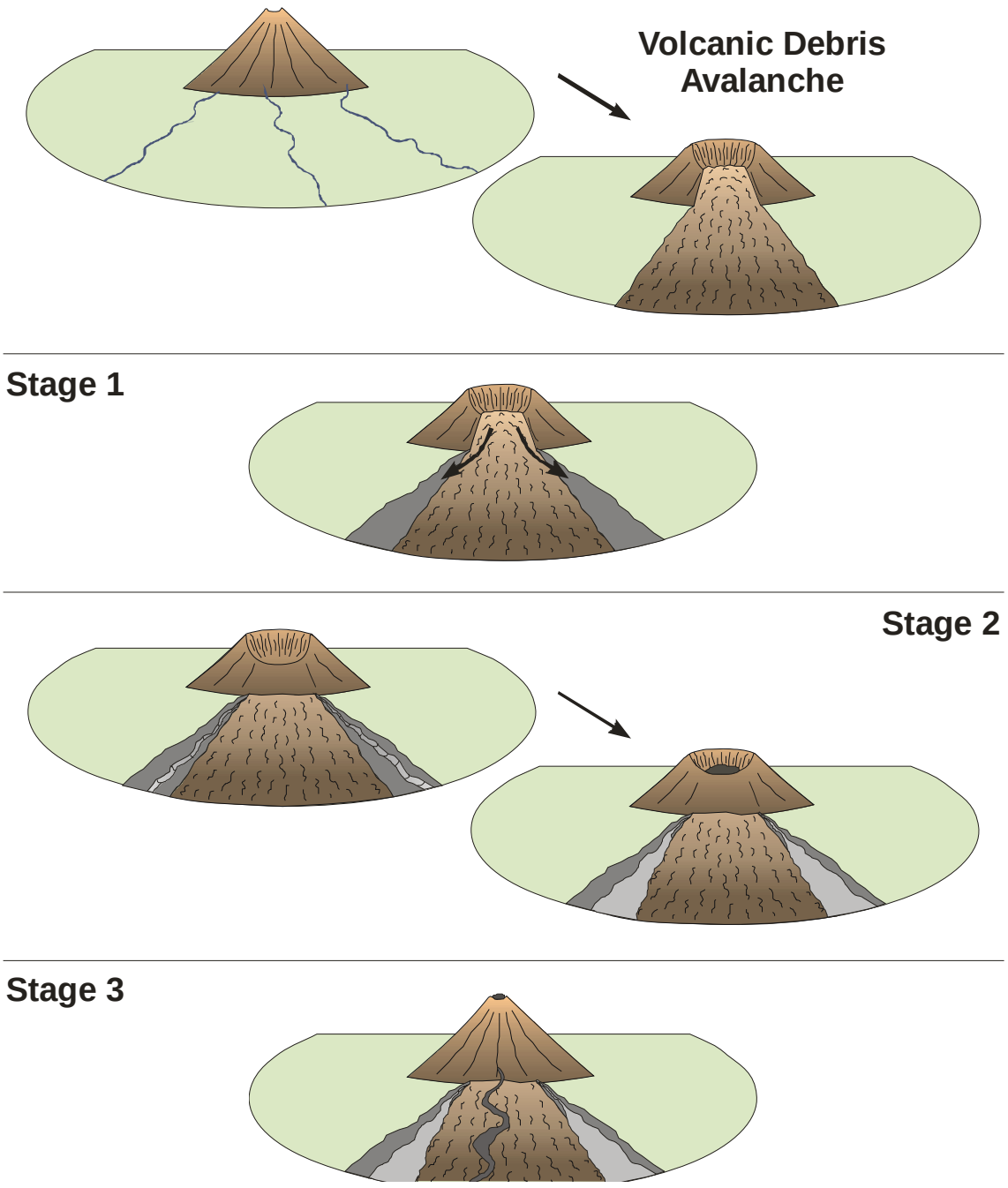

Figure 4-4. Phases of ring plain evolution following volcanic debris avalanche. Stage 1) lateral deposition; stage 2) channel formation and filling; stage 3) overland flow on debris avalanche surface.

4.6. Landscape and Sedimentary Response – Warea Formation

4.6.1. Stage 1 (16-22 ka B.P.)

A. Stony River

The deposits exposed in this area exist as a sequence of three packets of volcanic conglomerates and sandy gravel deposits, each of which exhibit central-channel facies, outer-channel facies and overbank facies variants (fig. 4.5).

A.1. Upper Catchment (0-13 km)

These deposits range from 0.2-3 m in thickness and are strongly influenced by paleo-channel morphology. The thickest units are those of the channel facies (fig. 4.5), while the greatest variations are found in the overbank facies units, which may wedge-out over 10 m laterally. The lateral distribution of the channel facies deposits are similar to the extent of the present day course of the Stony River; with widths ranging from c. 900 m at 9 km from source, increasing downstream to c. 2000 m at 13 km. Overall the deposits form broad tabular sheets, which due to their firm, indurated nature may form distinct flat-topped terraces. The units comprise poorly sorted volcanic breccias or conglomerates of black to dark grey basaltic andesite and grey to red-weathered dense andesite in a brown to yellow clay to sand-sized matrix, composed of andesites, pumice and clay, consistent with debris flow deposits (Major et al., 2005). The channel facies deposits are the coarsest, and contain 50-60% clasts in a coarse sandy matrix, whereas the overbank deposits are slightly better sorted with a median clast size of less than 0.1 m in a fine-sand matrix.


A
Hangatahua Gravels
Okato/Oakura Tephras
Warea Fm.
1m
B
Warea Fm.
Pungarehu Fm.
1m
C
1m
D
1m

Figure 4-5. (Previous page) Deposits from Stage 1 of the Warea Formation (Grid reference, NZMG E 2587351, N 6220968). A) Exposure of the sequence from within the Stony River lower units represent the channel facies of the debris flows/hyperconcentrated flows; B). Downstream equivalent hyperconcentrated flows deposited at 9 km; C) Graded hyperconcentrated flow unit; D) The channel facies deposit from the downstream-transformed, hyperconcentrated flow deposit.

Three distinct deposit sets occur. The lowest unit contains large metre-sized boulders in the channel facies and a pervasive pumice-rich matrix. In the outer-channel facies, clast-alignment and in places cross-bedding structures occur in the base. The clasts are sub-rounded, on average <0.2 m in diameter and dominantly consist of grey, crystal-rich (hornblende/pyroxene) dense andesites. The middle unit in outer-channel facies shows reverse grading, and in the upper part exhibits metre-scale, low-angle cross-beds. The uppermost unit is a massive, pebbly coarse sand. Both units contain sub-angular clasts <10-15 cm in size, ranging from black basaltic-andesite to grey and red andesite with occasional <3 cm pumice clasts. Overbank deposits from all three units are similar, comprising unstratified massive coarse-sand to silty-sand deposits. In the finest grained units, horizontally stratified beds and separation of pumice and lithic-rich layers occur. Contacts between deposits in the channel are erosional or represented by thin silt layers. In outer-channel and overbank facies, contacts are sharp and planar with minor low amplitude ripple beds and cm-sized silt layers (presumably formed by settling and dewatering c.f.; Cronin et al., 2000).

A.2. Lower Catchment (13-21 km)

Near the coastline, correlative deposits comprise three distinct, 1 m-thick finer grained units, with differences that result from apparent flow transition. These also form large tabular sheets, but with less distinctive terraces. The poorly sorted, matrix-dominated

deposits have similar lithologies to upstream sites (fig. 4.5). They comprise silty sands to silty gravelly sands, exhibiting weak planar bedding and common cm-sized pumice clasts. Clasts (<5-15 cm diameter) make up <40% of the unit, and are mainly subrounded dense andesite. Occasional > 1 metre-sized clasts occur either contained in isolation or associated with clast-rich lenses or trains in paleo-channel sites. Contacts between the three distinct units are planar and non-erosive, being marked by 5-10 cm thick layers of laminated silt and fine sand.

B. Oaonui Stream

At the southern edges of the Pungarehu Formation, similar deposits occur to those in the Stony River catchment, but with lithology and structure that may indicate different source areas and parent flow types. These deposits inundated a 1000-m-wide area at 200 m elevation (20 km from source) and at the coast they spread laterally over 2000 m. The deposits are covered in part by the c. 7000 yrs B.P. Opua Formation debris avalanche deposits. They are confined to a distinctive paleo-depression formed between the axial-A and marginal facies (Neall, 1979) of the Pungarehu debris avalanche deposits. Pockets of lignite, capping the avalanche and underling these deposits, show that the area had ponded-water/swampy conditions for some time after the debris avalanche deposition. The paleo-channel appears to have been similar to the present narrow (c. 30 m) and shallow (< 10 m deep) active channel cut into the clay-rich debris avalanche deposits.

The up to 10-m-thick combined deposit sequence is indurated, with individual beds forming tabular sheets but no distinctive terraces. Up to four distinct packets of deposits occur, each being 0.5-1.5 m thick. The volcanic conglomerates have higher matrix mud contents (yellow-grey silty sand) and higher proportions of fine pumice

pebbles (c. 5% by volume). They also show a lower clast content (~40%) of finer clasts (<20 cm). The lowermost deposit shows reverse grading with clast size increasing from coarse pebbles to ~25 cm in size. Overlying coarse sandy diamictons are 0.5 m thick packets which exhibit normal grading, while the upper units are weakly planar bedded and have clast alignment parallel to the bed. In places, low-angle lenticular, cross-stratified beds form and are several metres in length, with locally better sorting and dominantly finer grain-sizes than the rest of the deposit. The clasts comprise sub-angular, predominantly black, basaltic-andesite, red-grey andesite and pumice. The contacts between depositional units are marked by prominent laminar-bedded silt layers, 5-10 cm thick.

4.6.1.2. Interpretation

The deposits in these two catchments were identified as the Warea Formation (Neall, 1979), described as brecciated sands, and inferred to be lahar deposits (Alloway et al., 2005). Despite being prehistoric deposits with very little information pertaining to the parent flows, factors such as rheology, source and initiation can only be inferred by comparison to similar modern day analogues such as the Mt. St. Helens 1980 flows (Pierson, 1985; Major et al. 2005) and Mt. Ruapehu lahars from the 1995 eruptions (Cronin et al., 2000).

The deposits are characteristic of lahar deposits, being non-cohesive sandy diamicts, and their complex changes in sedimentary character imply flows that rapidly transformed between debris flows and turbulent hyperconcentrated flows (c.f. Pierson and Scott, 1985; Cronin et al., 1997a), as well as having vertical and time-dependent transformations causing complex deposition (e.g., Cronin et al., 2000). The most diagnostic feature is their transformation over ~7 km of run-out (13-20 km from

source), from a coarse sandy diamict to a better sorted, and stratified, sand-dominated deposit (fig. 4.5). This standard head to tail transformation is a result of deposition and loss of sediment rather than an increase or influx of water. Observed lahars that transform like this (Mt. Ruapehu 1995: Cronin et al., 2000) also exhibit a decrease in peak discharge and observed velocity.

One of the best recognised factors in the transformation from debris flow to hyperconcentrated flow is the normal grading of deposits in upper catchments, suggesting a flow that is slowing, with the larger particles progressively settling out (Pierson, 2005b). Subsequent deposits become finer and better sorted as the flow regime changes from a dominantly collisional and frictional granular flow, to turbulent flow of particles in short-term suspension or saltation (Pierson, 2005b). However, in these deposits, the basal layers show longitudinal (parallel to flow direction) cross-bedding indicating the formation of bars and berms. This may be attributed to deposition of the material from a watery head of the flow (c.f., Cronin et al., 1999), but more likely represents deposition by the waning stage flow tail, with lower sediment contents.

The source of the material is difficult to determine, since most Mt. Taranaki lithologies occupy a narrow compositional range (Neall et al., 1986). Very little highly weathered or hydrothermally altered material was observed; pumice/scoria clasts are typically confined to sand-grade and rare pebbles. Hence, in general the constituents are very similar to the underlying debris avalanche material, although having a sandy rather than clay matrix. This may imply that the materials are derived from the avalanche and avalanche scarp where this type of material is readily available. The lack of pumice and the presence of sorted sands would suggest that the source is not from

concurrent eruptives (as observed with younger deposits) (Platz, 2007). The initiation of the parent flows are probably related to the high rainfall of the area, coupled with huge areas of fresh and unvegetated debris avalanche deposits and scarp. The deposits reflect the filling of marginal and shallow surficial incipient drainages on the debris avalanche, forming temporary small braided river systems. After this period of redeposition, soil development and cutting of more stable channel systems occurred indicating that the landscape stabilised within 5 000-7 000 years of the Pungarehu debris avalanche.

4.6.2. Stage 2 (14-22 ka B.P.)

The next group of volcanic diamictons is differentiated by location, lithology, structure, age and stratigraphy. An intervening paleosol indicates that these units were formed some time after the Pungarehu Formation and a radiocarbon date places them at c. 3000 years younger than the Stage 1 units (fig. 4.3b). The deposits were confined to box-shaped river channels located between the Stage 1 deposits and the Pungarehu Formation. The underlying paleosol layer is absent in the channel facies of Stage 2 units, where the contact is unconformable (erosive). The deposits in this stage consist of a channel facies unit that grades rapidly laterally into an overbank facies. Stratigraphically equivalent units are found in the catchments of Oaonui, Oaoiti, Matanehunehu and Werekino Streams. Only the latter is described further.

A.1. Werekino/Matanehunehu Stream

Stage 2 deposits are best exposed between the Werekino and Matanehunehu Streams in western Taranaki, set within a 2000 m-wide flood plain. The channel facies deposit of a single unit occupies the Werekino Stream area valley, confined to a former 40 m-


A
1m
B
1m
C
25cm
D

Figure 4-6. (Previous page) Deposits from Stage 2 of the Warea Formation from the Werekino Stream (Grid reference, NZMG E 2582956, N 6224626); A) Central part or channel facies of deposits representative of Stage 2; B) Transition zone (over 20m) from channel to overbank facies; C) Bouldery channel facies. d. Bedded pumice and silt-rich layers within the overbank facies.

wide by 8 m-high valley (fig. 4.6). Its over-bank facies (up to 2m thick) forms a tabular sheet spreading laterally ~200 m from the channel (fig. 4.6). The transition between these two facies occurs rapidly, wedging over ~10 m laterally. The confined channel facies is coarse, bouldery (55% by volume), clast-supported conglomerate with an intervening poorly sorted yellow to greyish-brown coarse sandy matrix comprising 40% of the unit. Clasts are primarily rounded to sub-rounded, grey to greyish red and subordinate black (10% and <10 cm) porphyritic dense andesites. The broader overbank facies comprises a 2-3 m-thick silty-sand unit that is sorted and exhibits well-defined laminar, dune and lenticular bedding. The remainder of the flood plain comprises sheet-like over-bank deposits from a series of flows with similar sedimentary character. The units often form a thin sandy mantle in the depressions of the debris avalanche deposit, along with occasional thicker mounds former bars of coarser, indurated and cemented sands. Individual beds are 5 to 40 cm-thick, often with erosive basal contacts. Beds are commonly cross-stratified and have sharp upper boundaries defined by cm-thick layers of silt or fine sand, at times exhibiting weak paleosol development. Some beds are well sorted and some monolithologic, e.g., pumice-dominated, or grey, uniform andesite sands to dense pebbles. Units are often reversely graded with the upper portions containing occasional clasts of up to 20 cm diameter.

4.6.2.1. Interpretation

The second stage of evolution of the ring-plain drainage network following the Pungarehu debris avalanche was characterised by the formation of small, but well-defined box-shaped channels that may have formed as the avalanche and related scarp became re-vegetated. These channels were inundated by redistributed eruptive products, once the volcanic cone began to regrow. Evolution of active volcanic ring plains through the emplacement of lahars show very similar processes, e.g. at Mt. Ruapheu, (Cronin and Neall, 1997; Donoghue and Neall, 2001), Iliamna Volcano, (Waythomas et al., 2000), Kelud Volcano (Thouret et al., 1998), Borzsony Mountains (Karatson and Nemeth, 2001), Merapi Volcano (Lavigne et al., 2000) and Mt. St. Helens (Scott, 1988a). The lithology of the Stage 2 deposits implies that they were no longer being sourced directly from the debris-avalanche deposit, but instead from explosive (pumice) and dome-forming eruptions (dense-rock).

An illuminating feature of these Stage 2 deposits is the exposure of complete cross-sections of a bouldery channel facies that passes rapidly laterally into a sandy hyperconcentrated flow-like overbank facies (fig. 4.3 & 4.6). Ongoing rain-triggered lahars from the constantly-erupting Gunung Semeru, East Java, Indonesia (Lavigne and Suva, 2004; Thouret et al., 2007) provide an ideal modern analogue. Lahars at Mt. Semeru are considered to be of low velocity, resulting from the development of a frontal bouldery dam, dominated by a granular-collisional regime. Flow progression occurs in a series of pulses due to this self-inhibiting mechanism. The tail of the flow erodes into the initially emplaced boulder-dominated deposits, as well as spreading laterally depositing a sandy hyperconcentrated flow deposit. The result is normally graded deposits with a basal layer of rounded boulders. This model corresponds to the features of the Stage 2 deposits described from Taranaki, particularly the lack of downstream transformations from debris flow to hyperconcentrated flow (c.f. Stage 1). Thouret et al. (2007) identifies three controlling factors on Mt. Semeru for the

lahars observed: a source of easily erodible material (from dome or coulee collapse, tephra covered fans), high-intensity rainfall and small-immature channel systems.

It is envisaged that a similar process was occurring at Mt. Taranaki during Stage 2; a cone re-forms from effusive and explosive material and redeposits some of these products to lower altitudes during high-intensity rainfall events. These flows were initially confined to immature drainage structures formed between closely spaced events. Gradually the over-bank deposits of these flows filled a series of small flood plains between the last-stage deposits and the debris avalanche deposit.

4.6.3. Stage 3 (<22 ka B.P.)

The third stage of the ring-plain response is marked by deposits of sandy gravels located directly on top of Pungarehu Formation deposits or on top of Stage 1 and 2 debris-flow deposits, occupying areas between mounds in a pattern that gives rise to the idea that they flowed around the mounds (Neall, 1979) (fig. 4.3 & 4.7). The type section of the Warea Formation (Neall, 1979) is located abutting a 30 m-high Pungarehu mound (fig. 4.7). Deposits from this stage are best found parallel to the main depositional axis of the Pungarehu Formation, in the mid-sections of the present Waiweranui and lower Kapoaiaia Streams.

A.1. Waiweranui Stream

The flows inundated an area adjacent to the current Waiweranui Stream, spanning a width, perpendicular to the stream of 200-300 m at 9 km distance from source and ~1000 m wide at the coast. The units fill areas between debris avalanche mounds of

the axial b facies of the Pungarehu (c.f., Palmer et al., 1991). Sub-terraces are cut and filled by overlying deposits of similar character. Individual beds range between 0.5-1.8 m-thick and no clear channel vs over-bank facies is exhibited. Distinctive within each unit is a pebble-to boulder-rich basal layer that grades upwards into a finer sand-dominated and pebble/boulder-free layer. The overall deposits are muddy gravelly sands with a matrix of grey/red/black muddy coarse sand that weathers to yellow brown in oxidised outcrops; <5% pumice (<2 cm in size) occurs. The matrix is often friable and contains common pores/vesicles. Sub-angular clasts, dominantly <20 cm in diameter, are mostly grey to red dense andesites and black basaltic andesite with rare (<5%) pumice clasts. In basal layers, clast trains occur and many of the clasts are sub-rounded. Where the deposits on-lap debris avalanche mounds, they are commonly pebble rich and exhibit minor bedding and sorting (fig. 4.7). These marginal facies, distinctively also contain bread-crusted and radially fractured, 10-25 cm, black, scoriaceous porphyritic bombs (fig. 4.7). In addition to coarse-tail normal grading, the units (3-4) also exhibit lenses with better sorting and faint cross-bedding structures (1-3 m long). Contacts between units and at the base are planar and non-erosive, commonly with cm-thick layers of silt capping units.

A.2. Waiweranui Stream, Oaonui Stream

A suite of deposits, considered by Neall and Alloway (2004) to be of laharic origin, occur as capping units in the Oaonui Stream and on the lowest flood-plain surface in the Waiweranui Stream area (fig. 4.2). These units are here considered to represent parts of the Hangatahua Gravels (Neall and Alloway, 2005), derived from remobilisation of the block-and-ash flow deposits of the last 1000 yrs. located in their upper catchments (c.f., Platz et al., 2007). These moderately poorly sorted, and weakly cross- and laminar-bedded deposits comprise muddy gravelly sands with a greyish brown and grey sand-dominated matrix and <5 cm sub-rounded clasts.

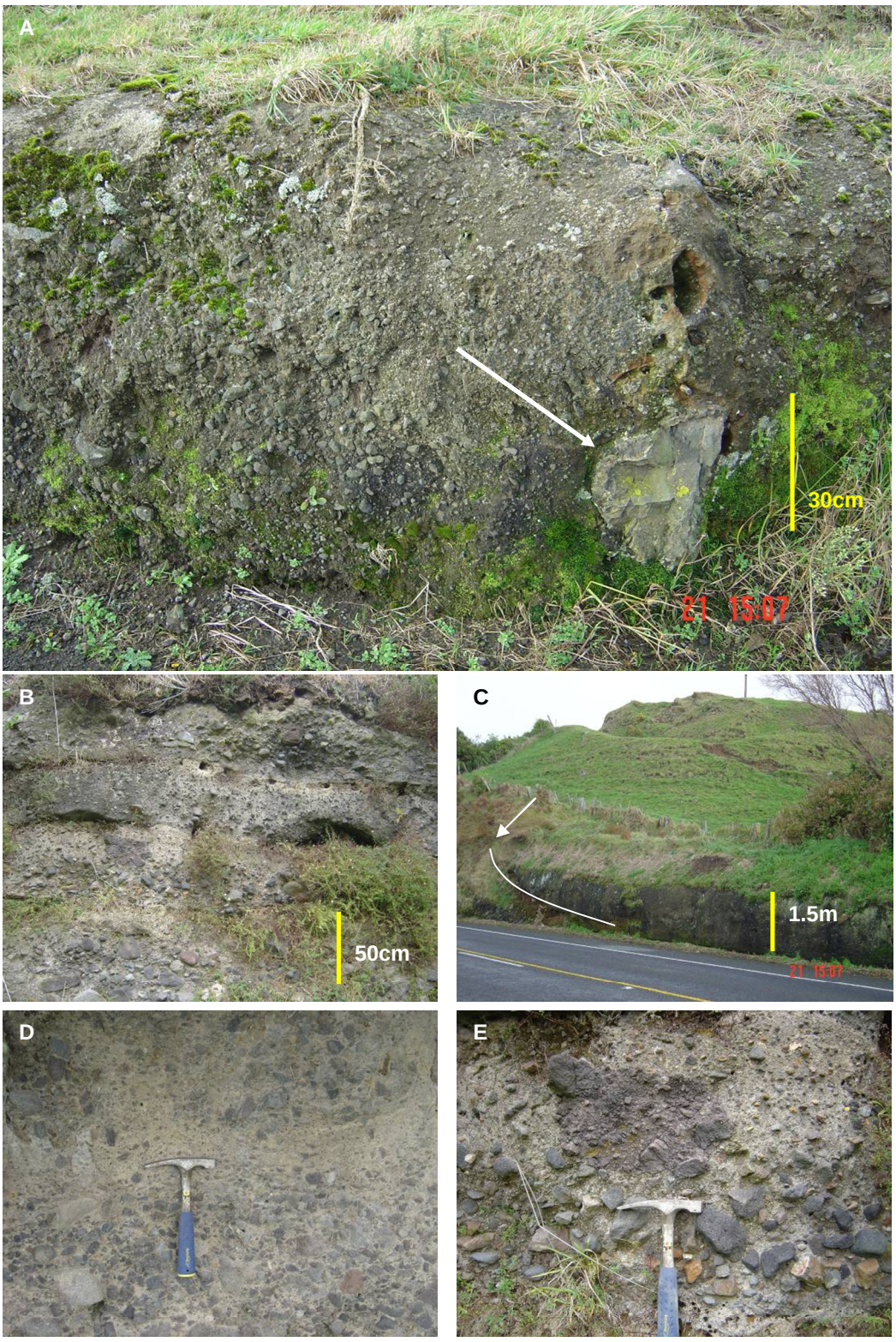

Figure 4-7. Photos of deposits from Stage 3 of the Warea Fm. (Grid reference, NZMG E 2582493, N 6222587); A) Overbank facies of the coarse, upper unit of the Stage 3 deposits; note ~30 cm breadcrusted, radially fractured bomb contained within the deposit (arrowed); B) Characteristic stack of debris flow/hyperconcentrated flow units (Channel facies) from Stage 3; C) Overbank facies on-lapping a Pungarehu Formation debris avalanche mound (as indicated); D-E) Lithology and structure (matrix and clast composition) of the Stage 3, hyperconcentrated flow deposits.

A.3. Stony River

Similar to the above two catchments, the Hangatahua Gravels (Neall and Alloway, 2004), occur in the Stony River as clast-supported bouldery gravels and gravelly sands.

4.6.3.1. Interpretation

The latest stage of evolution of the ring-plain, following the stabilisation of the Pungarehu deposit was the inundation of the lateral margins and stream valleys within the debris avalanche deposit by mass flows possibly derived from rainfall-reworked block-and-ash flow deposits or those that may have been initiated from hot ejecta upon snow and ice on the upper flanks (c.f., Neall, 1973). The units are representative of hyperconcentrated flows (c.f., Pierson, 2005b), but with minor restricted areas of slightly coarser facies reminiscent of near-channel units of eruption-related non-cohesive lahars (c.f., Cronin et al., 2000). The parent hyperconcentrated flows travelled down poorly-defined flow paths, progressively inundating areas ~20 km across in distal areas.

The broad and thin distribution of these deposits is similar to overbank hyperconcentrated flows observed on Mt. Pinatubo by Pierson et al. (1996), where very shallow flows spread laterally over wide areas gently flowing around intricate obstacles. The presence of pumice and jigsaw jointed, bread-crusted volcanic bombs implies an immediate triggering of the emplacing flow similar to that described by Rodolfo and Arguden (1991) within “hot” lahars. Initiation of the flow from pyroclastic flows interacting and melting snow and ice was also proposed by Neall (1973).

4.7. Computer Simulation of Debris flows

The simulation of volcanic mass flows or debris flows is common for hazard analysis (Saucedo et al., 2003; Sheridan et al., 2004a), but it has not often been applied to landscape-reconstruction studies. Current computer simulation of volcanic debris flows uses either: 1. slope-area or statistical methods with digital elevation models (DEMs) (Schilling, 1998); 2. commercially available hydrologic codes or flood models based on the movement of water in channelized flow (e.g., Carrivick et al., 2009), or 3. the application of more experimental granular-flow simulations, utilising an incompressible Coulomb continuum approach (e.g., Iverson, 1997a; Iverson & Denlinger, 2001; Pitman and Le, 2005). Titan2D is a depth averaged, "shallow water" flow model, with modules for simulating either a dry granular flow, or a two-phase viscous fluid + granular flow, developed by the Geophysical Mass Flow Modelling group at SUNY Buffalo (Pitman and Le, 2005). The major innovative feature of this family of codes is that they solve the movement of a granular or two-phase mass of an initially specified volume over natural terrains by using an adaptive grid (Patra et al., 2005). For the purpose of this study where large areas are covered by flows and channel-definition is low, Titan2D offers an advantage in its application of an adaptive grid, reducing computational power while enabling flows to be simulated across large areas with a digital elevation model (DEM) in original resolution. Titan2D was run over a DEM of 20 m resolution (constructed from contour data of the area) within the GRASS GIS package.

To accurately simulate the source areas for mapped deposits a catchment analysis was performed using ArcGIS (ESRI, 2007); from this the centre of each major drainage path identified was used as the starting point for each simulation. The starting piles were on

the upper Stony River, Waiweranui Stream, Okahu Stream and Oaonui River at start elevations of c. 400 – 700 m. These were determined by identifying the catchment or source areas of the current drainage paths as well as the cross-referencing from the most proximal known location of each deposit. Three different volumes, 1 x 10^6 m^3, 1 x 10^7 m^3 and 1 x 10^8 m^3 were modelled at each starting location with each starting pile being situated in the channel. Each flow was modelled in the two-phase Titan2D code, containing 70% granular material and 30% fluid as that ratio is suggested typical of lahars by Cronin et al. (1997a) and Pierson (2005b).

All simulated flows in the Stony and Waiweranui catchments were confined to the current flood plains or present-day channel. In the Okahu and Oaonui catchments, the flows spread laterally across the flank of the cone with the simulations readily alternating flow path at lower altitudes occupying other catchments and running-out through adjacent streams (fig. 4.8). This phenomenon actually occurred during a small lahar within Oaonui Stream during 1999 (Hancox, 1999), where a rock fall transformed into a lahar before infilling the channel and spilling out from its stream channel into an adjacent stream. In general each simulation had a very short run-out distance of 6-7 km (planar distance) before spreading out and dissipating. No flows reached or ran-out the distance of the current inundation areas of the described deposits or flowed to the coast. A series of simulations were then repeated in the Stony River with the starting locations at the final runout distance of the previously simulated flows. These showed channel confinement of flows and related inundation of flood plains in a similar pattern and runout to deposits of Stage 1 along the Stony River.

Figure 4-8. (Next page) Examples and outputs of final stages of flow (greatest inundation) from three Titan2D computer simulations of flows (1 x 10^8 m^3) with source areas from the; A) Oaonui Stream; B) Waiweranui Stream; C) Stony River (Werekino Stream) catchments.

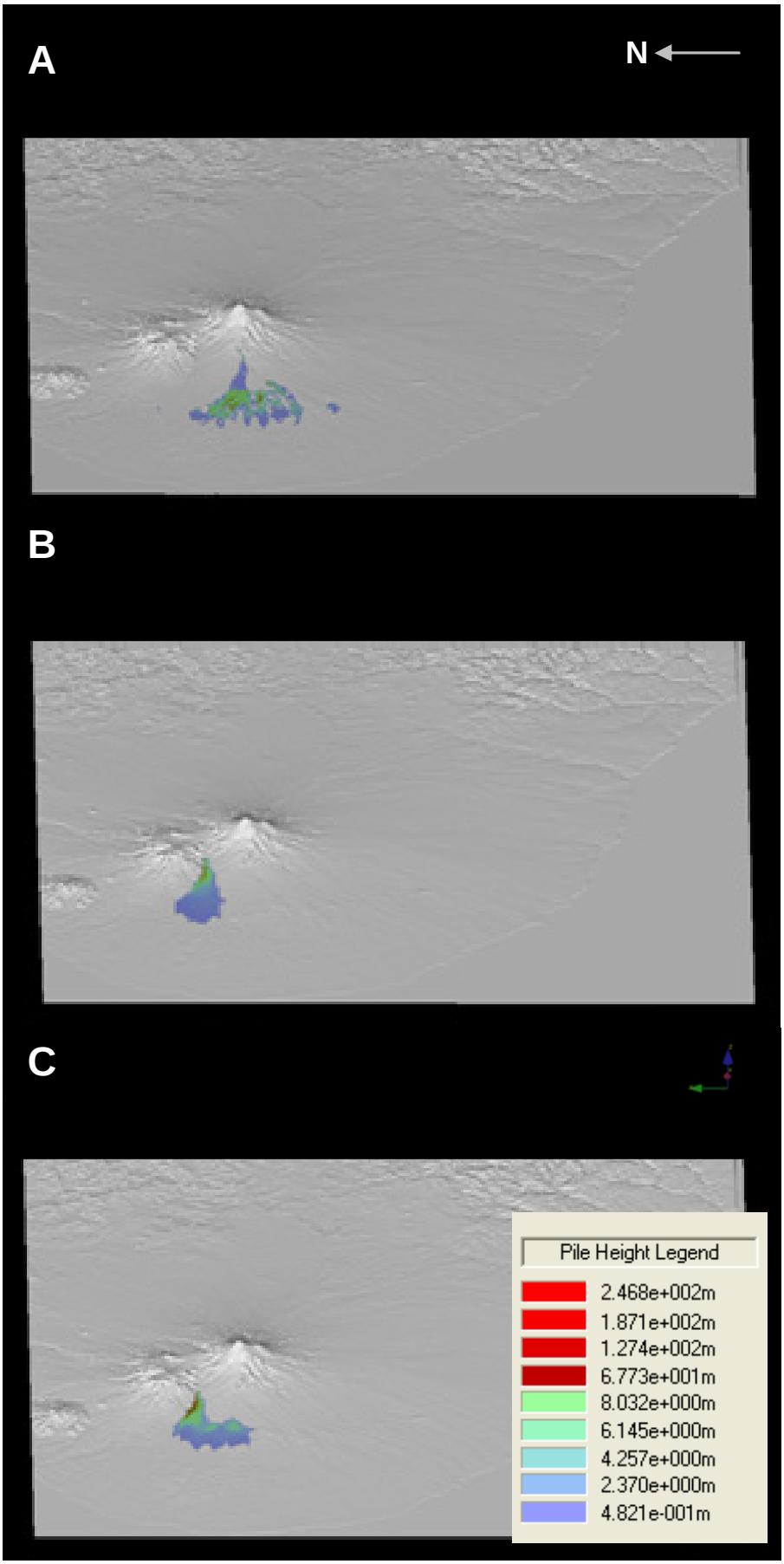
A
N
B
C
Pile Height Legend
2.468e+002m
1.871e+002m
1.274e+002m
6.773e+001m
8.032e+000m
6.145e+000m
4.257e+000m
2.370e+000m
4.821e-001m

4.7.1. Interpretation

The computer simulations are a useful tool to characterise and compare possible source and inundation areas as well as flow paths, but do not provide the detail to compare small-scale processes that form the texture and structure observed in deposits. All computer simulations also need to be rigorously optimised before small scale comparison can be undertaken.

The common output from the simulations that started at the highest point in each catchment is that the run-out distance is low, no single channel confines the flow and the flows spread out over an area of ~1000 m between the altitudes of 500-400 m (fig. 4.8). The simulations also suggest that the flows described here originated from an elevation consistent with the mid-flanks of the current cone, consistent with its collapsed and slowly rebuilding state at the time.

4.8. Volcanic Hazard Assessment and Mapping

Neall and Alloway (1996) produced a Taranaki Volcanic Flow Hazard Map that defined zones of risk from A-F (highest to lowest). The hazard map and the displayed zones were produced by estimating the return periods of surface inundation from mapped past pyroclastic flow, lahar and debris avalanche deposits. In this methodology, surfaces where the uppermost flow unit is the Pungarehu Formation had a return period of 23 000 yrs., and was hence zoned as “E”. The Warea Formation was

categorised as “D”, intermediate hazards, and with an estimated return period of between 3 500 – 23 000 yrs. (Alloway et al., 2005). The streams and their associated flood plains were categorised as “C”, the highest hazard from lahars, with an estimated return period of 500 – 3 500 yrs. Notably, these hazard zones are primarily based on prehistoric patterns of deposition and the effect of the terrain or landscape altering events are not able to be accurately portrayed on a map in an appropriate resolution. In addition, large-scale debris avalanches are known to be landscape-changing on this ring plain, hence drainage patterns following such events will be erratic and may re-establish in completely different locations as a new cone. Hence, such deposit-based hazard maps give only a broad overview of future mass-flow hazards. Hazard maps and predictive hazard zones need to be developed or constantly updated that take into account the variety of scenarios that could occur from a large-scale, catastrophic event or from rapidly changing drainage patterns.

4.9. Conclusions

Typical chronostratigraphic-based mapping of volcanic fans or ring plains often means that in the poor resolution of available tephra marker horizons, numerous deposits of possibly widely varying origin, mechanism and age are grouped into individual packets. This aids mapping and a general view of overall ring-plain growth, but does not allow detailed dynamic processes of ring-plain growth to be analysed. Emplacement of large volcanic debris avalanches changes the landscape in their source regions (on the cones) and the surrounding ring plains. This implies that in order to interpret ring-plain successions from repeatedly collapsing volcanoes, the dynamics of landscape response following debris avalanche emplacement must be considered. The sedimentary sequence developed following the emplacement of the Pungarehu Formation debris-

avalanche deposit on the western ring plain of Mt. Taranaki was formerly a single mapping unit comprising of deposits of mass flows of similar overall character aged between 13 000 - 22 000 yrs B.P. However, based on the sedimentological and geomorphological features of these units, the response to the landscape-altering Pungarehu event has been interpreted into three stages in the landscape recovery (fig. 2):

1. Deposition at the margins of the debris-avalanche fan, including filling the natural low points and channels developed along its side. Mass flows, including debris and hyperconcentrated flows, then developed from the proximal avalanche areas and possible scarp and debris avalanche deposit. Rainfall runoff from the non-vegetated landscape was extreme. This stage was probably confined to the first few decades following the debris avalanche.

2. Formation of narrow, box-shaped channels into the debris avalanche deposit, followed by their infilling and inundation by mass flows (dominantly hyperconcentrated flows) redistributing primary eruptive products from the regrowing cone. This stage occurred up to 9 ka after the debris avalanche.

3. From 9 ka to present, overland flow across broad and higher areas of the debris avalanche deposit form shallow, low-energy sheet-like hyperconcentrated flows. These units are typically generated from rainfall-induced redistribution of proximal deposits of block-and-ash flows, scoria/pumice-rich pyroclastic flows and tephra covered fans from the upper slopes of the massif.

From a hazards perspective, this implies that following a major debris avalanche event, the old drainage system is effectively erased. Instead, new channels and new loci of

mass-flow hazards are formed probably initially along the edges of the debris avalanche fan. Later channels are formed in relation to the morphology of the re-growing cone. Post-avalanche hazard continues as a threat in broad areas of the surrounding landscape for several thousand years, because the immature and small channels formed are often easily inundated by accelerated periods of volcanism that often follow major cone destruction events. This implies that Volcanic Flow Hazard maps should be regarded as continuing “works-in-progress” with major adaptations necessary following such large landscape changes.

CHAPTER 5

Emplacement Mechanisms of the Opua Debris Avalanche deposit from Mt Taranaki, New Zealand: Structural Analysis and Computer Simulation.

J.N. Procter, S.J. Cronin[1], A.V. Zernack[1], M.F. Sheridan[2], V.E. Neall[1].

1. Institute of Natural Resources, Massey University, Private Bag 11 222, Palmerston North, NZ.

2. Geophysical Mass Flow Modelling Group, State University of New York at Buffalo, NY 14260, USA.

Abstract

More than 14 unconfined debris avalanche deposits (DADs) <200 000 years old occur on the Mt. Taranaki ring plain demonstrating a high-impact but low-frequency hazard facing the surrounding community. The ~7000 yr B.P. Opua Fm is the youngest of these events and exhibits the typical chaotic, polymodal, polylithologic and extremely poorly sorted characteristics of DADs. Despite the apparent invariance of these large-scale properties within the Opua deposit, the proportion of clay:sand:gravel/boulders gradually changes from proximal to distal areas (>30 km from source) with the finer fractions, including clay contents, increasing with distance. Scanning Electron Microscope analyses of clay and silt grains show typical hackly textures and micro-cracks are common. There is no variation in the crack distribution or frequency in grains

from different parts of the deposit, suggesting the cracking process occurred at source. Analysis of the surface features of the deposit morphology shows consistent variation with distance, in particular its mounds and hummocky surface. A near-source initially chaotic surface gives way with distance to ridges of hummocks in flow-parallel direction. These eventually break-down into clusters of mounds and further to more widely spaced fields of individual mounds in distal areas. The Opua debris avalanche was generated by the gravitational collapse of a sector of the volcanic edifice that fragmented and flowed down a single catchment. Rapid changes in topography and slope resulted in the transformation of the flow into a more cohesive mobile body, which formed two major lobes marked by mound/hummock ridges. The granular flow model Titan2D was applied to evaluate possible emplacement conditions and collapse parameters. Titan2D, while useful for defining initial collapse parameters and major flow paths, could not adequately simulate the complex rheological transformations from a collapsing/sliding pile through a granular flow into a cohesive clay-rich flow with long runout and high apparent fluidity. It is also difficult to adequately define simulation parameters for this rapidly changing flow from the resulting geological deposits. Hence, computer simulations of major flow paths must be used alongside insights from geological mapping to provide future-focussed hazard zones for debris avalanches.

5.1. Introduction

Catastrophic volcanic debris avalanches present an infrequent yet highly destructive hazard on many stratovolcanoes worldwide (Siebert et al., 1987; Belousov et al., 1999; Scott et al., 2001). They dramatically alter the landscape inundating surrounding volcanic ring plains and valleys with several tens of meters of volcanic debris. The

infrequency of these events makes the observation of a volcanic debris avalanche extremely rare (Glicken, 1996), necessitating a holistic approach to fully understand flow rheology and emplacement mechanisms of these events at any given volcanic centre.

Prior to the 1980 eruption of Mt. St. Helens, volcanic diamictons emplaced by mass flow were commonly termed “lahars” without distinction between initiation and transport processes such as debris-flow vs. flank collapse (e.g. Neall 1976a & b, 1979; Crandell, 1971). The dramatic 18 May 1980 demonstration of a volcanic debris avalanche and studies of the resulting deposits provided a detailed model for these volcano collapse events (Voight et al., 1981, 1983; Glicken, 1996). Ongoing studies have differentiated the characteristics of debris avalanches and their deposits from other volcanic mass-flow types (e.g. Siebert, 1984; Ui, 1983, 1989; Crandell, 1989; Glicken, 1991, 1996). In addition, a series of models for volcanic mass wasting and volcanic ring-plain development have also been constructed (Palmer et al., 1991; Stoopes & Sheridan, 1992; Vallance et al., 1995; Vallance & Scott, 1997; Belousov et al., 1999; van Wyk de Vries et al., 2000; Capra & Macias, 2000; Capra et al., 2002; Waythomas & Wallace, 2002; Shea et al., 2008).

Debris avalanche processes have been inferred from interpreting features of their deposits such as shattered and jigsaw-cracked fragmental rock clasts, megaclasts, large rip-up clasts and matrix-properties as well as the shape of hummocks and mounds along the main axis of dispersal and in proximal areas (Palmer et al., 1991; van Wyk de Vries et al., 2000; Scott et al., 2001; Shea et al., 2008). Scott et al. (2001) described debris avalanches as sudden very rapid flows of variably wet (but unsaturated) mixtures of rock fragments and soil in response to gravity. These are typically

generated by large-volume landslides or slope failures (ranging from 0.05 to 45 km^3) from the flanks of volcanoes (Varnes, 1978; Ui 1983; Schuster & Crandell 1984; Pierson & Costa 1987). They may travel over 100 km from source and reach velocities as high as 100 m/s (Siebert et al., 1987; Crandell, 1989; Stoopes & Sheridan, 1992; Scott et al., 2001).

Debris avalanches are considered to behave initially as grain flows where particle collisions and frictional contact dominate during flow progression, in contrast to debris flows that can be supported by excess pore fluid pressures (Pierson and Costa, 1987; Scott et al., 2001). Despite this, Scott et al. (2001) showed that debris avalanches can be complex and variable, ranging from pure dry grain flows in proximal reaches, transforming to large debris flows or rapid successions of these with distance. The general model of debris avalanche emplacement suggests an initial sliding motion of a solid or coherent rock mass and involves the non-turbulent transport of material with shearing occurring mainly along internal fractures (Siebe et al., 1992; Coussot & Meunier, 1996; Shea et al., 2008). The transformation to a flowing particulate mass usually takes place at the base of the volcano, or at a major break in slope following disaggregation of the material (Siebe et al., 1992). Further transformation into a cohesive debris flow occurs towards the final phases of transportation when water or water-saturated sediments and soils are incorporated (e.g. Palmer et al., 1991; Scott et al., 1995; Vallance & Scott, 1997).

The most common measure of debris avalanche runout estimations is based on the ratio of maximum height versus maximum runout (H/L ratio; Hiem, 1932), which defines the coefficient of friction. This also provides the basis of many numerical models for simulation of flows (Ui et al., 2000). Models of rheology and emplacement

have been developed to explain the relatively low dissipation and deformation of fragmental clasts that preserve original edifice stratigraphy (Takarada et al., 1999). These models incorporate features such as air/gas fluidized basal layers, mechanical fluidisation on lubricated substrates, acoustically or seismically triggered fluidization through to non-Newtonian, Bingham flow mechanisms. Other models have focused on granular flow mechanisms involving low-density basal layers and low angles of (basal and internal) friction due to loss of mass through deposition or increased fluidization (Iverson et al., 1997). Ui et al. (2000) concluded that a combination of models probably apply to most volcanic debris avalanches depending on their composition, volume and environment.

Given that a range of rheological conditions and flow mechanisms apply to volcanic debris avalanches, modelling their future hazard potential by numerical simulation is likely to be very challenging. However, some of these hurdles must be overcome in order to provide the most realistic hazard assessment scenarios at frequently collapsing stratovolcanoes. To examine these constraints for modelling debris avalanches and debris flows a combined geological and modelling study was carried out at Mt Taranaki using the most recent major debris avalanche unit (the c. 6700 yrs. old Opua Formation) as an example (fig. 5.1). This single unconfined volcanic debris avalanche deposit displays a range of sedimentological variability with distance from source and the deposit margins and surface are well defined and observable. Using a combination of aerial photographic interpretation, GIS analysis and focussed sedimentological investigations, a model of emplacement for the Opua debris avalanche can be developed and compared to simulations based on the Titan2D granular flow model (cf. Patra et al., 2005).

5.2. Geological Setting of Mt. Taranaki/Egmont Volcano

The Taranaki volcanic succession consists of a group of Quaternary andesite volcanoes (Neall et al., 1986) that lie to the west of the major Taupo Volcanic Zone subduction-related volcanism (Cole, 1986; Gamble et al., 1993a; Wilson et al., 1995). The oldest of the Taranaki successions is Paritutu Volcano at the northwestern extreme, with a K-Ar age of 1.75 Ma (Price et al., 1999). The next youngest volcano is the c. 0.57 Ma Kaitake, followed by Pouakai around 0.25 Ma (Neall, 1979, Neall et al., 1986). Mt. Taranaki/Egmont Volcano is the youngest and most southerly expression of the NW-SE trending volcanic alignment. Its activity began >210 ka (Zernack, 2009) with at least one eruption known to have occurred after AD1755 (Platz, 2007).

Mt. Taranaki and its ring plain is situated unconformably upon a sedimentary marine basin sequence of weakly consolidated sand-, silt- and mudstones with intercalated shell beds that record fluctuating sea levels from the Late Cretaceous to early Miocene (King & Thrasher, 1996; Kamp et al., 2004). The sedimentary sequence is cut by numerous Quaternary faults, yet their common SSW-NNE orientation apparently reflects an earlier stress field (Sherburn & White, 2006). An indicator of the more recent stress field may be given by the alignment of volcanic vents, because these tend to lie perpendicular to the extension direction (Nakamura, 1977). Neall (1971) also identified a number of faults perpendicular to the current volcanic lineament particularly through Mt. Taranaki (the Oaonui Fault and Inglewood Fault). However, movements on these faults have not yet been correlated to any volcanic debris avalanche event.

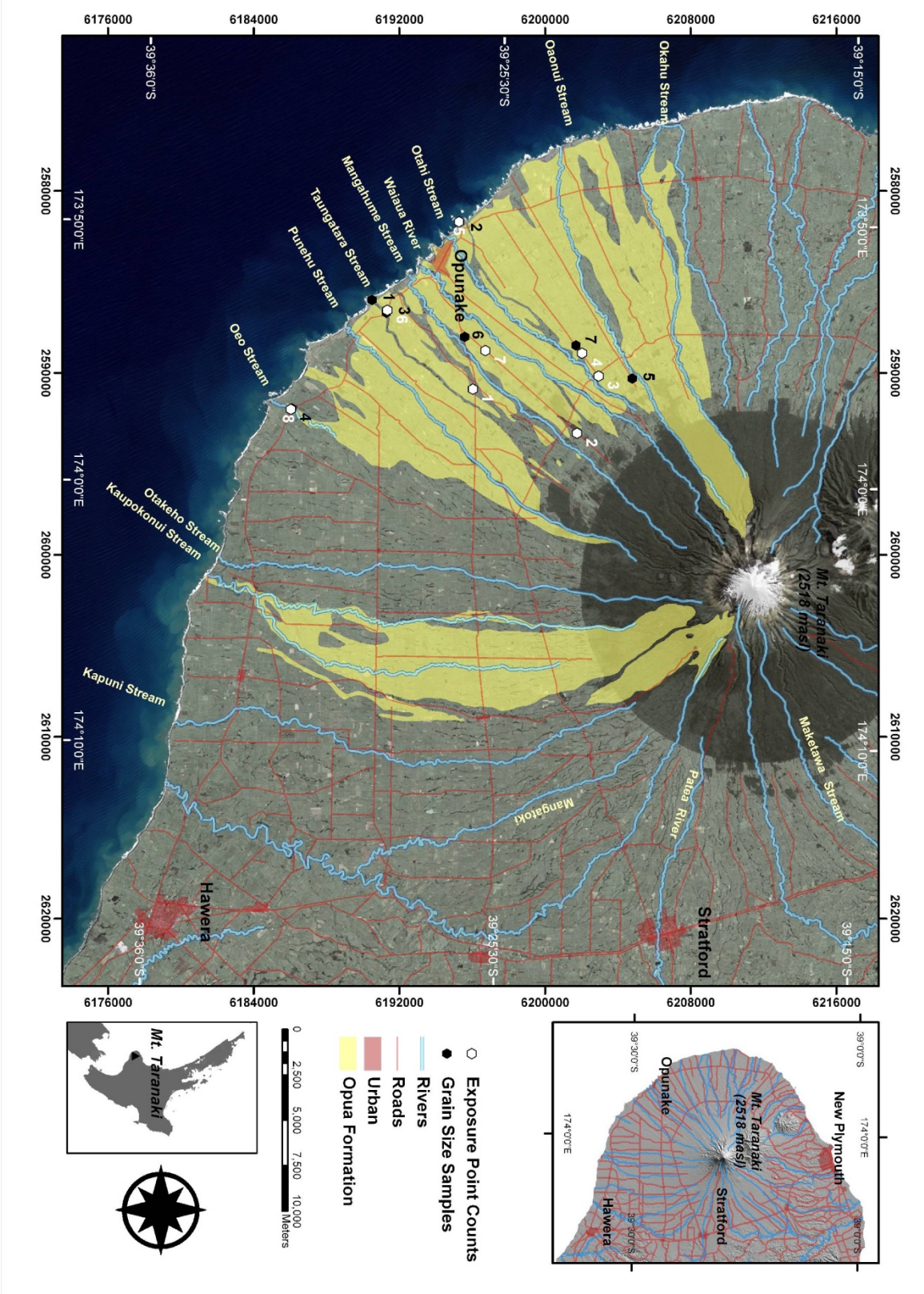

Figure 5-1. Location map of Mt. Taranaki and LandSat7 image of the ringplain. Shown in yellow is the Opua Fm. (Neall and Alloway, 2004). Indicated are also the location and identification numbers for grainsize samples and point count localities.

The current edifice of Mt. Taranaki rises to 2518 m above sea level and comprises c. 12 km^3 of lavas and pyroclastic deposits that are mostly younger than 14 ka (Neall, 1979). The edifice is surrounded by an apron of volcaniclastic diamictons, including debris avalanche, lahar, fluvial and pyroclastic deposits, that is an order of magnitude greater in volume (>150 km^3) (Neall et al. 1986). Volcanic debris avalanche deposits, attributed to the failure of former edifices, make up the largest component of volcaniclastic material within the near-circular Taranaki ringplain.

Four debris-avalanche deposits in west and south Taranaki were mapped by Neall (1979), including the Opua, Warea, Pungarehu and Stratford Formations and later Alloway et al. (2005) identified three additional debris avalanche deposits (Ngaere, Okawa and Motunui Formations) to the north-east and south-east of the volcano. Zernack (2009) has revised this record to include 14 debris avalanche deposits over the entire record known for Mt Taranaki. Palmer & Neall (1991) and Zernack (2009) also recognised that these debris-avalanche deposits record large-scale destruction of the cone. In contrast, the intervals between their emplacements are characterised by phases of edifice (re)growth and periods of quiescence, represented by eruptive products and lahar deposits as well as paleosols and fluvial sediments, respectively.

Only a minimum run-out distance can be estimated for the Taranaki debris avalanches because coastal erosion is continuously removing the toes of deposits around the Taranaki peninsula at c. 25-40 km from the edifice. These calculations indicate a minimum H/L ratio of 0.1. Uniquely, Mt. Taranaki volcanic debris avalanches could spread in an unconfined fashion onto the gently dissected ring-plain, forming broad fans around the volcano (Neall, 1979; Neall et al., 1986; Palmer & Neall, 1991; Zernack, 2009). The largest known edifice failure at Mt. Taranaki produced the <22.6 ka

Pungarehu Formation for which the onshore volume is estimated at 7.5 km^3 (Ui et al., 1986) covering an area up to 250 km^2. Its internal structure is characterised by two major components: fragmental rock clasts (FRCs) and matrix. FRCs are shattered or deformed pieces of lava and stratified volcaniclastic material that represent intact parts of the former volcanic edifice (Alloway et al. 2005). They are surrounded by interclast matrix, which includes clay-sized material. Mt. Taranaki lithologies, including those of FRCs within the avalanche deposits, range from vesicular red and black scorias through non-vesicular to holocrystalline, porphyric lavas of basaltic andesite to andesite composition (Neall et al., 1986; Stewart et al., 1996). One of the smallest known debris avalanche units is the Opua Formation, estimated at only 0.35 km^3 (Neall, 1979) yet spreading over a large area and exhibiting similar structural features to the Pungarehu deposit.

Mt Taranaki has a high mean annual rainfall with a strong altitude-related gradient, ranging from 2400 mm on the lower flanks at c. 300 m asl., up to 8000 mm near the summit (Stewart et al., 2006). Palmer et al. (1991) highlights that most drainage originates from the upper slopes and mean discharge of all the rivers draining the volcano out to a 12 km radius equals to 46 m^3/s. This discharge is relatively constant and indicates a large groundwater reservoir is located in the volcanic pile that may provide a considerable source of water during a collapse event as well as promoting weathering of the edifice interior.

The incorporation of clays, in particular allophane and ferrihydrite (andic material), into inter-clast matrix is an additional significant factor in increasing the mobility of debris avalanches and related cohesive debris-flows (Alloway et al., 2005). Under the humid-temperate climatic conditions of the western North Island, abundant andesitic

ash rapidly weathers to short-range-order clay minerals such as allophane (Neall, 1976c). Allophane consists of hollow spherules with diameters of 3.5-5 nm (Parfitt, et al., 1981), and hence has a very high specific surface area and capacity for water retention (up to 300% of the weight of dry soil). During debris avalanche propagation, these cover-bed deposits will directly contribute allophane-rich, fine-grained material into the flowing mass to greatly enhance its potential fluidity. Vallance and Scott (1997) suggested that clay-rich (cohesive) and wet flows might spread up to ten times farther than dry volcanic debris-avalanches.

5.3. Debris Avalanche Nomenclature

Standard grain size terminology is applied in this study such as: clay (<0.004 mm), silt (0.004-0.0625 mm), sand (0.0625-2 mm), granules (2-4 mm), pebbles (4-64 mm), cobbles (64-256 mm) and boulders (>256 mm). Matrix refers to the components of the deposit that make up the finest grainsize (<2-4 mm) and form an embracing interconnected body of particles that support or fill gaps between clasts (>4 mm). Clay refers to clay-sized particles as well as crystalline and short-range-order clay minerals. Debris avalanche deposits are distinguished from diamictons with similar textural characteristics by their content of mega-clasts (Neall, 1979, Palmer et al., 1991; Scott et al., 2001), which are single (encased) definable fragments of lithologically or stratigraphically coherent material derived from the original edifice. Other diagnostic features include jig-saw fragmented clasts, major zones of strongly sheared and deformed soft clasts and sheared basal margins with common rip-up clasts (Siebert et al., 1987; Glicken, 1991; Ui et al., 2000; Scott et al., 2001).

The internal structure of Taranaki debris avalanche deposits is characterised by fragmental rock clasts (FRC) and matrix. The matrix is unsorted and unstratified and may contain rip-up clasts of plastically distorted soil, peat and tephra layers as well as wood fragments derived from the terrain beneath. Intra-clast matrix is a separate entity that occurs within FRCs and megaclasts of original breccias from the edifice (Alloway et al., 2005). Scott et al. (2001) and Palmer et al. (1991) define megaclasts as being >1 m in diameter. These can be large coherent fragments of rock, intact portions of the original edifice strata, fragmented clasts that have been partially disaggregated and those that have completely disaggregated to form a "domain" of rock fragments that are recognisably related and could represent a jigsaw puzzle (Shreve, 1968; Gaylord et al., 1993). The lithology and ratio of matrix to FRCs can vary within each debris-avalanche deposit depending on the characteristics of the source area, related volcanic activity, as well as flow rheology and interaction with paleo-physiography.

The content of clay and/or clay sized particles is also a diagnostic feature of debris avalanche deposits and can provide information on source areas, initiation and emplacement processes. Wet debris avalanches and clay-rich (cohesive) debris flows are typically associated with the collapse of fluid-saturated portions of a volcanic edifice (Vallance & Scott, 1997). The available water, pore-water and alteration or weakness of the pre-avalanche mass contributes to the rapid transformation from debris avalanche to clay-rich debris flow.

5.4. The Opua Formation

The Opua Fm. (fig. 5.1) was first identified by Neall (1979) as a debris avalanche deposit on the south western ringplain that consists of a poorly sorted, coarse, brecciated axial facies flanked by marginal conglomerate and sands. Also described is a second deposit lobe farther east, which was later recognised as being a younger debris flow unit <3600 yrs B.P. in age (Alloway et al., 2005). The deposit forms a broad fan (7 km wide) of c. 4 m of deposit resulting in a volume of 0.35 km^3, a similar volume to that of the amphitheatre of the source area on the southern volcano flanks. The deposit exhibits a characteristic hummocky landscape along its axial facies with a higher density of larger hills along the main dispersal axis that reduce in spatial density and size laterally and longitudinally. Neall (1979) also considered the largest mounds to be protruding from beneath the Opua Formation and represented mounds from earlier deposits. The marginal facies does not exhibit mounds and was thought to have been emplaced by debris flows. Radiocarbon dates of wood from within the deposit returned an age of 6570 ± 110 yrs B.P. (Neall 1979).

Three facies were recognised in the deposit: axial a, axial b, and marginal facies (Neall, 1979; Alloway 1989; Palmer et al., 1991: Alloway et al., 2005).

- Axial a facies is where fragmental rock clasts dominate and interclast matrix occupies <30% of the deposit. The surface topography is dominated by large mounds up to 50 m high with basal areas of 500 m^2.
- Axial b facies occurs where inter-clast matrix comprises 30-90 vol.% and where the surface physiography is dominated by sparsely distributed mounds and hills. This corresponds to the mixed block and matrix facies of Glicken (1996).
- Marginal facies is where the proportion of inter-clast matrix is dominant, making up >90 vol.% of the deposit, and no mounds or hills occur.

In exposure the Opua debris avalanche deposit is a poorly-sorted diamicton consisting of a characteristic yellow to brown, poorly sorted, silty or clay-rich sand matrix with a variety of andesitic to basaltic-andesite fragmental rock clasts (fig. 5.2). The internal stratigraphy is generally consistent with distance. In distal areas the matrix exhibits higher contents of pumice and/or a wet, greasy clay-rich texture. The matrix is mainly composed of rock fragments of the same composition of the clasts, along with minor pumice fragments and pyroxene, hornblende and plagioclase crystals. The clasts are angular to sub-rounded, porphyritic, basaltic-andesite to andesite lithologies, ranging in colour from black and grey to red. Pumice clasts are typically weathered and sub-rounded. They occur in low proportions and are always <3 cm in diameter. Lava clasts exhibit a range of fracturing patterns from minor cracks and jigsaw-shaped fractures to completely dispersed fragments within a radius of <1 m. The clasts exhibit no preferred alignment or imbrications; however, some fragmented clast-trains are formed, aligned parallel to flow direction. Megaclasts of fragmented rock clasts, domains of fragmented rock clasts with an intraclast matrix and sections of source stratigraphy occur throughout, but are more prevalent in axial a and b facies (fig. 5.2A-D).

In distal areas, wood fragments and organic material become more prevalent near the base of the deposit (fig. 5.2E-F). In the southern axial a facies of Neall (1979), the deposit contains a conspicuously high content of logs, making up to 2% of the local deposit. Distal areas also have a greater abundance of rip-up soil clasts that are rounded and rotated but intact. The contact of the deposit to underlying soil or medial ash layers is generally planar. Little evidence is seen for erosion at the basal contact or shearing within the lower part of the deposit. In axial areas a weak <cm-sized silt layer can be

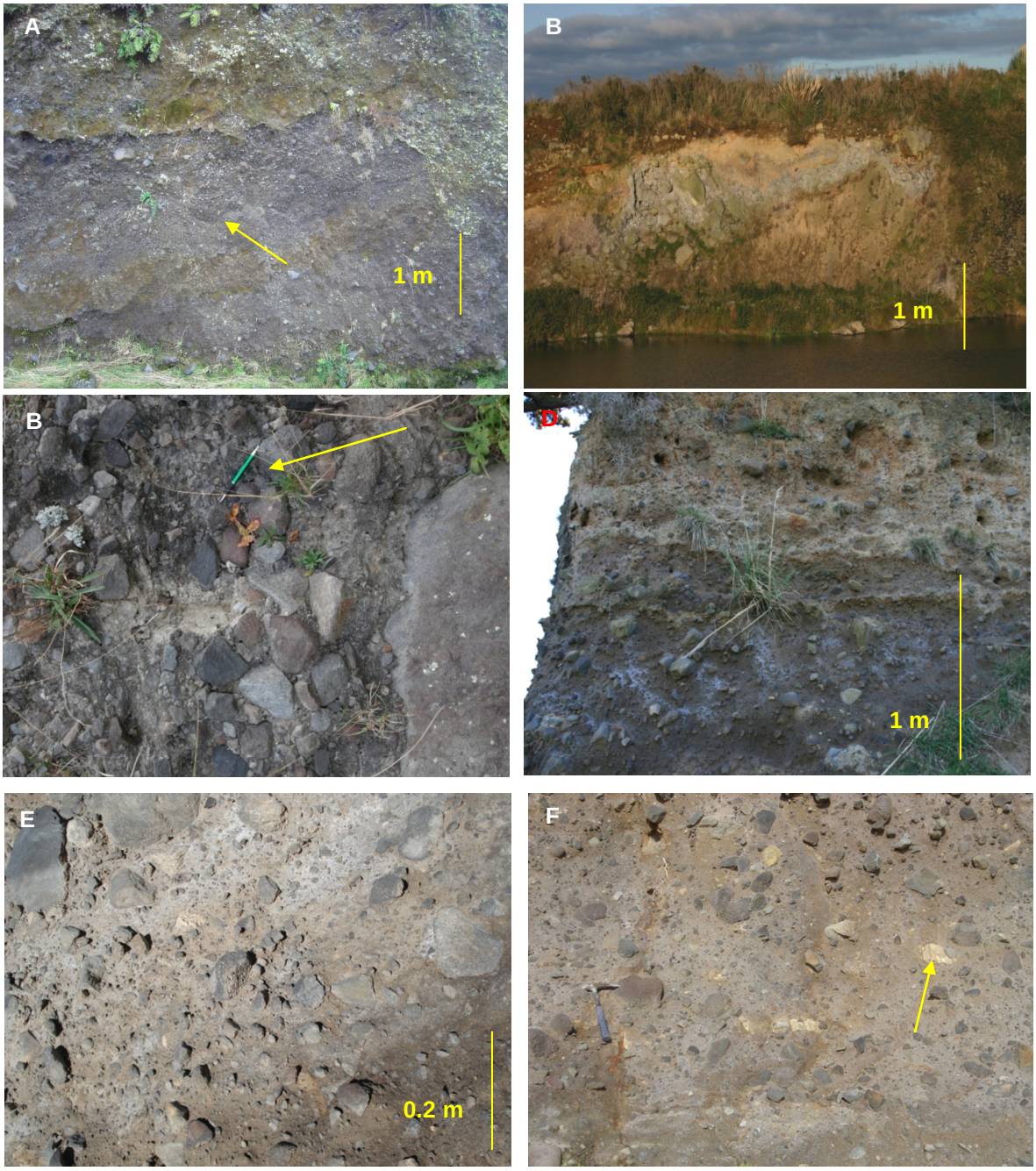

Figure 5-2. The internal structure of the Opua Fm. with photos A & B representing axial a facies, C & D the axial b facies and E & F the marginal facies (cf. Palmer et al., 1991). A) Arrow points to a shattered and stretched megaclast above a paleosol separating two debris avalanche deposits; B) Deposit characterised by predominantly FRCs; C) Deposit in axial b facies with groupings of FRCs (arrow points to 10 cm long pen for scale); D) Central distal section showing a layered deposit with a lower basal unit higher in FRCs; E) Texture and structure of the marginal distal facies, and F) Distal marginal facies texture and structure, yellow clast are ripped-up soil clasts (arrow points to soil clast).

distinguished at the base of the deposit in some locations. In coastal exposures, a weak internal stratigraphy occurs with a ~0.5 m-thick basal layer having a grey very firm matrix with a higher content of larger clasts than the upper (1.5 m) unit, which is characterised by a yellow-brown matrix (fig. 5.2D). In some locations a <cm sized grey silt layer is visible between the two units similar in appearance to settling and dewatering units described in non-cohesive lahars (Cronin et al., 2000).

5.4.1. Granulometry

Samples of matrix from lateral and longitudinal cross-sections were subjected to standard sieve analysis from -4 to 4 Φ (16 mm to <63 μm) (fig. 5.3). Analysis of the proportion and sizes of clasts was also made from counts at eight exposures using a 10 cm point spacing and recording either matrix or clast size (fig. 5.4).

The matrix materials are all polymodal sandy gravels with a mean grain size in the range 0.8 to 3.4 mm. Marginal facies samples have a mean grain size of ~3 mm compared to a mean of only ~1 mm in axial a facies. Axial b samples show the greatest range from 2.5 to 0.8 mm, representative of its transitional nature. All histograms show a polymodal distribution with major peaks at 2 and -4 Φ (fig. 5.3A). According to the statistics of Folk and Ward (1957), the samples are very poorly sorted, very coarse sand to fine gravel (fig. 5.3B-C). The most distal samples from the marginal facies have gravel-dominated grain-size distributions, possibly more representative of debris flow conditions.

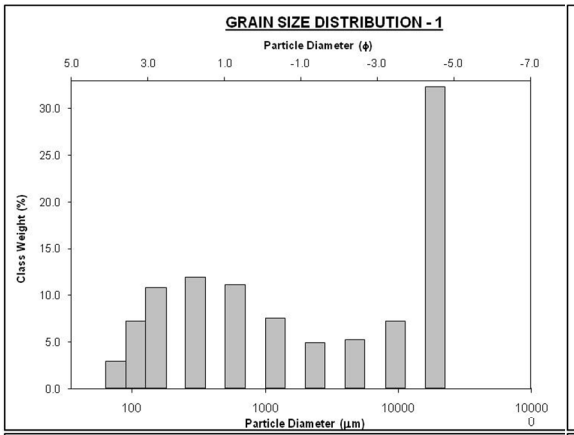
GRAIN SIZE DISTRIBUTION - 1
Particle Diameter (ϕ)
5.0 3.0 1.0 -1.0 -3.0 -5.0 -7.0
Class Weight (%)
0.0 5.0 10.0 15.0 20.0 25.0 30.0
100 1000 10000 100000
Particle Diameter (µm)

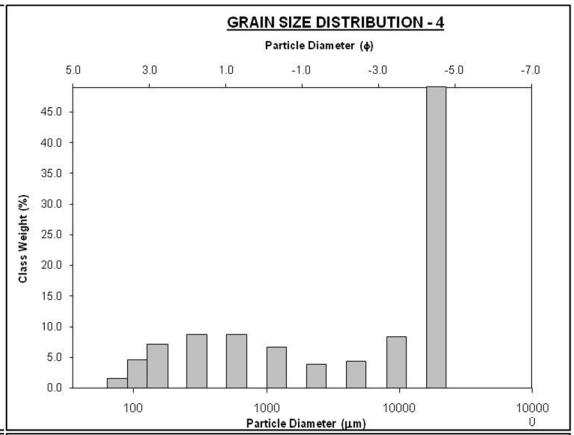
GRAIN SIZE DISTRIBUTION - 4
Particle Diameter (ϕ)
5.0 3.0 1.0 -1.0 -3.0 -5.0 -7.0
Class Weight (%)
0.0 5.0 10.0 15.0 20.0 25.0 30.0 35.0 40.0 45.0
100 1000 10000 100000
Particle Diameter (µm)

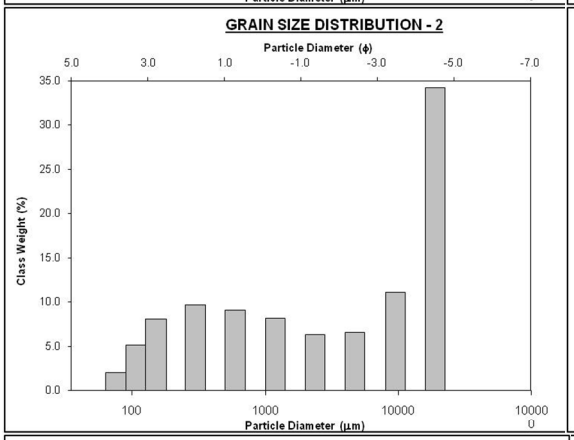
GRAIN SIZE DISTRIBUTION - 2
Particle Diameter (ϕ)
5.0 3.0 1.0 -1.0 -3.0 -5.0 -7.0
Class Weight (%)
0.0 5.0 10.0 15.0 20.0 25.0 30.0 35.0
100 1000 10000 100000
Particle Diameter (µm)

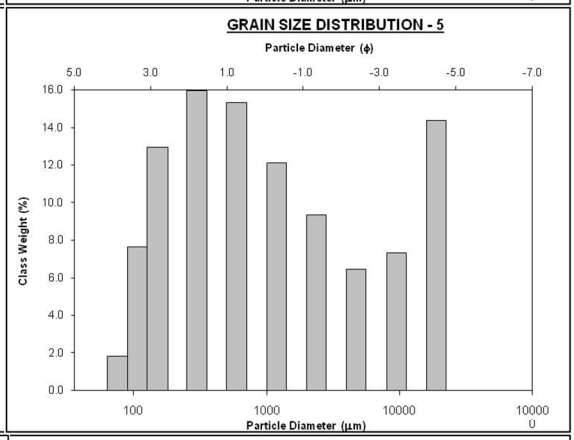
GRAIN SIZE DISTRIBUTION - 5
Particle Diameter (ϕ)
5.0 3.0 1.0 -1.0 -3.0 -5.0 -7.0
Class Weight (%)
0.0 2.0 4.0 6.0 8.0 10.0 12.0 14.0 16.0
100 1000 10000 100000
Particle Diameter (µm)

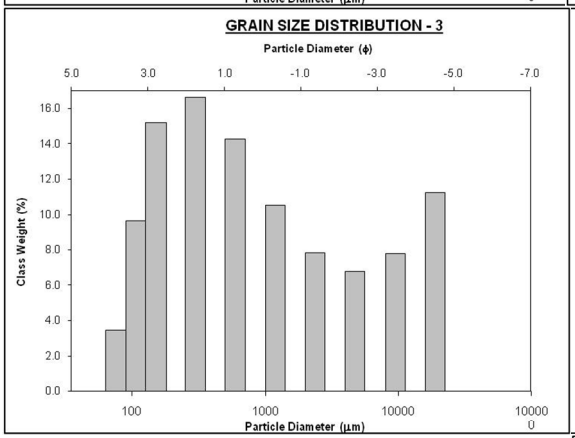
GRAIN SIZE DISTRIBUTION - 3
Particle Diameter (ϕ)
5.0 3.0 1.0 -1.0 -3.0 -5.0 -7.0
Class Weight (%)
0.0 2.0 4.0 6.0 8.0 10.0 12.0 14.0 16.0
100 1000 10000 100000
Particle Diameter (µm)

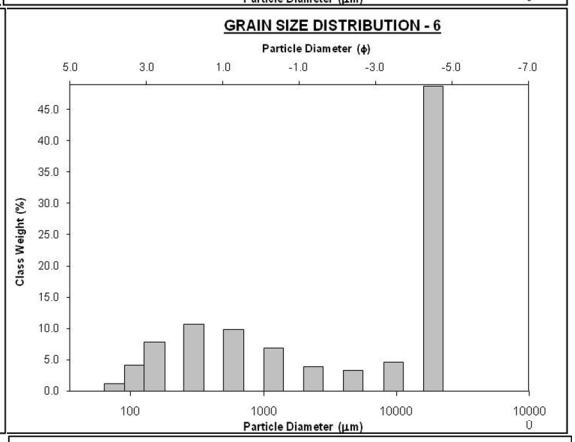
GRAIN SIZE DISTRIBUTION - 6
Particle Diameter (ϕ)
5.0 3.0 1.0 -1.0 -3.0 -5.0 -7.0
Class Weight (%)
0.0 5.0 10.0 15.0 20.0 25.0 30.0 35.0 40.0 45.0
100 1000 10000 100000
Particle Diameter (µm)

A

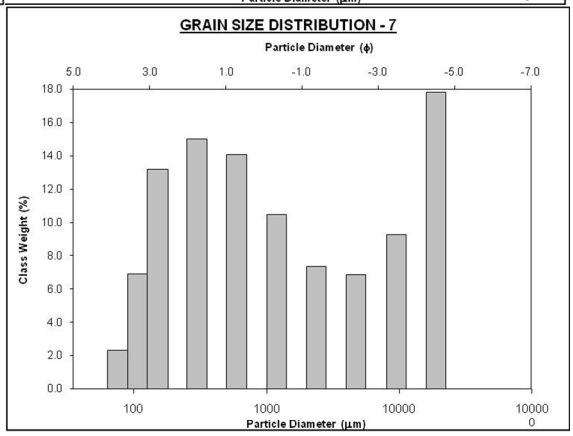
GRAIN SIZE DISTRIBUTION - 7
Particle Diameter (ϕ)
5.0 3.0 1.0 -1.0 -3.0 -5.0 -7.0
Class Weight (%)
0.0 2.0 4.0 6.0 8.0 10.0 12.0 14.0 16.0 18.0
100 1000 10000 100000
Particle Diameter (µm)

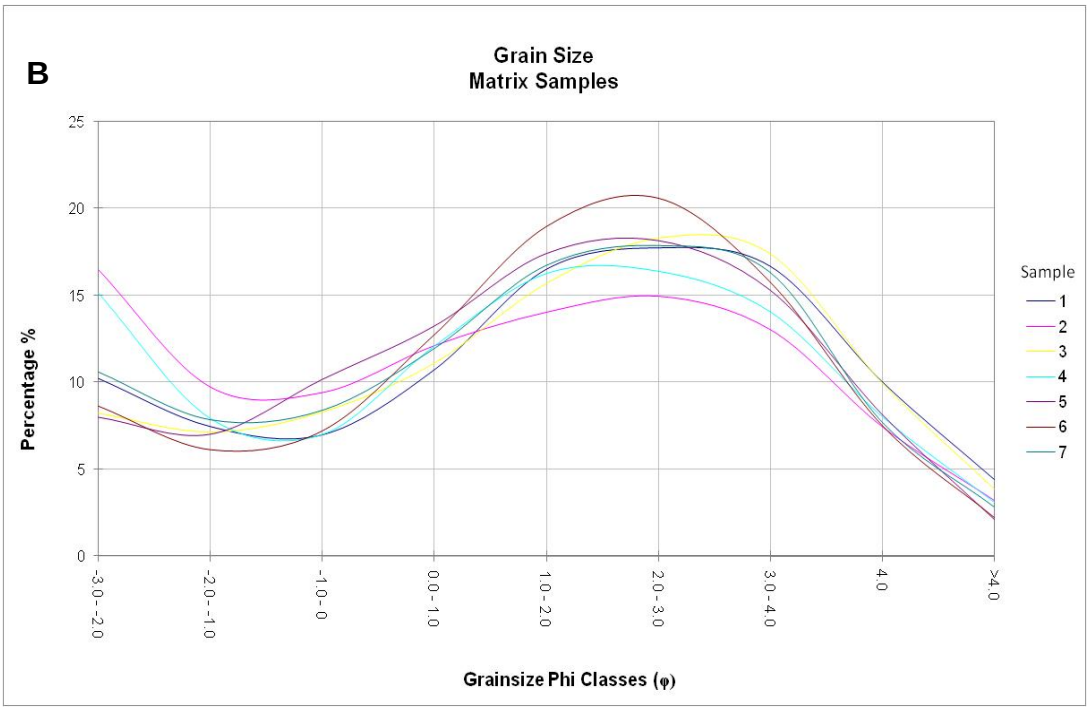

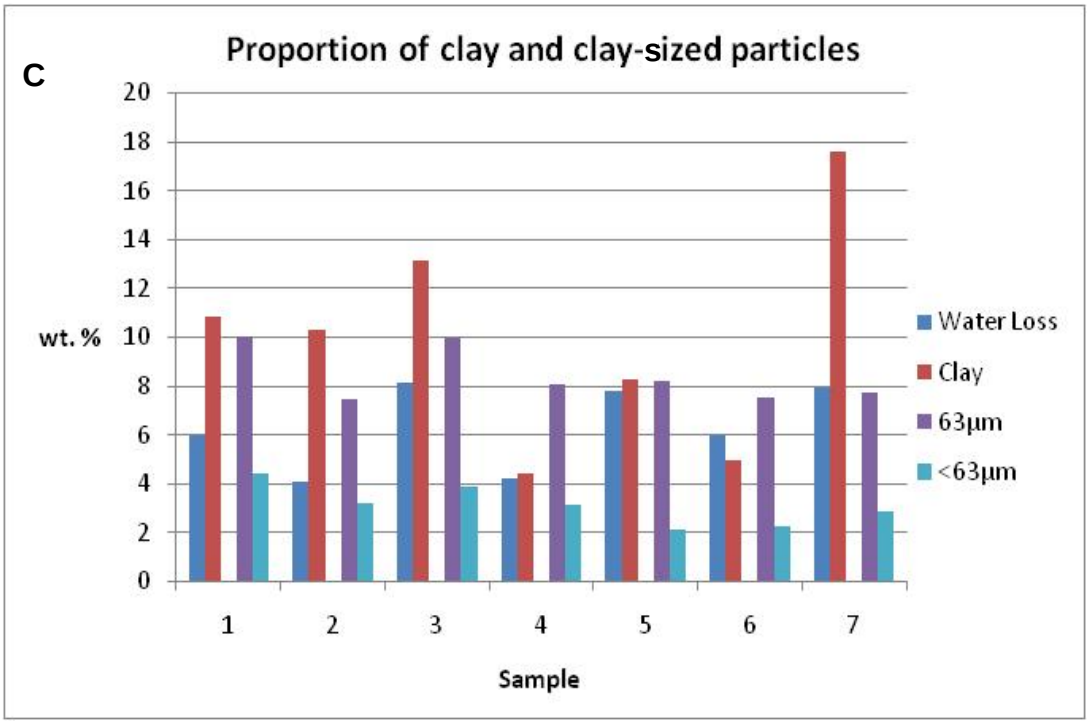

Figure 5-3. Grainsize distribution within Opua matrix samples (sample locations cf. fig. 5-1) samples 1-4 distal, 5-7 proximal. A) Graphs 1-7 display the grainsize distribution within the 7 matrix samples gathered; B) Combined plot of all samples; C) Histogram showing the loss of water (wt.%) after drying, loss of clay after sonic bath as well as proportions of the 63 µm and <63 µm fractions.

Samples after drying exhibit a consistent water loss of 4-8 wt% (fig. 5.3). Clay-sized particles make up 5-17 wt.% of the total sample with axial facies matrix ranging from 8-17 wt.%. Axial b facies has clay contents of ~10 wt.% while samples of the marginal facies contain only 4 wt.%. Silt-sized particle (<63 μm) contents are consistent around 10 wt.% of the total sample, with up to 14 wt.% in two matrix samples taken from distal areas (fig. 5.3).

The clast/matrix proportion analysis also illustrates a gradational increase of matrix portion with increasing distance from source (fig. 5.4) similar to that inferred by Palmer et al. (1991). More proximal areas (axial a facies) show a consistent matrix proportion of 45 vol.%, while axial b and marginal facies consist of c. 60 vol.% matrix. The most distal exposure exhibits 75 vol.% matrix. Most clasts counted have a mean diameter in the range of 8.5-12 cm, with the largest clasts measured being 50-100 cm across. Distal axial b and marginal exposures contain <7 vol.% boulder-sized clasts while more proximal axial a and b facies exhibit up to 10 vol.% boulders.

5.4.2. Microcracks

In order to characterise the morphology and surface features of debris avalanche matrix components, the coarse sand (<2 mm) fraction of the Opua samples was separated and the particles analysed using a scanning electron microscope (SEM). Common features observed in debris avalanche samples are the presence of microcracks (lateral displacement separations and intersecting relations) and hackly (concave fracture) surfaces. These features have been described as being diagnostic of debris avalanches and originating during their initiation (Komorowski et al., 1991; Belousov et al., 1999).

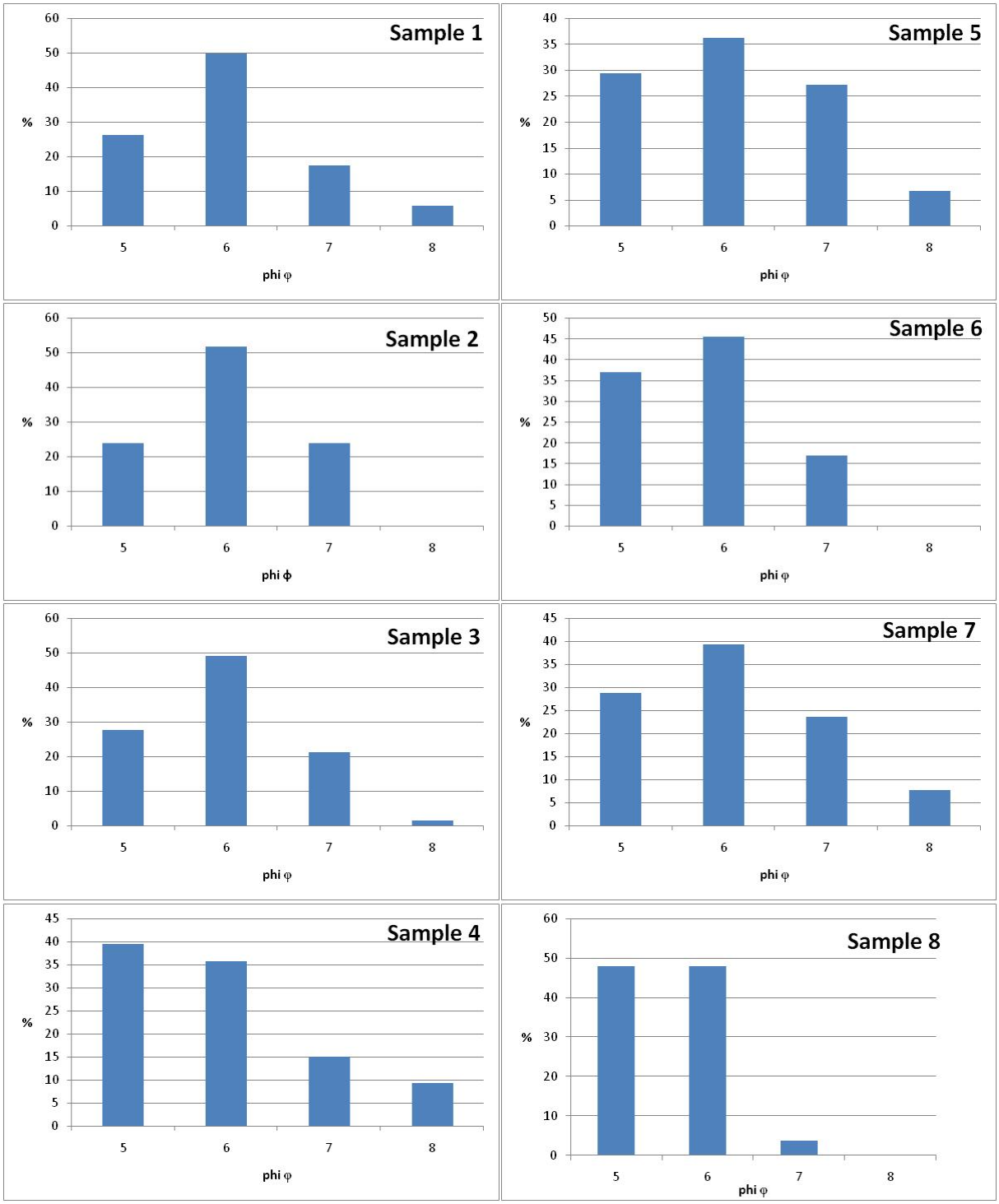
Sample 1
%
phi φ
Sample 5
%
phi φ
Sample 2
%
phi ϕ
Sample 6
%
phi φ
Sample 3
%
phi φ
Sample 7
%
phi φ
Sample 4
%
phi φ
Sample 8
%
phi φ

A

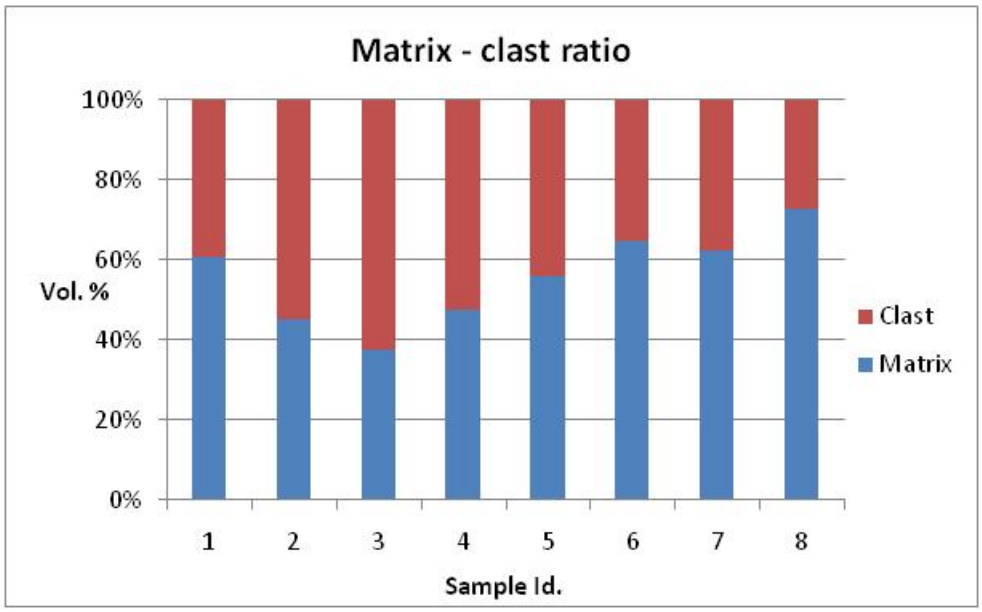

B

Figure 5-4. Point count analysis from exposure (locations of point counts cf. fig. 5-1). A) (previous page) Grainsize distribution at locations 1-8 from 100 counts per exposure; B) Proportion of matrix to clasts at exposures 1-8.

Rock fragments, pyroxene and hornblende crystals within the Opua matrix typically show microcracks from impacts and splitting of the particles. The rock fragments are subrounded to subangular with curved conjugate pairs of microcracks visible at 90-350x magnification, yet very little jointing was observed (fig. 5.5A-B). Little evidence was found for surface friction or scratching from other grains and only a small number of grains (<10%) exhibits hackles in one or two locations on the grain. Occasional glass shards are characterised by an extremely hackly surface at times with the entire surface exhibiting a fish-scale like pattern. Microcracks present are typically one or two large cracks that have migrated across the entire shard. The greatest impacts on the surfaces of glass shards may not be attributed to a decompression or explosion during initiation of the debris avalanche but rather to the relative softness of the glass.

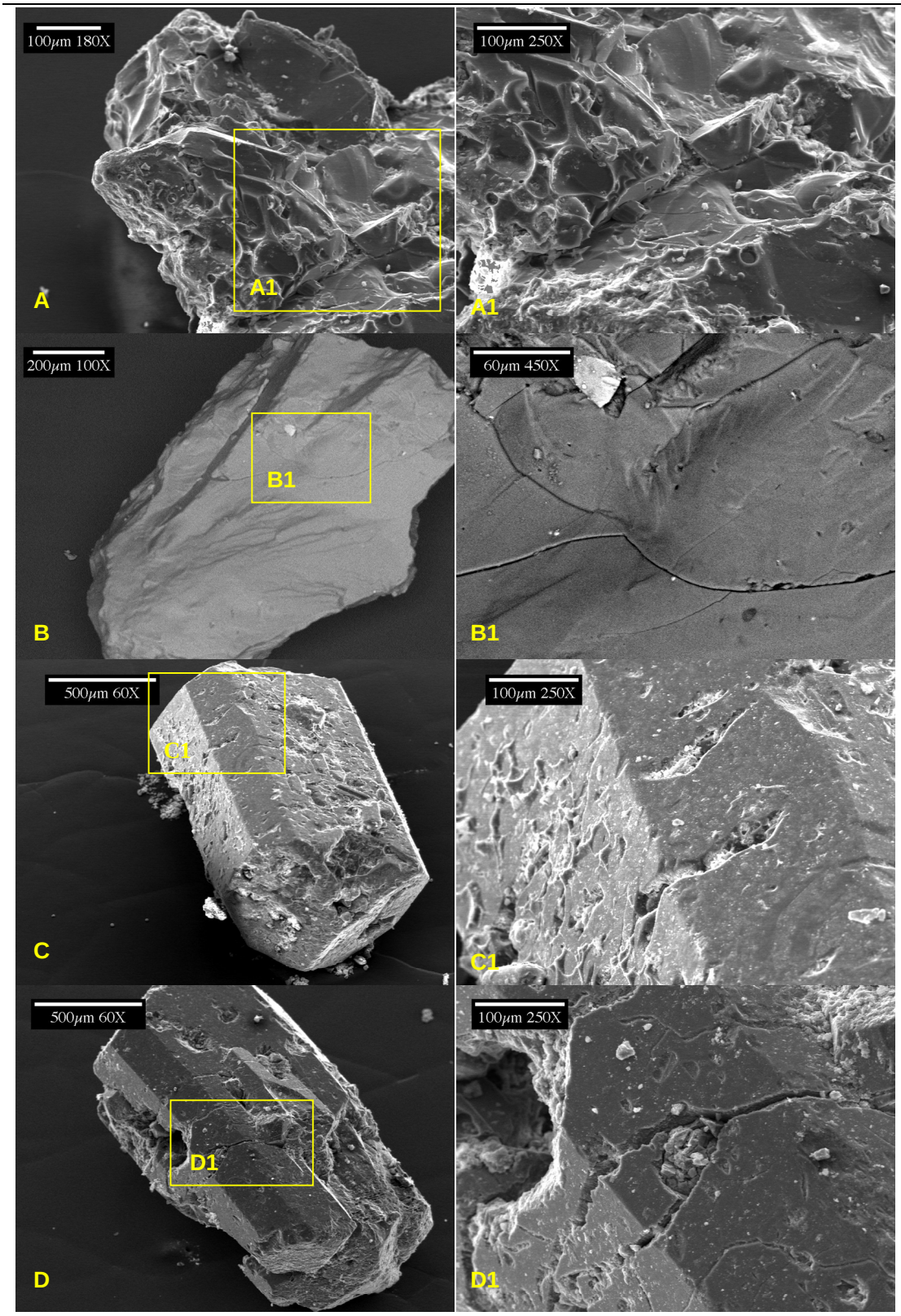

Figure 5-5. SEM pictures with examples of diagnostic features. A) Sub-angular rock fragment exhibiting collision surfaces and fracturing (A1); B) Rock fragment exhibiting conchoidal fracturing and close-up (B1); C) Pyroxene crystal showing impact marks, rounding at edges and fracturing (C1); D) Pyroxene crystal showing fracturing and close up (D1).

Since hackles are concentrated in localised areas it also suggests that they result from grain to grain contact during flow.

The most striking examples of impact scouring, indentations, microcracking/shear fractures and discrete plumose hackles occur on pyroxene and hornblende crystals. Their distinctive faces, cleavage and shape make the identification of post-formation impacts easier to determine. At ~50-100x magnification, when the entire mineral is visible, faces show 10-20 μm long scours or triangular indentations over ~30 % of the surfaces (fig. 5.5C). Hackly features are not prominent on the crystal surfaces; however, rare concave fracture patterns are visible at high magnification in areas where parts of the crystals were broken off. Crystals have subrounded edges as well as common microcracks and shear fractures forming joints that propagate through the majority of mineral faces (fig. 5.5D). At higher magnification the microcracks form a network of conjugate shear fractures throughout the entire face.

The proportion of fragments displaying microcracks has been determined from longitudinal and lateral cross-sectional samples. Samples exhibit either 30-50 % or 70-90 % of microcracked fragments with few consistent variations. Overall, axial deposits show the highest proportions of microcracked crystal grains compared to those from marginal areas of the deposit.

5.4.3. Geomorphology/Physiographic extents

A re-analysis of the Opua debris avalanche deposit has been carried out using new (c. AD2000), high resolution orthophotography combined with mapping via GIS (ArcGIS;

ESRI) at a greater resolution than previously possible. While the broad previously mapped extent of the unit (Neall, 1979) has only slightly been adjusted here, boundary details and deposit geometry are significantly refined. The only available Digital Elevation Model (DEM) has 20 m resolution and is too coarse for some of the analysis needed, meaning that only planar rather than 3-dimensional measurements can be made. The newly mapped deposit is up to 20 km wide at its maximum extent and covers an area of 243 km^2. However, it is only exposed at the surface below the 280 m contour, ~14.2 km from the current coastline. GIS catchment analysis of the intersecting drainages within the current deposit (fig. 5.6) indicates a source area around the headwaters of the Mangahume and Waiaua Streams, presently a valley between Bob's Ridge and Skeet Ridge (2440 m). The lava flows that make up these ridges postdate the Opua debris avalanche, with coverbeds indicating they were emplaced around 1400-3300 yrs B.P. (Neall, 1979). A secondary source area/catchment could have been the head waters of the Oaonui Stream c. 1100 m lower on the >7000 yrs old Warwick Castle lava flows. The catchment analysis implies a minimum run-out distance of 26 km due to the uncertain final extent of the deposit offshore. These suggest an H/L (height/length) coefficient (cf. Heim, 1932) of 0.09, which is at the more mobile end of the spectrum for debris avalanches of this volume.

The volume of the deposit is difficult to determine accurately due to poor exposure of its base over most of its aerial distribution. Neall (1979) suggested 0.35 km^3, but the spatial extent from this study and an average thickness of 5 m results in a calculated minimum volume of 1.22 km^3. When including the area obscured by overlying younger deposits and the reconstructed extent from the catchment analysis, the deposit volume increases to 1.62 km^3 but still represents a minimum since it does not count any offshore deposits. Using a graduated approach by assigning average thicknesses to the three identified facies (axial a – 10 m; axial b – 8 m and marginal – 4 m) a

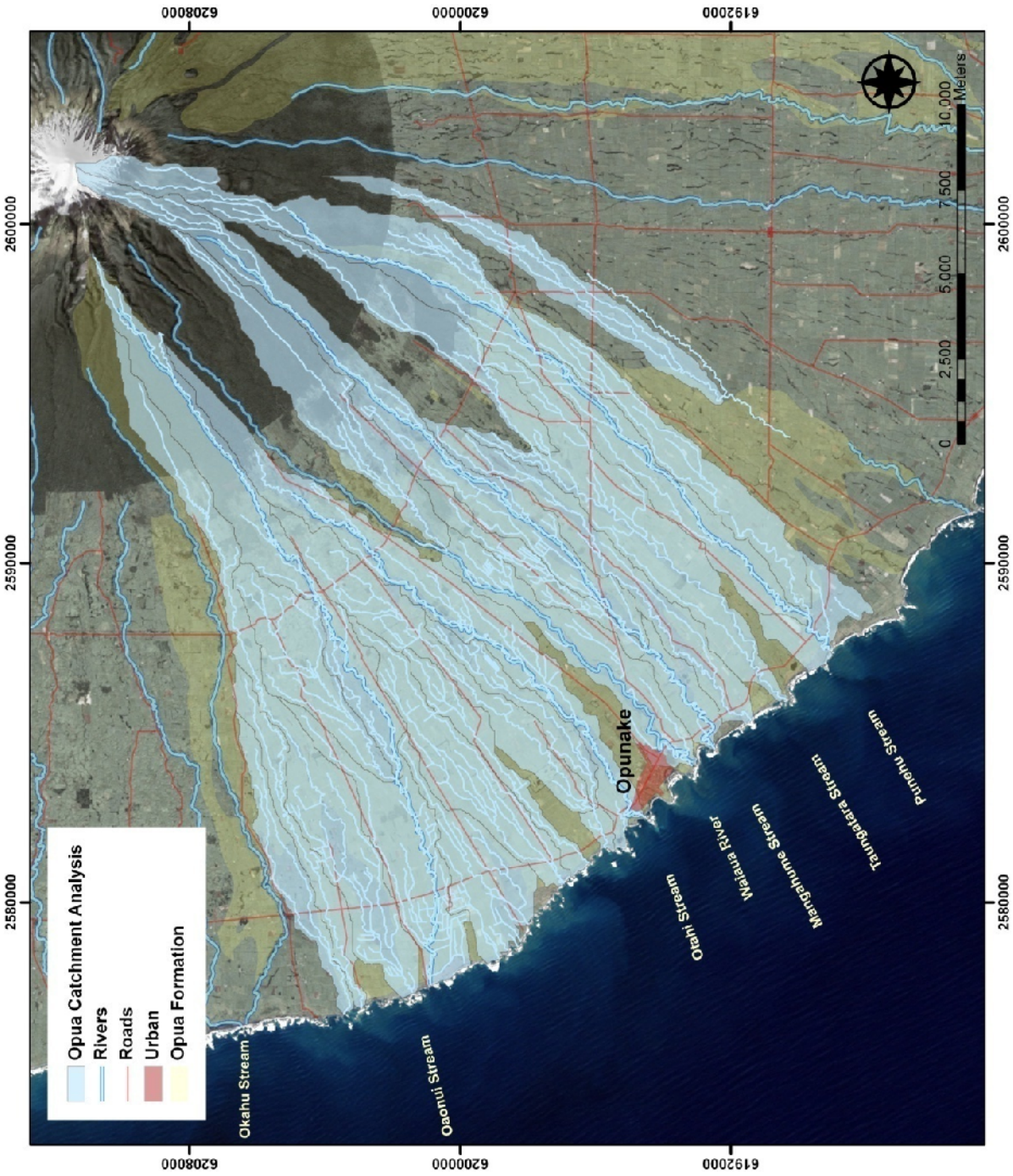

Figure 5-6. GIS catchment analysis of the drainage from mapped extents of the Opua Fm. indicating the source and flow path of the deposit.

volume of 1.98 km^3 is calculated and the maximum reconstructed volume is 2.38 km^3. The true volume of the Opua debris avalanche deposit lies within this range. However, in order to improve these estimates a high resolution DEM of the deposit surface is needed as well as sufficient basal exposure to correlate thicknesses.

5.4.4. Hummocks/Mounds distribution

Hummocks and mounds are characteristic surface features of debris avalanche deposits (eg Ui, 1983; Siebert et al., 1987; Crandell, 1989; Glicken, 1991). Hummock shape, distribution and structure vary considerably within and between units with no overall consistent model being determined for all debris avalanche deposits (Ui et al., 2000). Neall (1979) and Palmer et al. (1991) described the Opua debris avalanche mounds in detail and used their abundance and morphology to help subdivide the deposit into three facies. This subdivision gave rise to a model of mound emplacement and sedimentation resulting from increasing friction due to loss of mass, and mound formation due to the inability of the flow to distribute the clots of fragmental rock clasts or megaclasts. However, Neall (1979), Ui et al. (1986) and Alloway et al. (2005) emphasise that not all Taranaki debris avalanche mounds contain megaclasts, or a high proportion of FRCs.

In this study the Opua deposit surface morphology and the spatial patterns of different features were analysed (figs. 5.7 & 5.8) in order to determine a subdivision of the deposit using high resolution orthophotos (2.5 m) and a 20 m DEM. Four distinct Opua surface morphologies were identified (figs. 5.9 & 5.10).

5.4.4.1. Opua 1

Towards the edge of the deposit is a mound-poor relatively smooth surface. This is called the Opua 1 facies. The smooth, flat runout surface of the debris avalanche deposit has been described as marginal facies by Palmer et al. (1991). It consists of a ~5 m thick mantle of poorly sorted matrix-rich deposit with <1 m-sized clasts and rounded FRCs, overlying a low-relief paleophysiography. Mounds are rare and subtle covering only ~3% of the surface. They can be scattered with 1-2 km between mounds or located in distinct clusters of 3-30 bodies (figs. 5.7 & 5.9). They are <10 m in height with basal diameters of ~20-50 m and distinct flat inter-mound surfaces.

Coastal cross-sections of rare mounds show that they relate to megaclasts of intact, remnant stratigraphy from the source area up to 8 m in diameter. Other rare examples consist of domains of similar matrix texture, colour and FRCs, suggesting once-coherent blocks. However, the majority of mounds in cross-section are identical to the surrounding deposit.

5.4.4.2. Opua 2

This unit is similar to the axial b facies of Palmer et al. (1991) containing singular mounds defined by one or more closed contours (c.f., Glicken, 1996). This facies makes up the majority of the exposed deposit (fig. 5.10). Mound-density is significantly higher than for Opua 1, at up to 60 identifiable mounds per 0.5 km^2 (figs. 5.7 & 5.8). Within the deposit, the interclast matrix is still dominant (at 30-90%), there is a greater clast size range (0.1-5 m), and greater variability in the lithologies of sub-angular FRCs. Megaclasts show many fractures and domains of FRCs are commonly fractured and stretched parallel to the main flow direction.

Mounds are up to 15 m in height and >30 m in diameter and exhibit more irregular, commonly elliptical shapes, with axis ratios of 2:1 and long-axes aligned parallel to flow direction. Mounds are grouped or clustered together with contacting ends meeting to form small irregular ridges in the landscape (fig. 5.9). Between these clusters a distinctive flat surface is present, consisting of a deposit with a higher matrix portion than observed in the mounds. In cross-section, ~50 % of mounds show a gradation to increasing clast and FRC size from their margin to the centre.

5.4.4.3. Opua 3

The most distinct surface feature of the Opua deposit was termed axial a facies (Palmer et al., 1991). It consists of larger mounds that form interfluves of greater heights due the unit mantling older debris avalanche deposits through which the mounds of the older units were believed to occasionally protrude through. Here, through examining cross sections and surface patterns, we re-interpret these mounds to be purely compound mounds of the Opua debris avalanche deposit.

The mounds in this landscape are indistinct as single mounds and form steep-sided conical hills with no distinctive flat areas between them (fig. 5.9). On a larger scale, this hummocky landscape is made up of long lobes of ridges of mounds originating from source areas and oriented parallel to flow direction. The mounds are 30 to 50 m in height forming elongate ridges that extend up to 700 m in length and 500 m in width. These mound-ridges consist predominantly of angular to sub-angular FRCs with <30 % of interclast matrix, a chaotic mixture of lithologies and a clast-supported framework. Many of the more proximal ridges/hummocks exposed consist entirely of shattered lava blocks. The termini of lobes show a gradation into matrix-richer textures with interclast matrix surrounding domains of contacting fragmental rock clasts.

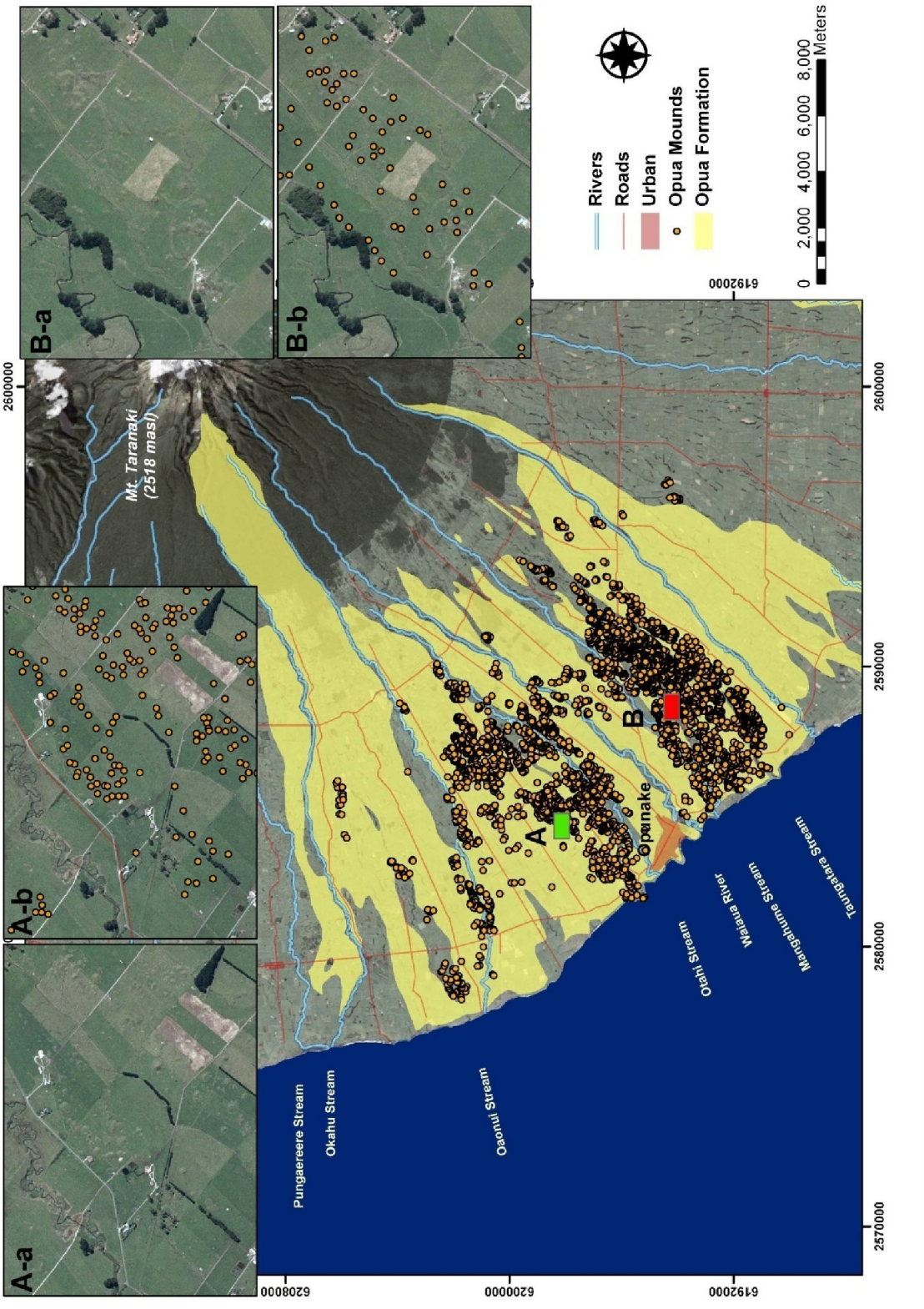

Figure 5-7. Distribution of debris avalanche mounds with each mound in the exposed distal areas being mapped as single point in GIS. Insets Aa-b and Ba-b show close-up of the terrain with and without the identified mounds and mapped points. Note the clustering patterns and groups of mounds.

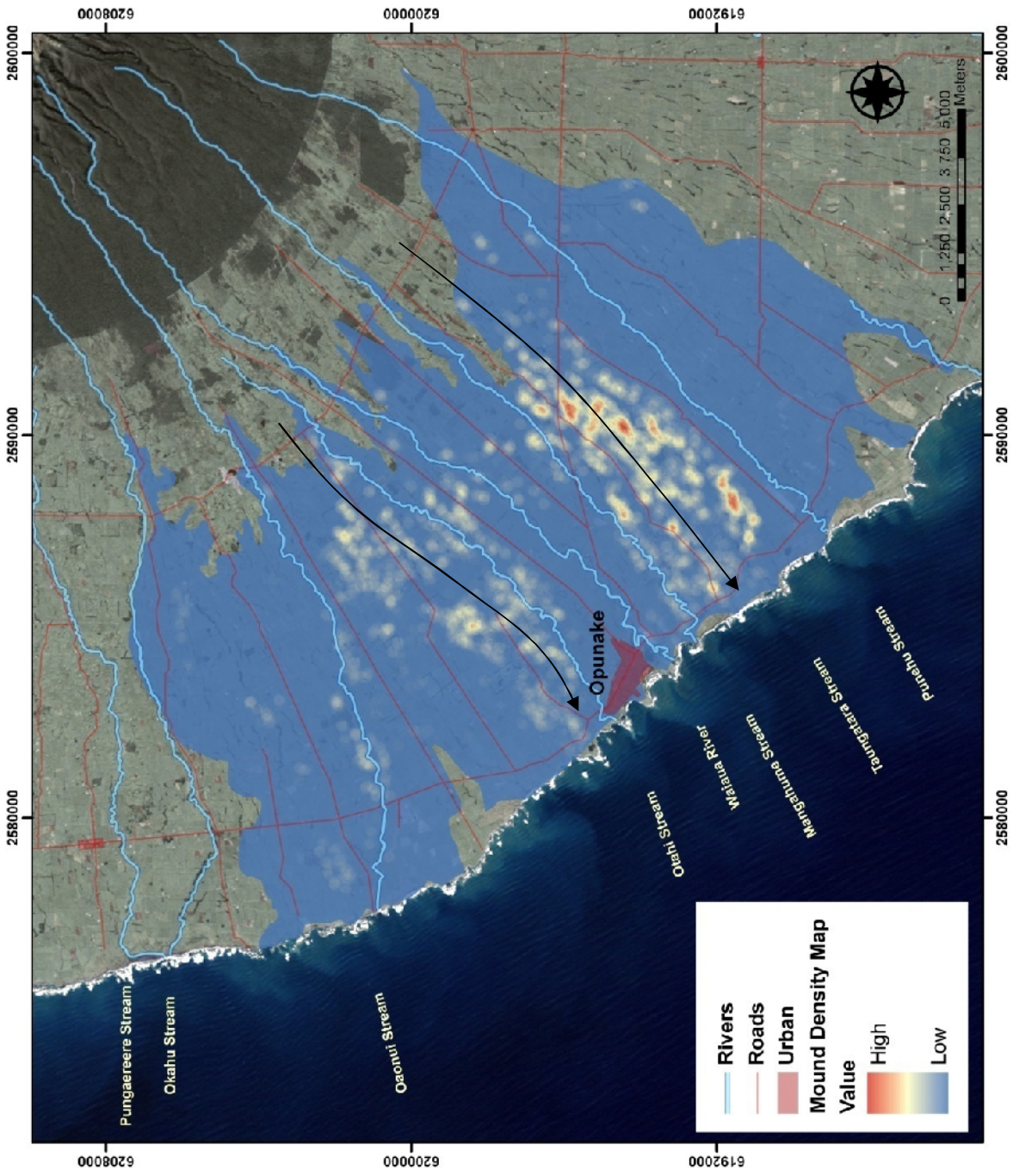

Figure 5-8. GIS raster map of the density of mounds across the landscape. Indicated are the clustering of mounds and groupings forming ridges parallel to flow direction as well as the two dominant flow paths (as indicated by the arrows).

5.4.4.4. Opua 4

This is another form of axial facies a, but characterised by proximal hummocky surfaces overlain by deposits of smaller, later debris avalanche lobes that stalled in proximal areas. This surface is extremely chaotic with multiple compounding mounds/hummocks that form an elevated (terrace-forming) set of ridges showing only weak alignment in flow direction (fig. 5.9). One distinct lobe is ~1-2 km long with its terminus at the 200 m asl. contour (fig. 5.10). Down slope of this steep front a number of distinct large compounded mounds of similar height (~50-80 m) trail for another ~1 km. The southern side of this lobe grades into the "Opua 3" facies.

The unique feature of this surface is that the defined composite mounds are separated by fine sediment inter-beds representing a compounded deposit of several events of a very similar nature. The similar lithological properties of these later units make distinction from the main deposit difficult and they could in fact record ongoing instability and land sliding in the Opua source area following the main phase of collapse.

5.4.5. Density Map

GIS analysis of the distribution of the mapped mounds uses a density algorithm to determine a raster image of clusters of mounds (fig. 5.8). This combined with the physiographic mapping described above results in two distinct patterns: one strongly longitudinal and the other defining two major flow paths (fig. 5.9).

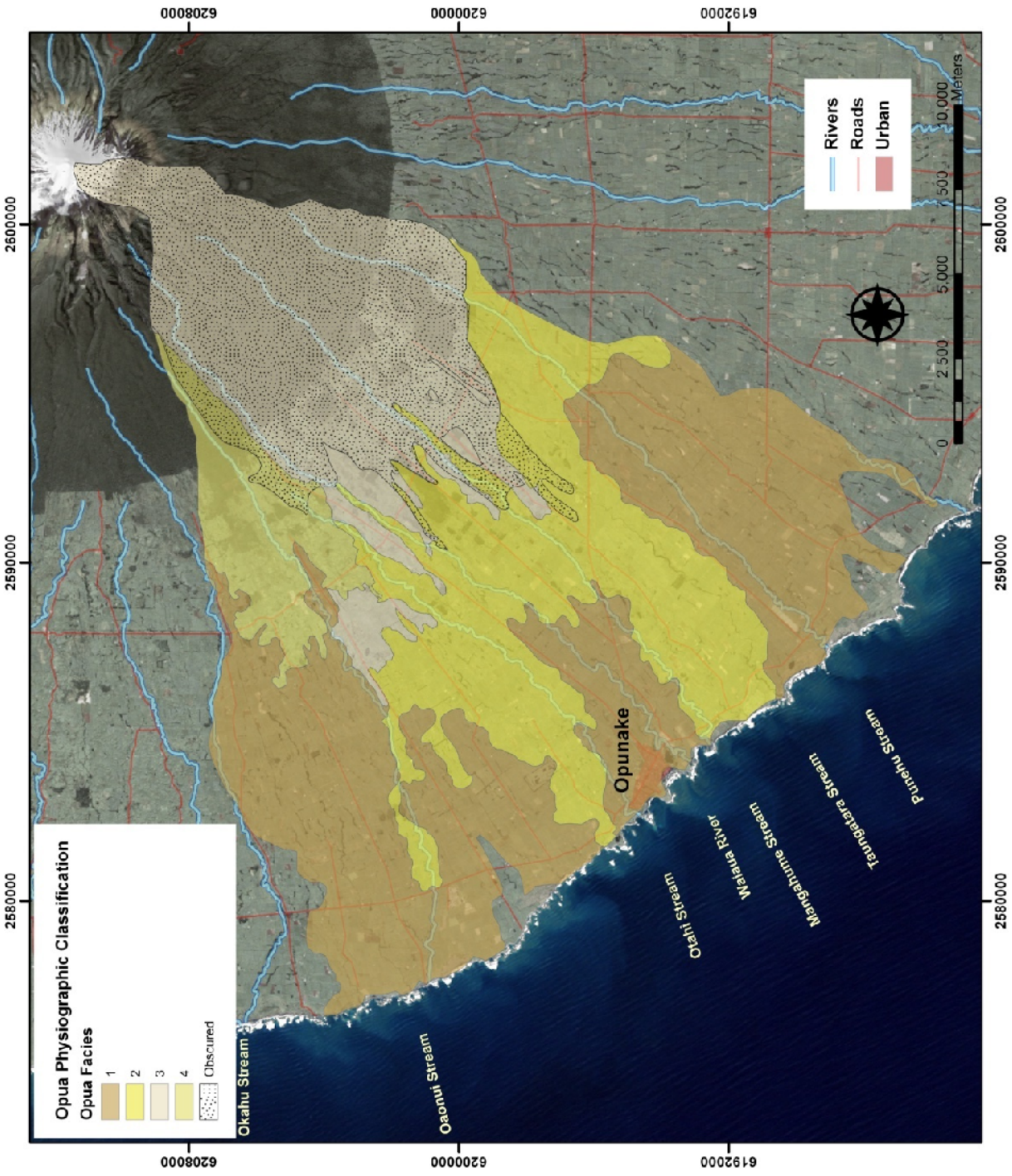

Figure 5-9. Physiographic map of the Opua Fm. showing the distribution of Opua facies 1-4 from this study.

From proximal to distal areas there is a gradual transition from a hummocky surface to clusters of single conical mounds, through to dispersed occasional conical mounds in a flat planar surface (fig. 5.10). This gradation may represent the rheological transition from sliding rock avalanche and frictional granular flow conditions to more cohesive viscous flow conditions as the large clasts break up.

The two distinct flow paths outlined by this analysis have not previously been identified and are clearly visible, both in the distribution of mounds at low scales in GIS and in the density map (fig. 5.8). The two lobes bear ~220° and 230° from true north, feeding lobes that separate at ~260 m altitude, 15 km from source. The lobes also correlate with present day catchment and drainage patterns of the major rivers in the area of the present Mangahume and Heimama/Waiaua Streams. Both lobes are seen in coastal cross-sections to be partly confined between low paleo-ridges consisting of more erosion-resistant, channelised, non-cohesive debris flow and promontories of older debris avalanche deposits (Zernack, 2009).

Also visible within the mound density map in the Opua 2 surface is a distinct pattern of ridges ~1.5-2 km long oriented parallel to flow direction over a 600 m wide band within each lobe (fig. 5.8). These ridges form strong lineations with intermittent 200 m gaps from the up-slope facies. They all coincide with paleo-drainages as indicated by the few basal exposures of underlying channelised laharic deposits.

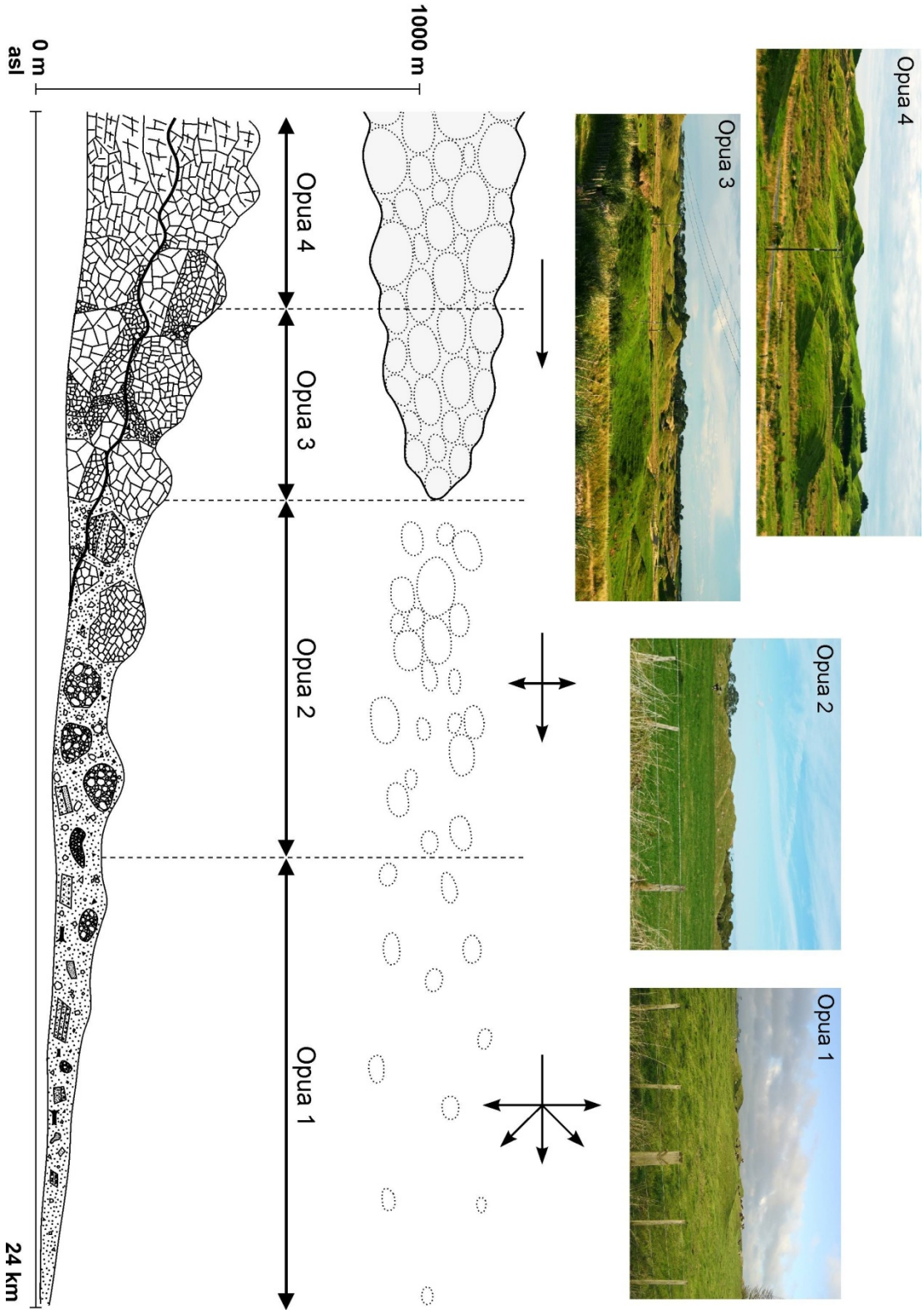

Figure 5-10. Sketch and photos of the dominant landscapes in relation to each of the four identified Opua facies. Lower sketch shows a longitudinal cross-section of the Opua debris avalanche deposit (modified from Palmer et al., 1991; Zernack, 2009). Upper sketch displays the plan view and distribution of mounds. Arrows indicate preferred flow direction.

5.5. Titan2D

Titan2D, developed by the Geophysical Mass Flow Group at SUNY Buffalo (Pitman et al., 2003), is based on a model for an incompressible Coulomb continuum; a "shallow-water" granular flow (after Iverson & Denlinger, 2001). It is designed primarily for "dry" granular masses, not wet debris flows or highly fluidised pyroclastic flows. However, certain parameter combinations may be used to provide some basic comparisons to these types of flows. Titan2D then offers a chance to simulate mass flows throughout the mobility spectrum at Mt. Taranaki, especially that of flank-collapse induced debris avalanche events.

The main variables in the model are the pile dimensions and angles of "internal" and "basal" friction. Initial tests of the Titan 2D model have been undertaken on Ruapehu Volcano attempting to calibrate the model to observed debris flows. Over 90 runs (on both Ruapehu and Egmont Volcanoes) have been evaluated, by comparing model outputs to historic data (Procter et al., in review; refer to chapter 6). Internal friction controls the lateral spread of the moving mass, and best results were at 30-35°, close to the angle-of-repose for typical mass-flow sediment. Basal friction angles should vary considerably for different types of flow; we used a range between 9-30° based upon gradients at which deposition began for each type of flow (Procter et al., in review; refer to chapter 6).

Using a P4 3.0 GHz processor and 1.5 GB of RAM, simulations with low (200-400) initial computational mesh densities produced poor results because Titan2D was not sampling the DEM with enough precision to adequately represent the terrain.

Increasing the initial computational mesh density up to 800 was possible, producing more realistic results. Large-scale multi-processors are required to improve on this.

Titan2D operates under a LINUX environment utilizing GRASS GIS to supply the topography data through a DEM. A variety of DEMs of 20 m resolution were used, e.g. Triangular Irregular Network (TIN) and Inverse Distance Weight (IDW) Grid derived. It was also found that the Titan2D model is very sensitive to the quality of DEM and the outputs improve with the DEM being more representative of the real topography. Parameters such as the initial pile volume and location can also be crucial to accurately simulate mass-flows on a cone such as Mt. Taranaki. Yet for some pre-historic flows these parameters can be difficult to determine.

5.5.1. Titan2D Application

To simulate the emplacement of the Opua debris avalanche deposit an internal friction angle of 28° (estimated sediment repose angle) and a basal friction angle of 20° (slope of the start of deposition fan) was initially used with this being lowered to 5° in attempt to recreate the conditions for an increased run-out. The initial pile was placed to fill the valley of the Waiaua/Mangahume catchments, which lead to an initial volume of $6.3x10^8$ m^3. In follow-up runs multiple (3-4) piles were used (dividing the volume equally) and also placed within the source area either laterally or longitudinally to flow direction.

Initial piles that replaced the parasitic cone Fanthams Peak and variable friction maps were also applied with varying degrees of success. Simulations with source areas on

Fanthams Peak (volume ~0.6x10^7 m^3) failed to join with the Mangahume piles and travelled only 6 km from flow. Variable friction maps similar to those used by Sheridan et al. (2005) were applied but showed no significant difference to runs with single basal friction values.

5.5.2. Titan2D Results

The modelled flows had very similar outputs despite adjusting source pile volume, friction value inputs and the number of initial piles. They inundated an area of the cone and ringplain that contains the deposits of the Opua Fm (fig. 5.11). Only ~30 mins of simulated time was required before the bulk of the flow came to rest suddenly. The simulated flow (>0.5 m) inundated a path 6 km wide for 10 km from source. Beyond 10 km, the simulated flows form two distinct lobes with the southern one following the Waiteika/Mangahume/Taungatara catchments for a further 13 km and the other following the Heimama/Otahi stream catchments for another 10 km.

The animation of the simulation shows that the flow responds to minor topographical changes such as being directed down subtle stream valleys and catchments. Also, despite only using a 20 m DEM the simulations responded to the representation of these features in proximal areas where they are recorded in the DEM.

The simulations provide very good comparison to the Opua 2-3 facies, although they are not able to reproduce the full Opua 1 run out facies. This may indicate that the Opua Fm. was either much larger than first considered, or its deposition was very strongly modified by secondary processes. The most northern lobe of the Opua 4

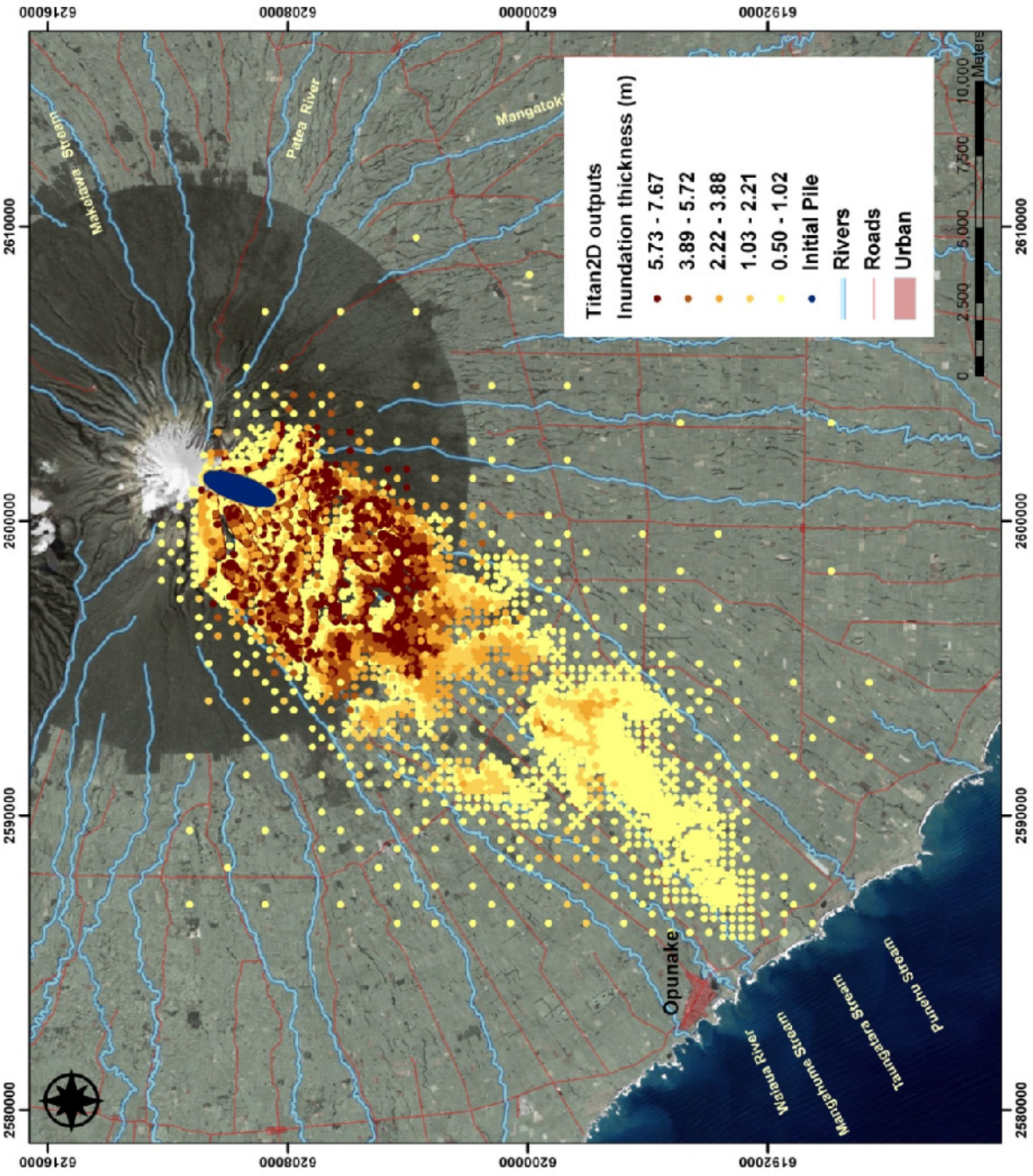

Figure 5-11. Map of example outputs from the computer simulation Titan2D and the location of the initial pile.

facies (mixed deposit/mound facies), located in the Oaonui Stream area could not be simulated. This indicates that the present-day geomorphology as given by the DEM provides a barrier that stops flows from inundating this particular area.

5.6. Discussion

Analysis of the Opua Fm. provides important insights into the emplacement processes of debris avalanches onto low-relief and unconfined surfaces at andesitic volcanoes in temperate areas. The modelling, surface topography analysis and internal sedimentary descriptions explain more clearly some of the features recognised by Neall (1979) and Palmer et al. (1991). This analysis provides some components that contribute to developing a model of collapse, flow and deposition of debris avalanches and provides strong constraints on hazard maps for the area.

5.6.1. Mound Formation

Mounds or hummocks are important and unique diagnostic features of debris avalanche emplacement. Deposition concepts to explain their formation need to be consistent with rheological models. In the context of the Opua debris avalanche deposit it is important to note that around ⅔ of the surface area and up to ¾ of its volume consists of mounds or hummocks. The identification of similar surface or patterns of distribution of mounds provides several insights into emplacement of this debris avalanche.

Neall (1979) and Palmer et al. (1991) considered the Opua hummocks to be primarily lithologically controlled, related to distribution and proportion of FRCs. Neall (1973) described the process of mound formation in the older Pungarehu debris avalanche deposit as being similar to progressive aggradation where coarser material, fragmental rock clasts and boulders were subjected to increasing friction from the base and forced to come to rest or deposit. This engendered segregation of finer-grained flowing materials that continued onward. At distal areas of the flow the size and density of mounds were thought to gradually decline due to a loss of coarser material. Palmer et al. (1991) also suggested a similar process of mound formation through the progressive loss and reduction of the velocity of the coarser fragmental rock clasts, creating a segregated water and clay-rich phase that remains highly mobile. The mound shapes under this type of model indicate angles of repose for the various phases of flow.

Glicken (1996) provided three mechanisms for mound formation each forming a different type of hummock: (1) those formed from blocks/megaclasts in matrix; (2) those in proximal areas from the pieces of the old mountain; and (3) those of predominantly matrix. The Opua debris avalanche deposit consists predominantly of category 1 and 3 mounds, thought to form due to deceleration resulting from increasing basal shear (Glicken, 1996). The mounds with their long axis parallel to flow direction are considered to represent a type of levee while those orientated randomly indicate the terminal areas of lobes.

The formation of compressional ridges, longitudinal ridges (flow bands) and mounds/hummocks are common surface features on both experimental and natural deposits of granular flows (Davies & Dufresne, 2009), although not so common in fluvial-dominated regimes such as debris flows. Dufresne and Davies (2009) attribute the formation of mounds to the velocity of the emplacing grainflow, material density and shape, the internal frictional behaviour and controls and the interaction with basal topography and substrate. For volcanic debris avalanches to produce hummocks, they propose that the flow must be thick and consist of highly competent material (such as angular fragmental clasts) that is propagating on a basal shear layer. This results in extensional ridges of blocks of coarser material exhibiting a longitudinal gradation of proportionally finer material or fewer blocks/fragmental rock clasts. Note that these features are well developed for the Opua debris avalanche deposit but are not seen in distal areas of deposition despite containing dense fields of hummocks. Dufresne & Davis (2009) also imply there is a gradual process of breakup of ridges from extension relating to the velocity of frontal regions being greater than the tail. The pattern of extensional ridge break-up would seem to match the pattern of distribution and clustering of hummocks parallel to flow direction of the Opua debris avalanche deposit. However, the concept of front flow velocities being greater due to basal shearing cannot be directly supported in the Opua unit, because depositional patterns that exhibit layering of variable texture, grading or granulometry (as observed at Cantal Volcano, France; Schneider and Fisher, 1998) are not observed other than a coarser, more poorly sorted basal layer that has been observed in distal axial parts of the Opua Fm., most likely related to a pulsing in the flow.

The presence of clay particles in a debris avalanche or mass flow can strongly change the coherence of the flow and affect its velocity, rheology and runout (Breien et al., 2008). Shea and van Wyk de Vries (2008) through analogue modelling show that when

cohesion is increased in the mass flow through inclusion of clay there is a prevalence for hummocky surfaces to form, while if the material is homogeneous then ridges form with the inclusion of water. This is also the case in the Socompa debris avalanche where it has been envisaged that the incorporation of finer substratum material into the flow increased cohesion and formation of ridges (van Wyk de Vries et al., 2001). Major (1996) also considers that increased fines in debris flow content decreases lobe thickness and apparent strength, because the fines help sustain high pore pressures that reduce frictional resistance and enhance lobe spreading. The highest clay content within the Opua debris avalanche deposit occurs in the Opua 3 facies (axial b), which exhibits the most recognisable hummocky surface with mounds being related to the breakup of longitudinal ridges.

From these findings, hummocky surfaces should hence be considered as features resulting from the movement of a flowing mass that is undergoing basal frictional changes, internal shearing as well as changing fluid pressures and grain sizes. These factors result in changes in velocity and eventually deposition.

5.6.2. Concept of emplacement

Models of debris avalanche emplacement can be difficult to determine from a historical deposit that is only partially exposed. Also, examination of emplacement mechanisms from other more recent and better exposed deposits can only be done when similar patterns of deposition exist. Hence, emplacement models from analogue experiments provide further insights into large-scale debris avalanches such as the Opua Formation, although issues of scale must be strongly noted.

All models of debris avalanches describe the process of a rigid mass transforming into a fluid-like flow and then back into a partially rigid mass (Iverson, 1997a). Most recent numerical models of debris flow emplacement have evolved from grain flows (Takahashi, 1981) to Coulomb grain flows (Savage and Hutter, 1991) to models including the effects of pore fluid pressure (Major and Iverson, 1999). Conceptual models of emplacement of debris avalanches postulated from depositional features generally infer a grain flow mechanism where grain interaction dominates (Davies, 1986; Glicken, 1996; Schneider & Fisher, 1998; Kelfoun and Druitt, 2005). However the incorporation of clays in the flow or the development of a low friction basal layer seems the only way to explain the long runout of many debris avalanches (Shea et al., 2008; Davies and McSaveney, 2008).

Exposure and surface mapping of the Opua debris avalanche deposit beyond 10 km indicates that although it has an extremely hummocky surface with a high proportion of fragmental rock clasts, it is relatively thin compared to its width. This implies a very mobile flow that is essentially granular and able to flow over surfaces with little basal erosion. The collapsing mass may have been near saturation, aiding this mobility. Campbell et al. (1995) provides a simulation (Hopkins, 1987) of the initial phases of flow generation, with shearing and fracturing of rock increasing with the volume of material being added to the initial failure, in turn lowering the basal friction. However, in the Opua case this type of flow must have transformed at some point to develop into a flow that exhibits a very low basal friction and little shearing allowing preservation of the underlying soil surface. The development of very low basal friction layers as described by Davies and McSaveney (2008) is a possibility to allow the Opua flow to later transform and split into two main lobes controlled by low-relief paleo-topography.

Transformation may also be aided by incorporation of or internal production of clay particles. Van Wyk de Vries et al. (2001) attributed the long run out of the Scomopa debris avalanche to the inclusion of finer grained substratum. Schneider and Fisher (1998) also recognised a process of isotropic spherical dispersion where the fragmentation and inflation of rock clasts and megaclasts contributed to the interclast matrix increasing mobility and the development of lobate plugs of flowing mass. The Opua Formation deposit at ~10-12 km from source is emplaced across a rapid change in slope at the base of the volcano, associated with strongly increased fragmentation and dispersion of FRCs (yet with little impact on paleo-surfaces) and the development of a facies (Opua 2) characterised by splitting into two lobes controlled by subtle underlying physiography.

The Opua 2 facies (axial b) is dominated by mounds clustered and aligned to the flow direction. Davies & McSaveney (2008) explain the formation of such mounds through the development of fluid basal layers with blocks of more rigid mass riding atop. However, at this distance the sedimentology of the Opua debris avalanche deposit shows that rather than shear being concentrated at the base, the flow may have been somewhat more viscous with higher contents of clay and fluid. At the other end of this spectrum, experiments by Major and Iverson (1999) simulating debris flow conditions on a flume highlighted the importance of pore-fluid pressure and the differences a loamy (10% silt and clay) mixture can have on flow and deposition of material. They described that the flow decelerated after a major break in slope resulting in debris accumulating and thickening at the flow front. This increased the fluid pressure in its central parts, leading to surges or waves that may overrun already deposited material to create lateral deposits of coarser material similar to levees. The Opua appears not

to have been so strongly dominated by fluid pore-pressures, but it is possible that this process could have generated lobes or ridge-like forms in more distal reaches.

The boundary between the axial b and marginal facies of Palmer et al. (1991) was thought to represent the transition of the flow from a rock-avalanche to a lahar. Here, it is considered that there was a more gradual process of change from the outset of a rigid mass to a cohesive flow over distance, possibly due to an increase in fluid pressure, matrix content, clay content and changing internal and basal stresses and friction. The only major feature of distinction between the two facies (axial b and marginal) is thickness and mantling of the landscape, which cannot always be used to determine rheology of the flowing mass (Major and Iverson, 1999).

In general emplacement processes progressed from a collapsing and granular/fragmenting rock mass into a cohesive flow as a response to terrain change, flow thinning, and/or an increased frictional regime at the flow front. This inturn liquefied and concentrated the internal sections of the flow creating two lobes that progressed as cohesive flows forming the characteristic ridges and hummocks/mounds.

5.6.3. Titan2D Comparison

The Titan2D simulations and catchment analysis are not consistent with the northern lobe or Opua 4 facies distribution representing a single Opua collapse, unless mass was also lost from the northern side of Bob's Ridge or generated as low as the ~300 m contour. This matches with the sedimentological and geological evidence that implies

several later phases of collapse compounded to form the Opua 4 landscape. Titan2D running on a present-day terrain model simulated Opua-3 axial areas well, although the same simulation was not able to account for the entire runout and Opua 1 facies, despite attempts to change input parameters such as the basal friction angle. However, changing these parameters increased the run out of each simulated lobe to a certain degree with a general overall increase in velocity. The simulation provided comparable thicknesses for areas of deposition and responded to small changes in topography by flowing around mounds represented on the DEM and being directed by drainage patterns despite being poorly defined by the 20 m DEM.

It is important to recognise that a granular flow (Coulomb) model cannot be expected to simulate a mass flow undergoing such a dramatic range of transformations as exhibited by the Opua debris avalanche. However, by combining geological analysis with simulation studies, attributes of the flows can be examined and the usefulness of the Titan2D model for these types of flows can be evaluated. As a hazard analysis tool these simulations were able to most importantly provide a reliable indication of the main flow axes, proximal and medial inundation areas and deposition thicknesses as well as reasonable estimates of arrival times for similar types of volcanic flank collapses. The simulations greatly underestimate the distal hazard area for such flows. However, if this is recognised, useful projections of this can be made from the proximal and medial areas of inundation.

5.7. Conclusions

Morphological and geological analysis of the Opua debris avalanche deposit suggests that the flow was initiated from a gravitational collapse and fragmentation of an initially rigid mass of volcanic material. SEM analysis and distribution of grains show fracturing and rounding resulting from the initial collapse and emplacement rather than from an eruptive episode. During propagation and especially beyond a major slope-break this mass broke up and became gradually more cohesive through the internal production of a fine-grained matrix along with possible inclusion of ripped-up clay-rich material. This transition to more viscous flow was probably also aided by the concentration of original pore water in the growing matrix phase. Micro-crack features imply there was no major decompression event at the onset of this collapse, and most fracturing occurred on the most-susceptible particles during collisional and frictional flow. The formation of four major landscape elements in this deposit does not accurately represent that the transformation of the flowing mass was gradual from a sliding block to a cohesive and viscous flow. The mounds/hummocks are a distinctive surface feature of the deposit that arise from the development of a cohesive flow and changing basal friction as a result of developing shear layers post the break in slope at the base of the volcano massif. The distribution, alignment and clustering of the mounds displays the gradual development of a mobile cohesive flow that forms two distinctive lobes in response to very subtle changes in paleogeomorphology.

Titan2D models are effective in simulating the initial and medial phases of emplacement, but changing parameters during simulations were not able to replicate internal transformations in the debris avalanche that fundamentally changed its properties and increased its mobility and runout. The Titan2D toolkit is also unable to

simulate the complex processes of erosion (bulking) and deposition (de-bulking) which are highly influential factors on the rheology of lahars. The simulations are highly useful, however, to define major axes of flow expected on current terrain models, investigation of locations for paleo-collapses and providing proximal and medial hazard zones that can be used to project distal hazards. In addition, they show good realistic sensitivity to effects of topography and surface roughness that can be used to examine flow propagation over variably eroded ringplain landscapes.

CHAPTER 6

Mapping block-and-ash flow (BAFs) hazards based on Titan2D simulations: a case study from Mt. Taranaki, NZ

J.N. Procter, S.J. Cronin[1], T. Platz[1], A. Patra[2], K. Dalbey[2], M. Sheridan[2], V. Neall[1]

1. Volcanic Risk Solutions, Institute of Natural Resources, Massey University, Private Bag 11 222, Palmerston North, NZ.

2.Geophysical Mass Flow Modelling Group, State University of New York at Buffalo, NY 14260, USA.

Abstract

Numerical models for simulation of mass flows are typically focussed upon accurately predicting the paths, travel-times and inundation from a single flow or collapse event. When considering catchment-based hazards from a volcano this is complicated by often being faced with several possible scenarios. Over the last 800 years at Mt. Taranaki/Egmont a number of dome growth and collapse events have resulted in the genesis and emplacement of block-and-ash flows (BAFs). Each BAF was directed north-westward by a breach in the crater rim. The latest dome-collapse events in the AD1860 and AD1755 inundated the north-western flank with run-out lengths 10 km from source. Future activity of this type could have a devastating effect on the Taranaki region's communities, infrastructure and economy. Hazard planning has involved constructing volcanic hazard maps based upon the areas inundated by past volcanic

flows, with little consideration of present-day topography. Here, a numerical geophysical mass-flow modelling approach is used to forecast the hazards of future comparable BAF events on NW Mt. Taranaki. The Titan2D program encompasses a "shallow water", continuum-solution based, granular-flow model. Flow mechanical properties needed for this approach include estimates of internal and basal friction as well as the physical dimensions of the initial collapse. Before this model can be applied to Taranaki BAFs the input parameters must be calibrated by simulating a range of past collapse events. By using AD1860 and AD1755 scenarios, initial collapse volumes can be well constrained and internal and basal friction angles can be evaluated through an iterative approach from previous run-out lengths. A range of possible input parameters were therefore determined to produce a suite of potentially inundated areas under present-day terrain. A suite of 10 forecasts from a uniformly distributed range were combined to create a map of relative probabilities of inundation by future BAF events. These results were combined in a GIS package to produce hazard zones related to user-specified hazard thresholds. Using these input parameter constraints, future hazard forecasts for this scale and type of event can also take into account changing summit and topographic configurations following future eruptive or collapse events.

6.1. Introduction

Repeated block-and-ash flows (BAFs) formed from the partial or total collapse of viscous lava domes are common and deadly hazards on many composite volcanoes with lava domes, as shown recently at Unzen, Japan (1991-95; Nakada and Fuji, 1993), Gunung Merapi, Indonesia (1984, 1994, 1997-98, 2006; Schwarzkopf et al., 2005), Colima, Mexico (1991, 1998; Saucedo et al., 2004), and Soufrière Hills on Montserrat

(1995-present day; Sparks and Young, 2002). Between eruptive events, current methods to evaluate BAF hazards rely primarily on reconstructions from historical and stratigraphic records to ultimately produce a hazard map. These hindcasting methods, particularly with respect to inundation maps, are based on paleo-topography and paleo-drainage, and it is not clear how these can be applied to current landscapes or the prediction of future events.

Methods to define volcanic hazard zones were outlined by Crandell et al. (1984) and Scott et al. (2001). These highlighted the use of detailed geological investigations, combined with return period information, to produce high-quality hazard assessments. By combining return periods of volcanic mass flows of differing inundation patterns, Crandell et al. (1984) displayed a progressively changing risk of the likelihood of impact by using a system of graduating colours. This process, however, was rarely transferred into practice. With the development of Geographical Information Systems (GIS) and increasing computer power, numerical simulations of volcanic events are becoming more common (Canuti et al., 2002; Iverson et al., 1998; Bonadonna et al., 2005, Magill et al., 2006). Typically, these methods are applied in combination with geological mapping and focus on individual scenarios, where impacts are on restricted points of interest.

For assessment of pyroclastic flow hazards, Malin and Sheridan (1982) used the Heim coefficient ($\Delta H/L$) to identify runout length-based hazard zones in relation to the current topography. Sheridan et al. (2000) and Toyos et al. (2007) continued to apply computer models to identify hazard zones based on the run-out and velocity of small-volume pyroclastic flows, yet these zones usually encompassed the entire cone and ignored confining topography. Similar BAF modelling was undertaken by Saucedo et al.

(2004) and Itoh et al. (2000) on Colima and Merapi volcanoes, respectively, with the outputs from individual scenarios being the basis for hazard assessment. Related work in lahar hazards analysis (Canuti et al., 2002; Schilling, 1998; Stevens et al., 2003) compared the effectiveness of the computer simulations from FLO-2D and LAHARZ.

The varying input parameters used in this broad range of models highlight a need for developing clearly definable constraints on the range of input parameters required for simulations. This would ensure accurate identification of hazard, and provide a robust method of optimisation against real events. In addition, an effective display of the associated uncertainties or sensitivity of these scenarios also needs to be devised.

Recently developed depth-averaged 2D simulation codes offer a new potential to incorporate the effect of present (and changeable) terrain on the inundation and runout of mass flows. The SUNY-Buffalo developed "Titan2D" granular flow code has proven effective for modelling dry rock collapses, either in cold (Little Tahoma Peak: Sheridan et al., 2005) or hot conditions (Volcán Colima: Rupp et al., 2003; 2006). These provided validation information for individual scenarios. However, for long-term hazard forecasts, considerable uncertainty exists in factors controlling future events, including: volume of material collapsing, initiation points, triggering mechanisms and the conditions of collapsing and flowing materials. Hence, a single modelled scenario may not lead to a reliable hazard map. In the ideal case, a map or dynamic hazard assessment should incorporate the probability of any area being inundated by a mass flow within a range of known (or geologically possible) events from the eruptive centre, or within a particular catchment studied.

This problem exists for hazard assessment in the case-study area of the Hangatahua (Stony) River catchment, Mt. Taranaki, New Zealand (fig. 6.1). The catchment has been repeatedly affected over the past 800 years by BAFs resulting from dome growth and collapse from the summit area of Mt. Taranaki (2518 m). Hot BAFs (above Curie-point temperatures ~350°C) have travelled up to ~10 km from the current summit and inundated an area of up to 40 km^2 with primary flow deposits (Platz et al., 2007). The range of recent BAFs (<1000 years) on Mt. Taranaki (Platz, 2007) provide an opportunity to compare a range of scenarios produced by numerical modelling using Titan2D. In addition, techniques are explored that combine differing scenarios and lead to the development of a method to display a collective or overall hazard forecast.

6.2. Mt. Taranaki mass-flow hazards

The andesitic stratovolcano Mt. Taranaki (2518 m) is situated in the western North Island of New Zealand. Since inception at ~130 ka, the cone has experienced a cyclic pattern of growth through accumulation of lava flows and pyroclastic deposits, alternating with destruction through debris avalanches (Alloway et al., 2005; Zernack et al., 2009). The latest constructional phase of the stratocone (<10,000 yrs) is focussed around two main vents; at the volcano's summit and a parasitic cone (Fanthams Peak) located directly to the south (fig. 6.1). The dominant Holocene style of volcanism has involved frequent dome emplacement and collapse events with associated tephra falls (Turner et al., 2008). The last 1000 years of explosive and extrusive activity has produced at least ten major ash fallout-producing episodes (Platz et al., 2007; Turner et al., 2008). In addition, Neall (1979) identified up to 14 mass flow

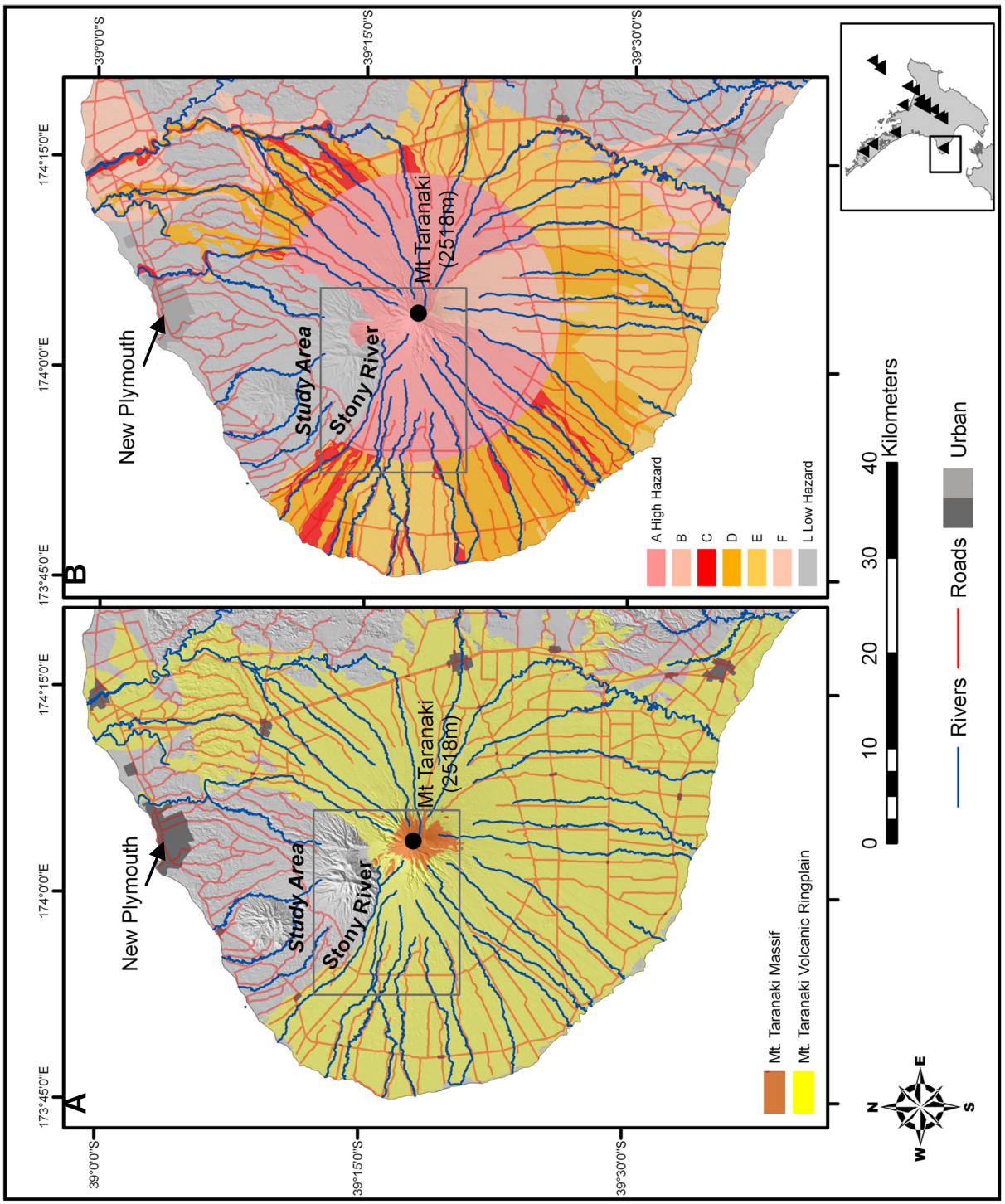

Figure 6-1. Location map. A) Taranaki region and study area located along the Stony River, northwestern sector of Mt. Taranaki/Egmont Volcano; B) Volcanic Flow Hazard zones (Neall and Alloway, 1996) overlayed on shaded relief terrain of the Taranaki peninsula. The study area is contained within the hazard zone A represented by 1:300 yr return period of pyroclastic flows.

units (debris flow, pyroclastic flow deposits) associated with eruptive activity during the last 500 years concentrated on the NW flanks. An update of this work by Platz (2007) indicates that 10 separate eruptive episodes occurred, between 878 ± 39 yrs B.P. and c. AD1850, almost all of which produced domes in the summit crater and one or several mass flows (BAFs or cold rock avalanches) on the NW flanks. The lack of a defined crater rim to the NW has resulted in mass flow hazards being orientated to the NW flanks (Platz, 2007).

BAFs resulting from summit-dome collapse over the past 1000 years have travelled up to 15 km from source (with a 2270 m drop) and mantled areas of up to 40 km^2 with avalanche deposits and associated surge and fall deposits (Neall, 1979; Platz, 2007) (fig. 6.2). Individual depositional units range between 1-6 m in thickness, depending mainly on their position in relation to paleo-channels. Estimated unit volumes range from 5 to 15 x 10^6 m^3; however, these are almost certainly the collective deposits from many small pulse-like collapses, cf Merapi-type dome collapse small-volume BAFs (Ui et al., 1999). The BAF deposits in paleochannels are very poorly sorted breccias with minor amounts of ash matrix containing abundant coarse block clasts of up to 2.5 m in diameter. Clasts and matrix are composed of dense, angular to sub angular, andesite (trachy- to basaltic- andesite), which is typically monolithologic and grey, although in some cases contain up to 30% of other weathered clast types. Deposits, <1 m thick, on the interfluves also have ashy matrixes, which support typically only up to lapilli-sized clasts. These lateral deposits, particularly at flow margins, also contain higher proportions of lower-density vesicular clasts. Aside from these vesicular, clast-rich margins, no pure pumice flows are found on this sector of the volcano (according to Platz et al., 2007).

The internal structures of the Mt. Taranaki BAFs are similar to those described from many historical examples (e.g., Boudon et al., 1993; Miyabuchi, 1999; Cole et al., 2002). They commonly contain evidence of hot emplacement, including partially or fully charcoalised wood, gas escape (pipe) structures (typically above large charcoalised logs) and oxidised haematite-stained upper portions. Many units show poorly sorted, pinching, bedded ash ground surge units, containing soil rip-up clasts beneath the main body of deposit. Coarse-tail reverse grading is common (e.g. Palladino and Valentine, 1995), along with weakly developed clast trains and localised clast-supported lenses.

The bedding characteristics, relatively thin deposits and coarse-grained nature of the Taranaki BAFs could be produced by modified granular flows, with low internal gas pressures (see Savage, 1987; Drake, 1990). Similar vertical height loss:runout ratios of these flows to normal rock avalanches of similar volumes (Table 6.1; e.g., Fisher and Schmincke, 1984; Hayashi and Self, 1992) is also indicative of granular-like flow processes with little initial energy input (in contrast with lateral blast-triggered pyroclastic flows). Observations of the generation of these types of flows (Ui et al., 1999; Nakada & Fujii, 1993) show that they typically start by the sudden break-off of large intact portions of hot lava domes that rapidly disintegrate to generate abundant ash, gas and blocky particles as they tumble down slope.

Table 6-1. Constraints on the best exposed BAF deposits preserved on the NW Flanks (from Platz, 2007).

Age	Mass flow type	Min. volume estimate (m^3)	Runout distance (km)	H/L
c. AD 1880	Rock Fall/Collapse	1-2 x 10^6	5.3	0.31
c. AD 1755	BAF	5 x 10^6	10.0	0.21
c. AD 1655	BAF	10-15 x 10^6	12.7	0.18
c. AD 1555	BAF	7-11 x 10^6	8.2	0.25
AD 1400-1500	BAF	11-15 x 10^6	13.5	0.17
AD 1200-1400	BAF	7-11 10^6	8.2	0.25

6.3. Titan2D geophysical mass-flow simulation code

The Titan2D code was designed by the Geophysical Mass Flow Modelling Group at SUNY Buffalo (Pitman et al., 2003; Patra et al., 2005) to simulate a dry granular flow from an initial point of collapse over a natural terrain. These pre-conditions are highly suited to simulating landslides and BAFs that form from the collapse of large portions of lava domes. The code is based on a model for an incompressible Coulomb flow adapted from the work of Savage and Hutter (1989). It uses a "shallow-water", depth-averaged approximation, simplifying the complex 3D phenomena (after Iverson and Denlinger, 2001). This assumption is grounded on the fact that compared to the entire area over which a long-runout mass flow travels and deposits, its thickness is small. Mass and momentum conservation equations are solved with a Coulomb friction term for the interface between the granular material and basal surface and for the internal friction of the flowing media (Pitman et al., 2003). Conservation of energy is neglected in the first order since it is assumed that a pure coarse-grained rock avalanche has insufficient heat to affect a propagating avalanche.

This hyperbolic system of equations is solved using a parallel adaptive mesh, Godunov solver (Patra et al., 2005). Adaptive gridding and the use of a Message Passing Interface (MPI) allows for calculations to be spread across multiple processes, increasing the computational power and decreasing the computing time. This combination can also produce a more accurate simulation (Patra et al., 2005) when the computational mesh is able to sample a grid of digital terrain data at a high resolution. The use of an adaptive grid refines the simulation according to the region likely to be affected, or where rapid changes in mass distribution occur, i.e. at the flow front. The process also allows the mesh to be unrefined in tail areas. In general, this allows large

(detailed) terrain grid files to be used without re-sampling, while also minimising memory requirements and computer power.

Titan2D operates in a LINUX environment via a Python scripted Graphical User Interface (GUI). Terrain data is entered into the simulation via the GRASS (Geographic Resources Analysis Support System; U.S. Army Corps of Engineers' CERL) GIS environment and format. Simulations on real terrain usually require a large amount of pre-processing and re-sampling of the original DEM to generate a new grid. This is avoided in Titan2D by integrating the model with GRASS GIS and adaptive gridding.

The main ways in which a user controls simulations using the Titan2D are through:

1. Defining dimensions of an initial “pile” of material; including shape, footprint, height, volume, position, and initial velocity (if required);

2. A variable that nominally represents the angle of internal friction of the granular pile;

3. A variable that nominally represents the angle of basal friction between the granular pile and the substrate;

4. A grid by which differing substrates (based on roughness, vegetation and slope) can be defined, each with differing basal-friction angles (if needed)

5. Stopping criteria to halt the simulation (normally a limit on “simulated –real time” or the number of computational time steps);

6. Providing a 3D grid containing topographic information (x, y, z; i.e., a Digital Elevation Model (DEM) for the simulation area.

Outputs of the model (at user-defined time-steps) typically show for each point in the computational mesh: x grid coordinate, y grid coordinate elevation, pile height, x-momentum and y-momentum.

Titan2D has been applied to and evaluated against small-scale pyroclastic flows, BAFs and rock avalanches on Volcan de Colima, Mexico (Pitman et al., 2003; Rupp et al., 2006), El Misti Peru (Delaite et al., 2005) and Little Tahoma Peak (Sheridan et al., 2005). The outcomes of these studies have highlighted the uncertainties in objectively defining model input parameters for realistic simulation of local flow conditions. These have hence only taken a first-order approach to hazard evaluation. For the creation of a hazard map that encompasses all geologically reasonable possibilities there is a need to: 1) create a more encompassing range of probable scenarios for each of these; and 2) include a range of model-controlling parameters.

6.4. Case Study – BAF and rock avalanche scenarios at Mt. Taranaki

The last major sequence of dome building, AD1700-1850, from Mt. Taranaki was followed by the westward collapse of around 5 x 10^6 m^3 of rock from the summit area (fig. 6.2), leaving a half-sectioned dome structure at the summit of approximately 2 x 10^6 m^3 (Platz, 2007). This collapse is characterised by at least two stages; one occurring in the late AD1860s, involved pre-cooled dome rock (<Curie Point temperatures of 350 °C) and parts of the underlying hydrothermally altered crater rim. The unit was

confined to within 5.3 km planimetric distance of the summit (Platz, 2007). In contrast to this event, the penultimate eruption episode (Tahurangi episode) dated at AD 1755, was one of the largest eruptions of the last 800 years. Hot BAF deposits (Tahurangi Breccia, a and b) extend on the NW sector to between 8 km (b) and >10 km (a) from source (fig. 6.2).

The low-energy characteristics of the recent Taranaki BAF and rock avalanche deposits (Table 6.1) mean that the Titan2D approach is well suited. In addition, at Mt. Taranaki, a well-constrained fixed point for flow onsets can be assumed, with broad constraints on potential collapse volumes given from events in the recent past. The limited record of runout/volumes of past flows is used to determine a first-order estimate of initial volume.

6.4.1. Digital Elevation Model (DEM)

The identification of the source area in the Titan2D computer simulation is one of the key input parameters, but developing an appropriate DEM provides the basis for any realistic flow modelling. As with all simulation studies that attempt to use existing depositional records to evaluate model outputs, the topography representation or DEM used is normally that of the present day, rather than the ideal of a pre-event terrain model. The only way to get around this in normal conditions is to create a detailed geological model of the stratigraphy of mass flow deposits and subtract these thicknesses from the current terrain. This is made impractical by the fact that BAFs have highly variable deposit thicknesses within a network of deep, narrow channels and interfluve areas that may change considerably between events. Despite this, the present topography (as represented by a 20 m DEM) at Taranaki (over

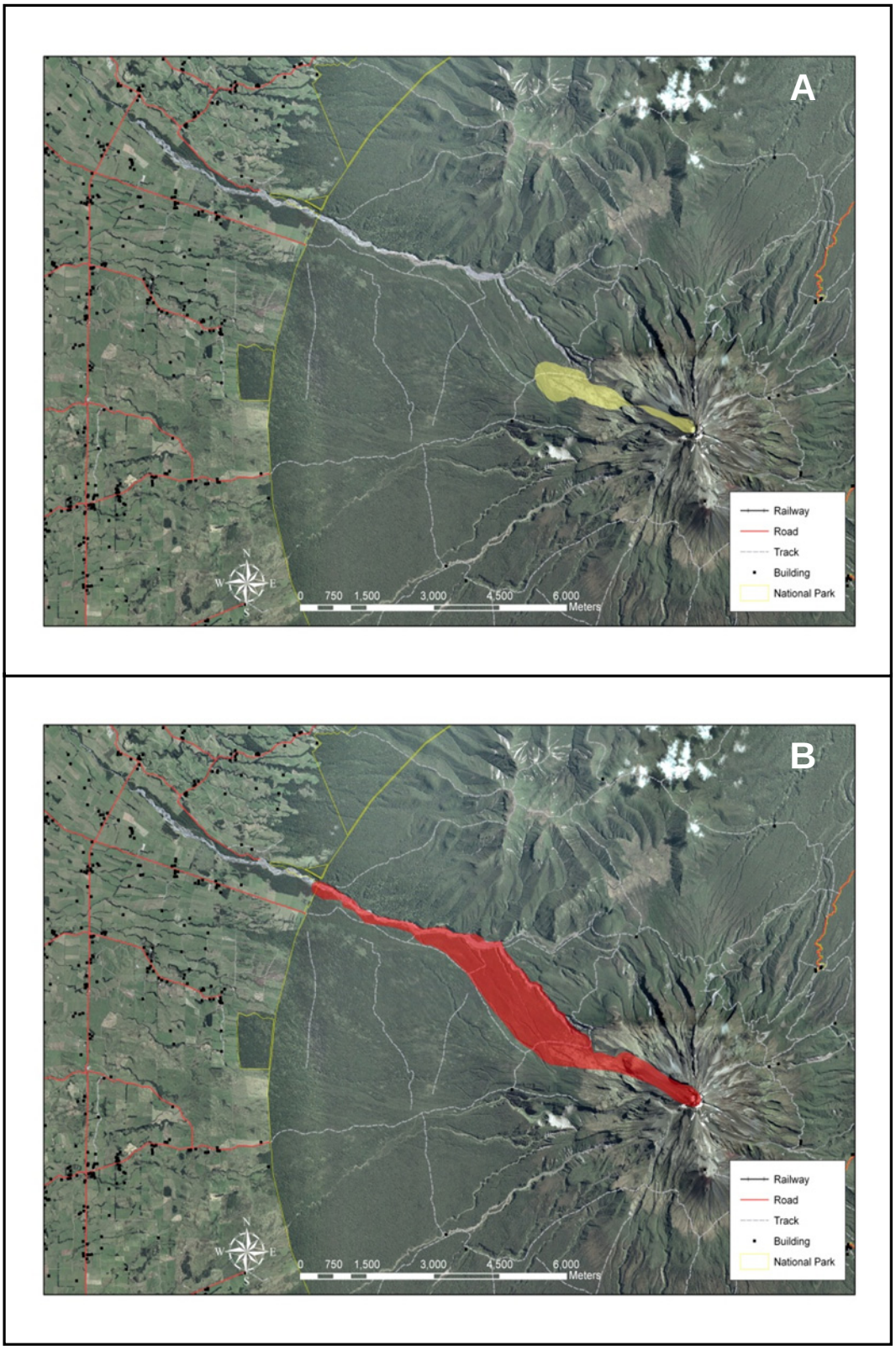

Figure 6-2. Most recent inundation areas from dome collapse and BAFs. A) Recently identified "cold rock collapse" of the remnant dome (Platz, 2007) B) Most recent BAF deposits inundation area (Platz, 2007; Cronin et al., 2003).

the last 500 yrs.) retains the same overall broad morphology and channel system down the northwestern slopes into the Hangatahua River as well as the same type of channel/erosion landforms and vegetation (Lees and Neall, 1993) that existed previously. In addition, using a DEM of the current landscape is more applicable to development of future hazard forecasting and hazard zonation.

The DEM used of Mt. Taranaki was produced from national topographic GIS datasets (NZMS 260 series, Land Information New Zealand), containing height data as contours and spot-heights. Using the ArcGIS TOPOGRID (ESRI, 2007) routine, a DEM was created with a cell dimension of 20 m. Major drainages and distinctive geomorphic features on the volcano are well defined on the DEM, although, in the surrounding ring plain area with low slopes and few dominant geomorphological features, morphological resolution is lost. The arcgrid DEM was then imported into GRASS GIS as an ascii file and converted to a GRASS DEM format for use in Titan2D.

6.4.2. Source Area and Initial Pile

To effectively simulate BAF or dome collapses, the initial volume and shape of the collapsing pile was constrained by the present crater configuration. The present summit consists of a remnant dome (fig. 6.3a), part of which collapsed in the 1860's. This structure lies above the main conduit system of Mt. Taranaki, and hence is expected to be readily destabilised at the onset of new activity. Following its removal, new domes are likely to be emplaced in the same location if activity were to repeat the pattern of the recent past. Hence new domes would be located within the westward-opening crater basin as well as possibly extending down the breached western rim.

The bulk of the present (and pre-collapse) dome mainly comprises a single endogenous lobe (Platz, 2007) within a 420 m radius crater (fig. 6.3b). The present remnant dome is ~100 m high, a height-limit apparently constrained by magma viscosity at Mt. Taranaki (Platz, 2007). The crater is essentially flat, but has a distinctive slope to the northwest of about 32°. This apparently generated the ellipsoid shape of the last dome.

Titan2D requires an initial starting pile. To effectively simulate a BAF or dome collapse, the initial volume and shape of the collapsing pile must be defined within the context of the present crater configuration, including an accurate representation of the sub-dome surface. An estimation of the pre-dome surface was needed, along with an idealised complete dome reconstruction. To carry this out, a combination of GPS and aerial ortho-photography was used in GIS, ArcMap/ArcScene (ESRI, 2005), to extrapolate a full parabolic dome shape (fig. 6.3). Using the volume and shape of the remnant dome (1.6×10^6 m^3) the maximum height of the original dome was 105 m and a (parabolic) basal outline of 450 m and 320 m radii in the x and y directions, respectively. This yields a parabolic dome shape stretched over the sloping surface with a full volume of 5×10^6 m^3 (fig. 6.3). The centre-point of the re-constructed dome and its dimensions were applied to the Titan2D simulations. Most dome collapses involve only small proportions of the overall structure (e.g., Ui et al., 1999), although at Soufriere Hills large proportions of the domes were incorporated in dome collapse at times (Sparks and Young, 2002). For the purposes of these simulations, a typical volume of 1×10^6 m^3 was used to replicate partial dome-collapse events or pulses on Mt. Taranaki.

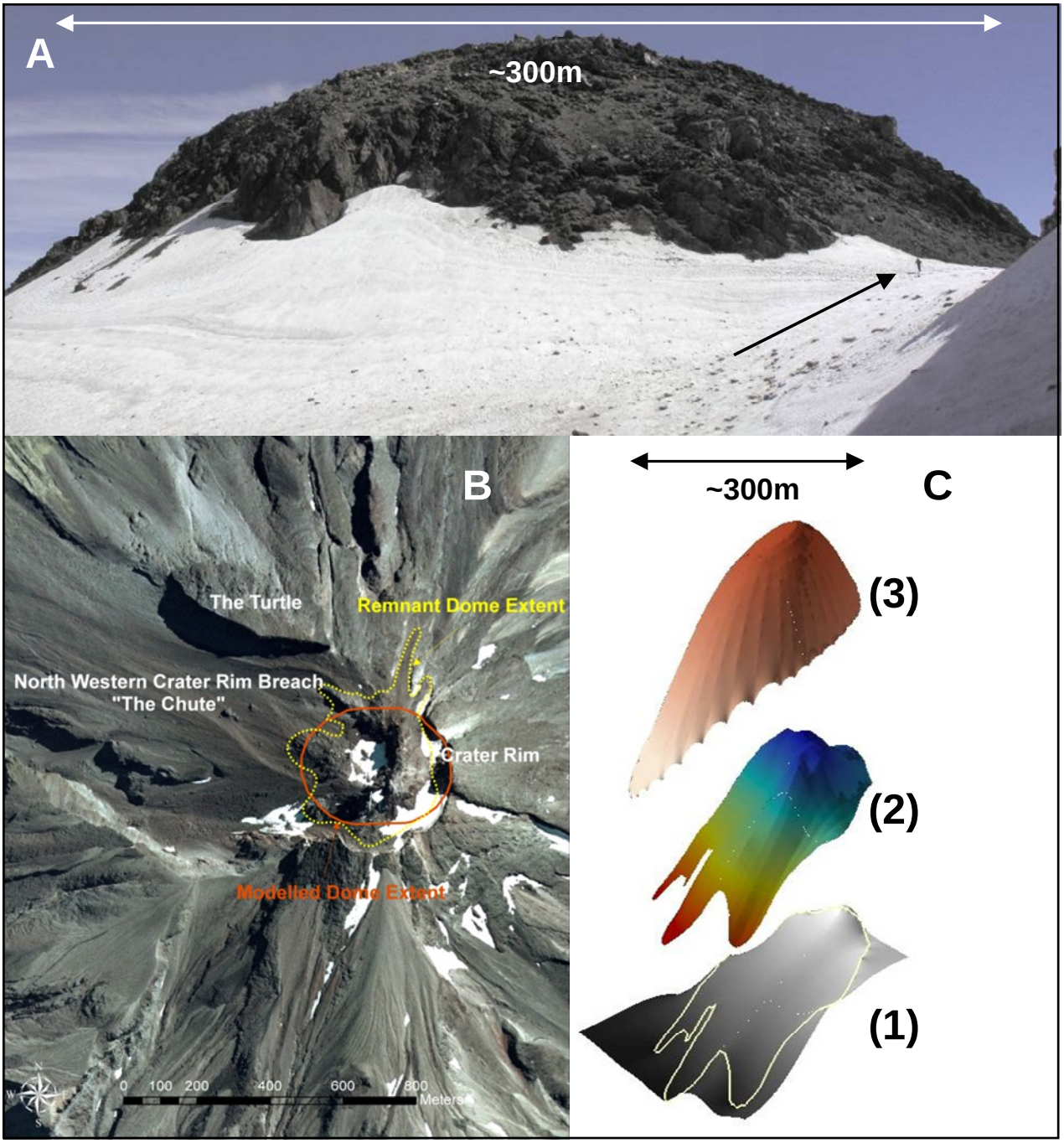

Figure 6-3. The dome and reconstruction of initial pile for BAF simulations. A) Mt. Taranaki, the current remnant dome, view of the northern side (note person for scale as indicated by the arrow); B) Ortho-photograph of the summit and remnant dome, dashed lines indicate the current outline of the remnant dome, solid lines represent the reconstructed modelled dome; C) GIS representation of dome, 1. Underlying summit surface with solid line representing the margins of the remnant dome. 2. 3D representation of the current remnant dome, 2 x 10^6 m^3. 3. Reconstructed dome used for BAF simulation 5 x 10^6 m^3.

6.4.3. Titan2D Parameters - Basal/Internal Friction angle

The two “friction angle” parameters used in Titan2D have not been directly related to physical parameters that can be measured in the laboratory or field. These are normally calibrated by matching simulation travel times and inundation areas to known values (e.g. Schilling, 1998; Oramas Dorta et al., 2007). Attempts to determine these parameters experimentally (e.g. Iverson et al., 1998; Iverson and Denlinger, 2001; Bursik et al., 2005) have focused on the measurement of collapsing piles on tilt tables and on flume experiments. Results are highly variable and it is arguable whether the laboratory conditions can be scaled to real-world situations. The most commonly used comparator between diverse types of mass flows is the H/L ratio (Heim friction coefficient; Heim, 1932, revised by Hayashi and Self, 1992), which can be used to estimate resistance to flow of a sliding avalanche by interaction with its underlying surface. Sheridan et al. (2005) used this method to determine the optimal basal friction parameter for simulating the Tahoma Peak Avalanche with Titan2D. Sensitivity analysis showed a dramatic effect on increasing runout lengths with reductions in the basal friction angle parameter, whereas changes in the internal friction angle have shown less dramatic or no noticeable impacts in middle-value ranges (Sheridan et al., 2005).

For the Mt. Taranaki flows, the only comparative measures available are inundation area, estimated volume, runout length and minimum H/L estimates. Rather than choosing specific values based on this imperfect dataset, a batch of 80 simulations were run for a controlled initial volume and location with every possible combination of internal and basal friction angle parameters at intervals of 5°.

6.5. Simulation results

Most simulated BAF deposition surfaces compared well to mapped deposits, without anomalies, such as overtopping known major topographic barriers or crater walls and without entering alternative catchments. All simulations exhibited a partial collapse from the initial pile with flow to the northwest of the current amphitheatre. Within the first 2.5 km from source, simulated flows were confined to a 500 m-wide amphitheatre-like structure. The flows either stopped on this slope (with high basal friction angles), or continued into box-shaped gullies of major stream channels (Maero and Pyramid Streams). After 3.5 km, these tributary flows combined in the Hangahatua (Stony) River valley for a further 9.5 km of travel.

Each simulation output was processed using GIS to develop an inundation-area map of maximum flow (pile) thickness. With extremely low basal friction angles (5°-10°) a series of "bounce footprints" resulted from flows that accelerated unrealistically rapidly down slope (see fig.6.4). At the opposite end of the spectrum (80-90° basal friction) piles collapsed and halted within <1 km of source. As discovered by Sheridan et al. (2005) variations in the internal friction angle had very little effect on the final inundation area and runout of the flow. This parameter appears to play a more important role on affecting the velocity outputs of the simulation at particular points in time.

The inundation areas, H/L ratio and run-out planar distance from mapped BAF deposits were most similar to those of simulated BAFs at basal friction angles between 15-25° (fig. 6.4).

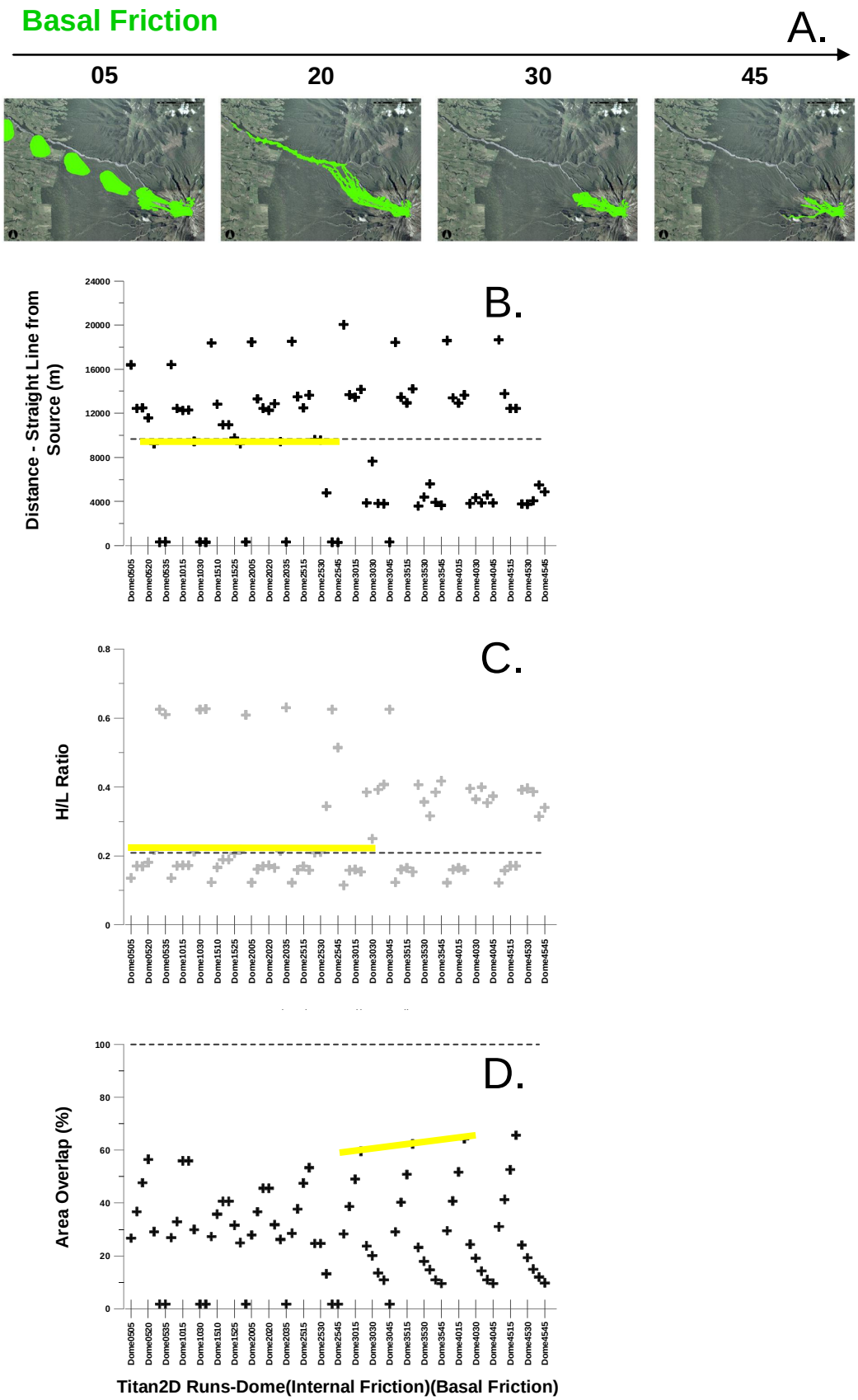

Figure 6-4. Simulation outputs analysis. Yellow lines highlight best fit. A) Summary of initial visual analysis; B) Comparison of simulations to run-out distance,; C) Comparison of simulations to H/L ratio; D) Comparison of simulations to inundation area.

6.5.1. Deriving hazard representations from the modelled flows

Converting Titan2D simulations of BAFs at Mt. Taranaki to an overall hazard representation required a method that combined all valid outputs. The approach developed takes into account variation resulting from the possible range in model input parameters that were used to infer the variation within realistic geological (or rheological) possibilities for hot and cold flows and source regions as described above.

Using a single volume/source example that is representative of the most recent BAF events, the model variation is broad with basal friction angles between 15°-25°. A Gaussian distribution was assumed for this range (median = 22°) to determine a set of new basal friction angles (Table 6.2) that is more representative of the range of possible events. The Gaussian distribution was used as it was best suited to find the range around and ideal parameter (mean = 22°) based on one set of input parameters. Using the same initial pile starting conditions, the same DEM, and a fixed internal friction angle of 30° (based on the previous 80 runs), a series of new simulations was used to produce a range of outputs that encompass the spectrum of inundation areas and run-outs expected by BAFs and/or major cold rock avalanches on NW Mt. Taranaki (fig. 6.5).

These simulations provide a range of scenario layers that can be further analysed in a GIS to display estimated flow depths, velocity and discharge. Using ArcGIS (ESRI, 2007), the outputs of each simulation were processed to produce a point layer containing the maximum pile height at each processed point. The point dataset was

interpolated to create a raster grid of pile-heights across the region. This produces a laterally and longitudinally gradational continuous layer. Raster layers from each of

Table 6-2. Basal Friction angles used in the Titan2D simulations for the hazard zone model for BAFs at Mt. Taranaki.

Run	**Basal friction**	**Gaussian Distribution %**
1	17.6305	0.0333
2	18.1747	0.0747
3	19.103	0.1095
4	20.333	0.1346
5	21.7556	0.1478
6	23.2444	0.1478
7	24.667	0.1346
8	25.897	0.1095
9	26.8253	0.0747
10	27.3695	0.0333

the simulations were combined into a single height/thickness layer using the ArcGIS raster calculator tool. This combined "thickness" layer was chosen to be directly represented as a gradational hazard zone (fig. 6.5). A similar process can also be paralleled for velocity or momentum outputs depending on user engineering or human hazard needs.

This combined layer highlights the Stony River and catchments as areas of greatest hazard, as expected. It can be queried at user-defined points and displayed using a variety of underlying images, maps or infrastructure networks, as well as displayed in 3D with a shaded relief model or ortho-image draped over a DEM (fig. 6.5).

6.6. Discussion

6.6.1. Combined Simulated Results

The results and a 1:300 yr (based on Neall and Alloway, 1996, return period for hazard zone A) hazard zone from BAFs is defined by the area (darker red central hazard zone on fig. 6.5) associated with the drainage patterns of the north-western sector of the volcano. These areas have been inundated by all BAFs in the past c. 800 years (Platz, 2007). The gradational zone, however, shows a lessening decrease in hazard on the interfluves between the main drainages, indicating the lower possibility of flows inundating these (fig. 6.5). Of particular interest is the length of the hazard zone, highlighting that flows would only rarely reach lower altitudes (700 m, >10 km runout), which is consistent with field evidence (Platz, 2007).

6.6.2. Mass flow hazard simulation

The majority of volcanic flow hazard maps are generalisations based solely on extrapolating the past inundation areas of each type of flow (e.g., pyroclastic flow, lahar, debris avalanche) onto present topography (Scott, et al., 1995; Waitt, et al., 1995; Hoblitt, et al., 1998; Wolfe and Pierson, 1995). These become redundant when either new mapping identifies additional constraints on event frequency or inundation, or when eruptions collapses substantially change the topography. In addition, hazard maps for land-use planning, workplace and recreational area management require more precision to reliably indicate differing degrees of relative hazard. In addition, other information, such as flow velocity, depth and mass flux is essential for assessing

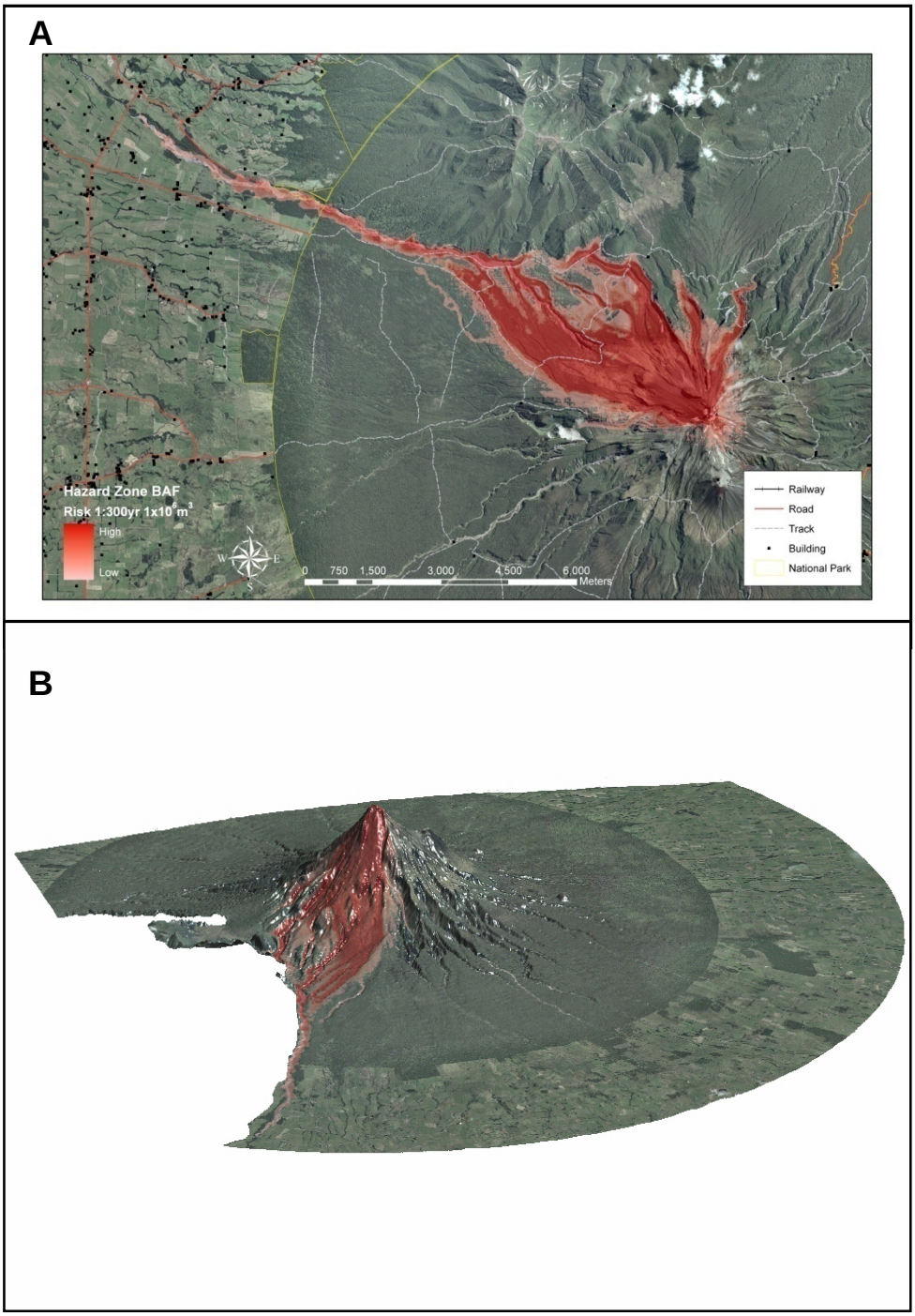

Figure 6-5. A) Hazard zone created from Titan2D computer simulations based on the 1:300 yr BAF event from a dome collapse and B) 3D representation of the created Hazard zone in relation to the outline of the Hazard Zone C from Neall and Alloway (1996).

the stability of any structures in the flow path and planning any new infrastructure. However, hazard maps showing increasingly more complexity, including those with some probabilistic component (e.g., Nevado del Ruiz; Parra and Cepeda, 1990), are typically less well understood by users.

For current tephra fall hazards, Magill et al. (2006) used the numerical model ASHFALL (Hurst, 1994) to forecast the probability of volcanic ashfalls from all major sources to affect the city of Auckland. From these data, they determined and displayed tephra inundation maps of a similar nature to those presented here. Using an alternative approach, Bebbington and Lai (1996) and Turner et al. (2008) developed a time-variable, probabilisitic, ashfall forecast for Taranaki. These statistical approaches may be divorced by varying degrees from the physical hazard generation processes, particularly those that combine various physical models without considering their inherent uncertainties. Other limiting factors with these methods are the inability to produce spatial representations (i.e. hazard maps) of the predictions that can be easily understood and applied by local authorities, land-use planners and hazard/emergency managers.

A similar approach to the Taranaki example presented here was undertaken for mass-flows landslide and rock/debris flow hazards in the District of North Vancouver (Jacob, 2005; KWL Ltd., 2003) using Flo-2D software (FLO-2D Software Inc.) to recreate the discharge/inundation of flows of a particular recurrence period. Inundation maps of each simulated flow in the various catchments studied were combined in a GIS to give a representation of the hazard to downstream areas. A gradation of increasing relative hazard was defined on the basis of the likelihood of areas being affected. The range of volumes modelled also provides a good method for encompassing and compensating

for the lack of uncertainty around the volume of future events. This method does not, however, take into account the variability in the physical properties of the flow and whether these can be accounted for by the model. The recognition of the variability that may exist due to changing or contrasting flow sediment concentrations and differing flow paths was entirely assumed to be a factor of volume. The methods presented for the Taranaki example differ by attempting to identify a range within the input (physical) parameters that influence the flow rheology (largely unknown here) and resulting inundation area. This is then used as a proxy to encompass all the realistic possible outcomes within the constraints of recent past events. As identified by Platz et al. (2007) we can identify or infer from deposits that flows and their behaviour (linked to emplacement processes) can vary greatly and this can have an effect on runout and inundation. It is assumed that in the Titan2D model friction input values are the most influential parameters in the flow model that control the modelled flow's mobility. For the Mt. Taranaki BAFs the rheology of the flow (rather than source conditions) is one of the more dominant factors in determining the runout and inundation.

To expand this by including the variability amongst all known or possible BAFs on Taranaki events (such as variations in initial volume and source) would require either having a complete event history with accurately known volumes and inundation areas, or developing a probabilistic model to describe the known limits of variation in these that could then be coupled to Titan2D.

Given the relative dominance of BAF and related mass flows over the last 800 years, the simulations made are likely to encompass the main initial hazards of the next unrest at Mt. Taranaki. The present configuration means that collapses down the NW

slope will be highly likely if a new dome were to grow. The maximum volume that could be accommodated in the present crater is around ~10 x 10^6 m^3, similar to the total volume of the largest sets of flow-packages mapped to date. It is common that only small fractions of dome volumes collapse at any one time (Unzen 1991; Nakada and Fujii, 1993; Gunung Merapi, 1993; Schwarzkopf et al., 2005), which further reduces the probable volumetric range of flows expected.

6.6.3. Taranaki BAF hazard mapping

Grant-Taylor (1964) and Neall (1972) considered that potential risk from future pyroclastic flow (BAF) activity at Mt. Taranaki would be restricted to within a 9 km radius of the summit. This was followed by a hazard map for volcanic flows (Neall and Alloway, 1996) that defined six zones of risk, from various types of mass flows. This was based on mapped historical and prehistoric deposits of pyroclastic flows, lahars and debris avalanches along with their estimated return periods. The two zones relating to pyroclastic flows are defined by a radius of 15 km from the summit, with the highest hazard zone having a 1 in 300 year return period of impact. Recent studies (Platz, 2007; Turner et al., 2008) have revealed a much higher frequency of small-volume dome collapse and pyroclastic-flow producing eruptions, necessitating a revision of the hazard zones. In addition, questions remain as to how accurate the map remains in the context of present-day topography, particularly in relation to a future "typical" sequence of dome growth and collapse with a crater area open and sloping toward the NW.

The 15 km circular hazard zone of Neall and Alloway (1996) incorporates the extent of all possible pyroclastic flows that may originate from the volcano. This may be a useful

overall “exclusion zone” for emergency management during a volcanic crisis due to the unpredictable nature and path of pyroclastic flows, associated surges, ballistics, tephra and possible blast events. This approach does not allow distinction of varying degrees of mass-flow risk in the area, which would be useful for the managers of the recreational area (and workplace) to assess hazards between eruptions and even during prolonged eruptions. Nor does it allow identification of any key infrastructure elements that may be affected with greatest likelihood by mass flows, such as critical bridges, pipe lines and power cables. Given that BAFs and other mass flows since c.800 years have almost exclusively affected the NW sector, this is the area of highest apparent risk under present topographical conditions yet this is not represented in hazard zones due to larger events (with less probability of occurrence) overshadowing this area of higher risk. However, it must be recalled that the newly created hazard zone is scenario-based rather than encompassing all of these events possibly originating from the summit and considered by Neall and Alloway (1996) to have a return period of 1:300 yrs based on the last 1000 yrs of events.

There are few examples of applying a numerical model or computer simulation to hazard analysis and determination of future high risk zones other than that of Saucedo et al. (2005). The majority of computer model applications are related to the comparison of real and modelled simulations or the optimization of parameters within a model. The method presented here explores this premise in relation to a scenario in which BAFs from the same part of the volcano or sequence of dome-collapses may vary greatly. It is apparent that for the Titan2D model, friction input values are the most influential parameters, which appears also to be the case for the Mt. Taranaki examples, where source differences matter less.

By varying these factors we can account for expected variance in future Mt. Taranaki BAFs, during the course of a dome growth and collapse sequence. By modelling a range around an optimally compared flow, we can account for the variation that might exist by combining and displaying all results. The Gaussian distribution was used to encompass the variability observed in inundation areas. These give rise to GIS layers that can be displayed to show the gradational nature of hazard assessment, as implied by the early workers quoted above.

Haynes et al. (2007) provided important observations about the effectiveness of traditional hazard maps in relation to public interpretations of them. They found that respondents could better orientate themselves and interpret hazard zone information in 3D format or data that was superimposed onto photographs or aerial photos. Titan2D outputs and use of a GIS easily enables overlays of hazard zones onto aerial/satellite imagery or shaded-relief models to facilitate this knowledge transfer (fig. 6.5).

6.7. Conclusions

Titan2D provides a tool that can simulate granular flows and provide outputs that are testable within geological mapping constraints. Multiple runs can be undertaken rapidly on a desktop computer and allow for timely hazard assessments to be made on present day terrain, or on terrain that is rapidly changing. This case study shows that by undertaking an initial series of Titan2D runs that incorporate all reasonable combinations of basal and internal friction angles for BAFs while keeping the source

conditions constant, best-fit simulations can be determined by comparison to the spatial distribution of known BAF events (Platz, 2007). Here, reasonable Titan2D input parameters were 15-25° for basal friction and 30° for internal friction. Using a Gaussian distribution new input parameters could be derived to produce a series of new titan simulations. The combination of the inundation areas from these new simulations allowed for the creation of a graduated zone of inundation likelihood. This method provides a means to account for uncertainty related to differences in flow behaviour of BAFs or similar granular flows. The digital outputs from Titan2D can be displayed in GIS and presented with aerial, satellite imagery or in 3D to allow the user a greater understanding of the relationship between the possible hazard and the landscape.

Iverson (2005) remarks that ample scepticism should be used when scientific interpretations are made from models and all physical, mathematical and computational aspects need to be understood. This is applicable for hazard analysis also, particularly when volcanic flow hazard analysis methods and the display of hazard zones have developed little since Crandell et al. (1984). Flow modelling is becoming a more common practice in volcanic hazard analysis, but mostly in relation to single events or scenarios. Despite the rapid use and uptake of the results produced from computer simulations of flows (particularly by local government/authority in land use planning) there has been very little effort to transfer that information into publicly available hazard maps. This comes with the danger that appropriate representation of inherent uncertainties may be overlooked. Even in traditional hazard analysis and mapping based on geological field identification, uncertainty exists in both the inundation area and volume of a particular deposit as well as in the stratigraphic interpretation of the return period. However, these uncertainties are rarely transferred onto the cartographic display of the hazard. The identification and

quantification of uncertainty and display of model simulations related to hazard analysis is an area that requires more attention to provide both the geologist and the user with a simple display of the potential risk.

CHAPTER 7

Discussion: Hazard Map Creation and the Application of Numerical Modelling tools to Hazard Assessment

7.1. Introduction- Hazard Mapping

The concept of identifying places of volcanic danger and to warn the population of that danger was developed early by many indigenous communities and peoples, well before the written word and maps. For example, Cronin et al. (2004) and Cashman & Cronin (2008) show that oral tradition and cultural practices were used in many parts of the world to define exclusion zones around areas of volcanic vents and flow paths and to pass on practices for coping with changing and hazardous environmental conditions, thus creating some of the earliest volcano hazard assessments and risk-management practices.

Methods of identification and representation of hazard mapping are best described by Crandell et al. (1984) (refer to Chapter1.). The shortcomings of these methods are also identified by Crandell et al. (1984) to be limitations on the completeness or detail of the stratigraphic record of events, especially in relation to recording the highest-frequency but smallest-volume events in a spectrum of behaviour. In addition, depending on the time-interval that can be accessed in the geological record, very large low-frequency events may be missed, or their frequency poorly estimated. Other provisos in using this method include the fact that it is based on the volcano continuing to behave in the future as it has done in the past. Hence, if magma supply or behaviour

of the volcano significantly transforms, such as from a phase of vesiculating-magma driven explosive eruptions through to a phase of dome-forming, the consequent hazardscape could effectively change over short intervals. This inturn would make any hazard assessment based on previous styles of activity highly misleading. One of the biggest influences on the distribution and runout of mass flows are changes in the topography of the source volcano particularly constructional and erosional changes that occur during eruption episodes and large-scale flank collapses, including changing drainage patterns, flow paths and likely inundation areas. Some of these changes may be subtle, such as the growth of a dome over the previous barrier of a crater rim, or small changes in crater rim openings or elevation. Most current hazard maps use stratigraphic methods for the base information but attempt to take account of the associated uncertainties by providing a series of probabilities that encompass the entire area previously affected.

These methods require a subdivision of mass-flow types (e.g. pyroclastic flow, lahar, debris avalanche) that creates an assumed hierarchy of volcano-related events that pose various levels of risk. There is also an implied assumption in these discretised mapping approaches that different types of events occur in isolation in particular areas or catchments. These maps are also almost exclusively based on inundation patterns and runout in relation to paleo-landscapes. There is very little account for the fact that during an eruption sequence landscapes may change dramatically by aggradation and erosional processes. In the case of long-term series of events, hazard maps can be regularly updated to reflect these changes, e.g. Pinatubo lahars following the 1991 eruptions (Scott et al., 1996). In other cases, the changes may occur too rapidly for maps to be developed quickly enough (e.g. Mount St. Helens, 1980). Finally, interpretation of standard hazard maps requires some degree of specialised

knowledge of volcanic processes and products that could be confusing for the average public and governmental user.

Crandell et al. (1984) also highlights the basics of a probabilistic assessment of volcanic hazard and risk at Mount St. Helens as proposed by Newhall (1982) by considering the probability of an initial volcanic event and developing a tree of conditional probabilities for subsequent and increasingly specific derivative events. Newhall (1982) created volcanic hazard maps from this method that provided hazard zonation depending on particular scenarios at certain times during an eruptive sequence. These methods are highly suitable for emergency management, but have not yet successfully been transferred into general hazard zonation maps commonly used in inter-event times for land-use planning.

The approach of spatially extrapolating past events and inundation areas to develop hazard zones continues to the present day. Tilling (1989a) and Chester (1993) described “general prediction” as being the identification of the past volcanic behaviour to determine frequency and variety of primarily low-frequency and large landscape-impact events. They also defined “specific prediction” as monitoring the geophysical processes and signals preceding event initiation. General prediction has provided the basis of volcanic hazard zonation, while specific prediction has lead to simulation and modelling in order to forecast specific sequences of events. While the latter does not easily lend itself to a spatial representation of hazard or risk to the entire landscape, it provides information on the types of individual scenarios (in best cases with likelihood estimates) that can be modelled by computer simulations.

Blong (1996) suggested that volcanic hazard assessment should not only be focused on the development and strict adherence to spatial hazard zones, but instead use a more analytical process of identifying the variety of volcanic hazards, their physical characteristics and the probabilities of these physical processes occurring. Following this is the need to develop scenarios to determine the vulnerability of people and infrastructure. These scenarios need to take into account temporal variations (in best cases time-varying hazard) and the limits of the probable maximum or catastrophic event. The full complexity of this type of analysis is, however, difficult to incorporate into a single cartographic spatial representation, although it could be developed using a GIS database.

Present day volcanic hazard analysis uses computational/numerical modelling tools in two main approaches;

1. Probabilistic modelling, where the likelihood of events or specific impacts are the focus. This has primarily been used in developing forecasts of ash fall likelihood or damage thresholds (e.g. Tavenui, Fiji; Cronin et al., 2001; Tarawera, New Zealand; Bonnadonna et al., 2005; Taranaki, New Zealand; Bebbington et al., 2008).

2. Deterministic scenario-based geophysical modelling, where the area of inundation or impact on the landscape is the focus. This has primarily been the method used to examine volcanic mass flow hazards (e.g. Denlinger and Iverson, 2001; Sheridan et al., 2005; Patra et al., 2005), but it has also been well applied to ash fall (e.g., Hurst and Smith, 2004).

GIS analysis or decision support tools (Pareschi et al., 2000; Renschler, 2005; Emmanuel and Ofelia, 2006) are developed to incorporate a variety of hazard forecast inputs and provide emergency managers or hazard scientists means to develop scenarios for planning response to, or mitigation of, impending events. Despite this, GIS is often complex and the software is often a barrier to adoption. Hence, GIS methods need to be further developed to better communicate forecasts of impending hazards (Haynes et al., 2007).

Chester et al. (2002) noted that over the last 30 years in volcanic hazard analysis there has been a shift from determining physical hazards to incorporating the vulnerability of societies and infrastructure and the inclusion of social factors in hazard and risk analysis and communication. One important factor Chester et al. (2002) identified is that volcanic hazard research particularly in Western Europe has four times more pure volcanological/hazard mapping research than studies into the vulnerabilities of societies affected. This also highlights the slow uptake of many of the new computational scenario-building methods and hazard-based GIS into comprehensive land-use and economic developmental planning.

7.2. New Zealand hazard mapping and computer flow simulation

Volcanic hazard analysis in New Zealand, like in many countries, was re-prioritised and standardised after the 1980 Mount St. Helens eruptions. Neall and Alloway (1996) and Neall et al. (2001) published volcanic flow hazard maps at scales of 1:100 000 for Mts.

Taranaki and Ruapehu, respectively. These maps are based on detailed mapping and stratigraphy of volcanic mass flow deposits in all catchments, incorporating in part the results of several postgraduate studies. The most recent (highest frequency) lahar hazard zones were defined by current topographic drainage patterns and identification of the main likely affected catchments. The maps are more detailed, showing more specific zonation and likelihoods of mass-flow inundation. These are of a sufficient scale that they can be used for basic GIS cross-referencing to highlight specific infrastructure at risk. However, the scale does not allow specific land-use planning activities and boundaries are often not as specific or precise as implicit by being marked by lines. These maps are useful for providing information on inundation areas affected by past events and a robust general indication of future events.

By the mid-1990's, hazard mapping in New Zealand was mostly complete; however, the hazard maps were primarily based on historic interpretations of stratigraphy and flow types. Flow hazards were also combined into single or few categories, mostly because the series of separate maps needed to distinguish different styles; and, rheologies of events can be confusing for non-expert users. More recent advances in hazard assessments in New Zealand by Magill et al. (2006), Magill and Blong (2005) and Bebbington et al. (2008) have focused on merging physical and probabilistic models with estimates of impacts on infrastructure. While the focus of these simulations is on providing a probability of impact or damage from a number of scenarios, these are rarely converted into a region-wide hazard analysis at a resolution suitable for landuse planning.

Numerical and computer simulation of mass flow hazards in New Zealand has principally focused on Mt. Ruapehu and the most recent lahars in the Whangaehu

River. Vignaux & Weir (1990) developed a 1D numerical simulation that considers the flow rate as a simple power function of depth and channel slope, with a Mannings-type law to account for frictional losses. This method produced results that were out by a factor of 3, which was determined to be an impact of bulking that was not accounted for by the model. Following this, Stevens et al. (2003) applied the empirical statistically based LAHARZ model (Schilling, 1998) to examine the effect of using variable Digital Elevation Models (DEM) on the hazard analysis. Being water rich flows, Whangaehu river lahars have been modelled by a range of hydraulic codes simulating Newtonian flow, including the 1D MIKE11, BOSSBREACH and BOSS DAMBRK (Manville, 2004) and the 2D DELFT 3D (Delft Software Inc.) software (Carrivick et al., 2007). All of these approaches have effectively used known examples and their physical details to validate and test modelling methods. An additional study at Ruapehu by Hancox et al. (2001) went beyond this, utilising 1D, Mannings n, calculations to provide information for hazard forecasting of the anticipated breakout lahar which eventually occurred in 2007.

It is common to carry out studies of model validation on well-known and well-characterised events (e.g., at Mount St. Helens, USA, Julien and O'Brien, 1997; Guagua Pichincha Volcano, Ecuador, Canuti et al., 2002). This is an important step in order to convince researchers or policy makers of the usefulness, accuracy and appropriateness of new simulation techniques. Extending from this, the application of numerical simulation techniques to volcanic hazard mapping is not a single and simple step. Several other factors, including good geological background information and a good understanding of the model are required to most reliably add flow modelling to the arsenal of tools for mass-flow hazard analysis.

7.3. Requirements and Constraints for the Computer Simulation of Volcanic Flows

To apply any computer model to simulate a volcanic mass-flow scenario, the following must be understood:

- The flow rheology and any changes it may undergo during runout;
- The physical dimensions and travel times known from past flows, and those required for hazard analysis;
- The erosional and depositional characteristics of the flow;
- The properties of any related deposits that provide information about the rheology and physics of the flowing mass;
- The numerical basis (i.e., granular, vs. Newtonian, vs. viscous etc) and applicability of the computer simulation to the scenario;
- Input parameters required for the simulation and how they influence the model behaviour;
- How the flow is propagated across 1, 2 or 3D representations of the natural terrain;
- The computing requirements for the simulation and how limitations of this may affect the simulation progressing; and
- Finally the associated uncertainties of simulation inputs and outputs.

Defining the above factors as well as the external influences on the scenario will lead to producing the most accurate and reliable deterministic simulations and consequent basis for hazard forecasting.

7.3.1 Historical mass flow event simulation lessons

Based on the results of this PhD study, Titan2D simulations of the 1995 and 2007 Ruapehu lahars (Chapters 2 and 3) showed good comparison for the flow paths, average velocity, areas and depths of inundation and flow travel times for the upper 10 km of flow. However, in these cases the scenario being simulated was well understood and characterised from detailed observations, flow samples, along with information available on sedimentology of deposits and comparisons to contemporaneous flows and deposits. This allowed recognition of the limitations of using a granular-flow-only model, and highlighted that it was essential to apply the 2-phase fluid-granular-flow code (Pitman and Le, 2005). One of the major issues in translating from field geological data to the numerical simulation was relating the input parameters of the numerical code to a natural flow event. For the Mt. Ruapehu example, the starting conditions were well defined at the Crater Lake, although this may not be so simply defined at many other volcanoes.

The simulation also revealed the limitations of applying a model with invariant physical properties to a natural flow scenario that exhibits dramatic changes in rheology. One of the greatest influences on the flow rheology in non-cohesive lahars is their ability to bulk-up and de-bulk by entraining and depositing sediment, respectively. This is

impossible to simulate on a 3D natural terrain by Titan or any numerical model or computer simulation presently available. Bulking clearly occurs during the first 9 km of flow on Mt. Ruapehu (Procter et al., in press) and can only be accounted for in simulations by setting the initial volume to the fully bulked value. This may create non-comparable inundations and properties of flow over the first few kilometers of travel. Had the Titan2D simulations transited the Whangaehu Fan beyond 10 km, they would have still maintained their fully bulked up volume. However, it is known from the 1995 lahars (Cronin et al., 1997a; 2000) that large-scale de-bulking through deposition can occur, inducing changes from debris flow to hyperconcentrated flow rheology.

The implication of these modelling limitations must be taken into account when providing a hazard forecast. The simulation information must be presented in a way to either provide a hazard zonation that encompass such uncertainties, or clearly identify that the forecasts are either minimum or maximum end members of the possible scenario at various locations.

7.3.2 Prehistoric mass-flow event simulation lessons

In the case of simulating prehistoric events to provide a hazard forecasting scenario, difficulties arise from the lack of measured or observed parameters to constrain flows. In addition, there is often great uncertainty surrounding source area location and conditions, triggering mechanisms and geomorphology at the time. In the case of the Warea Formation sequence of lahars at Mt. Taranaki (Chapter 4), the pattern of deposition is related to a broad spectrum of flow types (debris flow, hyperconcentrated flow and transitional types), as well as different and changing source areas and initiating conditions. Most importantly, the distribution of lahars and

subsequent deposits was controlled primarily by major landscape changes induced by an extremely large debris avalanche deposit. The Titan2D toolkit could be used in a general way to simulate how these events may behave on the present day landscape, however, the simulations highlighted that defining the source areas and flow genesis are the most important parameters to carry out a numerical hazard forecasting study. Detailed behaviour of the simulations is also likely to be subject to rheological variations in response to the available sediment and water; neither factor can be reconstructed from deposit sedimentology alone.

Numerical modelling methods can conversely be applied as a tool to reconstruct likely paleo-conditions. In Chapter 4 it was demonstrated that running a range of scenarios in Titan2D with variations in starting pile positions and volumes allowed definition of the most likely drainage patterns and source areas of prehistoric flows. Also, running a range of scenario types, with variable rheological, source location and volume properties was a good way to identify the most susceptible channels for future lahar events across the otherwise broad and flat ring-plain around Mt. Taranaki. Once primary flow paths are identified by a broad-scale analysis, simulations can be targeted in a probabilistic manner by testing a geologically appropriate range of volume and rheology input parameters to forecast potential ranges in lahar velocity, discharge and inundation. The Chapter 4 results also imply that following major flank collapse, the subsequent focus of lahars may dramatically change so that hazard forecasts must be made on updated DEM's.

When examining large scale debris avalanche events, such as the Opua debris avalanche at Mt. Taranaki (Chapter 5), it is apparent from analysis of deposit sedimentology and morphology that paleo-topography has a primary influence on flow

processes. The Titan2D reconstructive simulations of events of this scale and rheology show this also, but applying these methods to future forecasting is not straightforward. Scott et al. (2001) identified a range of reasons why the analysis of past (debris flow and debris avalanche) events may not provide an accurate forecast for future events. These include variations in bulking or de-bulking, flow behaviour and rheology, scale effects such as initial volumes, changes in present topography and flow surface roughness and variable source areas or initiation conditions.

Computer simulations of debris avalanches (LAHARZ; Schilling, 1998; Titan2D; Patra et al., 2005) can be used to take into account some aspects of volume, paleo-topography and scale effects, because these can be controlled and varied by the user and built into a range of reasonable simulations. Titan2D runs on present-day topography provide an accurate simulation of source volumes and the behaviour of the flow in relation to topographic features. Titan2D and other similar styles of computer simulations can also be used to determine how pre-historic debris avalanches may have interacted with terrain, to help identify critical points of where future debris avalanches may transform into related flows, such as cohesive debris flows.

The computer simulation forecasts of velocity and discharge based on prehistoric events may not be independently verifiable, but they may provide first-order information usable for hazard analysis along potential flow paths. Runout can be modelled using relatively simpler methods, such as those developed by Malin and Sheridan (1982) and Sheridan et al. (2004a) which use the energy line principle and varying initial volumes. The advantage of using Titan2D and other similar computer simulations is the ability to provide an indication of transient flow depths. However, it must be noted that these may or may not be comparable to deposit thickness (Iverson,

1997a). Following a statistical analysis of the relationship between past event volumes, sources, styles, lithology and other relevant factors, a series of computer simulations modelling this range can be carried out and combined on the basis of relative probability of each scenario to provide an overall combined hazard zonation.

7.4. Creating Hazard Maps from Computer Simulations

The methods to create a hazard map for volcanic mass flows were originally introduced by Crandell et al. (1984) and they rely on the identification of past inundation areas and the frequency of past events. The fact that zones defined based on this information are gradational or have gradational boundaries was also recognised at the time. Achieving gradational forecasts requires identification and measurement of a range of characteristic properties (e.g. thickness) from past mass-flow events, which could possibly be replicated on modern terrains using 2D modelling methods as described in this thesis. To incorporate all these data into a gradational hazard map coverage requires statistical analysis and extrapolation.

The Swiss "Platform Natural Hazards" or PLANAT (a Federal Government advisory body) provided a categorisation of hazard mapping in response to all mass flow types, along with guidelines on map compilation, use of computer simulation and their application to planning (Table 7.1). This classification of mapping strategies should be seen as a hierarchical sequence that supplies increasingly detailed information. While these provide guidelines for hazard classification and useful methods for mapping, some of the statistical methods for cartographic display are undefined and rely on the

definition of sharp rather than gradational boundaries. To create any hazard zone with gradational properties or values requires defining a range or scale of values within a related intersecting spatial area. This can be easily achieved with computer simulation outputs as long as the process being modelled is within a logical continuum or has a known statistical distribution, with input parameters being well-constrained and well-understood.

To achieve this, a systematic method must be applied to input parameter selection such as applying a simple Gaussian distribution to a realistic range of values, then sub-sampling for test runs using Monte Carlo methods, latin-hypercubed sampling or even polynomial chaos methods (Dalbey et al., 2008). This process allows a measure of parameter uncertainty to be developed that can be applied to simulations and their spatial outputs on a map.

For Mt. Taranaki a Volcanic Flow Hazard Map (Neall and Alloway, 1996) and an Evacuation Map (Taranaki Regional Council, 2004) exist. The current pyroclastic flow hazard zone on Mt. Taranaki is a circular area based on the maximum run-out distance of recent block-and ash-flows. The event frequency and inundation probability is based on the number of defined events of this type over the last 1000 yrs. This zone definition is similar to the energy cone principle proposed by Sheridan et al. (2004b) and provides a useful exclusion zone for emergency management in this low-population area. However, more specific catchment-based information is also important to provide prioritisation of areas for evacuation and to identify potential downstream population and infrastructure at risk from transforming flows. The circular zone does not provide enough information for local level specific risk analysis, especially where some catchments host large iconic infrastructure (Bebbington et al.,

2008), or where relative hazard assessment is required for defining land-use planning priorities for mitigation efforts.

Table 7-1. Identification and categorisation of mapped hazards in relation to volcanic mass flows and volcanic events, based on a scheme created by the Swiss "Platform of Natural Hazards" (PLANAT).

Map type	*Content*	*Purpose*	*Creation*
Event Map	Record of events and affected areas	Provides indication of hazardous conditions and initial record of events for statistical analysis. Basis for hazard maps	– Database – GIS files created from anecdotal records
Hazard Map	Representation of the types of hazard and the spatial extent of each type of hazard	Displays the spatial extent of a hazardous event	– GIS DEM analysis – Deterministic scenario-based computer simulation
Danger Map	Representation and spatial extent of the hazard as well as representation of the degree of danger – magnitude and frequency	Probability of an event happening and display of the spatial extent or intensity. Particularly used in land-use mapping	– GIS DEM analysis – Historical analysis (frequency) of event with the combined spatial extents of all events – Deterministic scenario-based computer simulation combined with probabilities of event happening
Vulnerability Map	An analysis of the exposure of the population and infrastructure as to a particular event	Hazard/danger map combined with GIS analysis of economic assets affected by hazard. Used primarily for landuse planning and emergency management planning.	A probabilistic analysis; – Historical analysis (frequency) of event with the combined spatial extents of all events – Deterministic scenario-based computer simulation combined with probabilities of event happening In combination with Cadastral or GIS analysis of assets.
Risk Map	A qualitative or quantitative analysis of the probability of an event occurring and the impacts it will have.	A qualitative classification of risk from high to low combined with a likelihood of average loss resulting from the event	GIS analysis or extrapolation of risk values determined from the probability of event happening.

In Chapter 6 the method was applied in the way that the block-and ash-flow (BAF) hazard in the pyroclastic flow zone of Neall and Alloway (1996) for Mt. Taranaki was determined by the largest known event within the last 1000 years. For this maximum likely scenario, initial conditions of the event, including volume and rheology can be estimated from depositional and theoretical evidence. Varying volumes of initial source material may change the run out and inundation area of the flow, while avulsion processes and inundation depth is probably controlled by the initiating process and internal flow processes (Lube et al., 2007). Varying the volume and rheological conditions by adjusting the friction input factors of Titan2D can be used to create a range of outputs that can be combined into a gradational hazard/danger zone.

Esposti et al. (2002) developed a pyroclastic flow hazard assessment at Vesuvius (Italy) by applying the 1D numerical model of Todesco et al. (2002). Analysis of flow variables was able to show that the internal characteristics of the simulated flows such as density, velocity, temperature and pressure when encountering structures greatly affected its propagation. This highlighted that for hazard analysis there is a need to define not only the range and uncertainties in geological variability possible for scenarios, but also the variability in computer simulation outputs relating to how they are parameterised.

The simplest, and arguably best, method to examine the variability of modelling input parameters for scenario assessment is to start by assuming they fit within normal (Gaussian) distributions. For the Mt. Taranaki example used in Chapter 6, geological information was used to define the source area with the highest probability, based on the current crater configuration and present lava dome (after Platz, 2007). The spatial distribution of the <1000 yr. BAFs, including the largest events, was also available from

field mapping by Platz (2007) which also reaffirmed the source dome and volume. The variables of greatest control were those influencing flow processes; by varying those parameters (based on a Gaussian distribution within the best fit range) allowed for a series of output raster's of pile height that could then be combined (or averaged) and reclassified to define a gradational zone of hazard.

Tilling (1989b) and Scott (1989) recognised a process of determining pyroclastic flow hazard zones as well as methods of identifying a variable hazard zone based on frequency of events occurring in certain areas or at certain distances. They suggested that the principal factors in determining pyroclastic flow hazards are vent location, topography and volcano height/steepness. The most appropriate methods include the use of computer simulations or computer-assisted methods (such as Sheridan and Malin, 1983) to determine a range of run out values and identify any topographic influences on the flow. Saucedo et al. (2005) implied that pyroclastic hazard zones on Colima Volcano, Mexico, required updating due to changes in topography and suggested the use of computer simulation to define the catchments of greatest future hazard.

In one of the more comprehensive hazard assessments of El Chichón Volcano, Mexico, involving a range of volcanic hazards, Macias et al. (2008) combined flow models to simulate pyroclastic flows with Flo3D (Kover, 1995) and Titan2D (Patra et al., 2005), and lahar events with LAHARZ (Schilling, 1998). All simulations were based on the geological parameters of the most recent "maximum-likely" events. The only semi-gradational zone portrayed was within the lahar simulations, based on variations in simulated flow volumes. A similar methodology was replicated by Williams (2006) on the southern catchments of Cotopaxi Volcano, Ecuador, using Titan2D. Lahar

inundation and a representative hazard zone were determined by calculating a probability tree of a lahar of a particular volume occurring in relation to eruption size and violence. The varying probability and related simulations based on the maximum representative volumes were combined in GIS to develop a semi-gradational hazard zone used for vulnerability analyses maps of local infrastructure.

Lessons from all these studies, including that of Chapter 6, show that when combining probabilistic methods and multiple deterministic methods that involve modeling and creation gradational hazard zones for mass flows that these must encompass both, the variability relating to parameter uncertainties as well as providing a valid geological range of possible scenarios. Ideally, variability from these two sources should be distinguished in order for users to independently validate modelling results before using them for risk analysis.

7.5. Probabilistic Modelling vs. Deterministic Geophysical Computer Simulations

Probabilistic and deterministic methods to forecast the likelihood of an event or the spatial extent of its impacts should ideally be combined in hazard and risk studies. The use of probabilistic methods are currently in the forefront of hazard analysis, with the studies of Turner at al. (2008) and Bebbington et al. (2008) determining likelihoods of explosive eruptions and ash fall thicknesses from Mt. Taranaki. Magill et al. (2005; 2006) used a combination of probabilistic methods to determine vent location and a physical model, ASHFALL (Hurst, 1994), to forecast ashfall for the Auckland region of

New Zealand. Hurst and Smith (2004) used Monte Carlo methods to determine the input parameters (with associated probabilities) for the physical ASHFALL model. This was extended by Bonadonna (2006) who applied a range of scenarios and methods to simulate ashfall from the Okataina volcanic centre for the New Zealand area and developed probability curves of impact for the region. Bonadonna (2006) also indicated that a comprehensive hazard analysis has to be based on developing a range of scenarios. From these, Monte Carlo techniques can be used to re-sample input parameters. The resulting scenarios and their analysis could account for gaps or unknown events not found in the stratigraphic record.

Despite having many examples of probabilistic and physical modelling methods being combined for ashfall analysis in New Zealand, the same combination has not often been applied to volcanic mass flow hazards. This could possibly be due to a greater number of unknown factors relating to mass flows such as source, initiating factors, volume and rheological characteristics not being accurately quantified and described.

A detailed stratigraphy of volcanic ring-plains provides the best possible record of mass flows events with parameters such as deposit thickness, age and runout that could be analysed probabilistically. Zernack (2009) provided a detailed stratigraphy of the Mt. Taranaki ring-plain and identified a repeated cyclic pattern of cone collapse and re-growth as well as information on the preferred direction of major edifice failures. The cyclic sedimentation pattern includes thick debris avalanche deposits, followed by increasingly larger and longer-runout lahar deposits reflecting increasing cone growth. Having an understanding of systematic change provides another dimension to hazard analysis, by applying similar probability tree methods (Williams, 2006). In this way the forecasting of future scenarios and event sequences as well as responses to landscape

and cone changes can be built into a scenario tree with an associated probability for each type of mass flow occurring at different points within the cycle. This would create a system for evaluating time-varying hazard, because following each type of event or mass flow type the probability of other types of mass flow would change, e.g., following a large debris avalanche event the probability of another catastrophic debris avalanche occurring in a short time period is relatively low. Once the present situation is determined, the scenario tree can be developed with associated probabilities and each scenario modelled and combined to identify areas most likely to be impacted. One limitation of this method, however, is that after each scenario is modelled, the DEM would have to be adjusted accordingly.

In general there are three methods that could be applied to developing a gradational probabilistic hazard zone for inundation by mass flows around Mt. Taranaki;

1. Probabilistic analysis of volume, source area and friction values for a range of scenarios or variability in a maximum-likely scenario, before combining outputs of all scenarios into a matrix in GIS,

2. Carrying out a probabilistic analysis of past flow directions, volumes, thicknesses and frequency of each mass flow type and using computer simulations (e.g. Titan2D two-phase model) to simulate the most likely of these on the present terrain/topography,

3. Developing a probability tree of the scenarios (categorised by rheology) that are likely to occur in response to changing volcanic conditions and simulate each event using an appropriate rheological model combining the outputs with the probability of each event occurring.

No matter which method is applied, the analyst and the users of the results need to be fully aware of the hazard-analysis process, events being simulated, computer simulation or probabilistic calculation inputs and associated uncertainties, the terrain models or DEMs used and the needs of the communities and infrastructure at risk. In addition, Haynes et al. (2007) also pointed out that the hazard information needs to be communicated and understood, using methods most acceptable by the public and policymakers.

CHAPTER 8

Conclusions

Mass flows of all types from high elevation stratovolcanoes, such as Mt. Taranaki and Mt. Ruapehu in New Zealand, pose considerable hazard to the surrounding communities. The two example volcanoes discussed in this thesis show great differences in the nature of mass flow hazards posed regarding their relative frequency, magnitude and potential impacts on surrounding communities and infrastructure. This is exemplified by the fact that all stratovolcanoes pose a very individual set of hazards to their surrounds, hence methods for evaluating hazards must cope with a huge range of hazard types. Despite this, hazard evaluation methods should be also standardised as best as possible between locations to aid their conception by public, planners and policy makers.

Mts. Ruapehu and Taranaki have volcanic flow hazard maps based on comprehensive mapping of deposits and analysis of past mass flow events. Hazard has been interpolated into spatial zones on the basis of rheological criteria (debris flow, pyroclastic flow/BAF, debris avalanche), and event size. Frequencies for each of these hazard types and magnitudes are based on the known record of these events over time. The compilation of these hazard maps has allowed identification of how changes in topography, crater or cone configuration have resulted in changes in the focus of mass-flows between a range of catchments over time. This allowed each sector of the ring plain to be categorised within an overall relative ranking of hazard. These maps are based on the principle that the volcanic system will continue to behave in the

future as it has done in the past, and that changes in landscape will not materially affect assessment of future lahar hazards.

The rapid switching of hazardous catchments from one side of the volcano to another in the geological past at these two centres (c.f., Neall, 1979; Cronin et al., 1997c; Zernack, 2009) raise the spectre that geologically based hazard maps may not provide the complete picture of future hazard possibilities. In particular, topographic changes along individual channels mean that mass-flow inundation zones must only be seen as a general guide. In addition, upon the onset of major volcanic activity, changes in the upper edifice geometry may render these geological "averaging" hazard maps unusable as an emergency management guide. To add to the geological mapping approach, methods to incorporate the present day topography and more detailed catchment hazard analyses are needed. The development of new numerical models and computer mass-flow codes has opened the door for this possibility.

This thesis has attempted to address the question of how such computational mass flow hazard models can help us improve hazard forecasts at Mts. Taranaki and Ruapehu. The widely available granular mass flow model Titan2D, in several forms of its development over the last five years, has been applied to a range of mass-flow hazard problems at these two New Zealand stratovolcanoes, displaying a typical range of mass flow types and magnitudes. The original form of the code can be applied to simulate granular flows, applicable to dry rock avalanches or dome-collapse generated block-and-ash flows (BAFs). It also has a two-phase version (granular + fluid) which can be used to simulate water-mass flows, such as debris avalanches and various types of lahars. The model works by mathematically propagating a mass over real terrain replicated as a 3-dimensional digital elevation model (DEM). The codes can be run and

replicated in reasonable times on a desktop PC or more intensively on a super-computer array. Titan2D can be used in emergency management applications by providing the user or a decision maker with outputs that can be quickly analysed or viewed as a response to a volcanic event or emergency.

8.1 Lahars and Mt. Ruapehu

To analyse the effectiveness and applicability of Titan2D simulations to lahars the model was tested, verified and optimised by comparison with parameters observed and measured from recent lahar events on Mt. Ruapehu (Chapter 2). At Mt. Ruapehu the community hazard focus is on lahars generated by eruptive perturbation and loss of water from Crater Lake, such as occurred most recently in 1995 (Cronin et al., 1996b; 2000; Lube et al., 2009). During the course of this study, the fragile tephra dam that blocked parts of the main crater lake outlet collapsed, generating a break-out lahar on 18 March 2007 (Manville and Cronin, 2007; Procter et al., in press). The characteristics of this event were particularly well-characterised allowing detailed comparison with Titan2D modelling outputs (Chapter 3).

A critical risk factor for Ruapehu lahars is related to the integrity of the landscape at the top of the Whangaehu Fan, c. 10 km lahar travel distance from the Crater Lake. At this point, lahars if large enough may spill northwards into the Tongariro catchment, posing a risk to larger populations and nationally critical infrastructure (Cronin et al.,

1997a & b). In response to this a lahar deflection (stop-bank) structure, "the bund", was built to prevent flows from avulsing northward (Keys, 2007). Observations from the 1995 lahars provided the opportunity to simulate potential similar future events and thus "test" the model applicability as well as the possible future effectiveness of the bund structure.

The Titan2D simulations could be easily tuned to replicate the broad features of inundation areas, flow behaviour and travel time for floods generated from the Crater Lake to the bund structure. To achieve this, however, several features had to be accounted for, which highly depended on the availability of detailed historical data. This includes information of the fully bulked volume of the lahar and the awareness that small volumes of water expelled from Crater Lake may generate lahars 3-4 times greater in volume (c.f. Cronin et al., 1997a; Pierson, 2002). Since Titan2D works via conservation of mass and momentum, this fully bulked volume must be applied to such simulations. Careful consideration also has to be paid to source conditions and model initiation to avoid spurious computational results. It was assumed during this study that Mt. Ruapehu debris flows contained > 60% sediment, and hence the dominantly "granular" model of Titan2D provided a good fit to earlier tested hydrological models that were based on Newtonian flow (c.f., Manville, 2004). In this way, the two approaches provided an opportunity to simulate opposite ends of the mass flow rheological spectrum, allowing a balanced hazard assessment.

In undertaking a hazard analysis at the bund site it must be recognised that the apex of coalescing alluvial and laharic fans are highly dynamic and small changes in bed level or channel form may lead to major changes in flow path, rheology and downstream hazard. The Whangaehu fan apex has been recognised as a critical point where

previous lahars transformed from being dominantly erosive to depositional (Cronin et al., 2000). Detailed land surveying of this channel area during this study showed that large changes may occur through intense erosion or deposition, both, between and during lahar events. The study of the channel adjacent to the bund has shown that, despite periods of rapid channel aggradation following a series of small lahars (i.e., 1995-96), longer-term recovery results in net erosion. The response to a single event such as the March 2007 lahar showed that while aggradation occurred, the main effect was erosion of the main channel, which cut a deeper channel closer to the bund. This raises a new concern; despite net erosion causing greater channel capacity for future lahars, repeated erosive events may simply remove the protection structure in as few as two events. The study clearly shows that the ongoing effectiveness of such deflection structures must be continually reassessed and monitored to account for ever changing channel morphology.

In applying Titan2D to test the effectiveness of the bund, model outputs were not able to be automatically applied to calculate a mass-flux or "discharge" for comparison with the hydrological approaches used in bund design. Possibly more useful, mass flow simulation for hazard analysis should supply factors such as impact forces and shear stresses to also provide accurate analysis of specific areas of erosion and deposition.

A long-anticipated lake-breakout lahar from Mt. Ruapehu occurred during the period of this study on the 18 March 2007 (Manville and Cronin, 2007). Prior to this, the two-phase version of Titan2D was used to forecast the flow path and inundation area of the breakout lahar. The simulations were able to replicate the following comparable features with the real event:

- discharge at the dam break-out area,
- pulses of flow through the outlet and along the upper channel,
- bifurcation of the flow at 2 km from source and minor super-elevation prior to that,
- convergence of the flow at 5-7 km and hydraulic ponding, leading to multiple stage peaks,
- bifurcation of the flow at 7.5 km with the flow in the alternative channel (the chute) passing more rapidly across to the lower Whangaehu fan,
- similar inundation, stage height, velocity and discharge at 9-10 km from source.

Fine-scale details of inundation area and peak flow height along the upper 10 km of the Whangaehu channel were very well-forecasted. Outputs from the new model could be re-calculated to compare mass-flux with the 2007 event. However, it is important that, if a real-world event is to be used for evaluating model performance or models are to be used for real-event forecasting, data outputs of simulations must match the types of data that can be accurately observed for real events (such as travel time, peak height, deposition, flow tide-lines etc). This requires both an understanding of the simulation tool and its outputs, as well as an understanding of the flow and its physical characteristics.

8.2. Use of Computer Modelling in Geological Reconstruction and Simulation of Prehistoric Volcanic Mass Flows

In Chapter 4, the Titan2D code was applied alongside sedimentological and mapping studies to investigate a sequence of Mt. Taranaki-derived lahars (debris flow-hyperconcentrated flows) whose deposits were originally mapped by Neall (1979) as the Warea Formation. An important result from this study was that it demonstrated a need for detailed mapping of the sources and relationship between individual areas of volcanic mass flows that are otherwise grouped only on chronostratigraphic grounds. Due to the often poor resolution of chrono-stratigraphic markers, numerous deposits of possibly widely varying origin, flow mechanism, rheology and age are grouped together, hindering a clear understanding of the frequency and drivers behind hazard processes at the source volcano. Through detailed mapping, this study was able to reconstruct the process of landscape recovery after the emplacement of an extremely large debris avalanche deposit. This in-turn could be used to examine systematic changes over the next few thousand years in the source regions, lithological composition and flow paths for mass flows in the aftermath of catastrophic debris avalanches. Following the emplacement of the Pungarehu debris-avalanche deposit on the western ring plain of Mt Taranaki at c. 22 000 yrs B.P., the Warea Formation was emplaced between 13-22 000 yrs B.P., comprising mass flow deposits of broadly similar overall character. Initial flows were debris flows transforming to hyperconcentrated flows with distance from the debris avalanche scarp. During the next phase debris flows and hyperconcentrated flows, originating from the amphitheatre or possibly a growing lava dome within it, occupied newly created

drainage paths between the previously deposited debris flows and debris avalanche units.

The response to the landscape-altering Pungarehu event thus occurred in three distinct stages affecting different areas of the ring plain with differing types of hazard. Future events will similarly re-arrange drainage systems producing new channels and new mass-flow hazards, initially along the edges of the debris avalanche deposit, and expanding inwards as the lateral zones aggrade.

A hazard analysis derived from this geological scenario is difficult to apply with confidence to modern terrain, because it depends on the distribution of the initiating debris avalanche deposit. Results from Titan2D simulations, however, are useful to indicate the most likely catchments and flow paths affected in future events across the low-relief landscape. The Titan2D simulation results were also extremely useful for identifying or confirming characteristics with which to reconstruct the flow source-areas and genesis mechanisms. The short runout distances of all simulations, despite using natural internal and basal friction parameters (based on the Ruapehu lahar experiences) suggest that the depositional pattern of the Warea flows results from source areas on the lower flanks of the volcanic edifice (possibly from the proximal or medial portions of the Pungarehu debris avalanche deposit), or from the collapse scarp of the original debris avalanche. The simulations confirm the sedimentological evidence that a complex and wide variety of rheological conditions are needed within these flows to account for their distribution. This complexity, involving large numbers of events, is beyond the capabilities of numerical simulation, unless many hundreds of simulations are carried out.

In terms of hazard analysis, deposit-based hazard maps covering such complex periods of ring plain history give a low-resolution but holistic view of future mass-flow hazards. To extend from this, predictive hazard zones should be developed and constantly updated taking into account a variety of scenarios that could occur on the volcano and ring plain and may rapidly change drainage patterns.

8.3. Application of Numerical Modelling to Debris Avalanche Hazard Analysis and Event Reconstruction

In Chapter 5 the youngest Mt. Taranaki debris avalanche deposit (Opua Formation) provided the best exposed example of an unconfined deposit distribution on the low-relief ring plain. A morphological and structural analysis of the Opua deposit showed that it was emplaced by a progressively transforming flow, initiated by collapse of a portion of the volcano flanks that travelled in a granular fashion before breaking down as pore water and clay within the pile, and clay entrained along its path, formed a cohesive matrix. The resulting cohesive flow retained large granular bodies, forming the characteristic surface mounds of this deposit. The distribution, alignment and clustering of the mounds show that the deposit formed two distinct lobes in response to very subtle changes in the paleo-topography. The most distinctive avalanche mounds represent the gradational breakdown and transformation of the sliding and granular flowing mass into a cohesive and eventually viscous flow.

The Titan2D simulations of Opua-scaled debris avalanches on the modern ring plain of Mt. Taranaki produced comparable thicknesses for areas of deposition and responded to small changes in topography, such as flowing around pre-existing mounds represented on the DEM. The simulations were directed by very subtle drainage patterns, despite these being poorly defined on a relatively low-resolution (20 m grid) DEM. The limitation of this computer modelling approach was restricted to the model being based on a granular flow numerical framework. Despite attempting to change parameters during simulations, these could not reproduce the strong transformation that the disintegrating debris avalanche underwent during flow. Its fundamentally changed properties, particularly development of cohesive debris flow characteristics, significantly increased its mobility and extended its runout.

For geological reconstructions of the emplacement processes of the Opua Formation, the simulations were useful to define flow paths. The models show realistic sensitivity to effects of topography and surface roughness that can be used to examine flow propagation over variably eroded ring-plain landscapes. As a hazard analysis tool these simulations were able to provide a reliable indication of the main flow axes, proximal and medial inundation areas and deposition thicknesses. However, the simulations greatly underestimated the distal hazard area and runout for such flows, primarily due to their inability to simulate the complex rheological transformations that occurred.

8.4. Application of Numerical Modelling to Block-and-Ash Flow Hazards

The recent block-and-ash flows (BAFs) from Mt. Taranaki (Chapter 5) provided an excellent scenario to test the application of the Titan2D code. New research (Platz, 2007) had identified a higher frequency and longer runout of BAFs over the last 800 yrs of activity than previously thought (c.f. Neall, 1979). This prompted a review of the current hazard zones focusing on the inundation and runout of future BAFs in the context of present-day topography. The current hazard zone, comprising a 15 km circle around Mt. Taranaki, provided a useful exclusion zone, but given that BAFs over the last 800 yrs have been confined to the NW sector, due to the NW crater wall having collapsed away from this time creating a channel (Platz, 2007) focusing all impact on this area renders the zone somewhat over exaggerated.

Titan2D was used to explore the scenario of a sequence of BAFs or lava-flow collapses from the NW summit area, with variations in initial conditions and rheology parameters. It is apparent that for the Titan2D model application to Mt. Taranaki BAFs, friction input values were the most influential parameters, with source differences mattering less. The systematic variation of these parameters was used to produce a series of optimised model parameters. The combined result gave rise to a GIS layer that can be displayed as a gradational hazard forecast. The advantage of such GIS layers is that they can also be displayed in a variety of ways, such as being combined with aerial/satellite imagery, or shaded-relief models. These enable clear communication to the public, and since they are GIS layers with data associated with them, they can also be queried to extract local information from the scenarios, such as local velocity and mass flux. This case study showed that by undertaking a full series of Titan2D runs that incorporate all reasonable combinations of flow parameters, a range of best-fit simulations can be determined by comparison to the spatial distribution of mapped BAF events.

8.5. Concluding remarks

Computer simulation of floods and volcanic mass flows are becoming an increasingly common practice in hazard analysis. Most applications of these are constrained to a single event scenario that is usually hind-cast from historic events, often with very little comparable data to be incorporated into the flow simulation.

Despite the rapid use and demand for results produced from computer simulations of flows (particularly by local government/authority in land use planning), there has been very little effort to incorporate them into risk analyses, or transfer their information into hazard maps. However, without the appropriate representation of inherent uncertainties associated with computer simulations, or a detailed understanding of the event or range of events being analysed, any hazard zone created from computational modelling could be erroneous or misleading. Computer modelling of mass flows can never replace a program of geological mapping and analysis of the past record of mass flows in order to develop the basis for hazard maps. The geological studies also provide essential inputs for computational modelling to increase the resolution of hazard maps in certain areas or to develop scenario-forecasts for specific events. However, with geological studies great uncertainties arise in defining the spatial extents of past mass flows and the areas potentially affected by similar flows in the future, and interpretation of the return period of different types of flows. These uncertainties are rarely included in hazard maps. Similarly, computer modelling that uses constraints based on geological mapping propagates uncertainties through the process. These geological uncertainties are additional to those associated with the computer model itself and its simulation errors. Identification and quantification of uncertainties and their display within hazard zonation requires more attention to provide, both, the

geologist and the user with a more reliable tool for decision making and a focus to reduce these as much as possible.

The studies outlined in this thesis highlight that improved volcanic mass flow hazard forecasts can be developed through a holistic approach that combines geological analysis and interpretation of the past mass flow deposit record with targeted computer modelling. At this stage, a major drawback is that the majority of numerical and computational flow models are used to simulate flows in motion and cannot simulate the deposition of material, providing a fundamentally different dataset to mapped deposits. This raises the question of whether the depth of moving flow or the resultant deposit is a better measure of hazard. If the flowing depth is the hazard of focus, then analysis must concentrate on the initiation, source, flow paths (topography), velocity and discharge of a forecasted event. With any computational modelling, the forecasted event type or scenario must be constrained within the known bounds of what can occur at the volcano, based on a detailed understanding of the stratigraphy and geologic characteristics. Analysis of the frequency and occurrence of past deposits in a catchment or ring plain sector provides a means to incorporate a probabilistic analysis of event types. This in combination with computer modelling, would allow development of a systematic forecast of the likelihood of events and the basis for a new generation of volcanic hazard mass flow mapping approaches.

References

Acheson, D. J. (1990), Elementary Fluid Dynamics, Oxford Applied Mathematics and Computing Science Series, Oxford University Press, ISBN 0198596790.

Adams, R.D., Ware, D.E. (1977) Structural earthquakes beneath New Zealand: location determined with a laterally inhomogeneous velocity model. New Zealand Journal of Geology and Geophysics 20: pp. 59-83.

Allen, G. F. (1902). Supplementary edition of Willis' guide book of new routes for tourists. Willis, Wanganui. 240 p.

Alloway B, Neall VE, Vucetich CG (1995) Late quaternary (post 28,000 year BP) tephrostratigraphy of northeast and central Taranaki, New Zealand. Journal of the Royal Society of New Zealand 25: pp. 385–458

Alloway, B. (1989) Late Quaternary cover-bed stratigraphy and tephrochronology of north-eastern and central Taranaki, New Zealand. Unpublished PhD thesis, Massey University, Palmerston North, New Zealand.

Alloway, B. V., Lowe, D. J., Barrell, D. J. A., Newnham, R. M., Almond, P. C., Augustinus, P. C., Bertler, N. A. N., Carter, L., Litchfield, N. J., McGlone, M. S., Shulmeister, J., Vandergoes, M. J., Williams, P. W. and NZ-INTIMATE members. (2007) Towards a climate event stratigraphy for New Zealand over the past 30 000 years (NZ-INTIMATE project). Journal of Quaternary Science, 22: pp. 9-35.

Alloway, B., McComb, P., Neall, V., Vucetich, C., Gibb, J., Sherburn, S., Stirling, M. (2005) Stratigraphy, age, and correlation of voluminous debris avalanche events from an ancestral Egmont Volcano: implications for coastal plain construction and regional hazard assessment. Journal of the Royal Society of New Zealand 35: pp. 229-267.

Anderson, K., Sundaresan, S. & Jackson, R. (1995) Instabilities and the formation of bubbles in fluidized beds. Journal Fluid Mechanics. 303: pp. 327–366.

Anderson, T. B. & Jackson, R. (1967). A fluid mechanical description of fluidized beds: equations of motion. Industrial and Engineering Chemistry Fundamentals. 6: pp. 527–539.

Apmann, R. P., (1973). Estimating discharge from superelevation in bends: American Society of Civil Engineers, Hydraulics Divison Journal, v. 99, no. HY1: pp. 65-79.

Arguden, A.T., Rodolfo, K.S., (1990) Sedimentological and dynamic differences between hot and cold laharic debris flows of Mayon Volcano, Phillipines. Geological

Society of Americal Bulletin. 102: pp. 865-876.

Bagnold, R.A. (1954) Experiments on a gravity free dispersion of large solid spheres in a Newtonian fluid under shear. Proceedings of the Royal Society London A 225: pp. 49-63.

Bates, P.D., De Roo, A.P.J. (2000) A simple raster-based model for flood inundation simulation, Journal of Hydrology 236: pp. 54–77

Bebbington, M., Cronin, S.J., Chapman, I., Turner, M.B. (2008) Quantifying volcanic ashfall hazard to electricity infrastructure. Journal of Volcanology and Geothermal Research 177: pp. 1055-1062.

Bebbington, M.S., Lai, C.D. (1996) Statistical analysis of New Zealand volcanic occurrence data. Journal of Volcanology and Geothermal Research 74: pp. 101-110.

Belousov, A., Belousova, M., Voight, B. (1999). Multiple edifice failures, debris avalanches and associated eruptions in the Holocene history of Shiveluch volcano, Kamchatka, Russia. Bulletin of Volcanology 61: pp. 324-342.

Beverage, J.P., Culbertson, J.K. (1964) Hyperconcentrations of suspended sediment. American Society of Civil Engineers, Proceedings, Hydraulics Division Journal 90, no. HY6: pp. 117-128.

Bibby, H.M., Caldwell, T.G., Davey, F.J., Webb, T.H. (1995) Geophysical evidence on the structure of the Taupo Volcanic Zone and its hydrothermal circulation. Journal of Volcanology and Geothermal Research 68: pp. 29-58.

Bird, P. (2003) An updated digital model of plate boundaries, Geochemistry Geophysics Geosystems, 4(3), 1027, doi:10.1029/2001GC000252.

Blong, R.J., (1996) Volcanic Hazards risk assessment. In: Scarpa, R., Tilling, R.I. _Eds.., Monitoring and Mitigation of Volcanic Hazards. Springer, pp. 675–698.

Bonadonna, C. (2006) Probabilistic modeling of tephra dispersion. In: Mader HM, Coles S, Connor C, Connor L (eds) Statistics in Volcanology. IAVCEI series 1. Geol Soc Lond, pp. 243–259.

Bonadonna, C., Connor, C.B., Houghton, B.F., Connor, L.J., Byrne, M., Laing, A., Hincks, T.K. (2005) Probabilistic modeling of tephra dispersal: Hazard assessment of a multiphase rhyolitic eruption at Tarawera, New Zealand. Journal of Geology and Geophysical Research, 110, B03203, doi:10.1029/2003JB002896.

Boudon, G., Camus, G., Gourgand, A., Lajoie, J., (1993) The 1984 nuée ardente deposits of Merapi volcano, Central Java, Indonesia: stratigraphy, textural

characteristics, and transport mechanisms. Bulletin of Volcanology. 55: pp. 327– 342.

Branney, M., Kokelaar, P. (1992). A reappraisal of ignimbrite emplacement: progressive aggradation and changes from particulate to non-particulate flow during emplacement of high-grade ignimbrite. Bulletin of Volcanology 54, 504–520.

Breien, H., Pagliardi, M., Elverhoi, A., de Blasio, F. (2008). On the Dynamics of Debris Flows - the Influence of the Ambient Fluid and the Sand/Clay Ratio. American Geophysical Union, Fall Meeting 2008, abstract #H42C-04

Bursik, M., Patra, A., Pitman, EB., Nichita, C., Macias, JL., Saucedo, and Girina, O. (2005) Advances in studies of dense volcanic granular flows. Reports on Progress in Physics, 68: pp. 271-301, doi:10.1088/0034-4885/68/2/R01.

Burton, I.R., Kates, G.W., White, F. (1978) The Environment as Hazard. New York: Oxford University Press.

Campbell, C. S., Cleary, P. W., and Hopkins M. (1995), Large-scale landslide simulations: Global deformation, velocities and basal friction, Journal of Geophysical Research., 100(B5): pp. 8267–8283.

Canuti, P. Casagli, N., Catani, F. and Falorni G. (2002) Modeling of the Guagua Pichincha volcano (Ecuador) lahars. Physics and Chemistry of the Earth Parts A/B/C, 27(36), 1587.

Capra, L., Macias, J.L. (2000). Pleistocene cohesive debris flows at Nevado de Toluca Volcano central Mexico. Journal of Volcanology and Geothermal Research 102: pp. 149-168.

Capra, L., Macias, J.L. (2002). The cohesive Naranjo debris-flow deposit (10 km^3): A dam breakout flow derived from the Pleistocene debris-avalanche deposit of Nevado de Colima Volcano (México). Journal of Volcanology and Geothermal Research 117: pp. 213-235.

Capra, L., Macias, J.L., Scott, K.M. (2002). Debris avalanches and debris flows transformed from collapses in the Trans-Mexican Volcanic Belt, Mexico behaviour, and implications for hazard assessment. Journal of Volcanology and Geothermal Research 113: pp. 81-110.

Carrivick, J.L. (2006) 2D modelling of high-magnitude outburst floods; an example from Kverkfjöll, Iceland. Journal of Hydrology 321: pp. 187–199.

Carrivick, J.L., (2007) Modelling coupled hydraulics and sediment transport of a high magnitude flood and associated landscape change. Annuals Glaciology. 45: pp. 143–154.

Carrivick, J.L., Manville, V., Cronin, S.J., (2009) A fluid dynamics approach to modelling the 18th March 2007 lahar at Mt. Ruapehu, New Zealand. Bulletin of Volcanology 71: pp. 153–169. doi:10.1007/s00445-008-0213-2.

Cashman, K.V., Cronin, S.J., (2008) Welcoming a monster to the world: Myths, oral tradition, and modern societal response to volcanic disasters. Journal of Volcanology and Geothermal Research 176: 407-418. http://dx/doi.org/10.1016/j.jvolgeores.2008.01.040.

Chen, C. (1988). Generalized viscoplastic modeling of debris flow, Journal of Hydraulic Engineering, 114: pp. 237–258.

Chester, D. (1993) Volcanoes and Society, Edward Arnold, London

Chester, D.K., Dibben, C.J.L., Duncan, A.M. (2002) Volcanic hazard assessment in western Europe. Journal of Volcanology and Geothermal Research, vol. 115, no. 3-4: pp. 411-435.

Christenson, B.W., Wood, C.P., (1993). Evolution of a vent-hosted hydrothermal system beneath Ruapehu Crater Lake, New Zealand. Bull. Volcanol. 55: pp. 547–565.

Cole, J.W. (1978) Andesites of the Tongariro Volcanic Centre, North Island, New Zealand. Journal of Volcanology and Geothermal Research 3: pp. 121-153.

Cole, J.W. (1979) Structure, petrology and genesis of Cenozoic volcanism, Taupo Volcanic Zone, New Zealand: a review. New Zealand Journal of Geology and Geophysics 22: pp. 631-657.

Cole, J.W. (1982) Tonga-Kermadec-New Zealand. In: Thorpe RS (ed.) Andesites: Orogenic andesites and related rocks. Wiley, New York.

Cole, J.W. (1986) Distribution and tectonic setting of late Cenozoic volcanism in New Zealand. In: Smith IEM (ed.) Late Cenozoic Volcanism in New Zealand. Bulletin of the Royal Society of New Zealand 23: pp. 7-20.

Cole, J.W., Graham, I.J., Hackett, W.R., Houghton, B.F. (1986) Volcanology and petrology of the Quaternary composite volcanoes of Tongariro Volcanic Centre, Taupo Volcanic Zone. Royal Society of New Zealand Bulletin 23: pp. 224-250.

Cole, J.W., Darby, D.J., Stern, T.A. (1995) Taupo Volcanic Zone and Central Volcanic Region: Backarc Structures of North Island, New Zealand. In: Taylor B (ed.) Backarc Basins: Tectonics and Magmatism, Springer Heidelberg, p. 1-24.

Cole, P.D., Calder, E.S., Sparks, R.J.S., Clarke, A., Druitt, T.H., Young, S.R., Herd, R.A.,

Harford, C.L., Norton, G.E., (2002) Deposits from dome collapse and fountain collapse pyroclastic flows at Soufrière Hills Volcano, Montserrat. In: Druitt, T.H., Kokelaar, B.P. (Eds.), The Eruption of Soufrière Hills Volcano, Montserrat, from 1995 to 1999. Memoirs, vol. 21. Geological Society, London: pp. 231–262.

Costa J.E. (1984). Physical geomorphology of debris flows, in Costa J.E. & Fleisher P.J. (eds), Developments and Applications of Geomorphology, Springer, Berlin and New-York, p. 268-317

Costa, J.E., Williams, G.P. (1984) Debris-flow dynamics (videotape, 22.5 min). US Geological Survey Open File Report 84-606.

Coussot. P., Meunier, M. (1996) Recognition, classification and mechanical description of debris flows. Earth-Science Reviews 40, 2: pp. 09-227.

Coussot, P., Proust, S. (1996) Slow unconfined spreading of a mudflow. Journal of Geophysical Research101: pp. 25,217-25,229.

Crandell, D.R. (1971) Post-glacial lahars from Mt. Rainier volcano, Washington. US Geological Survey Professional Paper 1444, 91 p.

Crandell, D.R. (1973) Potential Hazards from Future Eruptions of Mount Rainier, Washington. U.S. Geological Survey Miscellaneous Geologic Investigations Map, I-836.

Crandell, D.R. (1975) Assessment of Volcanic Risk on the Island of Oahu, Hawaii. 18 pp. U.S. Geological Survey Open-file Report, 75-287.

Crandell, D.R. (1980) Recent Eruptive History of Mount Hood, Oregon, and Potential Hazards from Future Eruptions. 81 pp. U.S. Geological Survey Bulletin, 1942.

Crandell, D.R. (1989) Gigantic debris avalanche of Pleistocene age from ancestral Mount Shasta volcano, California, and debris-avalanche hazard zonation. US Geological Survey Bulletin 1861, 29 p.

Crandell, D.R., Booth, B., Kazumadinata, K., Shimozuru, D., Walker G.P.L., Westercamp, D. (1984) Source book for volcanic hazards zonation. UNESCO, Paris.

Crandell, D.R., Mullineaux, D.R. (1978). Potential hazards from future eruptions of Mount St Helens. US Geological Survey Bulletin, 1383-C: pp. 1-26.

Cronin, S. J. (1996) Late Quaternary volcanic stratigraphy within a portion of the northeastern Tongariro volcanic centre. Unpublished PhD Thesis. Massey University, Palmerston North. 181 pages.

Cronin, S. J., Neall, V.E., Palmer, A. S. (1996a) Geological history of the north-eastern ring plain of Ruapehu volcano, New Zealand. Quaternary International 34-36: pp. 21-28

Cronin, S.J., Neall, V.E., Lecointre, J.A. and Palmer A.S., (1996b) Unusual 'snow slurry" lahars from Ruapehu volcano, New Zealand, September 1995. Geology 24: pp. 1107-1110.

Cronin, S. J., Neall, V.E. (1997) A late Quaternary stratigraphic framework for the northeastern Ruapehu and eastern Tongariro ring plains, New Zealand. New Zealand Journal of Geology and Geophysics 40(2): pp. 185-197.

Cronin, S.J., Neall, V.E., Lecointre, J.A. and Palmer, A.S., (1997a) Changes in Whangaehu River lahar characteristics during the 1995 eruption sequence, Ruapehu volcano, New Zealand. Journal of Volcanology and Geothermal Research, 76: pp. 47-61.

Cronin, S.J., Hodgson, K.A., Neall, V.E., Palmer, A.S., Lecointre, J.A. (1997b) 1995 Ruapehu lahars in relation to the late Holocene lahars of Whangaehu River, New Zealand. New Zealand Journal of Geology and Geophysics 40: pp. 507–520.

Cronin, S.J., Neall, V.E. and Palmer, A.S., (1997c) Lahar history and lahar hazard of the Tongariro River, northeastern Tongariro Volcanic Centre, New Zealand. NZ Journal of Geology and Geophysics 40: pp. 383-393.

Cronin, S.J., Neall, V.E., Lecointre, J.A. and Palmer, A.S. (1999) Dynamic interactions between lahars and stream flow: a case study from Ruapehu volcano, New Zealand. Geological Society of America Bulletin 111: pp. 28-38.

Cronin, S.J., Lecointre, J.A., Palmer, A.S., Neall, V.E. (2000) Transformation, internal stratification, and depositional processes within a channelised, multi-peaked lahar flow. New Zealand Journal of Geology and Geophysics 43: pp. 117-128.

Cronin, S.J., Bebbington, M., Lai, C.D., (2001) A Probabilistic assessment of eruption recurrence on Taveuni volcano, Fiji. Bulletin of Volcanology 63: pp. 274-289.

Cronin, S.J., Stewart, R.B., Neall, V.E., Platz, T., Gaylord, D. (2003) The AD1040 to present Maero Eruptive Period of Egmont Volcano, Taranaki, New Zealand. Geological Society of New Zealand Miscellaneous Publications 116A:43.

Cronin, S.J., Gaylord, D.R., Charley, D., Wallez, S., Alloway, B., Esau, J. (2004) Participatory methods of incorporating scientific with traditional knowledge for volcanic hazard management on Ambae Island, Vanuatu. Bulletin of Volcanology 66: pp. 652-668.

Dade, W.B. (2007) Tectonic and climatic controls of alluvial-fan size and source-catchment relief. Journal of the Geological Society of London, 164: pp. 353-358.

Dalbey, K., Patra, A. K., Pitman, E. B., Bursik, M. I., Sheridan, M. F. (2008) Input uncertainty propagation methods and hazard mapping of geophysical mass flows, Journal of Geophysical Research, 113, B05203, doi:10.1029/2006JB004471.

Davies, T.R., McSaveney, M.J. (2008) The role of rock fragmentation in the motion of large landslides. Engineering Geology. doi:10.1016/j.enggeo.2008.11.004.

Davies, T.R.H. (1986) Large debris flows: A macro-viscous phenomenon. Acta Mechanica 63: 161-178.

Delaite, G., Thouret, J-C., Sheridan, M., Labazuy, P., Stinton, A., Souriot, T. and Van Westen, C. (2005) Assessment of volcanic hazards of El Misti and in the city of Arequipa, Peru, based on GIS and simulations, with emphasis on lahars, Zeitschrift für Geomorphol N.F., Suppl. vol. 140: 209–231.

Denlinger, R. P. (1987). A model for generation of ash clouds by pyroclastic flows, with application to the 1980 eruptions at Mount St Helens. Journal of Geophysical Research. 92: 10284–98.

Denlinger, R. P., Iverson, R. M. (2001) Flow of variably fluidized granular material across three dimensional terrain 2. Numerical predictions and experimental tests. Journal of Geophysical Research. 106: pp. 553–566.

Donoghue, S. L. (1991) Late Quaternary volcanic stratigraphy of the south-eastern sector of Mount Ruapehu ring plain, New Zealand. Unpublished PhD thesis, lodged in the Library, Massey University, Palmerston North, New Zealand. 336p.

Donoghue, S. L., Neall, V.E., Palmer, A. S., Stewart, R. B. (1997) The volcanic history of Ruapehu during the past 2 millenia based on the record of Tufa Trig tephras. Bulletin of Volcanology 59(2): pp. 136-146.

Donoghue, S. L., Neall, V.E. (2001) Late Quarternary constructional history of the Southeastern Ruapehu ring plain, New Zealand. New Zealand Journal of Geology and Geophysics 44(3): pp. 439-466.

Doyle, E.E., Cronin, S.J., Cole, S.E., Thouret, J-C., in review: Wave changes, sediment concentration and lahar evolution at Semeru, Indonesia. Submitted to Geophysical Research Letters.

Doyle E.E., Huppert H.E., Lube G., Mader H.M., Sparks R.S.J. (2007). Static and flowing regions in granular collapses down channels: Insights from a sedimenting shallow water model. Physics of Fluids, 19, 1.

Drake, T.G., (1990) Structural features in granular flows. Journal of Geophysical Research. 95 (B6): pp. 8681– 8696.

Druce, A.P. (1966) Tree-ring dating of recent volcanic ash and lapilli, Mt. Egmont. New Zealand Journal of Botany 4: pp. 3-41.

Druitt, T. H. (1998). The eruption, transport and sedimentation of pyroclastic flows. In: Gilbert, J. & Sparks, R.S.J. (Ed.), The Physics of Volcanic Eruptions, Geological Society of London Special Publication, 145: 147–200.

Dufresne, A., Davies, T.R. (2009) Longitudinal ridges in mass movement deposits, Geomorphology 105: pp. 171–181

Emmanuel, J.M.C., Ofelia, O.T. (2006) Predicting Lahar-Inundation Zones: Case Study in West Mount Pinatubo, Philippines. Natural Hazards 37: pp. 331–372, DOI 10.1007/s11069-005-6141-y.

Esposti Ongaro, T., Neri, A., Todesco, M., Macedonio, G. (2002) Pyroclastic flow hazard assessment at Vesuvius (Italy) by using numerical modeling. II. Analysis of flow variables, Bulletin Volcanology, 64: pp. 178–191, doi:10.1007/s00445-0010190-1.

ESRI, ArcGIS 9.2, Software [DVD-ROM]. (2007) Redlands, CA: Environmental Systems Research Institute.

Ewart, A., Brothers, R.N., Mateen, A. (1977) An outline if the geology and geochemistry, and the possible petrogenetic evolution of the volcanic rocks of the Tonga-Kermadec-New Zealand island arc. Journal of Volcanology and Geothermal Research 2: pp. 205-250.

Fagents SA, Baloga SM (2005) Calculation of lahar transit times using digital elevation data. Journal of Volcanology Geothermal Research, 139: pp. 135–146

Fisher, R.V., Schmincke, H.U., (1984) Pyroclastic Rocks. Springer, Berlin, pp472.

Folk, R.L., and Ward, W.C., (1957) Brazos River Bar: A study in the significance of grain size parameters: Journal of Sedimentary Petrology, v. 27, no. 1, p. 3-26.

Fread, D. L., (1987) BREACH: An Erosion Model for Earthen Dam Failures, Hydrologic Research Laboratory, NOAA, NWS, U.S. Department of Commerce, Silver Spring, Maryland, June, 34 pp.

Fread, D.L., (1988) The NWS DAMBRK Model: Theoretical Background/User Documentation. HRL-256, Hydrologic Research Laboratory, National Weather Service, Silver Spring, Maryland, 325 pp.

Gamble, J.A., Smith, I.E.M., McCulloch, M.T., Graham, I.J., Kokelaar, B.P. (1993a) The geochemistry and petrogenesis of basalts from the Taupo Volcanic Zone and Kermadec Island arc, SW Pacific. Journal of Volcanology and Geothermal Research 54: pp. 265-290.

Gamble, J.A., Wright, I.C., Baker, J.A. (1993b) Sea floor geology and petrology in the oceanic to continental transition zone of the Kermadec/Havre/Taupo Volcanic Zone arc system, New Zealand. New Zealand Journal of Geology and Geophysics 36: pp. 417-435.

Gamble, J.A., Price, R.C., Smith, I.E.M., McIntosh, W.C. and Dunbar, N.W. (1998) "40Ar/39 Ar geochemistry of the Whangaehu Gorge and eastern Ruapehu Volcano, Taupo Volcanic Zone, New Zealand". Geological Society of New Zealand, Miscellaneous Publication 101A. p97.

Gamble, J.A., Price, R.C., Smith, I.E.M., McIntosh, W.C., Dunbar, N.W. (2003) 40Ar/39Ar geochronology of magmatic activity, magma flux and hazards at Ruapehu volcano, Taupo Volcanic Zone, New Zealand. Journal of Volcanology and Geothermal Research 120: pp. 271-287.

Gardner, C.A., Scott, K.M., Miller, C.D., Myers, B., Hildreth, W., Pringle, P.T. (1995) Potential Volcanic Hazards from Future Activity of Mount Baker, Washington: U.S. Geological Survey Open-File Report 95-498.

Gaylord, D.R., Neall, V.E., Palmer, A.S. (1993) The Maitahi Formation, A Mid-Pleistocene volcanic debris avalanche assemblage, Taranaki, New Zealand. Abstract in: Volcanic activity and the environment, abstracts of the IAVCEI, Puerto Vallarta, Mexico 1997 General Assembly. Gobierno de Jalisco, Unidad Editorial, Guadalajara, Mexico.

Gillon, M., Fell, R., Keys, H.J.R., Foster, M. (2006) A contribution to public safety studies – failure modes and likelihood analysis for a tephra dam on an active volcano. Bulletin of ANCOLD (Australian National Committee on Large Dams), 134: pp. 11–22.

Glicken, H. (1991) Sedimentary architecture of large volcanic debris avalanches. In: Fisher RV, Smith GA (Eds.) Sedimentation in Volcanic Settings, SEPM Special Publication 45: 99-106.

Glicken, H. (1996) Rockslide-debris avalanche of May 18, 1980, Mount St. Helens volcano, Washington, US Geological Survey, Open File Report 96-677, 90 p.

Grant-Taylor, T. L. (1964) Geology of Egmont National Park. In: Scanlan, A. B. ed. Egmont National Park. New Plymouth, Egmont National Park Board. 13-26.

Grindley, G. W. (1960) Sheet 8—Taupo. Geological map of New Zealand. 1:250 000.

Wellington, New Zealand. Department of Scientific and Industrial Research.

Hackett, W. R. (1985) Geology and petrology of Ruapehu volcano and related vents. Unpublished PhD Thesis. Geology Department. Wellington, Victoria University of Wellington.

Hackett, W. R. and B. F. Houghton (1987) A facies model for an active composite volcano: Ruapehu, New Zealand. Pacific Rim congress 87. Proc. international congress, 1987, Gold Coast, Queensland. Parkville, Australasian Institute of Mining & Metallurgy: pp. 141-144.

Hackett, W. R., Houghton B.F. (1989) A facies model for a Quaternary andesitic composite volcano: Ruapehu, New Zealand. Bulletin of Volcanology 51(1): pp. 51-68.

Hadley, K.C. and LaHusen, R.G. (1995) Technical manual for an experimental acoustic flow monitor: U.S. Geological Survey Open-File Report 95-114, 26 p.

Hancox, G.T. (1999) Debris avalanche and debris flow lahar in Oaonui Stream on Mt Egmont, 16 September 1998. 18p. Sr99/6, Institute of Geological and Nuclear Science, NZ.

Hancox, G.T., Nairn, I.A., Otway, P.M., Webby G., Perrin, N.D., and Keys, J.R. (1997) Stability assessment of Mt Ruapehu crater rim following 1995-1996 eruptions. Client Report 43605B Institute of Geological and Nuclear Sciences Limited.

Hancox, G.T., Otway, P.M., Webby G. (1998) Possible effects of a lahar caused by future collapse of the tephra barrier formed at the Mt Ruapehu Crater Lake outlet by the 1995-96 eruptions. Client Report 43711B Institute of Geological and Nuclear Sciences Limited.

Hancox, G.T., Keys, H.J.R., Webby, M.G. (2001) Assessment and mitigation of dam-break lahar hazards from Mr Ruapehu Crater Lake following the 1995–96 eruptions. In Proceedings of the New Zealand Geotechnical Society Symposium – Engineering and Development in Hazardous Terrain, Christchurch 2001. Wellington, New Zealand. NZ Geotechnical Society, Institution of Professional Engineers New Zealand, pp. 385–409.

Harvey, A.M. (1996) The role of alluvial fans in the mountain fluvial systems of southeast Spain: implications of climatic change. Earth Surface Processes & Landforms, 21: pp. 543-553.

Hatherton, T. (1969) The geophysical significance of calc-alkaline andesites in New Zealand. New Zealand Journal of Geology and Geophysics 12: pp. 436-459.

Hayashi, J.N., Self, S., (1992) A comparison of pyroclastic flow and debris avalanche

mobility. Journal of Geophysical Research. 97: pp. 9063– 9071.

Haynes, K., Barclay, J. and Pidgeon, N. (2007) Volcanic hazard communication using maps: an evaluation of their effectiveness. Bulletin of Volcanology 70(2): 123-138.

Healy, J. (1954) Origin of flood and Ruapehu Lahars in. Submission on Tangiwai Railway Disaster, Report of Board in Inquiry, pp. 6-8, Tangiwai Railway Disaster 31 Wellington: Government Printer.

Heim, A., (1932) Der Bergstruz von Elm. Geol. Gesell. Zeitschr. 34: pp. 74– 115.

Hluchy, L., Tran, V.D., Astalos, J., Dobrucky, M., Nguyen, G.T., Froehlich, D. (2002) Parallel Flood Modelling Systems. In: Proc. of the 2002 International Conference on Computational Science, Amsterdam, The Netherlands, April 21-24, LNCS 2329, Springer-Verlag: pp. 543-551.

Hobden, B.J., Houghton, B.F., Lanphere, M.A., Nairn, I.A. (1996) Growth of the Tongariro volcanic complex: new evidence from K–Ar age determinations (Note). New Zealand Journal of Geology and Geophysics 39: pp. 151-154.

Hoblitt, R.P., Walder, J.S., Driedger, C.L., Scott, K.M., Pringle, P.T., Vallance, J.W. (1995) Volcano hazards from Mount Rainier, Washington, USGS Open-File Report 95-273: pp. 4–6.

Hoblitt, R.P., Walder, J.S., Driedger, C.L., Scott, K.M., Pringle, P.T., Vallance, J.W. (1998) Volcano Hazards from Mount Rainier, Washington, Revised 1998: U.S. Geo. Surv. Open-File Report, 98-428.

Hochstein, M.P. (1995) Crustal heat transfer in the Taupo Volcanic Zone (New Zealand): comparison with other volcanic arcs and explanatory heat source models. Journal of Volcanology and Geothermal Research 68: pp. 117-151.

Hodgson, K.A. (1993) Late Quaternary lahars from Mount Ruapehu in the Whangaehu River valley, North Island, New Zealand. Unpublished PhD thesis, Massey University, Palmerston North, New Zealand. Vol. 1. 256 p.

Hodgson, K.A., Manville, V.R. (1999) Sedimentology and flow behavior of a rain-triggered lahar, Mangatoetoenui Stream, Ruapehu volcano, New Zealand. Geological Society of America Bulletin, 111(5): pp. 743–754.

Hodgson, K.A., Lecointre, J.A., Neall, V.E. (2007). Onetapu Formation: the last 2000 yr of laharic activity at Ruapehu volcano, New Zealand. New Zealand Journal of Geology and G ophysics, Vol. 50: pp. 81-99

Hopkins, M.A. (1987) Particle simulation: Vol 1, Rep. No. 87-7, Dep of Civil and

Environmental Engineering, Clarkson Univ., Postdam, N.Y.

Houghton, B.F., Latter, J.H., Hackett, W.R. (1987) Volcanic hazard assessment for Ruapehu composite volcano, Taupo Volcanic Zone, New Zealand. Bulletin of Volcanology, 49(6): pp. 737–751.

Houghton, B.J., Nairn, I.A. (1991) The 1976-1982 Strombolian and phreatomagmatic eruptions of White Island, New Zealand: eruptive and depositional mechanisms at a 'wet' volcano. Bulletin of Volcanology 54: pp. 25-49.

Hull, A.G., Dellow, G. (1993) Earthquake hazards in the Taranaki region. Institute of Geological and Nuclear Sciences Client Report 1993/03, Institute of Geological and Nuclear Sciences Ltd, Lower Hutt.

Hungr, O., Morgan, G.C., Kellerhalls, R. (1984) Quantitative analysis of debris torrent hazards for design of remedial measures. Canadian Geotechnical Journal. 21: pp. 663-677.

Hungr, O. (1995) A model for the runout analysis of rapid flow slides, Canadian Geotechnical Journal. 32: pp. 610–623.

Hurst, A. W. (1994) ASHFALL—a computer program for estimating volcanic ash fallout. Report and users guide. Institute of Geological & Nuclear Sciences Science Report 94/23. 22.

Hurst, A.W., Smith, W. A. (2004) Monte Carlo methodology for modelling ashfall hazards, Journal of Volcanology and Geothermal Research 138 (3–4): pp. 393–403.

Hyde, J. H., Crandell, D.R., (1978) Postglacial Volcanic Deposits at Mount Baker, Washington, and Potential Hazards from Future Eruptions. 17 pp. (U.S. Geological Survey Professional Paper, 1022-C.

Itoh, H., J. Takahama, M. Takahashi and K. Miyamoto (2000) Hazard estimation of the possible pyroclastic flow disasters using numerical simulation related to the 1994 activity at Merapi. Journal of Volcanology and Geothermal Research 100(1-4): pp. 503-516.

Iverson, R.M. (1997a) The physics of debris flows. Reviews of Geophysics 35: pp. 245-296.

Iverson, R.M. (1997b) Hydraulic modelling of unsteady debris-flow surges with solid-fluid interactions. In: Chen CL (Ed.) Debris-flow Hazards Mitigation: Mechanics, Prediction, and Assessment. American Society of Civil Engineers, pp. 550-560.

Iverson, R. (2005) Debris-flow Mechanics. In: Jakob M, Hungr O (eds), Debris-Flow

Hazards and Related Phenomena Praxis-Springer, Heidelberg: pp. 105-134.

Iverson, R.M., Denlinger, R.P. (1987) The physics of debris flows - A conceptual assessment. In: Beschta RL, Blinn, T., Grant, G.E., Ice, G.G., Swanson, F.J. (Eds.) Erosion and Sedimentation in the Pacific Rim. International Association of Hydrological Sciences Publication 165: pp. 155-165.

Iverson, R. M., Reid, M.E., LaHusen, R.G. (1997) Debris-flow mobilization from landslides, Annual Review of Earth and Planetary Sciences. 25: pp. 85–138.

Iverson, R.M., S.P. Schilling, Vallance, J.W. (1998) Objective delineation of lahar-inundation hazard zones, Geological Society of America Bulletin, 110: pp. 972-984.

Iverson, R.M., Denlinger, R.P., (2001) Flow of variably fluidized granular material across three dimensional terrain 1: Coulomb mixture theory. Journal of Geophysical Research Letters 106 (B): pp. 537–552.

Iverson, R.M., Vallance, J.W. (2001) New views of granular mass flows. Geology 29, pp. 115–118.

Jacob, M. (2005) Debris-flow Hazards Analysis. In: Jakob M, Hungr O (eds), Debris-Flow Hazards and Related Phenomena Praxis-Springer, Heidelberg: pp. 411-443.

Janda, R.J., Daag, A.S., Delos Reyes, P.J., Newhall, C.G., Pierson, T.C., Punongbayan, R.S., Rodolfo, K.S., Solidum, R.U., Umbal, J.V. (1997) Assessment and response to lahar hazard around Mount Pinatubo, 1991 to 1993. In: Newhall, C.G., Punongbayan, R.S., (Eds.), Fire and Mud: Eruptions and Lahars of Mt. Pinatubo, Philippines. University of Washington Press, pp. 107–139

Johnson, A.M., Rodine, J.R. (1984) Debris flow. In: Brunsden D, Prior DB (Eds.) Slope Instability. Wiley, New York, pp. 257-361.

Julien, P.Y., O'Brien, J.S., (1997) Selected notes on debris flow dynamics. In: Armanini, A., Michiue, M. (Eds.), Recent Developments in Debris Flows. Springer, Berlin, pp. 144–162.

Kamp, P.J.J., Vonk, A.J., Bland, K.J., Hansen, R.J., Hendy, A.J.W., McIntyre, A.P., Ngatai, M., Cartwright, S.J., Hayton, S., Nelson, C.S. (2004) Neogene stratigraphic architecture and tectonic evolution of Wanganui, King Country and eastern Taranaki Basins, New Zealand. New Zealand Journal of Geology and Geophysics 47: pp. 625-644.

Karatson, D., Nemeth, K. (2001) Lithofacies associations of an emerging volcaniclastic apron in a Miocene volcanic complex: an example from the Borzsony Mountains, Hungary: International Journal of Earth Science. (Geologische Rundschau.) v. 90: pp.

776–794

Kelfoun, K., Druitt , T.H. (2005) Numerical modeling of the emplacement of Socompa rock avalanche, Chile. Journal of Geophysical Research, 110, B12202, doi:10.1029/2005JB003758.

Keys, H.J.R. (2007) Lahars of Ruapehu Volcano, New Zealand: risk mitigation. Annals of Glaciology, Volume 45, Number 1: pp. 155-162(8)

Keys, H.J.R., Green, P.M. (2008) Ruapehu Lahar New Zealand 18 March 2007: Lessons for Hazard Assessment and Risk Mitigation 1995-2007. Journal of Disaster Research 4: pp. 284-296.

King, P.R. (1991) Physiographic maps of the Taranaki Basin - Late Cretaceous to Recent. New Zealand Geological Survey report, G155.

King, P.R., Thrasher, G.P. (1996) Cretaceous–Cenozoic geology and petroleum systems of the Taranaki Basin, New Zealand. I Institute of Geological and Nuclear Sciences Monograph 13, Institute of Geological and Nuclear Sciences Ltd, Lower Hutt, 243 p.

Komorowski, J.C., Glicken, H., Sheridan, M.F. (1991) Secondary electron imagery of microcracks and hackly fractures in sand-size clasts from the 1980 Mount St. Helens debris-avalanche deposits, implications for particle-particle interactions. Geology 19: pp. 261–264

Kover, T.P. (1995) Applications of a digital terrain model for the modeling of volcanic flows: a tool for volcanic hazard determination. Master Thesis, SUNY, Buffalo, 62 pp.

KWL Ltd. (2003) Debris Flow Study and Risk Mitigation Alternatives for Percy Creek and Vapour Creek. (Final Report, December). District of North Vancouver.

Lavigne F., Thouret J.C., Voight B., Suwa H., Sumaryono, A. (2000) Lahars at Merapi volcano, Central Java: an overview. Journal of Volcanology and Geothermal Research 100: pp. 423-456.

Lavigne, F., Suva, H. (2004) Contrasts between debris flows, hyperconcentrated flows and stream flows at a channel of Mount Semeru, East Java, Indonesia. Geomorphology 61: pp. 41-58.

Lecointre, J. A., Neall, V.E., Palmer, A. S. (1998) Quaternary lahar stratigraphy of the western Ruapehu ring plain, New Zealand. New Zealand Journal of Geology and Geophysics 41(3): pp. 225-245.

Lees, C.M. and Neall, V.E. (1993) Vegetation response to volcanic eruptions on

Egmont volcano, New Zealand, during the last 1500 years. Journal of the Royal Society of New Zealand 23: pp. 91–127.

Lowe, D.R. (1979) Sediment gravity flows - Their classification and some problems of application to natural flows and deposits. In: Doyle LJ, Pilkey OH Jr (Eds.) Geology of continental slopes. Society of Economic Paleontologists and Mineralogists Special Publication 27: pp. 75-82.

Lube, G., Cronin, S.J., Platz, T., Freundt, W., Procter, J.N., Henderson, C.J., Sheridan, M.J. (2007) Flow and deposition of pyroclastic granular flows: a type example from the 1975 Ngauruhoe eruption, New Zealand. Journal of Volcanology and Geothermal Research, 161: pp. 165-186.

Lube, G., Cronin, S.J., Procter, J.N., (2009) Explaining the extreme mobility of volcanic ice slurry flows, Ruapehu Volcano, New Zealand. Geology 37: pp. 15-18. doi:10.1130/G25352A.1

Macías, J. L., Capra, L., Arce, J. L., Espíndola J. M., García-Palomo, A. (2008) Hazard map of El Chichón Volcano, Chiapas, México, in Taran, Y. A., J. L. Macías and J. M. Espíndola, editors: Special Issue on El Chichón Volcano, Journal of Volcanology and Geothermal Research, 175: pp. 444-458.

Magill, C., Blong, R. (2005) Volcanic risk ranking for Auckland, New Zealand. I: Methodology and hazard investigation. Bulletin of Volcanology 67: pp. 331-339.

Magill, C.R., McAneney K.J, Smith, I.E.M. (2005) Probabilistic assessment of vent locations for the next Auckland Volcanic Field event, Mathematical Geology 37 (3): pp. 227–242.

Magill, C.R., Hurst, A.W., Hunter, L.J., Blong, R.J. (2006) Probabilistic tephra fall simulation for the Auckland Region, New Zealand, Journal of Volcanology and Geothermal Research 153: pp. 370–386.

Major, J.J. (1993) Rheometry of natural sediment slurries. In: Proceedings of ASCE National Conference on Hydraulic Engineering 1993, San Francisco. American Society of Civil Engineers, New York. 7 pp.

Major, J.J. (1996) Experimental studies of deposition by debris flows: Process, characteristics of deposits and effects of pore-fluid pressure, Unpublished PhD Thesis, University of Washington, Seattle, 341 pp.

Major, J.J. (1997) Depositional processes in large-scale debris-flow experiments. Journal of Geology 105: pp. 345-366

Major, J.J. (2003) Post-eruption hydrology and sediment transport in volcanic river

systems. In: Water Resources IMPACT, 5, no. 3: pp. 10-15.

Major, J.J. (2004) Posteruption suspended sediment transport at Mount St. Helens: Decadal-scale relationships with landscape adjustments and river discharges. Journal of Geophysical Research, 109, F01002.

Major, J.J., Voight, B. (1986) Sedimentology and clast orientations of the 18 May 1980 southwest-flank lahars, Mount St. Helens, Washington. Journal of Sedimentary Petrology 56: pp. 691-705.

Major, J.J., Pierson, T.C. (1990) Rheological analysis of fine-grained natural debris-flow material. In: French RH (Ed.) Hydraulics/Hydrology of Arid Land (H2AL). ASCE, New York, pp. 225-231.

Major, J.J., Pierson, T.C. (1992) Debris flow rheology: Experimental analysis of fine-grained slurries. Water Resources Research 28: pp. 841-857.

Major, J.J., Iverson, R.M. (1999) Debris-flow deposition - Effects of pore-fluid pressure and friction concentrated at flow margins. Bulletin of the Geological Society of America 111: pp. 1424-1434.

Major, J.J., Pierson, T.C., Scott, K.M. (2005) Debris flows at Mount St. Helens, Washington, USA. In: Jakob M and Hungr O (Eds.) Debris-flow hazards and related phenomena. Springer Berlin Heidelberg, p. 685-731.

Malin, M.C. and Sheridan, M.F. (1982) Computer assisted mapping of pyroclastic surges. Science 217: pp. 637–640.

Manville, V. (2004) Palaeohydraulic analysis of the 1953 Tangiwai lahar New Zealand's worst volcanic disaster. Acta Vulcanologica, XVI: pp. 137–152.

Manville, V. and Cronin, S.J., and members of the Crater Lake Research Team, (2007) Breakout lahar from New Zealand's Crater Lake, EOS, Transactions (AGU) 88(43): pp. 441-442.

Manville, V., Wilson, C.J.N. (2004) The 26.5 ka Oruanui eruption, New Zealand: a review of the roles of volcanism and climate in the post-eruptive sedimentary response. New Zealand Journal of Geology and Geophysical Research, 47: pp. 525-547.

Manville, V., Cronin, S.J., (2007) Breakout lahar from New Zealand's Crater Lake, EOS, Transactions (AGU) 88(43): pp. 441-442.

McCuen, R.H. (1998) Hydrologic Design and Analysis; Prentice Hall, New Jersey, 814 p.

Meyer, G.A., Wells, S.G., Balling, R.C. and Jull, A.J.T. (1992) Response of alluvial systems to fire and climate change in Yellowstone National Park. Nature, 357: pp. 147-150.

Miller, C. D. (1980) Potential Hazards from Future Eruptions in the Vicinity of Mount Shasta Volcano, Northern California. 43 pp. U.S. Geological Survey Bulletin, 1503.

Miyabuchi, Y., (1999) Deposits associated with the 1990–1995 eruption of Unzen volcano, Japan. Journal of Volcanology and Geothermal Research 89: pp. 139–158.

Mizuyama, T., S. Kobashi, Ou G. (1992) Prediction of debris flow peak discharge, Interpraevent 1992, Bern, vol. 4: pp. 99–108.

Mullineaux, D. R., Peterson, D. W. (1974) Volcanic Hazards on the island of Hawaii. 61 pp. (U.S. Geological Survey Open-file Report 74-239.

Nairn, I. A., Kobayashi, T., Nakagawa, M. (1998) The ≈10 ka multiple vent pyroclastic eruption sequence at Tongariro Volcanic Centre, Taupo Volcanic Zone, New Zealand: Part 1. Eruptive processes during regional extension. Journal of Volcanology and Geothermal Research 86(1-4): pp. 19 44.

Nairn, I.A., Wood, C.P., Hewson, C.A.Y. (1979) Phreatic eruptions of Ruapehu, April 1975. New Zealand Journal of Geology and Geophysics 22: pp. 155-173.

Nakada, S., Fujii, T. (1993) Preliminary report on the activity at Unzen Volcano (Japan), November 1990-November 1991: Dacite lava domes and pyroclastic flows. Journal of Volcanology and Geothermal Research 54, 3-4: pp. 319-333

Nakagawa, M., Nairn, I.A., Kobayashi, T. (1998) The ≈10 ka multiple vent pyroclastic eruption sequence at Tongariro Volcanic Centre, Taupo Volcanic Zone, New Zealand: Part 2. Petrological insights into magma storage. Journal of Volcanology and Geothermal Research 86(1-4): pp. 45-65.

Nakamura, K. (1977) Volcanoes as possible indicators of tectonic stress orientation - principle and proposal. Journal of Volcanology and Geothermal Research 2: pp. 1-16.

Neall, V.E. (1971) Volcanic domes and lineations in Egmont National Park. New Zealand Journal of Geology and Geophysics 14: pp. 71-81.

Neall, V.E. (1972) Tephrochronology and tephrostratigraphy of western Taranaki, New Zealand. NZ J. Geol. Geophys. 15: pp. 507-557.

Neall, V.E. (1973) Some aspects of western Taranaki geology and pedology. Unpublished PhD thesis. Victoria University of Wellington, Wellington, New Zealand.

Neall, V.E. (1976a) Lahars as major geological hazards. Bulletin of the International Association of Engineering Geology 14: pp. 233-240.

Neall, V.E. (1976b) Lahars - Global occurrence and annotated bibliography. Victoria University Wellington, New Zealand, Publication 5, 18 p.

Neall, V.E. (1976c) Genesis and weathering of Andosols in Taranaki, New Zealand. Soil Science 123: pp. 400-408.

Neall, V.E. (1979) Sheets P19, P20 and P2l New Plymouth, Egmont and Manaia, Geological Map of New Zealand 1:50,000. 3 maps and notes, 36 p. New Zealand Department of Science and Industrial Research, Wellington.

Neall, V.E. (2003) The volcanic history of Taranaki. Institute of Natural Resources - Massey University, Soil & Earth Sciences Occasional Publication No. 2.

Neall, V.E., Alloway B.E. (1996) Volcanic Hazard Map of Western Taranaki. Massey Uni. Dep. Soil Sci. Occ. Report 12.

Neall V.E., Alloway B.E. (2004) Quaternary Geological Map of Taranaki. INR, Massey Uni. Dep. Soil Sci. Occ. Pub No.4.

Neall, V.E., Cronin, S.J., Donoghue, S.L., Hodgson, K.A., Lecointre, J.A., Palmer, A.S., Purves, A.M., Stewart, R.B. (2001) Lahar Hazards Map for Ruapehu Volcano. Institute of Natural Resources – Massey University, Soil and Earth Sciences Occasional Publication No. 1.

Neall, V.E., Houghton B.F., Cronin, S.J., Donoghue, S.L., Hodgson, K.A., Johnston, D.M., Lecointre, J.A., Mitchell, A.R., 1999: Volcanic hazards at Ruapehu volcano. Volcanic hazard information series 8. Ministry of Civil Defence, Wellington, Volcanic hazards information series, No. 8.

Neall, V.E., Stewart, R.B., Smith, I.E.M. (1986) History and petrology of the Taranaki volcanoes: Royal Society of New Zealand Bulletin 23: pp. 251-263.

Neri, A., Dobran, F. (1994). Influence of eruption parameters on the thermofluid dynamics of collapsing volcanic columns. Journal of Geophysical Research, 99: pp. 11833–11857.

Newhall, C.G. (1982) A Method for Estimating Intermediate- and Long-term Risks from Volcanic Activity, with an Example from Mount St Helens, Washington. U.S. Geological Survey Open File Report, 59: pp. 82-396.

Norris, R.J., Cooper, A.F. (2000) Late Quaternary slip rates and slip partitioning on the

Alpine Fault, New Zealand. Journal of Structural Geology 23: pp. 507-520.

O'Brien, J.S., Julien, P.Y. (1988) Laboratory analysis of mudflows properties. Journal of Hydraulic Engineering 14: pp. 877-887.

O'Brien, J.S., Julien, P.Y., Fullerton, W.T. (1993) Two-dimensional Water Flood and Mudflow Simulation, J. Hyd. Eng., ASCE, 119(2): pp. 244–261.

O'Shea, B.E. (1954) Ruapehu and the Tangiwai Disaster. New Zealand Journal of Science and Technology B36: pp. 174-189.

Oramas Dorta D, Toyos G, Oppenheimer C, Pareschi MT, Sulpizio R, Zanchetta G. (2007) Empirical modelling of the May 1998 small debris flows in Sarno (Italy) using LAHARZ. Natural Hazards 40: pp. 381-396.

Palladino, D.M., Valentine, G.A., (1995) Coarse-tail vertical and lateral grading in pyroclastic flow deposits of the Latera Volcanic Complex (Vulsini, Central Italy): origin and implications for flow dynamics. Journal of Volcanology and Geothermal Research 69: pp. 343– 364.

Palmer, B.A., Alloway, B.V., Neall, V.E. (1991) Volcanic debris-avalanche deposits in New-Zealand: lithofacies organisation in unconfined, wet-avalanche flows, in Fisher R.V. and Smith G.A. (Eds.) Sedimentation in Volcanic Settings, SEPM Special Publication, n°45, pp. 89-98.

Palmer, B.A., Neall, V.E. (1991) Contrasting lithofacies architecture in ring plain deposits related to edifice construction and destruction, the Quaternary Stratford and Opunake Formations, Egmont Volcano, New Zealand. Sedimentary Geology 74: pp. 71-88.

Pareschi, M.T., Cavarra, L., Favalli, M., Giannini, F., Meriggi, A. (2000) GIS and volcanic risk management. Natural Hazards 21: pp. 361–379

Parfitt, R., Pollok, J.A., Furkert, R.J. (Eds) (1981) Guide Book for Tour 1, Pre-Conference North Island. Soils with Variable Charge Conference, Palmerston North New Zealand. PD Hasselberg, Government Printer, Wellington, New Zealand, 153 p.

Parra, E. & Cepeda, H. (1990) Volcanic hazard maps of the Nevado del Ruiz Volcano, Colombia. Journal of Volcanology and Geothermal Research 42: pp. 117-127.

Patra A.K., Bauer A.C., Nichita C.C., Pitman E.B., Sheridan M.F., Bursik M., Rupp B., Webber A., Stinton A.J., Namikawa L.M., Renschler C.S., (2005) Parallel adaptive numerical simulation of dry avalanches overnatural terrain. Journal of Volcanology and Geothermal Research 139, Issues 1-2: pp. 89-102.

Pender, G., Neelz, S. (2007) Use of computer models of flood inundation to facilitate communication in flood risk management. Environmental Hazards, 7(2): pp. 106-114.

Pierson, T.C. (1980) Erosion and deposition by debris flows at Mount Thomas, North Canterbury, New Zealand. Earth Surface Processes 5: pp. 227-247.

Pierson, T.C. (1985) Initiation and flow behavior of the 1980 Pine Creek and Muddy River lahars, Mount St. Helens, Washington. Geological Society of Americal Bulletin, 96, No. 8: pp. 1056–1069

Pierson, T.C. (1997) Transformation of Water Flood to Debris Flow following the Eruption-Triggered Transient-Lake Breakout from the Crater on March 19, 1982. IN: Pierson, T.C., (Eds.) 1997. Hydrologic Consequences of Hot-Rock/Snowpack Interactions at Mount St. Helens Volcano, Washington, 1982-1984: USGS Open-File Report 96-17.

Pierson, T.C. (1998) An empirical method for estimating travel times for wet volcanic mass flows. Bulletin of Volcanology 60: pp. 98-109.

Pierson, T.C. (2002) Evaluation of lahar mitigation proposals at Mt. Ruapehu: New Zealand Dept. of Conservation, DOC Science Internal Series 63, 18 p.

Pierson, T.C. (2005a) Distinguishing between Debris Flows and Floods from Field Evidence in Small Watersheds. U.S. Geological Survey Fact Sheet 2004-3142.

Pierson, T.C. (2005b) Hyperconcentrated flow - transitional process between water flow and debris flow. In: Jakob M, Hungr O (Eds.) Debris-flow Hazards and Related Phenomena, Springer, Heidelberg, pp. 159-202.

Pierson, T. C. (1986) Flow behavior in channelized debris flows, Mount St. Helens,Washington, In: Abrahams, A. D., (Eds.) Hillslope processes: Boston, Allen and Unwin, p. 269–296.

Pierson, T. C., Costa, J.E. (1987) A rheologic classification of subaerial sediment-water flows, in Debris Flows/Avalanches: Process, Recognition, and Mitigation, Reviews in Engineering Geology, vol. 7, (Eds.) J. E. Costa and G. F. Wieczorek, pp. 1–12, Geological Society of America, Boulder, Colorado.

Pierson, T. C., Scott, K.M. (1985) Downstream dilution of a lahar: Transition from debris flow to hyperconcentrated streamflow, Water Resour. Res., 21, pp. 1511–1524.

Pierson, T.C., Janda, R.J., Thouret, J.C., Borrero, C.A. (1990) Perturbation and melting of snow and ice by the 13 November 1985 eruption of Nevado del Ruiz,

Colombia and consequent mobilization, flow and deposition of lahars. J. Volcanol. Geotherm. Res. 41 1–4: pp. 17–66.

Pierson, T.C., Daag, A.S., Delos Reyes, P.J., Regalado, M.T.M., Solidum, R.U., Tubianosa, B.S., (1996) Flow and deposition of posteruption hot lahars on the east side of Mount Pinatubo, July –October 1991. In: Newhall, C.G., Punongbayan, R.S. (Eds.), Fire and Mud, Eruptions and Lahars of Mount Pinatubo, Philippines. PHIVOLCS Press, Quezon City, and University of Washington Press, Seattle, pp. 921–950.

Pillans, B.J. (1983) Upper Quaternary marine terrace chronology and deformation South Taranaki, New Zealand. Geology 11: pp. 292-297.

Pitman, E.B., Le L. (2005) A two-fluid model for avalanche and debris flows. Philosophical Transactions of the Royal Society of London A 363: pp. 1573–1601

Pitman, E.B., Nichita, C. C., Patra A., Bauer, A., Sheridan, M.F., and Bursik, M.I., (2003) Computing granular avalanches and landslides. Phys. Fluids, 15 (12): pp. 3638-3646

Platz, T. (2007) Aspects of Dome-forming Eruptions from Andesitic Volcanoes through the Maero Eruptive Period (1000 yrs BP to Present) Activity at Mt. Taranaki, New Zealand. Unpublished PhD Thesis, INR, Massey University, New Zealand.

Platz, T., Cronin, S.J., Cashman, K.V., Stewart, R.B., Smith, I.E.M., (2007) Transitions from effusive to explosive phases in andesite eruptions – a case-study from the AD1655 eruption of Mt. Taranaki, New Zealand. Journal of Volcanology and Geothermal Research 161: pp. 15-34.

Price, R.C., McCulloch, M.T., Smith, I.E.M., Stewart, R.B. (1992) Pb-Nb-Sr isotopic compositions and trace element characteristics of young volcanic rocks from Egmont Volcano and comparisons with basalts and andesites from the Taupo Volcanic Zone, New Zealand. Geochimica et Cosmochimica Acta 56: pp. 941-953.

Price, R.C., Stewart, R.B. Woodhead, J.D., Smith, I.E. (1999) Petrogenesis of High-K Arc Magmas: Evidence from Egmont Volcano, North Island, New Zealand. Journal of Petrology 40: pp. 167-197.

Price, R.C., Gamble, J.A., Smith, I.E.M., Stewart, R.B., Eggins, S., Wright, I.C. (2005) An integrated model for the temporal evolution of andesites and rhyolites and crustal development in New Zealand's North Island. Journal of Volcanology and Geothermal Research 140: pp. 1-24.

Procter, J., Cronin, S., Sheridan, M., Patra, A. (2004) Application of titan2D mass-flow modelling to assessing hazards from a potential lake-breakout lahar at Ruapehu volcano, New Zealand. Abstract S11a_pth_031 in proceedings IAVCEI General Assembly, Pucon, Chile.

Procter, J., Cronin, S.J., Patra, A., Dalbey, K., Sheridan M., Neall. V.E. (in review) Mapping block-and-ash flow (BAFs) hazards based on Titan 2D simulations; a case study from Mt Taranaki, NZ. (Submitted to Natural Hazards 2008).

Procter, J.N., Cronin, S.J., Fuller, I.C., Lube, G., Manville, V., (in press) Quantifying the Geomorphic Impacts of a lake-breakout flood, Mt. Ruapehu, New Zealand. Geology.

Procter, J.N., Cronin, S.J., Zernack, A.V. (2009). Landscape and Sedimentary Response to Catastrophic Debris Avalanches, Western Taranaki, New Zealand. In: K. Nemeth, V. Manville, and K. Kano (Eds.) Source to sink: from volcanic eruptions to volcaniclastic deposits, Sedimentary Geology Special Volume. doi:10.1016/j.sedgeo.2009.04.027

Pudasaini, S. P., Hutter, K. (2003) Rapid shear flows of dry granular masses down curved and twisted channels. J. Fluid Mech. 495: pp. 193–208.

Purves, A.M. (1990). Landscape ecology of the Rangipo Desert. Unpublished M.Sc. thesis, lodged in the Library, Massey University, Palmerston North, New Zealand.

Renschler, C.S. (2005) Scales and uncertainties in using models and GIS for volcano hazard prediction. Journal of Volcanology and Geothermal Research 139: pp. 73–87.

Rickenmann, D. (1994) An alternative equation for the mean velocity in gravel-bed rivers and mountain torrents, Proc. 1994 Nat. Conf. on Hydraulic Engineering, Buffalo N.Y., U.S.A., ASCE, Vol. 1: pp. 672–676.

Rickenmann, D. (1995) Beurteilung von Murgängen [Assessment of debris flows], Schweizer Ingenieur und Architekt (48): pp. 1104–1108 (in German).

Rickenmann, D. (1999) Empirical relationships for debris flows. Natural Hazards, 19: pp. 47-77.

Rodolfo, K.S. (1989) Origin and early evolution of lahar channel at Mabinit, Mayon volcano, Philippines. Bulletin of the Geological Society of America 101: pp. 414-426.

Rodolfo, K.S., Arguden, A.T. (1991) Rain-lahar generation and sediment-delivery systems at Mayon volcano, Philippines, in Smith G.A. and Fisher R.V. (eds.) Sedimentation in Volcanic Settings, SEPM Special Publication n°45, pp. 71-87

Rupp, B., Bursik, M., Patra, A., Pitman, B., Bauer, A., Nichita, C., Saucedo, R., Macias, J. (2003) Simulation of Pyroclastic Flows of Colima Volcano, Mexico, Using the TITAN2D Program, AGU/EGS/EUG Spg. Meet., Geophysical Research Abstracts, 5, 12857.

Rupp, B., Bursik, M., Namikawa, L., Webb, A., Patra, A.K., Saucedo, R., Marcias, J.L. and Renschler, C., (2006) Computational modelling of the 1991 block-and-ash flows at Colima Volcano, Mexico. In: Seibe, C., Marcias, J.L. and Aguirre-Diaz, G.J. (Eds.) Neogene-Quaternary Continental Margin Volcanism: A Perspective from Mexico. Geological Society of America Special Paper, 402: pp. 237-250.

Saucedo, R., Macı´as, J.L., Bursik, M.I., (2004) Pyroclastic flow deposits of the 1991 eruption of Volca´n de Colima, Mexico. Bulletin of Volcanology 66: pp. 291– 306.

Saucedo, R., Macias, J.L., Sheridan, M.F., Bursik, M.I., Komorowski, J.C. (2005) Modeling of pyroclastic flows of Colima Volcano, Mexico: implications for hazard assessment. . Journal of Volcanology and Geothermal Research 117: pp. 129–153.

Savage, S.B. (1987) Interparticle percolation and segregation in granular materials: a review. In: Selvadurai, A.P.S. (Ed.), Developments in Engineering Mechanics. Elsevier, New York, pp. 347– 363.

Savage, S.B. Hutter, K. (1989) The motion of a finite mass of granular material down a rough incline. Journal of Fluid Mechanics 199: pp. 177-215.

Savage, S. B., Hutter, K. (1991) The dynamics of avalanches of granular materials from initiation to runout, I, Analysis, Acta Mech., 86: pp. 201–223.

Schilling, S.P. (1996) Digital data set of volcano hazards for active Cascade Volcanoes, Washington: U.S. Geological Survey Open-File Report 96-178.

Schilling, S.P. (1998) LAHARZ: GIS Programs for Automated Mapping of Lahar-inundation Hazard Zones. US Geo. Surv. Open-File Report 98-63.

Schmincke, H.U., Park, C., Harms E. (1999) Evolution and environmental impacts of the eruption of Laacher See Volcano (Germany) 12,900 a BP. Quaternary International 61, 1: pp. 61-72.

Schneider, J.L., Fisher, R.V., (1998) Transport and mechanisms of large volcanic debris avalanche: evidence from northwest sector of Cantal volcano (France). Journal of Volcanology and Geothermal Research. 83: pp. 141–165.

Schuster, R.L., Crandell, D.R. (1984) Catastrophic debris avalanches from volcanoes. Proceedings IV Symposium on landslides, Toronto 1: pp. 567-572.

Schwarzkopf, L.M., Schmincke, H-U., Cronin, S.J. (2005) A conceptual model for block-and-ash flow basal avalanche transport and deposition, based on deposit architecture of 1998 and 1994 Merapi flows. Journal of Volcanology and Geothermal Research 139: pp. 117-134.

Scott, K.M. (1985) Lahars and lahar-runout flows in the Toutle-Cowlitz River system, Mount St. Helens, Washington--origins, behavior, and sedimentology, USGS Open-File Report 85-500, 202p.

Scott, K.M. (1988a) Origins, behavior and sedimentology of lahar-runout flows in the Toutle-Cowlitz River system, U.S. Geological Survey Professional Papers, n°1447-A, 74 p.

Scott, K.M. (1988b) Magnitude and frequency of lahars and lahars-runout flows in the Toutle-Cowlitz River system, U.S. Geological Survey Professional Papers, n°1447-B, 33 p.

Scott, W. (1989) Volcanic and Related Hazards. Tilling, R.I., (Ed.), Ch. 2, in Volcanic Hazards, short course in geology, v. 1, p. 9-23.

Scott, W.E., Iverson, R.M., Vallance, J.W., Hildreth, W. (1995) Volcano Hazards in the Mount Adams Region, Washington: U.S. Geological Survey Open-File Report 95-492, 11p.

Scott, K.M., Vallance, J.W., and Pringle, P.T., (1995) Sedimentology, Behavior, and Hazards of Debris Flows at Mount Rainier, Washington: U.S. Geological Survey Professional Papers 1547, 56p.

Scott, K.M., Janda, R.L., de la Cruz, E.G., Gabinete, E., Eto, I., Isada, M., Sexon, M. and Hardley, K.C. (1996) Channel and Sediment Responses to Large Volumes of 1991 Volcanic Deposits on the East Flank of Mount Pinatubo. In Newhall, C.G and Punongbayan, R.S. eds, Fire and Mud, Eruptions and Lahars of Mt. Pinatubo, Philippines, Quezon City/Seattle, PHIVOLCS/ University of Washington Press, pp. 971-988.

Scott, K.M., Macías, J.L., Naranjo, J., Rodriguez, S., McGeehin, J.P. (2001) Catastrophic debris flows transformed from landslides in volcanic terrains: mobility, hazard assessment and mitigation strategies. US Geological Survey Professional Papers 1630, 59 p.

Sdrolias, M., Müller, R.D. (2006) Controls on back-arc basin formation. Geochemistry, Geophysics, Geosystems 7: Q04016, doi:10.1029/2005GC001090.

Segschneider, B., Landis, C.A., White, J.D.L., Wilson, C.J.N., Manville, V. (2002) Resedimentation of the 1.8 ka Taupo ignimbrite in the Mohaka and Ngaruroro river catchments, Hawke's Bay, New Zealand. New Zealand Journal Geology Geophysics, 45: pp. 85–102.

Shea, T., van Wyk de Vries, B. (2008) Structural analysis and analogue modelling of the kinematics and dynamics of rockslide avalanches. Geosphere; v. 4; no. 4; pp.

657-686; DOI: 10.1130/GES00131.1

Shea, T., van Wyk de Vries, B., Pilato, M. (2008) Emplacement mechanisms of contrasting debris avalanches at Volcán Mombacho (Nicaragua), provided by structural and facies analysis. Bulletin of Volcanology DOI 10.1007/s00445-007-0177-7

Sherburn, S., White, R.S. (2005) Crustal seismicity in Taranaki, New Zealand using accurate hypocentres from a dense network. Geophysical Journal International 162: pp. 494-506.

Sherburn, S., White, R.S. (2006) Tectonics of the Taranaki region, New Zealand: earthquake focal mechanisms and stress axes. New Zealand Journal of Geology and Geophysics 49: pp. 269-279.

Sheridan, M.F. and Malin, M.C., (1983). Application of computer-assisted mapping to volcanic hazard evaluation of surge eruptions: Vulcano, Lipari and Vesuvius. Journal of Volcanology Geothermal Research 17, pp. 187–202.

Sheridan, M. F. and Kover, T. (1996) FLOW3D: A computer code for simulating rapid, open-channel volcanic flows. In Proc. UJST workshop on the Technology of Disaster Prevention against Local Severe Storms. Norman OK: pp. 155–163.

Sheridan, M.F., Hubbard, B., Carrasco-Nuñez, G., and Siebe, C, (2000) GIS model for volcanic hazard assessment: pyroclastic flows at Volcán Citlaltépetl, México. In Parks, B.O., Clarke K.M., Crane M.P., (Eds.). Proceedings of the 4th international conference on integrating geographic information systems and environmental modeling: problems, prospects, and needs for research; 2000 Sep 2-8; Boulder, CO. Boulder: University of Colorado, Cooperative Institute for Research in Environmental Science.

Sheridan,M.F., Carrasco-Núñez, G.,Hubbard,B., Rodríguez -Elizarraras, S., Siebe, C. (2004a) Construction of the hazard map for Citlaltépetl (Pico de Orizaba) volcano, Mexico. Proceedings of the IAVCEI 2004 General Assembly. 14–29 November 2004, Pucon, Chile. Abstracts with Programs, unpaginated.

Sheridan, M.F., Hubbard, B., Carrasco-Nunez, G., Siebe, C., (2004b) Pyroclastic Flow Hazard at Volcan Citlaltepetl, Natural Hazards, 33(2): pp. 209-221.

Sheridan, M.F., Stinton, A.J., Patra, A.K., Bauer, A.C., Nichita, C.C., and Pitman, E.B. (2005) Evaluating TITAN2D Mass-Flow Model Using the 1963 Little Tahoma Peak avalanches, Mount Rainier, Washington. J. Volcanol. Geotherm. Res., 139 (1-2): 89-102.

Siebe, C., Komorowski, J-C., Sheridan, M.F. (1992) Morphology and emplacement of an unusual debris-avalanche deposit at Jocotitlan volcano, Central Mexico. Bulletin of

Volcanology 54: pp. 573-589.

Siebert, L. (1984) Large volcanic debris avalanches: Characteristics of source area, deposits, and associated eruptions. Journal of Volcanology and Geothermal Research 22: pp. 163-197.

Siebert, L., Glicken, H., Ui, T. (1987) Volcanic hazards from Bezymianny- and Bandai-type eruptions. Bulletin of Volcanology 49: pp. 435-459.

Skermer N.A., VanDine D.F. (2005) Debris flows in history. In: Jakob M, Hungr O (eds) Debris-flow hazards and related phenomena. Springer Berlin Heidelberg, Praxis, pp 25–47.

Smith, E.G.C., Stern, T, Reyners, M. (1989) Subduction and back-arc activity at the Hikurangi convergent Margin, New Zealand. Pure and applied geophysics, 129: pp. 203-231

Smith, G.A. (1986) Coarse-grained nonmarine volcaniclastic sediment: Terminology and depositional process. Bulletin of the Geological Society of America 97: pp. 1-10.

Smith, G.A. (1987) Sedimentology of volcanism-induced aggradation in fluvial basins: Examples from the Pacific Northwest, USA. In: Ethridge FG, Flores RM, Harvey MG (Eds.) Recent developments in fluvial sedimentology. Society of Economic Palaeontologists and Mineralogists Special Publication 39: pp. 217-228.

Smith, G.A., Fritz, W.J. (1989) Volcanic influences on terrestrial sedimentation. Geology 17: pp. 375-376.

Smith, G.A., Grubensky, M.J., Geissman, J.W. (1999) Nature and origin of cone forming volcanic breccias in the Te Herenga Formation, Ruapehu, New Zealand. Bulletin of Volcanology, 61: pp. 64-82.

Smith, G.A., Lowe, D.R. (1991) Lahars: Volcano-hydrologic events and deposition in the debris flow hyperconcentrated flow continuum. In: Fisher RV, Smith GA (Eds.) Sedimentation in Volcanic Settings. SEPM Special Publication 45: pp. 60-70.

Sparks, R.S.J, Self, S., Walker, G. (1973) Products of ignimbrite eruptions, Geology 1, 115–118.

Sparks, R.S.J., Young, S.R. (2002) The eruption of Soufrière Hills Volcano, Montserrat (1995-1999). In, Druitt, TH and Kokelaar, BP (Eds.), The Eruption of Soufrière Hills Volcano, Montserrat, from 1995 to 1999, Geological Society of London Memoirs 21: pp. 45-69.

Stern, T.A. (1985) A back-arc basin formed within continental lithosphere: the Central

Volcanic Region of New Zealand. Tectonophysics 112: pp. 385-409.

Stern, T.A. (1987) Asymmetric back-arc spreading, heat flux and structure associated with the Central Volcanic Region of New Zealand. Earth and Planetary Science Letters 85: pp. 265-276.

Stern, T.A., Stratford, W.R., Salmon, M.L. (2006) Subduction evolution and mantle dynamics at a continental margin: Central North Island, New Zealand. Reviews of Geophysics 44: pp. 1-36.

Stevens, N.F., Manville, V., Heron, D.W. (2003) The sensitivity of a volcanic flow model to digital elevation model accuracy: experiments with digitised map contours and interferometric SAR at Ruapehu and Taranaki volcanoes, New Zealand. Journal of Volcanology Geothermal Research, 119: pp. 89–105

Stewart, R.B., Price, R.C., Smith, I.E. (1996) Evolution of high-K arc magma, Egmont volcano, Taranaki, New Zealand: evidence from mineral chemistry. Journal of Volcanology and Geothermal Research 74: pp. 275-295.

Stilwell, W.F., Hopkins, H.J., Appleton, W. (1954) Tangiwai railway disaster. Report of the Board of Inquiry. Wellington, Government Printer. 31 p.

Stoopes, G.R., Sheridan, M.F. (1992) Giant debris avalanches from the Colima Volcanic Complex, Mexico: Implication for long-runout landslides (>100 km). Geology 20: pp. 299-302.

Takahashi, T. (1978) Mechanical characteristics of debris flow, Journal of Hydraulic Engineering Division of the American Society of Civil Engineers, 104: pp. 1153–1169.

Takahashi, T. (1980) Debris flow on prismatic open channel, Journal of Hydraulic Engineering Division of the American Society of Civil Engineers, 106: pp. 381–396.

Takahashi, T. (1981) Debris flows. Annual Reviews of Fluid Mechanics 13: pp. 57-77.

Takahashi, T., Sawada, T., Suwa, H., Mizuyama, T., Mizuhara, K., Wu, J., Tang, B., Kang, Z., and Zhou, B. (1994) Japan-China joint research on the prevention from debris flow hazards, Research Report, Japanese Ministry of Education, Science and Culture, Int. Scientific Research Program No. 03044085.

Takahashi, T., Tsujimoto, H. (2000). A mechanical model for Merapi-type pyroclastic flows Journal of Volcanology and Geothermal Research, 98: pp. 91–115.

Takarada, S., Ui, T. and Yamamoto, Y. (1999) Depositional features and transportation mechanism of valley-filling Iwasegawa and Kaida debris avalanches, Japan. Bulletin of Volcanology, 60: pp. 508-522.

Taylor, R. (1861) Journal of Rev. Richard Taylor 1833–1873. Wellington, Alexander Turnbull Library.

Thouret, J.C. (2004) Geomorphic processes and hazards on volcanic mountains. In: Owens Ph., Slaymaker O. (Eds.) Mountain Geomorphology, chapter 11, Arnold, London, pp. 242-273.

Thouret, J.C., Abdurachman, K.E., Bourdier, J.L., Bronto, S. (1998) Origin, characteristics, and behaviour of lahars following the 1990 eruption of Kelud volcano. Bulletin of Volcanology. 59,: pp. 460-480.

Thouret, J.C., Lavigne, F., Suwa, H., Sukatja, B., Surono (2007) Volcanic hazards at Mount Semeru, East Java Indonesia with emphasis on lahars. Bulletin of Volcanology, 70: pp. 221–244

Tilling, R.I., (1989a) Volcanic hazards and their mitigation: progress and problems. Reviews in Geophysics 27: pp. 237–269.

Tilling, R.I., (1989b) Volcanic Hazards, short course in geology: v. 1, Washington, D.C., American Geophysical Union, 123 p. 269.

Todesco, M., Neri, A., Esposti Ongaro, T., Papale, P., Macedonio, G., Santacroce, R., Longo, A. (2002) Pyroclastic flow hazard at Vesuvius using numerical modeling. I. Large-scale dynamics. Bulletin of Volcanology. DOI 10.1007/s00445-001-0189-7.

Topping, W.W., (1973) Tephrostratigraphy and chronology of late Quaternary eruptives from the Tongariro Volcanic Centre, New Zealand. New Zealand Journal of Geology and Geophysics 16: pp. 397 – 423.

Toyos, G., Cole, P., Felpeto, A., Martí, J. (2007) A GIS-based methodology for hazard mapping of small volume pyroclastic flows. Natural Hazards 41: 99 – 112.

Turner, M.B., Cronin, S.J., Bebbington, M.S., Platz, T. (2008) Developing a probabilistic eruption forecast for dormant volcanoes; a case study from Mt Taranaki, New Zealand. Bulletin of Volcanology 70: pp. 507-515. DOI: 10.1007/s00445-007-0151-4.

Ui, T. (1983) Volcanic dry avalanche deposits: identifications and comparison with nonvolcanic debris stream deposits. Journal of Volcanology and Geothermal Research 18: pp. 135-150.

Ui, T. (1989) Discrimination between debris avalanches and other volcaniclastic deposits. In: Latter JH (Ed.) Volcanic Hazards. Springer, Heidelberg, 625 p.

Ui, T., Kawachi, S., Neall, V.E. (1986) Fragmentation of debris avalanche material

during flowage – evidence from the Pungarehu Formation, Mount Egmont, New Zealand. Journal of Volcanology and Geothermal Research 27: pp. 255-264.

Ui, T., Matsuwo, N., Sumita, M., Fujinawa, A. (1999) Generation of block and ash flows during the 1990–1995 eruption of Unzen volcano, Japan. Journal of Volcanology and Geothermal Research 89: pp. 123– 137.

Ui, T., Takarada, S., Yoshimoto, M. (2000) Debris avalanches. In: Encyclopedia of Volcanoes, p. 617-626.

UNESCO. (1980) Natural disasters and vulnerability analysis: report of Expert Group Meeting (9-12 July 1979) Office of the United Nations Disaster Relief Co-ordinator.

Vallance, J.W. (2000) Lahars. In: Sigurdsson, H., Houghton, B., McNutt, S., Rymer, H., Stix, J. (Eds.) Encyclopedia of Volcanoes, Academic Press, San Diego, pp. 601-616.

Vallance, J. W. (2005) Volcanic debris flows, in Debris Flow Hazards and Related Phenomena, Jakob, Matthias, and Hungr, Oldrich, eds., Springer-Praxis, Heidelberg, pp. 247-274.

Vallance, J.W., Siebert, L., Rose, W.I. Jr, Giron, J.R., Banks, N.G. (1995) Edifice collapse and related hazards in Guatemala. Journal of Volcanology and Geothermal Research 66: pp. 337-355.

Vallance, J.W., Scott, K.M. (1997) The Osceola Mudflow from Mount Rainier; sedimentology and hazard implications of a huge clay-rich debris flow. Geological Society of America Bulletin, 109: p. 143–163.

Vallance, J.W., Cunico, M.L., Schilling, S.P. (2003) Debris-Flow Hazards Caused by Hydrologic Events at Mount Rainier, Washington – US Geological Survey Open-File Report 03-368.

Varnes, D. J. (1984). Landslide Hazard Zonation: Preview of Principals and Practices: Paris, UNESCO, Int. Association of Engineering Geologists, Commission on Landslides and Other Mass Movements on Slopes, Natural Hazards, V-3 pp176.

Van Wyk de Vries, B., Kerle, N., Petley, D. (2000) Sector collapse forming at Casita volcano, Nicaragua. Geology 28: pp. 167-170.

Van Wyk de Vries, B., Self, S., Francis, P.W., Keszthelyi, L. (2001) A gravitational spreading origin for the Socompa debris avalanche. Journal of Volcanology and Geothermal Research 105: 225-247.

Varnes, D.J. (1978) Slope movement types and processes. In, Schuster, R.L., Krizek, R.J. (Eds.) Landslides: Analysis and Control. National Academy of Sciences,

Washington, D.C. Transportation Research Board Special Report 176, l-33.

Vessel, R.K., Davies, D.K. (1981) Nonmarine sedimentation in an active fore arc basin. Society of Econonic and Paleontologists and Mineralogists, Special Publication 31: pp. 31-45.

Vignaux, M., Weir, G.J. (1990) A general model for Mt Ruapehu lahar. Bulletin of Volcanology, 52: pp. 381-390.

Villamor, P., Van Dissen, R., Alloway, B., Palmer, A., Litchfield, N. (2007) The Rangipo Fault, Taupo Rift, New Zealand: an example of temporal slip rate and single event displacement variability in a volcanic environment. Bulletin of the Geological Society of America, 119: pp. 529-54

Voight, B., Glicken, H., Janda, R.J., Douglass, P.M. (1981) Catastrophic rockslide avalanche of May 18. In: Lipman, P.W. & Mullineaux, D.R. (Eds.) The 1980 eruptions of Mount St. Helens, Washington, US Geological Survey Professional Papers 1250: pp. 347-377.

Voight, B., Janda, R.J., Glicken, H., Douglass, P.M. (1983) Nature and mechanism of the Mount St. Helens rockslide-avalanche of May 1980. Geotechnique 33: pp. 243-273.

Volker, H.X., Wasklewicz, T.A. and Ellis, M.A. (2007) A topographic finger print to distinguish alluvial fan formative processes. Geomorphology 88, 1-2: pp. 34-45.

Waight, T. E., Gamble, J.A., Price, R. C., Stewart, R. B., Smith, I. E. M. (1999) Stratigraphy and geochemistry of the Turoa area, with implications for andesite petrogenesis at Mt Ruapehu, Taupo Volcanic Zone, New Zealand. New Zealand Journal of Geology and Geophysics 42(4): pp. 513-532.

Waitt, R.B., Mastin, L.G., Begét, J.E. (1995) Volcanic-Hazard Zonation for Glacier Peak Volcano, Washington: U.S. Geological Survey Open-File Report 95-499

Walder, J.S. and O'Connor, J.E. (1997) Methods for predicting peak discharge of floods caused by failure of natural and constructed earthen dams. Water Resources Research 33: pp. 2337–2348.

Walker, G. P. L., Wilson, C. J. N. (1983). Lateral variations in the Taupo ignimbrite. Journal of Volcanology and Geothermal Research 18, 117–133

Wallace, L.M., Beavan. J., McCaffrey, R., Darby, D. (2004) Subduction zone coupling and tectonic block rotations in the North Island, New Zealand. Journal of Geophysical Research 109: B12406, doi:10.1029/2004JB003241.

Wang, C., Cheng, L-H., Chin, C-V. and Yu, S-B. (2001) Coseismic hydrologic response of an alluvial fan to the 1999 Chi-Chi earthquake, Taiwan. Geology, 29: pp.831-834.

Waythomas, C. F., Miller, T. P., Beget, J. E. (2000) Record of Late Holocene debris avalanches and lahars at Iliamna Volcano, Alaska: Journal of Volcanology and Geothermal Research 104: pp. 97-130.

Waythomas, C.F., Wallace, K.L. (2002) Flank collapse at Mount Wrangell, Alaska, recorded by volcanic mass-flow deposits in the Copper River lowland. Canadian Journal of Earth Sciences 39: pp. 1257-1279.

Webby, M.G. and Forster, D.J. (2002) Ruapehu Crater Lake Lahar Residual Risk Assessment - Lahar Flow Calculations - Opus International Consultants. Ministry of Civil Defence and Emergency Management, New Zealand.

Weir, G. J. (1982) Kinematic wave theory for Ruapehu lahars, N. Z. J. Sci., 25: pp. 197–203.

Whipple, K., Dunne, T. (1992) The influence of debris-flow rheology on fan morphology, Owens Valley, California. Bulletin of the Geological Society of America 104: pp. 887-900.

White, F.M. (2006) Viscous Fluid Flow. New York, NY: McGraw Hill.

Williams, R., (2006) Modeling lahars using TITAN2D for the southern drainage of Volcan Cotopaxi: impact on the city of Latacunga. Master Thesis, SUNY, Buffalo, 85 pp.

Wilson, C. J. N. (1986). Pyroclastic flows and ignimbrites. Science Progress, Oxford., 70, 171–207.

Wilson, C.J.N., Houghton, B.F., McWilliams, M.O., Lanphere, M.A., Weaver, S.D., Briggs, R.M. (1995) Volcanic and structural evolution of Taupo Volcanic Zone, New Zealand: a review. Journal of Volcanology and Geothermal Research 68: pp. 1-28.

Wolfe, E.W. and Pierson, T.C. (1995) Volcanic-Hazard Zonation for Mount St. Helens, Washington, 1995: U.S. Geological Survey Open-File Report 95-497

Yamamoto, T., Takarada, S., Suto, S., (1993) Pyroclastic flows from the 1991 eruption of Unzen volcano, Japan. Bulletin of Volcanology 55: pp. 166– 175.

Yu, Y., Hong, H., Wei, H., Zheng, X., Liu, P., Tao, W. (2004). Modeling of Potential Lahars Motivated by Landslides in Crater Lake of Baitoushan Volcano, *Eos Trans. AGU, 85*(47), Fall Meet. Suppl., Abstract #H44A-03.

Zernack, A. (2009) A Sedimentological and Geochemical Approach to Understanding Cycles of Stratovolcano Growth and Collapse at Mt. Taranaki, New Zealand. Unpubl. PhD thesis, Institute of Natural Resources, Massey University, Palmerston North, New Zealand.

Zernack, A.V., Procter, J.N., and Cronin, S.J. (2009). Sedimentary signatures of cyclic growth and destruction of stratovolcanoes: A case study from Mt. Taranaki, NZ. In: K. Nemeth, V. Manville, and K. Kano (Eds.) Source to sink: from volcanic eruptions to volcaniclastic deposits, Sedimentary Geology Special Volume. doi:10.1016/j.sedgeo.2009.04.024

Appendix (on DVD-ROM)

i. Titan2D User Guide. GMFG SUNY Buffalo

ii. Digital Elevation Models
    a. Mt. Taranaki 20m resolution
    b. Mt.Ruapehu 5m resolution

iii. Titan2D setup/initiation files – Mt. Ruapehu lahar simulations
    a. Chapter 2 simulations
    b. Chapter 3 simulations

iv. Titan2D setup/initiation files – Mt. Taranaki mass flow simulations
    a. Chapter 4 simulations
    b. Chapter 5 simulations
    c. Chapter 6 simulations

v. Western Taranaki stratigraphic section descriptions and field notes